به نام خدا

مرکز دانلود رایگان
مهندسی متالورژی و مواد

www.Iran-mavad.com

NATO Science for Peace and Security Series - C:
Environmental Security

# Integrity of Pipelines Transporting Hydrocarbons

## Corrosion, Mechanisms, Control, and Management

Edited by
Gabriella Bolzon
Taoufik Boukharouba
Giovanna Gabetta
Mimoun Elboujdaini
Mekki Mellas

Springer

NATO OTAN

*This publication is supported by* The NATO Science for Peace and Security Programme

# Integrity of Pipelines Transporting Hydrocarbons

# NATO Science for Peace and Security Series

This Series presents the results of scientific meetings supported under the NATO Programme: Science for Peace and Security (SPS).

The NATO SPS Programme supports meetings in the following Key Priority areas: (1) Defence Against Terrorism; (2) Countering other Threats to Security and (3) NATO, Partner and Mediterranean Dialogue Country Priorities. The types of meeting supported are generally "Advanced Study Institutes" and "Advanced Research Workshops". The NATO SPS Series collects together the results of these meetings. The meetings are co-organized by scientists from NATO countries and scientists from NATO's "Partner" or "Mediterranean Dialogue" countries. The observations and recommendations made at the meetings, as well as the contents of the volumes in the Series, reflect those of participants and contributors only; they should not necessarily be regarded as reflecting NATO views or policy.

**Advanced Study Institutes (ASI)** are high-level tutorial courses to convey the latest developments in a subject to an advanced-level audience

**Advanced Research Workshops (ARW)** are expert meetings where an intense but informal exchange of views at the frontiers of a subject aims at identifying directions for future action

Following a transformation of the programme in 2006 the Series has been re-named and re-organised. Recent volumes on topics not related to security, which result from meetings supported under the programme earlier, may be found in the NATO Science Series.

The Series is published by IOS Press, Amsterdam, and Springer, Dordrecht, in conjunction with the NATO Emerging Security Challenges Division.

**Sub-Series**

| | | |
|---|---|---|
| A. | Chemistry and Biology | Springer |
| B. | Physics and Biophysics | Springer |
| C. | Environmental Security | Springer |
| D. | Information and Communication Security | IOS Press |
| E. | Human and Societal Dynamics | IOS Press |

http://www.nato.int/science
http://www.springer.com
http://www.iospress.nl

**Series C: Environmental Security**

# Integrity of Pipelines Transporting Hydrocarbons

## Corrosion, Mechanisms, Control, and Management

edited by

**Gabriella Bolzon**
Politecnico di Milano, Dipartimento di Ingegneria Strutturale,
45 Milano, Italy

**Taoufik Boukharouba**
Université des Sciences et de Technologie Houari Boumediene (USTHB),
Laboratoire de Mécanique Avancée (LMA), Bab-Ezzouar, Algiers, Algeria

**Giovanna Gabetta**
Eni E&P Division – TEMM, San Donato Milanese, Italy

**Mimoun Elboujdaini**
CANMET Materials Technology Laboratory, Natural Resources Canada,
Ottawa, Ontario, Canada

and

**Mekki Mellas**
Université Mohamed Khider, Faculté des Sciences et de la Technologie,
Biskra, Algeria

Springer

Published in Cooperation with NATO Emerging Security Challenges Division

Proceedings of the NATO Advanced Research Workshop on
Corrosion Protection of Pipelines Transporting Hydrocarbons
Biskra, Algeria
26-28 April 2010

Library of Congress Control Number: 2011925853

ISBN 978-94-007-0594-4 (PB)
ISBN 978-94-007-0587-6 (HB)
ISBN 978-94-007-0588-3 (e-book)
DOI 10.1007/978-94-007-0588-3

Published by Springer,
P.O. Box 17, 3300 AA Dordrecht, The Netherlands.

*www.springer.com*

*Printed on acid-free paper*

# Foreword

Pipelines are becoming increasingly important vectors to transport large volumes of hydrocarbons over long distances in the Mediterranean region. If well constructed, carefully monitored and properly maintained, pipelines can be a safe and environmentally/economically solution of transport; otherwise they can pose a serious threat to our health and our environment.

Actually, pipeline integrity is a growing and challenging problem for oil companies since the age of the components is increasing and the responsibility and awareness about environmental protection is increasing too. Corrosion is one of the most active and dangerous damage mechanisms for pipes and corrosion defects can be assessed by Fracture Mechanics or Limit Analysis. Knowledge in both disciplines was increasing rapidly in the second half of past century, but the progress in some way slowed down more recently, due to the increasing complexity of parameters to be accounted for. One is clever at solving simple problems, but less when facing with complex and evolving situations that are not easy to handle. Considering pipelines, although they are operated with increasing care, there is still room for improvement. There is a need to raise awareness and share experience and good practices among the operators. The latest research results, when available, need a large effort to be applied. Communication between the scientific community, regulation offices and pipeline operators needs to be improved.

Moreover, research in the field of corrosion and integrity of metallic components is greatly affected by the increasing amount of experimental data and studies performed. Many new tools are now available to communicate and to share knowledge; they are increasingly used but their potential is not fully understood and exploited especially by older people. Social networks and the collection of information via the Web are often simply used to help connecting people, but a full exchange of knowledge is not easy to obtain.

In industry, available practices are always subjected to the need to “keep the plant running”, so that an action is foreseen in the shortest time. At the same time, more work is necessary to increase the awareness of long term consequences. Actually, due to high involved costs and increased competition, there is a need

for transmission and sharing experiences, not only between scientists working in the same sectors, but also within the operating companies and the regulation offices or to be short, the larger knowledge based community.

Under the leadership of NetMed, the network on Corrosion Prevention in the Mediterranean Countries, a workshop on ***Integrity of Pipelines Transporting Hydrocarbons*** was held to create links between the scientific community and the operating companies (owners, engineering companies, regulation offices), and to share the recent results and/or experimental programs. The meeting was divided into sessions where, after intervention of key note speakers, discussion and sharing of experience took place. Each discussion session was moderated by a chairperson selected between the key speakers.

The first session was devoted to ***Pipelines Integrity and Fracture Mechanics***, giving a starting overview of pipeline management related problems from a mainly theoretical point of view. Fracture mechanics is important for the structural integrity of pipes affected by corrosion mechanisms, particularly when stress corrosion cracking is developing and when hydrogen is the circumstance. Damage mechanisms and their evolution where described. Some models suggest that damage can accumulate and degrade the steel properties with time. The keynote session was followed by presentations on related numerical methods and modelling. Transfer of data from research laboratories to end users is a key point. Full scale tests are proposed to fulfil this objective, although full scale tests are known to be expensive and difficult to realize.

During the second session, focused on ***Pipeline Integrity Assessment***, methods to quantify the damage and to manage risks were presented, starting with coating assessment and cathodic protection. The debate on risk assessment is of interest for application, since the probability of failure is usually estimated using data banks of real cases, although an estimate based on damage mechanisms, if reliable, could be useful, easy to obtain and somehow more realistic. Cathodic protection was the object of two presentations by keynote speakers. Although this method can prevent damage development, it can also enhance hydrogen embrittlement as discussed by other experts. A further contribution was devoted to leakages, their management and their prevention. On the other hand, leak prevention is closely related to damage mechanisms and to the relevant modelling.

***Industrial applications*** were the object of the second workshop day. The experience of oil companies shows that a pipeline ageing does not necessarily lead to increased risks. In fact, relevant data to corrosion damage in pipelines as collected by different speakers coming from different countries are quite different. The impact of corrosion in pipelines transporting hydrocarbons seems to change as a function of region, transported fluid, manufacturing and age of the component, as well as many other parameters. Moreover, as shown for instance by *Sonatrach* experience, long pipelines behave differently in different location. Then, risk estimate cannot be the same along the entire pipeline.

***Hydrogen embrittlement*** of exploited pipeline steel was experimentally investigated at Karpenko Institute in Ukraina examining old pipeline materials, aged of at least 20 or 30 years. Damage is concentrated in zone where corrosion is active.

A relationship between degradation of mechanical properties and corrosion can therefore be proposed. An interesting comparison was raised in this session with the safety approach used in nuclear industry. Differently from other industrial components and for pipelines, material selection for nuclear plants requires prediction of material properties at the end of the design life. A debate about the feasibility of increasing the safety level to such a requirement was proposed.

The ***concept of acceptable risk*** (in terms of fatalities, damages to industry, damage to environment) has been also discussed. The level of acceptable risk is strongly related to costs. One should be aware that decreasing the risk of one order of magnitude may require increasing costs of two orders of magnitude. Risks are usually assessed on rational basis by engineers and other technicians, but common people are more sensitive about its emotional perception. So, while risks in terms of materials and financial costs can be relatively easily assessed, this becomes a really difficult task when injuries and environmental damage have to be considered.

The final session was focused on possible future actions based on the use of new communication tools and of ***Knowledge Management***. The first point addressed is the need for best trained and more numerous corrosion engineers. Apparently, young people are not much interested in starting and developing their professional careers in scientific/technical domains nowadays. Universities and associations in the USA are aware of the problem and a cooperation program is underway between the International Association of Corrosion Engineers (NACE International) and ASM International (the former American Society for Metals), implementing actions intended to introduce corrosion engineering to young people of high school age in such a way that science can be perceive as a challenging and interesting adventure. Knowledge Management (KM) addresses the ability of exploiting new tools, as for instance Social Networks, with their full potentialities. Often, people do not realize how quickly the explicit knowledge (collected in reports, papers and other documents) tends to become tacit (sitting only in the memories of people and/or personal computers) and to disappear totally with time. The knowledge cycle in a correct KM process shall proceed in the opposite direction, promoting the sharing of tacit knowledge, to let it become explicit and be disseminated in the company. The process cannot be completed if people do not recognize the value of past experience. A KM system should also generate networks of knowledge outside Companies. The contribution of existing networks such as technical associations and Working Parties (which are similar to Communities of Practice) can be very important to enhance the cooperation between scientists and experts all over the world.

In the specific case of internal corrosion of pipelines transporting hydrocarbon, a better use of knowledge could be helpful; as an example, the following conclusions were proposed:

- using codes with built-in corrosion rate calculations could be misleading,
- corrosion models are good for materials selection and for the understanding "backward" of failures; they are to be improved for a better prediction of integrity,

- the integrated use of different data bases, such as failure data, fluid properties, production data, and scientific findings can make the difference for integrity assessment.

The Workshop participants were aware that we need to solve problems, not to simply discuss them. On the other hand, while there are still many open problems worth to be investigated, in many countries it is not easy to raise money for research funds. However, the discussion on risk estimate shows that we still have a margin to improve risk assessment and to decrease the cost of damage. The cooperation between academia and industry is a win-win situation; different experiences can be shared to solve complex problems; industries are already in many cases joining efforts.

NATO ARW 983731/Co-Editors — Dr. Giovanna Gabetta
April 2010 — Prof. Taoufik Boukharouba

# Editors' Biographies

**Prof. Gabriella Bolzon**

Associate Professor of Structural Mechanics at the Politecnico di Milano, one of the main Engineering Schools in Italy, and Faculty member of the Ph.D. School in Structural, Earthquake and Geotechnical Engineering. She graduated in Civil Engineering at the University of Padova and received her Ph.D. in Mechanics of Materials and Structures from Bologna University. She has carried out research in academic and industrial environment, participating to several research projects sponsored by national and international agencies (Australian Research Council, EU, Japan Society for the Promotion of Science), with stays at: Laboratoire de Mécanique et Technologie, Cachan, France (1995); University of the New South Wales, Sydney, Australia (1996–1999); Okayama University, Japan (2001 and 2003); Technical University Darmstadt, Germany (2005); Instituto de Tecnologia Ceramica, Castellon de la Plana, Spain (2006). She has published more than 100 papers in international journals, books and conference proceedings and acts as reviewer of several international journals. Her main research topics focus on: constitutive modelling of multi-component materials; simulation of quasi-brittle fracture processes; mechanical characterization of materials; parameter identification by deterministic and stochastic techniques.

**Prof. Taoufik Boukharouba**

Received his Mechanical Engineering Degree (1987) from the University of Annaba, his Magister (1991) in Mechanical Engineering from Ecole Polytechnique of Algiers and then his Doctorate (1995) from the University of Metz in France. He joined the staff of University of Science and Technology, Houari Boumediene (USTHB) in 1996. He was Director of the Mechanical Engineering Institute (IGM of USTHB) from 1998 to 2000 and first advisory member in science and technology for the Algerian-French Advisory Board for higher education and scientific research (2004–2008). Presently, he is Director of the Advanced

Mechanics Laboratory (LMA) of USTHB. He is president of the Algerian Association of Mechanics and Materials and member of the "Commission Universitaire Nationale (CUN)". His research interest is in damage of composites, nanocomposites materials and materials in biomechanics. He has published 22 papers in refereed journals, 48 published communications to scientific meetings and book in English (Copyright: Springer 2009). He is member of the editorial board and reviewer of several journals and many international conferences and he organized several national and international conferences: the "Congrès Algérien de Mécanique de Construction" (Algiers 2007, Biskra 2009) and in Algiers the First African InterQuadrennial ICF Conference "AIQ-ICF2008". Presently, he is the general Chair (2009-2011) for the "Troisième Congrès Algréien de Mécanique (CAM2011) to be held in Guelma, Algeria in 2011.

**Dr. Giovanna Gabetta**

Giovanna Gabetta holds a degree in nuclear engineering (Politecnico of Milano, 1975). She worked 16 years at CISE, an Italian Research Centre in the power generation industry. The main interest was in Fracture Mechanics, Corrosion and Environmentally Assisted Cracking. Since 1994 she works for Oil&Gas Industry at eni, the Italian Oil&Gas industrial group, in the Engineering Division. The activity is focused on research in the same field of Corrosion and Materials characterization, with increasing interest towards pipelines safety and corrosion models. Since 2005, in the frame of a new project about Knowledge Management, she has the role of Facilitator in the Materials Community of Practice. She is a member of AIM (the Italian Association of Metallurgy), Nace International and ESIS (European Structural Integrity Society). For about 20 years (ending in August 2010), she acted as co-chairman of ESIS TC10 "Environmentally Assisted Cracking" together with Dr.-Ing. Wolgang Dietzel of GKSS. She acted as Editor of the Journal "Engineering Fracture Mechanics" in 1997–2004. Since 2000 she is a referee for the Journal "La Metallurgia Italiana", since 2007 is a member of the Scientific Committee of "Frattura ed integrità strutturale", Journal on line of the Italian Group on Fracture, IGF and since 2009 is a referee for the Academy of Scientific Research and Technology Informatics and Scientific Services Sector, National Information and Documentation Centre (NIDOC), Cairo, Egypt. She is author of more than 150 papers in journals and conferences. She published two books on the subject of "women and engineering". She is married with Carlo Zanotti since 1975 and they have three children.

**Dr. Mimoun Elboujdaini**

M. Elboujdaïni is currently a senior Research Scientist at CANMET–Materials Technology Laboratory in Ottawa, Canada. He received a mechanical engineering degree and Diplôme d'Etude Approfondie (DEA) from the University of Technology of Compiegne in France. He obtained his M.Sc. degree in physical metallurgy

from Ecole Polytechnique, Montreal and his Ph.D. in physical metallurgy and corrosion from the Laval University, Quebec, Canada. In 1989 he joined CANMET of Natural Resources Canada as a research scientist, leading projects dealing mainly with pipeline-oil/gas/petrochemical industries, including stress-corrosion cracking (SCC), corrosion fatigue, hydrogen-induced cracking (HIC) in H2S environment, hydrogen embrittlement, and liquid metal embrittlement. Dr. Elboujdaini has been active in various aspects of materials behavior and the author of several papers (over 150 papers) as well as editor of 16 proceedings, two books and contributions to two chapters in handbook and chaired several important committees (NACE, CIM, ESIS, ECF, ICF, ECS), chaired and organized several symposia of the Materials Performance and Integrity Section of the Metallurgical Society of CIM. Dr. Elboujdaini also served as a member of organizing committees of several national and international conferences. He has received the Morris Cohen Award, Fellow of the International Congress on Fracture (FICF) and is an adjunct professor at the University of Alberta and has been invited by many national and international organization/committees to deliver lectures. Group leader in managing of group of scientists and technologists for the Corrosion and Materials Degradation Group to Materials Technology Laboratory (MTL). Presently the Vice-President of the International Congress on Fracture (2009–2013).

**Dr. Mekki Mellas**

Dr. Mekki Mellas is a lecturer in civil engineering. He is, presently, a dean of faculty of sciences and technology at the University of Biskra. He was the Head of the department of civil engineering of the University of Biskra (1999–2009). He graduated in civil engineering from the National polytechnics school of Algiers (1984) and received his Master of Philosophy degree from the school of civil engineering at the University of Birmingham (United Kingdom) (1987), and received his Doctorate in civil engineering from the University of Biskra (2003). His main research topics focus on materials sciences, concrete, microstructures of cement, simulation in Soils mechanics, besides of the use of the scanning electron microscope and the x rays diffractions in the investigation of the materials properties. He is the member of the laboratory of research of the civil engineering. He organized several national and international conferences. He is member of the editorial board and reviewer of several journals.

# Acknowledgement

This book gathers together the presentations made during the NATO Advanced Research Workshop on 'Corrosion Protection of Pipelines Transporting Hydrocarbons', held in Biskra, Algeria on April 26–28, 2010, under the auspices of the NATO Science for Peace and Security Programme. Contributors are all known as experts in the areas of corrosion, fracture and reliability of structures, who are leading authorities in the current state of knowledge with regard to integrity of pipelines.

The editors would like to acknowledge the help of the organizing committee members for managing the event that resulted in this book. We also wish to thank the workshop participants and invited authors for their contributions, and the peer reviewers of the manuscripts. We are deeply grateful to the University of Biskra for hosting the meeting and contributing to its organization.

Finally, on behalf of all organizers and participants we gratefully acknowledge the NATO Program Committee for the award of a support grant which made this event possible.

Taoufik Boukharouba
Gabriella Bolzin
Giovanna Gabetta
Mimoun Elboujdaini
Mekki Mellas

# Contents

# The Use of Knowledge Management to Improve Pipeline Safety

**Giovanna Gabetta and Giulia Gori**

**Abstract** Since 2004, eni E&P Division is supporting a program on Knowledge Management (KM). The KM System of the Division, based on Communities of Practice (CoP), aims at helping professionals all over the world to address problems as they occur, and at capitalizing experiences and cases, not to loose precious know how. CoP Members are in contact via mailbox and they can share information and documents working together through a collaborative platform; after a few years of exchange, they recognize that a lot of experiences and cases are treated in the Group, as for instance failures analysis occurred in plants and industrial areas in many countries where our company is involved. These experiences are often kept as "tacit knowledge", stored in brains, computers, and shelves by the experts who are in charge of the problem. The CoP agreed to make an effort toward changing tacit knowledge into explicit knowledge, collecting cases examined in the past and using them to a better understanding of future developments. A CoP was established to create a network of experts in Corrosion and Materials related topics. This CoP is extended to a number of Companies inside eni Group. Only about 9% of the people active in KM are participating in the materials Community, which is nevertheless one of the most active. CoP members are in real time contact with corrosion engineers in Business Units all over the world, as for instance Congo, Egypt, Tunisia, Australia, Nigeria, Venezuela and many others. About 300 issues were posted in the CoP mailbox since it was established and each obtained two or three answers based on real experience, helping professionals to solve technical problems in a quick and easy way, saving time and money. Sharing of experience is only the beginning; the future challenge for the system is to get all the possible advantages from a better use of knowledge. Important questions are:

- Can we address technical problems from a different point of view with Knowledge Management?
- What are the advantages, if any, of such an approach?

G. Gabetta (✉) and G. Gori
Eni E&P Division, TEMM, via Emilia 1, San Donato Milanese, 29097 Milano, Italy
e-mail: giovanna.gabetta@eni.com; giulia.gori@eni.com

T. Boukharouba et al. (eds.), *Integrity of Pipelines Transporting Hydrocarbons*,
NATO Science for Peace and Security Series C: Environmental Security,
DOI 10.1007/978-94-007-0588-3_1, 

The application of the above philosophy to the management of asset integrity of pipelines seems to be a promising field; KM system can be an useful tool to get a better communication between new technological developments, expert knowledge and operational needs.

## 1 Introduction

Pipeline integrity is a growing and challenging problem for Oil Companies since the length of pipelines transporting hydrocarbons is increasing worldwide, and the responsibility and awareness about environmental protection is increasing too. Corrosion is one of the most active and dangerous damage mechanisms, while fracture mechanics help us to verify and predict pipeline stability. Knowledge in both disciplines was increasing at a fast pace in the second half of past century, but the progress in some way slowed down more recently, giving the impression that everything is known and the necessity for further research is lower.

At the same time, new tools are now available to communicate and to share knowledge; they are increasingly used but their potential is not fully understood especially by older people. Social networks and the collection of information via the web are often simply used to help connecting people, but not as a full exchange of knowledge. We are all aware of the difficulty in selecting what can be useful out of a huge amount of findings obtained by a search engine in the web; of the feeling of impotence when we are working and we get further and further interruptions by e-mail and phone calls. Neural science specialists are wondering if the human mind is going through a deep change from reading capabilities to digital information [1].

With a simpler goal in mind, as corrosion engineers in Oil Companies we are facing some problems peculiar of our times, as for instance:

- the retirement of a large amount of older experts is now taking place and will be completed in a few years; these people will be replaced by a much younger workforce without the time for a gradual change necessary to transfer knowledge,
- easy problems are known and can be quite simply solved; but much more complex problems are emerging and their solution – or their simple management – is probably far from the reach of a single human brain; moreover, the capability of human people to cooperate is still far too little, we have a habit for competition,
- the amount of time required to select what is useful in the huge amount of information automatically provided in the web is large; the use of human brain is still the only available resource to change information in applicable knowledge.

In summary, we tend to propose old solutions for new problems, and we do not use at their best the new available tools. It is worth some effort to think about these problems and to try an application of this philosophy to engineering problems such as pipeline management.

Knowledge Management is the name given to projects and efforts set up by organizations in different field to organize and share knowledge. The goal is ambitious; application to the solution of operational problems is promising, but not an easy task.

## 2 Knowledge Management System in Eni E&P Division

Eni E&P Division set up since 2004 a System of Knowledge Management (KM System), aimed at generating value and increasing efficiency by leveraging on Company knowledge and individual experience.

The KM System is designed to make competence and experience of experts available to all the Operational Line all over the world, to allow a better share of knowledge between people working on the same problems in different environments. The System tries to overcome the presence of functional and geographic silos in the transfer of knowledge, between different Business Units and project teams. The final objective is to improve operational processes through the use of best practices and lessons learned and to allow time and money saving thanks to the re-use of capitalized knowledge.

The spread of seniors' experiences promotes knowledge capitalization in the Company and helps younger people growing faster on operational activities.

We can define knowledge as a distillate of data and information, filtered through human experience. Usually, two kinds of knowledge are considered: what has been or can be codified, and stored in certain media and can be easily transmitted to others, and what lives in human mind and closely depends on individual experience. This second type of knowledge is difficult to transfer to another person by means of writing it down.

When knowledge is formally representable, is called *explicit* and can be transferred through procedures, standards, best practices, case histories, etc. It represents no more than 20% of the total knowledge circulating within enterprises.

The second kind of knowledge is called *tacit* and its exchange takes place only through direct contact between people. For this reason, its management requires knowing who holds knowledge (*who knows what*) and creating an environment supporting knowledge sharing and pro-activity behaviours. In this respect the KM System in E&P Division was thought and established, based on three concurrent factors: ICT (Information & Communication Technologies) tools, organizational tools and people's behaviour. A specific and functional ICT infrastructure is a critical factor to enable an efficient KM System, but of course it is not enough.

The introduction of the KM System in the Company also involved an organizational change. In 2004, a specific workflow was designed and formal structures were produced, necessary to coordinate and guide the activities related to Knowledge Management.

The whole System was based on Communities of Practice (CoP), virtual communities made of experts committed to a specific knowledge domain. CoP Members,

linked together informally, interact and build relationships, developing and sharing their knowledge and practice. CoP Members share a passion for something and interact regularly to learn by other's experience, to reach better performances and to avoid repeating mistakes. Members of the same Community work on the same problems and they are motivated to improve the global performance by leveraging on knowledge management.

Working collaboratively through CoPs implies a cultural change, because adopting a Knowledge Management approach means more attention to the motivation of people, insisting on principles like: trust, team-building and transparency rules. A facilitative leadership, rather than directive, is needed.

For these reasons, CoPs are without hierarchy, because people are all equal while facing knowledge and the right idea can spring from anyone. Every Community contemplates a Facilitator, in charge of coordinating the activities with the role of "primus inter pares".

The ensemble of the Communities is a network, which knots are the experts. This informal "fabric of communities" and shared practices make the official organization effective and able to contribute in the corporate business goals.

Nowadays 14 Communities are active within the division and they cover all the technical areas linked to the core-business. During their daily activities, CoP Members are in contact through a collaborative platform and a shared Mailbox and they can share information and documents working together. After a few years of exchange, they recognize that a lot of experiences and cases are available in the Group, and their better use can be of help to increase the Company performance.

KM and the solution of complex technical problems in a global world is an important challenge for the future. Inside companies and industrial organisations KM should be implemented with the aim at utilizing better the intangible resources and at creating a repository of internal knowledge with places where tacit knowledge is shared. There is also a need for a cultural change, namely to:

- explore new ways to afford old problems,
- implement methods and techniques for research and innovation,
- enhance cooperation between boundary disciplines.

## 3 Materials and Corrosion Community

There is a claim that corrosion is not in the core business of Oil Companies; however, its importance is correlated to cost. Studies on the cost of corrosion were carried on as early as in 1916 in the USA and since then in many countries of the World. In ASM handbook a comprehensive review is published [2] making reference to studies completed in more than 13 different countries. At least four different methods are proposed to calculate the cost of corrosion, and results can be quite different depending on the used method and on the examined industry. It is however a huge cost and a considerable share of it are proved to be avoidable [3].

Cost of failures has the highest impact in avoidable costs. To avoid failures, the Risk Based Approach is mainly proposed [4] and was proved useful. The risk evaluation should be made using available data bases of past failures.

With reference to the well known NACE study published in 2001 [5], a comprehensive figure for Oil&Gas Exploration and Production for corrosion costs in USA was about 0.40 $/boe (barrel of oil equivalent) produced. For gas and liquid transmission pipelines the same study gives an estimate of corrosion costs higher than $10^3$ $/km/year.

Corrosion cost issues range from added costs for new construction, to maintenance costs on aging/corroding equipment, to the costs of inspections and structural integrity evaluations, to the costs associated with corrosion-related failures and outages.

In addition, Oil&Gas industries are undergoing intense amounts of scrutiny from regulatory agencies and environmental groups. Releases of pollutants to air, soil or water caused by corrosion leaks are becoming high consequence events. Regulations force owners and operators to implement costly measures to reduce their impact on the environment. A recent paper [6] suggests that corrosion costs are increasing due to:

- lack of exchange of information on materials failures,
- retirement of qualified engineers.

A reduction by ¼ of corrosion costs can be achieved by promoting the exchange of information. Following this approach, an efficient KM system is a valuable tool to decrease corrosion costs.

In February 2005 the Materials and Corrosion Community (Fig. 1) was established in E&P Division to create a network of experts in Corrosion and Materials related topics. The objective of CoP Materials is to collect, archive and disseminate existing data and to give answer, based on experience, to the issues posted by colleagues working in the field. Since Corrosion is of interest to almost any


**Fig. 1** In Km system, materials CoP is a small community and a very active one

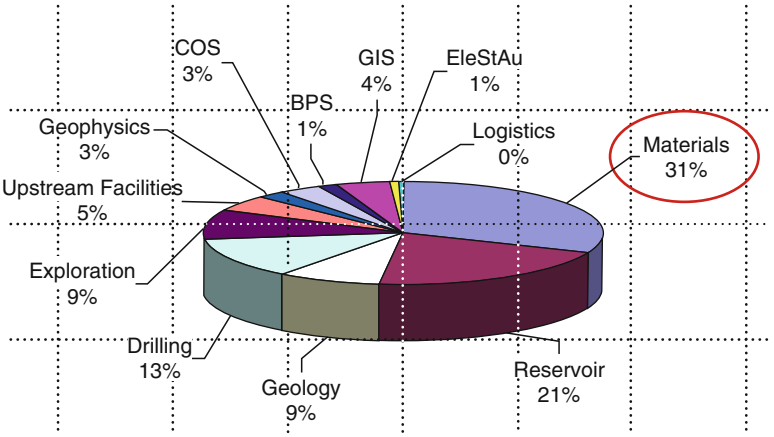


**Fig. 2** Contribute per CoP 2009

industrial field, this CoP is extended to a number of Companies inside eni Group. CoP members are in contact via mailbox and ICT instruments; after a few years of exchange, they recognize that a lot of experiences and cases are treated in the Group, as for instance analysis of failures occurred in plants and industrial areas in many countries where the company is involved. These experiences are often kept as "tacit knowledge", stored in brains, computers, and shelves by the experts who are in charge of the problem.

Eleven Communities were established in the KM System appointing a total of 562 members since 2005. Materials CoP members are 49 (22 from E&P Division and 27 from other Companies and/or Divisions of the Group). With about 9% of the people active in the KM System, Materials Community is the most active one in the Division (Fig. 2), having 31% of the total e-mail exchange. The number of issues proposed to CoP members is increasing with time as shown in Fig. 3. In addition to the managing of issues, two activities carried out by the Community are worth mentioning.

## *3.1 Event Management System (EMS)*

EMS is a data base where corrosion and damage cases are collected with the aim at to help the solution of new problems. The structure and characteristics of the program were developed to guarantee easy search ability and references to complete documents. The challenge is now the use of the tool, which must be kept alive, on one hand implementing the case content, and in the other hand using it for the solution of practical problems. The story of EMS can be significant. In a corrosion research centre operating between 1975 and 2002, about 8,000 issues on

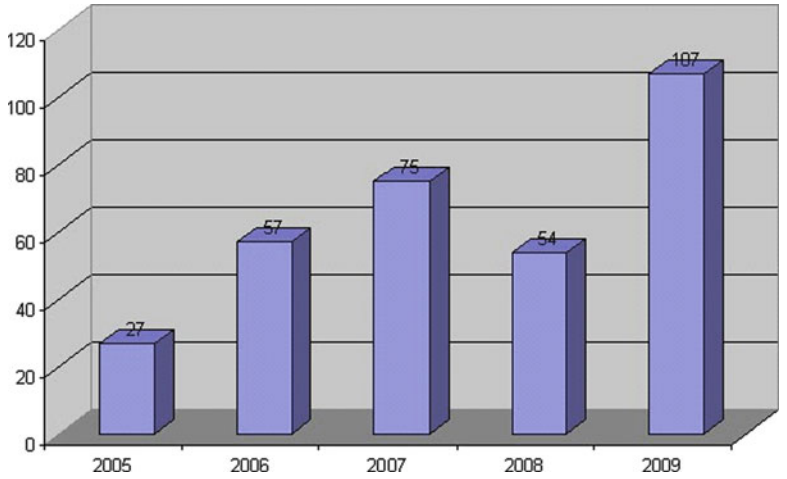


**Fig. 3** Proposed ISSUES – CoP materials

corrosion – materials – failure analysis were discussed and the same number of documents were prepared. As a simple ratio, about 300 issues per year where raised and examined. Since the centre was used mainly by petrochemical plants situated in the North of Italy, with only a small percentage of issues coming from different locations, we may imagine for comparison how many issues we should expect from the huge amount of plants managed by E&P Division and by the complete eni Group worldwide. (One may compare with the number of issues proposed to the Materials CoP, which is increasing, but remains no larger than about 100 per year). When the above Research Centre was closed in 2002, all documents were lost; however, a selected number of about 200 were analysed for the data base [7] promoted by eniMaterials Community of Practice.

The access to those documents was possible because they were intended to be disposed of; no complete data bases of failures are usually available in eni Group. Laboratories and research centres are often sold or become private, and their records on corrosion issues disappear, being no more available for company use. In fact, only a minor number of CoP issues deals with failures, since the large majority of problems are afforded by each Business Unit with the help of external consultants.

## *3.2 NetMed: Mediterranean Network on Corrosion and Protection*

NetMed is a group created inside an available professional Social Network (Xing). Within the working party ESIS TC10 (Environmentally Assisted Cracking) a discussion was open on the possible evolution of technical associations and groups with reference to the new available communication tools. TC10 promoted a

workshop [8] where the capability of Social Networks was discussed. The idea was to promote the use of Social Networks as a tool to connect experts in the field of Corrosion, Fracture Mechanics and other disciplines of Materials Science. With the support of the Knowledge Management team of E&P Division, the Group NetMed was launched within www.xing.com. The aim of this group is to connect people from the country around the Mediterranean (but not only), working and/or interested on corrosion related problems. The idea is also to verify the capabilities of Social Networks to connect people in this professional field. The experiment up to now cannot be defined as "successful". The number of participants is slowly growing, but the information exchange rate is quite slow. Apparently people do not have time to invest in keeping alive the network. However, it is worth to wait and give time to participants. Knowledge exchange and Knowledge Management require a cultural change that is not supposed to happen quick and easy. The passage from a culture of "Knowledge is Power" to a culture of "Shared Knowledge is Power" still needs time and passion.

In the time frame 2005–2009, 320 issues were discussed in the materials CoP, with an average of 2–3 given answers for each. Social Network Analysis was applied to analyze the activity of the Community.

As an example, Fig. 4 represents the relationship between subsidiaries promoting the issues, and Components:

- the activity of the Materials CoP is transversal to Eni Group, issues are proposed by engineering, refining, gas distribution and other sister companies, because corrosion problems are often similar in different plants/industrial activities,

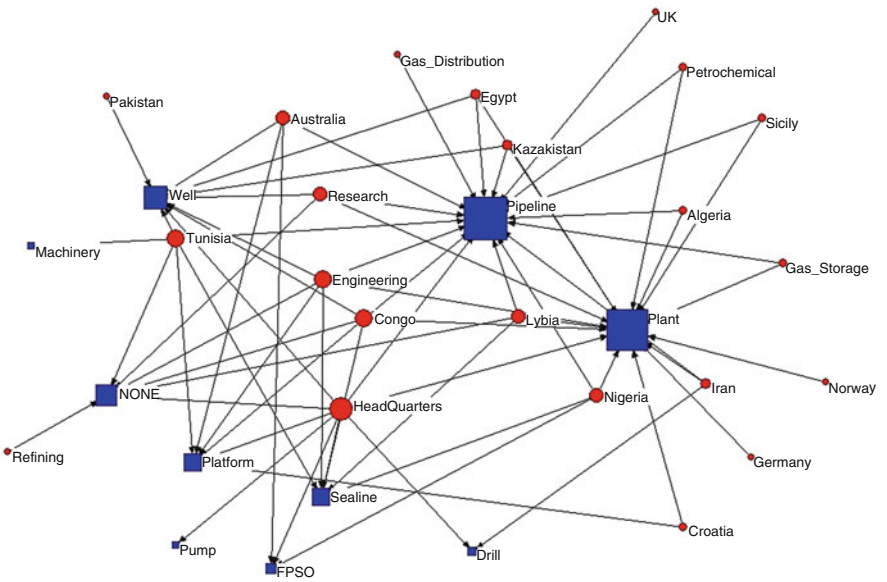


**Fig. 4** Interplay between countries and components

- the majority of studied components are engineering facilities (pipelines, plants). That happens because CoP members are mainly from the Headquarters Engineering professional family; CoP activity is still mainly superimposed to the activity of Engineering Headquarters units,
- the same can be observed when examining CoP issues with reference to the geographical location. Issues are raised mainly from E&P Italy, also when they are from external BUs. However, the relationship with a number of external units is growing.

Since pipelines are by far one of the two most often quoted components, an attempt is made in the second part of this paper to discuss the possible role of Knowledge Management in improving the assessment of pipeline integrity.

The challenge is to convince operating people that KM is not a waste of time; at the opposite they can take advantage – saving time and money – from a better use of knowledge. Important questions are:

- Can we address technical problems from a different point of view with Knowledge Management?
- What are the advantages, if any, of such an approach? Let us examine the case of pipelines transporting hydrocarbons.

## 4 Internal Corrosion in Hydrocarbon Transportation

$CO_2$ corrosion is a very important problem in the oil and gas industry, being the most effective and dangerous damage mechanism for components in contact with hydrocarbon based fluids. $CO_2$ corrosion is still to be considered an open issue, since many failures are experienced all over the world regardless of the large effort to understand and manage the phenomenon. The amount of data available and papers published annually in that topic is huge and growing very fast: for instance, if you insert in a research engine such as Google the key word "$CO_2$ Corrosion", you get as much as 36,500 documents (they were 9,320 in 2007). In the site of NACE international [9], 5,780 documents are quoted (466 in 2007), referring to books (old and new), documents, standards, reports and papers published by NACE. Those are only two examples. It is fully evident that a young person willing to start working in this field would be in difficulty about what to select for a complete and exhaustive state of the art. In fact, this young person would be quite old before getting a full insight of the problem from literature! The help of tacit knowledge in such situation is invaluable: older engineers should transfer their experience to younger people optimizing the effort and the time consumed.

$CO_2$ corrosion is described by predictive models, mainly based on empirical correlations with laboratory and/or field data [10]. Other models have been built based on a strict mechanistic analysis of the various processes involved in acid corrosion of carbon steel. Each oil company has its procedure to evaluate corrosion

and to apply these models, some of which are proprietary. A few oil companies have developed their own models.

In spite of the huge amount of available literature and models, while it is reasonably easy to understand a corrosion event "backward" with failure analysis methods, a large degree of uncertainty is associated to the attempt of predicting future damage. A risk estimate requires knowledge about the probability and the consequences of failure [11]. Probability figures should be derived from historical data analysis of failures. Since failure data are often incomplete and/or not available, an alternative method is to estimate Corrosion Rate (CR) using models [12].

In models application, users are often faced with the alternative between a very conservative approach, or not reliable figures [13]. Hence, there is a need for a suitable methodology to calculate risk by taking into account the qualitative (historical data analysis, experts' subjective opinion), and quantitative (inspection results, etc.) values to determine the probability of failure and its consequences [14]. Due attention is to be paid to statistical approaches and mathematical treatment of data, some of which seem to be promising [15].

Internal corrosion in a pipeline transporting hydrocarbons can lead to reduction of pipe wall thickness and ultimately to leak or burst failure. The presence of electrolytes such as water and species such as $CO_2$, $H_2S$, $O_2$ and other chemicals are some of the prominent factors causing internal corrosion. Consequently, periodic inspections and repairs are necessary to maintain pipeline integrity and to prevent failures. Despite recent advances in inline inspection (ILI) technology, not all portions of a pipeline can typically be inspected due to various geometrical and economic constraints. The surest way to determine the location and extent of internal corrosion is to excavate and examine the pipe.

In eni E&P a research project is underway to compare models results with field observation of failures in pipelines. The project is aimed at two main objectives:

1. to implement risk prediction methods for internal corrosion in pipelines. The objective is to identify locations where the risk of leakage is higher, using available corrosion models, past failure analysis and Non Destructive Testing, coupled with flow dynamic codes,
2. to test innovative materials characterization methods, scarcely or not invasive, to be applied in field.

The proposed procedure features the following steps:

- basic data are collected, evaluated and if necessary integrated. If any of those data are not available, assumptions have to be done and justified,
- a preliminary analysis of the pipeline geometry is done, looking for critical areas such as bends, joints, restrictions, sinking, etc.,
- a pipeline model with proper features is implemented in a mono dimensional code producing a general description of the flow regime as a function of pipeline geometry. Besides, by the results of $CO_2$ corrosion rate calculations, some pipeline sections will show a corrosion rate (and thus failure likelihood) higher than others.

Eventually, in the more risky sections of the pipeline, a 3D fluid dynamic simulation will be performed, using a CFD code. This simulation will be able to predict shear stress and the likelihood of localized damage. Boundary conditions and flow regime for the CFD simulation can be derived by the mono-dimensional calculation performed on the complete pipeline.

The main results obtained up to now are:

- investigation methods to assess accumulation of hydrogen and related mechanical degradation in old pipelines were tested and are now available for application [16, 17],
- technologies to measure mechanical properties on pipelines in service are available (ABI and Small Punch) [18]. The advanced system using inverse analysis, proposed by Politecnico di Milano, needs further work. Preliminary results are encouraging [19].
- coupling water wetting module with Corrosion Models allows to a better estimate of risk in different locations along the pipeline; however, the activity on Risk Evaluation is still to be completed.

Let us discuss an example of Corrosion Rate (CR) calculation applied to an onshore pipeline transporting multiphase heavy oil. Operating conditions are as follows: Initial Pressure: 30 bars; Temperature: 25–30°C; Water cut 40%; $CO_2$ 73% (flash conditions, gas phase).

The case is interesting because the internal corrosion process happened quite quickly and the damage was almost localized at the bottom of the pipeline in a small section.

Models application simply indicates that materials selection was inadequate; Carbon Steel is not supposed to be applied in such aggressive conditions. The failure was defined as a genuine $CO_2$ corrosion failure, and the models were applied in a retrospective analysis. CR measured in field by time to failure is at least 2.7 mm/year. Flow dynamic code output for the actual pipeline geometry is shown in Fig. 5, where Corrosion Rate obtained with two models (De Waard and Norsok implemented in the internal module of the mono dimensional code) are plotted.

Corrosion rate is high along the complete pipeline. The failure, whose position is indicated by the burgundy circle, could be expected; however, what is interesting now is to understand why a large part of the pipeline did not show internal damage, in spite of the high value of CR in the entire pipeline. The line is considered to be fully water wet during the complete life. Results of the two models (red and green lines) are of the same order of the actual Corrosion Rate estimated at the rupture (something more than 3 mm/year); however there are locations in the pipe where a higher CR should be expected, but no rupture was observed.

Further help can be obtained from the examination of a pipeline section in two locations in the pipeline, shown in Fig. 6. The section on the left is closer to the failure than the section on the right. At the left, one can see that a small extent of the pipe wall at 6 o'clock is affected; the damage is deep and remaining thickness is about half of the original. On the right, we can observe that the damage is spread in a larger zone and the thickness is only little affected.

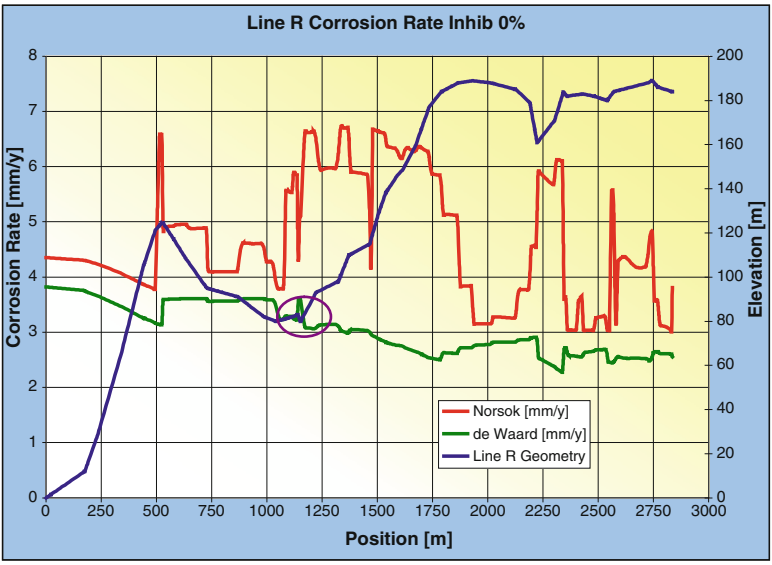


**Fig. 5** Example of corrosion rate for a pipeline

**Fig. 6** Comparison of internal corrosion in two locations of the pipeline

It is suggested to try a deeper insight on the water wetting effects. The results in Fig. 5 are based on the assumption of a total water wetting of the internal walls of the pipeline. Observation shows that water wetting is only partial and probably not diffused all over the pipeline length. Water Wetting effects are strictly correlated to flow dynamics and to the properties of oil. A simple calculation of water wetting/oil

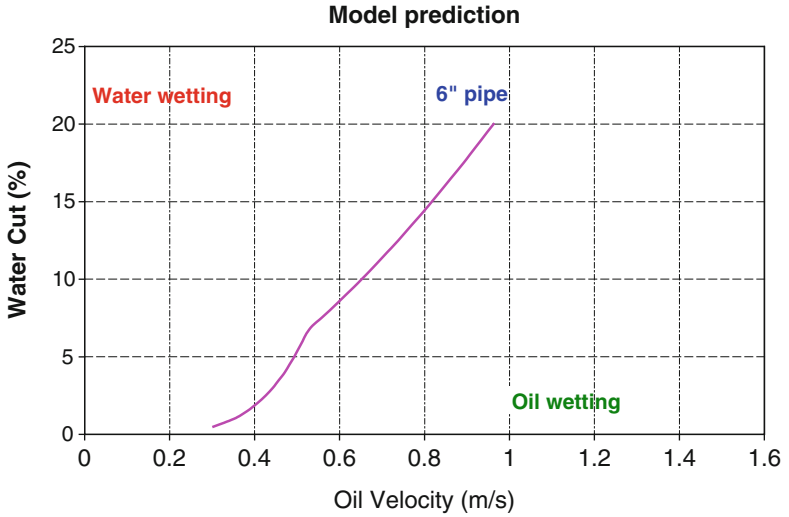


**Fig. 7** Example of application of WW module by Ohio University

wetting can be performed for the case of interest with software provided by Ohio University as the result of a Joint Industrial Project [20]. The output if this calculation is shown in Fig. 7. The plot shows the limit curve of water/oil wetting situation as a function of water cut and fluid velocity.

The pipeline under examination was carrying heavy oil. From an old report on a previous failure the information was obtained that this oil is able to capture – without releasing – up to 16% of water. Since this parameter is addictive, it means that the actual water cut is 24% instead than 40%. Fluid velocities were calculated with the mono dimensional code and are between 0.1 and 1 m/s, depending on location.

In short, oil wetting is expected in pipe section corresponding to higher velocities; while water wetting can be expected in zones were the fluid flows slowly.

The discussed case is only preliminary; the activity will be completed following the outline proposed above. The scope of the present paper is to highlight the role of KM in improving technical achievement. The case of corrosion models discussed above shows that, while the procedures mainly used to select properly the materials for pipelines are by now well known and reliable, they need further adjustment to be able of predicting corrosion damage that can develop in time.

KM approach can be useful to integrate many different data, such as failures, flow dynamics, fluid properties and so on. The example referred to internal corrosion, but similar discussion can be applied to other damage mechanisms, as for instance to external Stress Corrosion Cracking [21]. A well developed and tested KM system could be a helpful tool to operate industrial plants. There is a need for a larger effort in developing this tool. The investment in time and money will be productive at large.

## 5 Conclusions

The importance of collecting and re-using past knowledge is nowadays recognized in industrial companies; however, people often do not realize how quickly the explicit knowledge (collected in reports, papers and other documents) tends to become tacit (sitting only in the memories of people and/or personal computers), and, with time, to disappear totally. The knowledge cycle in a correct knowledge management process shall proceed in the opposite direction, promoting the sharing of tacit knowledge which shall become explicit and shall be disseminated in the company. The process cannot be completed if people do not recognize the value of past experience.

At the opposite, problems tend to repeat themselves and solutions previously applied can be useful in similar situations, to avoid duplicating past errors. Sometimes, solutions can be used again, with results in sparing of time and efforts. There is however a need to use KM as a tool to solve operating problems, to obtain trust and cooperation by operating people. To improve the use of KM tools, eni E&P is pursuing the following actions:

- make available Materials Community to a larger amount of Users,
- convince people that the Knowledge and Experience Exchange within the Community is effective in solving problems,
- collect past experience of failures and/or problems in order to spread the information about them and their feasible prevention/solution within the Group.

A KM system should also create a network of knowledge externally to the Company. The contribution of existing networks such as technical associations and Working Parties (which are similar to Communities of Practice) can be very important to enhance the cooperation between scientists and experts all over the world. Innovative tools as for instance Social Networks need to be used in their full potential. In the specific case of pipelines transporting hydrocarbon, preliminary results of an application seem to anticipate that:

- using codes with built-in CR calculations could be misleading,
- corrosion models are good for materials selection and for the understanding "backward" of failures; they are to be improved for a better prediction of integrity,
- the integrated use of different data bases, such as failure data, fluid properties, production data, and scientific findings can make the difference for integrity assessment.

**Acknowledgments** The authors thank the KM Team (Filippo Capriotti) for the help in Social Network Analysis and the participants in the ITA Pipeline project (Michele Margarone and Pierpaolo Zonta) for Flow Dynamic, Water Wetting and Failure Analysis data.

## References


1. M. Wolf, *Proust and the Squid, The Story and Science of the Reading Brain* (Harper Perennial, New York, 2008). ISBN 978-0-06-093384-5
2. *ASTM Handbook*, vol 13B, http://books.google.it/books?id=QV0sWU2qF5oC&pg=RA1-PA14&lpg=RA1-PA14&dq=hoar+method+corrosion+cost&source=bl&ots=7Pr3PBbh6q&sig=rr0c7pIQd9s-k9pt9NOL8a_8PO8&hl=it&ei=EVWlSfiJJuLBjAfsg7HQBQ&sa=X&oi=book_result&resnum=4&ct=result#PRA1-PA12,M1
3. LABS/Corm – Corrosione e materiali, Technical Note T1395, Impatto economico della corrosione, Giugno, 1995
4. American Petroleum Institute, Risk-Based Inspection – Base Resource Document, API Publication 581, Second Edition, Sept. 1, 2008
5. G.H. Koch, M.P.H. Brongers, N.G. Thompson, Y.P. Virmani, J.H. Payer, Corrosion Cost and Preventive Strategies in the United States, Final Report US Dept. Of Transportation, FHWA-RD-01-156, years 1999–2001, http://www.corrosioncost.com
6. K. Yamamoto, Technical proposals to prevent material failures and accidents in chemical process industries, Nace paper 06211, 2006
7. G. Gabetta, R. Riva, A. Vodarich, M.E. Gennaro, Raccolta di casistica industriale. Corrosion 2003, Italy, Taormina, Giardini di Naxos, 29–31 Oct 2003
8. ESIS Technical Committee TC10, Environmetally Assisted Cracking. Workshop, "Social networks for corrosion and life prediction of industrial components, VeneziaTecnologie, Porto Marghera (Venice), 06–07 Oct 2008
9. http://www.nace.org
10. G. Gabetta, P. Lattuada, M. Margarone, Guideline – Internal corrosion of pipelines in presence of CO2, TEMM Document 0034.TEMM.REL.0, 03 Sep 2008
11. American Petroleum Institute, "Risk-Based Inspection" API Recommended Practice 580, First Edition, May 1, 2002
12. S.A. Hameed, M. Ismail, P. Fassina, G. Hoxha, L. Lazzari, Corrosion risk assessment and planned maintenance for corrosion control: an application to an oil field in Egypt, in *17th International Offshore & Arctic Engineering Conference OMAE 1998*, Lisbon, Portugal, 5–9 July 1998
13. G. Gabetta, M. Margarone, Corrosion and flow models predictions compared using case histories, in *Corrosion NacExpo 2007*, Nashville, Symposium TEG 201X, paper no. 07522, March 2007
14. M. Singh, A methodology for risk-based inspection planning of oil and gas pipes based on fuzzy logic. Eng. Fail. Anal. **16**, 2098–2113 (2009)
15. G. Zangari, G. Gabetta, S.P. Trasatti, Analysis of $CO_2$ corrosion models by neural networks, in *Eurocorr 2006*, Maastricht, 25–29 Sept 2006
16. H. Nykyforchyn, E. Lunarska, O.T. Tsyrulnyk, K. Nikiforov, M.E. Gennaro, G. Gabetta, Environmentally assisted "in-bulk" steel degradation of long term service gas trunkline. Eng. Fail. Anal. **17**, 624–632 (2010)
17. H.M. Nykyforchyn, E. Lunarska, G. Gabetta, P. Zonta, Degradation of properties of long term exploited main oil and gas pipelines steels and role of environment in this process. To be presented at the workshop corrosion protection of pipelines transporting hydrocarbon, to be held in Biskra, Algeria, 26–28 April 2010
18. P. Zonta, B. Molinas, M. Gennaro, G. Gabetta, P. Lattuada, A. Cammi, S. Concari, C. Rinaldi, Messa a punto di metodologie poco invasive per la determinazione delle proprieta' di acciai per condotte in esercizio, *proceedings of the Conference Safap 2008*, Cagliari, Italy, June 2008
19. Vladimir Buljak, Assessment of material mechanical properties and residual stresses, by indentation, simulation and proper orthogonal decomposition, Doctorate thesis, Politecnico di Milano, March 2009

20. F. Ayello, W. Robbins, S. Richter, S. Nesic, Crude oil chemistry effects on inhibition of corrosion and phase wetting, in *17th International Corrosion Congress*, Las Vegas, Paper #3149, 6–10 Oct 2008
21. G. Gabetta, Aspect of Knowledge Management in corrosion modelling, in *International Workshop Corrosion Modeling to enable Corrosion Informed Material Selection to Life Prediction*, Cernobbio, 29–31 July 2006

# Development and Applications of a Specialty Nickel-Based Alloy and the Need for Corrosion Education

**Aziz I. Asphahani**

**Abstract** High-performance Nickel-based alloys are proven to be reliable, cost-effective corrosion control measures in many industries (e.g., Chemical/Petrochemical Processing, Pharmaceutical, Oil and Gas, Pollution Control, Energy,. . .). These alloys' resistance to corrosion (uniform, localized and stress cracking) and the role of alloying elements (Cr, Mo, W and Fe) are reviewed. The design concepts of a cost-effective corrosion-resistant alloy are presented in terms of optimum resistance to various forms of degradation, along with test data illustrating its improved resistance to pitting, crevice corrosion and to chloride/$H_2S$ stress cracking and hydrogen embrittlement. The increasing cost of maintenance/downtime, the concerns about the reliability of equipment along with the emphasis on the safety of personnel, the protection of the environment and sustainability are leading to greater awareness about the deleterious impact of corrosion. Design and Process Engineers, along with Maintenance Managers, are entrusted to ensure (from a corrosion perspective) that the "correct" materials selection and corrosion mitigation technologies are implemented upfront, at the design stage. Hence, there is a need for an engineering workforce, educated in the corrosion science fundamentals and trained in the applied corrosion engineering mitigation techniques. Such engineering workforce will be provided through a Bachelor of Science degree in "Corrosion and Reliability Engineering" (the first such degree in the USA) to start in the fall semester of 2010, at the University of Akron. Details are presented on the curriculum development, corrosion content, courses' sequencing and industrial interest/support.

A.I. Asphahani (✉)
Advanced Motion Technologies, Inc., Warrenville, IL, USA
and
"Corrosion Curriculum" Development, The University of Akron, Akron, OH, USA
e-mail: aziz.asphahani@yahoo.com

T. Boukharouba et al. (eds.), *Integrity of Pipelines Transporting Hydrocarbons*,
NATO Science for Peace and Security Series C: Environmental Security,
DOI 10.1007/978-94-007-0588-3_2, 

## 1 Introduction

For years, nickel-based alloys (e.g., INCONEL[1] and HASTELLOY[2] alloys) have been relied on to handle corrosive chemicals. While some metals (e.g., Ti, Zr, Ta, Nb) and their alloys offer excellent resistance to several corrosive media, these materials fail to provide the versatility of nickel-based alloys, especially when fluoride ions are present in process streams. Also, many of these metals and their alloys are rather cumbersome in terms of field weld-repairs. In contrast, the nickel-based alloys are well-known for their excellent mechanical properties (strength and ductility), as well as their good welding characteristics, which has augmented their acceptance as the most economical choices for solving severe/chronic corrosion problems.

Conventional corrosion-resistant alloys (e.g., stainless steels) and corrosion protective measures (e.g., coatings, inhibitors) are often selected on the basis of initial low-cost and perceived effectiveness in the intended service. However, the unsatisfactory performance of such conventional approaches is becoming an increased liability to long-term field operations. Recurring maintenance shutdowns and unscheduled downtimes are leading to a greater emphasis on cost reduction, as well as causing real concerns about the reliability of equipment and the safety of personnel. Such emphasis and concerns are the driving force behind the search by corrosion engineers for the correct choice of materials of construction at the design stage. As such, the uniqueness of the nickel-based alloys in providing excellent mechanical properties and corrosion-resistance characteristics is the reason for the increased demand for these high-performance alloys in critical/aggressive services.

It is the purpose of this paper to describe an advanced nickel-based product: Alloy G-50. The factors affecting corrosion and the role of alloying elements are reviewed. Corrosion test results are presented and potential applications in sour gas services are indicated.

In addition, the need for corrosion education is highlighted and information is provided on the first US Bachelor of Science degree in Corrosion Engineering.

## 2 Alloys Design for Sour Gas Services

The development of alloy G-50 (N06950) was one result of “Mid 1970s” extensive research programs on corrosion resistant alloys (CRA) for sour gas production. The extremely corrosive and toxic deep sour gas wells highlighted issues related to materials reliability and safety of operations [1]. Conventional carbon-steel tubing and other components were rapidly deteriorated by general weight loss, localized

[1] INCONEL is a registered trademark of Special Metals Corporation.

[2] HASTELLOY is a registered trademark of HAYNES International.

**Table 1** Nominal chemical composition (weight percent)

| Alloy | Ni | Fe | Cr | Mo | W | Orther |
|---|---|---|---|---|---|---|
| 718 | Bal | 19 | 18 | 3 | – | Nb + Ta = 5 |
| G-3 | Bal | 19 | 22 | 6 | – | Cu = 2 |
| 625 | Bal | 3 | 22 | 9 | – | Nb + Ta = 3 |
| C-276 | Bal | 3 | 16 | 16 | 4 | V = 0.35 |
| G-50 | 50 min | 17 | 20 | 9 | 1 | – |

**Table 2** Hydrogen sulfide stress craching 5% NaCl + 0.5% acetic acid/ saturated $H_2S$/room temp

| Resistant alloys | Yield (ksi) | Threshold (ksi) |
|---|---|---|
| 718 | 143 | 139 |
| G-3 | 217 | 213 |
| 625 | 193 | 189 |
| C-276 | 218 | 214 |
| Susceptible alloys | | |
| 17-4 PH | 125 | 13 |
| 410 SS | 90 | 30 |

crevice and under-deposit corrosion, stress corrosion cracking and hydrogen embrittlement. Furthermore, the effective use of inhibitors was faced with many limitations.

The inability to effectively inhibit corrosion of conventional steel tubing in deep sour gas production led to the testing of nickel-based CRA products (Table 1 lists the nominal chemical compositions of some of these alloys). In addition to the presence of the highly corrosive $H_2S$/brines and to bottom-hole temperatures approaching 450°F, the CRA tubular products must possess strength levels capable of handling bottom-hole pressures up to 23,000 psi at depths in excess of 13,000 ft [2, 3]. To meet these extreme stress levels, higher yield strength of CRA tubular products can be achieved by cold working (110–180 ksi), by precipitation strengthening (140–200 ksi) and by cold working plus aging heat treatment (180–280 ksi). Even at strength levels exceeding 140 ksi, the CRA tubular products retained their resistance to various forms of corrosive attack, including $H_2S$ stress cracking [2], and their threshold stresses were much higher than those for stainless steels (Table 2).

While initially the CRA were identified as "inert" in various laboratory tests, further evaluation uncovered the susceptibility of high-strength CRA tubular products to hydrogen embrittlement. This susceptibility was specifically observed for cold worked materials that were heat treated for a few hundred hours at temperatures as low as 400°F (simulating the aging of cold-worked tubes at bottom-hole temperatures). Cathodic hydrogen, produced by direct charging or via galvanic coupling to carbon-steel [4], induced stress cracking of the most corrosion resistant nickel-based alloy C-276, that was cold worked and aged (Table 3).

The least corrosion resistant of the tested nickel-based alloys (containing more iron than alloy C-276 and low to moderate amounts of molybdenum: i.e., alloys 718 and G-3) did not fail in this cathodic hydrogen stress cracking test at room

**Table 3** Cathodic hydrogen stress cracking: C-shape specimens (with galvanic coupling to carbon-steel) 5% NaCl + 0.5% acetic acid/saturated $H_2S$/room temp

| Alloys | Cold-work (10–60%) | 60% cold-work + 200 h at 400°F |
|---|---|---|
| 718 (19% Fe) | No cracking | No cracking |
| G-3 (19% Fe) | No cracking | No cracking |
| 625 (3% Fe) | No cracking | Failure |
| C-276 (3% Fe) | No cracking | Failure |

**Table 4** Anodic chloride/sulfide stress corrosion cracking: C-shape specimens (no galvanic coupling to carbon-steel) 5% NaCl + 0.5 acetic acid/saturated $H_2S$/400°F

| Alloys | Cold-work (10–60%) | 60% cold-work + 200 h at 400°F |
|---|---|---|
| 718 (19% Fe) | Failure | Failure |
| G-3 (19% Fe) | Failure | Failure |
| 625 (3% Fe) | Failure | Failure |
| C-276 (3% Fe) | No cracking | No cracking |

**Table 5** Cathodic hydrogen stress cracking: C-shape specimens (with galvanic coupling to carbon-steel) 5% NaCl + 0.5% acetic acid/saturated $H_2S$/room temp

| | Hours to failure | |
|---|---|---|
| | C-276 | G-50 |
| 40% cold-work | NC[a]/NC/NC | NC/NC/NC |
| 40% cold-work + 200 h at 400°F | 312/312/816 | NC/NC/NC |
| 40% cold-work + 100 h at 932°F | 24/24/90 | NC/NC/NC |

[a] NC = No cracking after 1,000 h

temperature. However, when tested at bottom-hole conditions ($H_2S$ plus brines at 400°F) alloys G-3 and 718 failed by anodic stress corrosion cracking, while alloy C-276 did not stress corrosion crack (Table 4). The high-iron containing alloys were extremely susceptible to anodic chloride-sulfide stress corrosion cracking [4, 5]. Furthermore, when evaluating the CRA for resistance to localized attack in chloride environments, alloys G-3 and 718 suffered pitting corrosion [2, 4, 5].

In view of the need for the Ni-Cr-Mo-W system's resistance to localized corrosion and to anodic stress corrosion cracking at bottom-hole conditions ($H_2S$, Chlorides, Temperatures near 400°F), along with the beneficial effect of iron content in enhancing the nickel-based alloys resistance to cathodic hydrogen stress cracking, the alloy G-50 was formulated to provide an optimum product for sour gas production tubing [6]. The increased iron level to about 17% (compared to less than 5% in alloy C-276) permitted alloy G-50 to better resist the deleterious effect of low temperature aging and cathodic hydrogen stress cracking (Table 5). In addition, the increased nickel content to more than 50% in alloy G-50 favorably improved its resistance to anodic stress corrosion cracking in hot chloride, sulfide and bromide containing environments (Table 6).

**Table 6** Anodic stress corrosion cracking: C-shape specimens (exposed 240–1,500 h/400°F)

| | 825 | G-3 | G-50 | C-276 |
|---|---|---|---|---|
| 20% $MgCl_2$ (30% cold-work) | 2[a]/2 | 1/2 | NC[b] | NC |
| % NaCl + 0.5% acetic acid + $H_2S$ | 2/2 | 2/2 | NC | NC |
| 4.7% $ZnBr_2$ | 2/2 | 2/2 | NC | NC |

[a] 2/2 = two specimens failed out of two tested specimens
[b] NC = no cracking

**Table 7** Resistance to uniform corrosion in acidizing environments: corrosion rates in mils per year

| Temperature (°F) | 15% HCl | | 12%HCl + 3% HF | |
|---|---|---|---|---|
| | G-3 | G-50 | G-3 | G-50 |
| 150 | 73 | 55 | 57 | 36 |
| 200 | 313 | 199 | 689 | 323 |
| 300 | 20,516 | 6,896 | 17,536 | 8,170 |

The alloy G-50 (minimum 50% Ni) exhibited resistance to anodic stress corrosion cracking close to that of alloy C-276 and much improved over those of alloy 825 (nominal 41% Ni) and alloy G-3 (nominal 44% Ni). Furthermore, the higher molybdenum content of alloy G-50 (9% Mo compared to 6% Mo in alloy G-3 and 3% Mo in alloy 825) was proven beneficial to improved resistance to localized attack (pitting/crevice and under-deposit corrosion) as well as an essential alloying element to resist uniform corrosion in acidizing environments (Table 7).

The G-50 alloy has been produced in various size tubular destined for the Mobile Bay deep sour gas fields in the USA. Extensive quality control evaluation, based on slow strain rate tests, confirms the reported excellent stress corrosion cracking resistance of this alloy [7]. Such improved corrosion resistance (better than alloys 825, 718 and G-3) along with its moderate cost (lower cost than alloy C-276) are leading to greater interest in alloy G-50 for offshore applications, where seawater and sour services represent tough challenges to the safe and reliable performance of many stainless alloys. Also, the alloy G-50 optimum mechanical properties and ease of weld repairs make it an excellent choice of material as bi-metallic tubing and piping for aggressive sour gas transmission pipelines (thus avoiding the use of inhibitors) and processing equipment.

## 3 The Need for Corrosion Education

The impact of corrosion on the industrial sectors, the public and daily life is very significant. Corrosion and materials reliability affect industrial complexes, public infrastructures, personnel safety and health, along with severe damages to the environment and sustainable development. The deleterious effects of corrosion are often described in economic terms: as materials degradation/replacement costs and as financial losses. A 2002 report on the "Corrosion Costs and Preventive

Strategies in the USA" calculated the corrosion direct costs to the US economy to be $ 276 Billion (about 3.2% of the annual GDP).

The report identified technical and organizational barriers to reducing the costs of corrosion and recommended strategies to overcome these barriers (http://www.corrosioncost.com/preventive/index.htm). Of the total corrosion cost, 25–30% of the cost is avoidable, if best practices are implemented. Also, it was indicated that savings can be realized through training and corrosion education.

As a follow-up, the importance of corrosion education was highlighted in the 2009 report "Assessment of Corrosion Education" (ACE), by the National Research Council of the US National Academies (http://www.nap.edu/catalog.php?record_id=12560). This ACE report mentioned that among the corrosion prevention strategies, consideration should be given to "improve education and training of staff in recognition and control of corrosion". Furthermore, the ACE report included a tactical recommendation that the "engineering department in universities should incorporate elective learning outcomes and course work on corrosion into all engineering curricula. Improving the overall awareness of corrosion control will require that more engineers have a basic exposure to corrosion/education/".

It is evident that many engineers recognize that materials degradation and corrosion negatively affect durability and systems integrity. Yet, at the design onset, most efforts are often placed on the materials' mechanical properties, fabricability, availability and cost. It is believed that the absence of full awareness of the direct costs of corrosion (and its societal impact in terms of safety, health and the environment) may have been the reason for the common neglect, at the design stage, to accurately factor in the belated corrosion damages to many engineered systems and infrastructural components. Eventually, corrosion considerations are then taken into account in more details, ONLY after a first failure case, involving large financial losses along with grave consequences to the public and serious damage to the environment. Hence, there is a need for engineering curricula to include corrosion courses, as well as to emphasize the societal impact of corrosion and to highlight the awareness of its deleterious effects on safety, health and the environment. Such need is best addressed through a comprehensive corrosion engineering education, along with effective corrosion technologists' training and certification programs.

## 4 The University of Akron Bachelor of Science Degree in Corrosion and Reliability Engineering

To address the need for corrosion engineering education, the University of Akron-Ohio (with seed money from the US Department of Defense) is establishing a comprehensive baccalaureate program for a corrosion-specific engineering degree through its College of Engineering: the first of its kind in the USA. Also, U. Akron is simultaneously establishing an industry-accredited workforce development

certification course for technical training, through its Summit College (which delivers the U. Akron's 2-year associate degree programs). Housed within the Department of Chemical and Bio-molecular Engineering, the baccalaureate degree in "Corrosion and Reliability Engineering" (CARE) program will be multidisciplinary and will take advantage of the U. Akron's well-known status as a leader in chemical and polymer engineering, as well as being one of the fastest growing colleges of engineering in the USA.

The U. Akron CARE program will be receiving its first-year students in the fall semester of 2010. The program objective is to ensure an effective corrosion education and to address the shortage of qualified corrosion engineers in the USA and around the world. A 2007 NACE survey of its USA members [8], indicated that in the following 10 years it is expected that about 44% of the active "Corrosion Workforce" (engineers and technologists) will retire, without anticipated replacement! In addition, a U. Akron survey (conducted by a market search firm with input from Industry and Associations) evaluated the job prospects for what would be graduates with a bachelor's degree in corrosion engineering. The survey results validated the employment opportunities in a multitude of industrial and governmental sectors for engineers graduating with a "corrosion degree". Also, the survey highlighted the need for effective corrosion engineering education, with 66% of employers perceiving that recent engineering graduates are ill equipped to understand and manage critical corrosion problems. Furthermore, nearly 75% of surveyed managers reported that they had experienced a shortage of qualified job candidates with valid "corrosion skill" sets. In order to ensure an effective corrosion education program and future accreditation, the CARE curriculum development team undertook a systematic approach to the selection and sequencing of the courses and their contents. This approach was based first on identifying the "learning outcomes" that are expected by interested stakeholders as to what future corrosion engineers "must know" and what they should be "able to do" (Table 8). These "learning outcomes" were then incorporated into a sequence of courses that fit within a comprehensive college education. The resulting CARE curriculum stands as a 5-year corrosion engineering degree built on:

- maintaining strong engineering-core,
- ensuring corrosion-centered content,
- emphasizing corrosion management.

The CARE corrosion-centered curriculum is "knowledge-based", through learning the fundamentals of corrosion science and focusing on applied corrosion engineering technologies. Also, this curriculum promotes "skill-based" techniques through apprenticeship models. Furthermore, the CARE curriculum covers various managerial aspects of corrosion problems involving inspection/detection, diagnostic/assessment, prediction and prevention. Such an approach should yield graduating engineers that are capable of addressing issues related to life-cycle costs, fitness for service, future performance/reliability and overall asset management. The corrosion management segment of the CARE curriculum and its learning modules will be developed through collaboration with industrial and interested

**Table 8** Stakeholders input on "corrosion engineers": knowledge/capabilities

| "Must know" | "Be able to do" |
|---|---|
| Industries (Chem. Proc., Oil and Gas, Infrastructure, Energy/Nuclear, Medical, Electronics) | |
| Corrosion basics/fundamentals | Organize risk-based inspection |
| Materials selection | Conduct failure analysis |
| Mechanical properties | Evaluate fitness for service/performance |
| Chemistry/process environment | Guide maintenance/rehabilitation |
| Fabrication/manufacturing | Ensure quality control and reliability |
| Testing/evaluation/standards/specs | Define life-cycle/life-extension/prediction |
| Government (Department of Defense, Department of Transportation) | |
| "Knowledge of" | "Ability to do" |
| Inspection/detection | Prevention |
| Diagnostics | Assessment |
| Prognostics | Prediction |
| Mitigation technologies | Management/optimal design |
| Maintenance/rehabilitation | Life-extension/materials selection |
| Expected benefits | |
| Improved safety | |
| Cost reduction/asset preservation | |
| Reduced environmental impact | |
| Enhanced readiness/productivity | |

partners. The educational products will be tested and refined at U. Akron, before being incorporated into the curriculum. The 5-year CARE curriculum also includes industrial work periods in job sectors related to corrosion/materials reliability. Upon graduating, the students will have completed 12 fundamental/"corrosion-centered" courses and 2–4 elective/"corrosion-focused" courses (Table 9).

Overall, this 5-year program will include: 15 basic Science and Math courses, 9 additional engineering courses (Mechanical, Chemical, Electrical and Civil engineering) and typical undergraduate engineering and general education courses, for a total of 136 credit hours (Table 10). Also, the CARE program strategy is to develop modularized instructional materials for use in other engineering curricula/courses and for adaptation to distance learning and outreach/partnership programs.

To ensure applied learning experiences, the corrosion engineering students will participate in co-operative programs to enhance their education. These co-op students will be immersed in a couple of full-time, semester-long work periods with the same company, each time with increasing level of responsibility and trust. The students are to be personally mentored by industrial professionals and will become an integral part of the company team. The interpersonal connections will serve as motivation for success on the job, which is reflected back in the classroom. The co-op students will demonstrate greater self-esteem, more confidence in their abilities, and a deeper understanding of the connections between fundamentals taught in the classroom and their application on the job.

**Table 9** Listing of corrosion-centered courses and some elective courses

| |
|---|
| Fundamentals/"corrosion-centered" courses |
| Laboratory tools for corrosion engineers |
| Materials science for corrosion engineers |
| Materials and energy balance for corrosion engineers |
| Fundamentals of aqueous corrosion |
| Corrosion lab/electrochemistry |
| Prevention of aqueous corrosion |
| Aqueous corrosion lab/protection technologies |
| Fundamentals of Hi-temp/gaseous corrosion |
| Prevention of Hi-temp/gaseous corrosion |
| Hi-temp/gaseous corrosion lab/protection technologies |
| Corrosion management-I (diagnostic, prognostic, mitigation) |
| Corrosion management-II (life-cycle costing, optimal design) |
| Electives/"corrosion-focused" courses |
| Risk-based inspections |
| Corrosion in the chemical processing industries |
| Refinery and petro-chemical processing corrosion |
| Oil and gas/pipeline integrity |
| Cathodic protection and anodic protection |
| Metallic coatings/electroplating |
| Organic coatings/polymers |
| Infrastructures/bridges life-extension |
| Reliability/systems integrity |
| Sensors/condition-based inspections |
| Failure modes and effects analysis |
| Microbiologically induced corrosion |
| Bio-materials/medical implants |
| Safety, health and corrosion |
| Environmental sustainability and corrosion |

**Table 10** Overall courses: corrosion and reliability engineering B.S. degree

| | |
|---|---|
| Fundamentals/"corrosion-centered" courses | 12 |
| Electives/"corrosion-focused" courses | 4 |
| Basics/"engineering-core" (Math and Sci) courses | 15 |
| Other engineering (Chem., Mech., Elec., Civil) courses | 9 |
| General education courses | 10 |
| Total | 50 courses[a] |

[a] 5-Year program (136 Credit Hours)

The CARE students will also be engaged in their prospective fields through participation in numerous U. Akron's student design teams that compete in regional, national and international student competitions. These activities, combined with a required capstone design project for all seniors, ensure that students graduate with hands-on experience in applying engineering principles to real world problems and

with an understanding of the skills that are critical to project management (e.g., scheduling, budgeting, time management, teamwork, communication).

The educational aspects of the U. Akron CARE program are crucial to continuing success in mitigating corrosion and, in the longer term, are likely to have the greatest positive impact for increased reliability and safety of engineered systems. Also, this program is poised to provide the next generation of corrosion experts and to develop education and training tools for a broader range of engineers, managers and policy makers. Furthermore, the CARE program addresses the goal of creating a "pipeline" of baccalaureate-level engineering graduates who will understand the impact of corrosion-related decisions in the early design stages and who are well trained to conduct valid analyses of materials selection and corrosion-protection measures, in order to ensure reliability and life-cycle cost effectiveness.

**Acknowledgments** Technical data and general information were taken from 1980s lectures/presentations and recent postings on the University of Akron's website (http://engineering.uakron.edu).

## References

1. T. Hamby, L. Broussard, D. Taylor, Producing Mississippi's deep, high-pressure sour gas. J. Petrol. Technol. **28**(6, June), 629–638 (1976)
2. M. Watkins, J. Greer, Corrosion testing of highly alloyed materials for deep, sour gas well environments. J. Petrol. Technol. **28**(6, June), 698–704 (1976)
3. R. Tuttle, Corrosion in oil and gas production. J. Petrol. Technol. **39**(7, July), 756–762 (1987)
4. A. Asphahani, F. Hodge, H2S interaction with corrosion-resistant alloys, in *T-1F Symposium/Panel Discussion, Corrosion/77*, NACE, San Francisco, 1977
5. A. Asphahani, High performance alloys for deep sour gas wells, in *Proceedings of the 7th International Congress on Metallic Corrosion*, Rio de Janeiro, 1978, p. 976
6. A. Asphahani, F. Hodge, R. Leonard, P. Schuur, Corrosion-resistant nickel alloy, U.S. Patent 4,171,217, 16 Oct 1979
7. H. Ahluwalia, V. Ishwar, G. Petersen, Corrosion characteristics of g-50 alloy, in *An improved Material for Sour Gas Applications, Corrosion/91*, NACE, Cincinnati, 1991
8. A. Asphahani, The need for a corrosion engineering curriculum: a nace foundation perspective, *NACE/Materials Performance*, Houston, August, 2007, p. 86

# Pipeline Regulation in Canada

**Alan Murray and Joe Paviglianiti**

**Abstract** Canada has been endowed with an abundance of Hydrocarbon natural resources which started the development of the Canadian pipeline system nearly 60 years ago. Today that system comprises about 585,000 kilometres of pipelines. Fortuitously for pipeline owners and operators, the Federal and pertinent Provincial regulators have adopted, by reference, the national pipeline standard Oil and Gas Pipeline Systems CSA Z662 within their respective regulations thus giving this standard the force of law. In general terms this means that pipelines in Canada are designed, constructed and operated in accordance with the normative requirement of a common standard. However the respective regulatory requirements, of each jurisdiction, are overlaid on the prescriptive elements of Z662 and reflect both the nature of the entities being regulated and the particular philosophical approach taken to regulation. The purpose of this paper is to attempt to describe the main differences to be found across the country and to expand upon the goal oriented approach favoured by the National Energy Board. Further, it will be helpful to also consider the importance of research in the development of standards and regulations.

## 1 Introduction

Canada has been endowed with an abundance of Hydrocarbon natural resources – the immense oil sands deposits in Northern Alberta and Saskatchewan, the shale gas plays of NE British Columbia, the natural gas and oil contained in the high arctic and off our eastern coast and not least those found in the Western Canada sedimentary basin (Fig. 1). It was the exploitation of the latter which started the development of the Canadian pipeline system nearly 60 years ago.

A. Murray
Principia Consulting, Calgary, Alberta, Canada
e-mail: ma-murray@shaw.ca

J. Paviglianiti (✉)
Avantitec Ltd., Calgary, Alberta, Canada
e-mail: avantitec@shaw.ca

T. Boukharouba et al. (eds.), *Integrity of Pipelines Transporting Hydrocarbons*,
NATO Science for Peace and Security Series C: Environmental Security,
DOI 10.1007/978-94-007-0588-3_3, 


**Fig. 1** Supply sources and pipeline markets for Canadian hydrocarbons

Today that system comprises about 585,000 km of pipelines, most of which are in the form of comparatively small diameter, low pressure gathering and distribution pipes. Since all of the distribution and almost all of the gathering lines are located within an individual Province, they are subject to provincial jurisdiction. A few so called "sausage link" gathering lines cross provincial boundaries and thus, in common with the much larger diameter high pressure transmission lines, come under federal jurisdiction and the watchful eye of the National Energy Board (NEB, or the Board). In addition to these inter provincial pipelines, the Board also has jurisdiction for pipelines crossing the international border to the USA.

Fortuitously for pipeline owners and operators, the Federal and pertinent Provincial regulators have adopted, by reference, the national pipeline standard Oil and Gas Pipeline Systems CSA Z662 [1] within their respective regulations thus giving this standard the force of law. In general terms this means that pipelines in Canada are designed, constructed and operated in accordance with the normative requirement of a common standard. However the respective regulatory requirements, of each jurisdiction, are overlaid on the prescriptive elements of Z662 and reflect both the nature of the entities being regulated and the particular philosophical approach taken to regulation. The purpose of this paper is to attempt to describe the main differences to be found across the country and to expand upon the goal oriented approach favoured by the National Energy Board. Further, it will be helpful to also consider the importance of research in the development of standards and regulations.

## 2 Pipeline Infrastructure in Canada

In 2008 Canada produced 993 million barrels of oil equivalent and 3.95 trillion standard cubic feet of natural gas. Approximately 32% of our oil and 37% of our natural gas production is consumed within the country, the remainder being exported, primarily to the United States, an export business worth $69 billion annually. The vast majority of these hydrocarbons are transported by pipeline economically and safely, over long distances, since the major demand centres are considerably removed from the primary supply source- the Western Canada sedimentary basin, (WCSB). It is essential to the Canadian economy that the transmission pipeline infrastructure remains competitive and reliable since these are the attributes upon which energy contracts are signed. Many other producing basins in the continental United States are closer to the market place than the WCSB, so in order to maintain a competitive advantage, Canadian pipelines have had a long history of incorporating technological innovation. The regulatory system has also been supportive in terms of setting just and fair tolls and tariffs and encouraging incentive regulation whereby the pipeline operators and shippers reach agreement on CAPEX and OPEX cost savings. The resulting agreements are submitted to the relevant regulator for approval to ensure transparency and preservation of the public interest (Currently all of the major pipeline operators in Canada have incentive tolling agreements in place). As with other mature producing regions, Canada's pipeline infrastructure consists of gathering systems which are largely, but not exclusively, owned by the producers, transmission lines owned and operated by pipeline companies and, in the case of natural gas, a localized distribution network. On any given day about 71 different types of hydrocarbon product are to be found in the Canadian transmission pipeline system, the vast majority being treated sweet product, (Fig. 2). It is not surprising therefore, that internal corrosion is a very uncommon threat to the integrity of the transmission infrastructure. Rather as Fig. 3 illustrates, on NEB regulated pipelines external corrosion is the predominant failure mechanism, followed by cracking and external damage. This is reflective of the aging nature of the transmission system, and the deterioration over time of various types of external coating, as well as the sparse population density along the major routes. By contrast, provincial regulators, having a higher preponderance of upstream gathering systems, find internal corrosion to be the dominant failure mechanism.

## 3 The Canadian Pipeline Regulatory Landscape

Protecting the public and the environment from untoward events are among the primary responsibilities of a regulator of physical facilities such as pipelines. How it chooses to do so however varies from one jurisdiction to another. A quick study of the history of major regulatory and standards changes in Canada shows a similarity with other developed countries, indicating a lagging response to major incidents. For example in 1985, during a pipeline repair incident at Camrose, Alberta, several

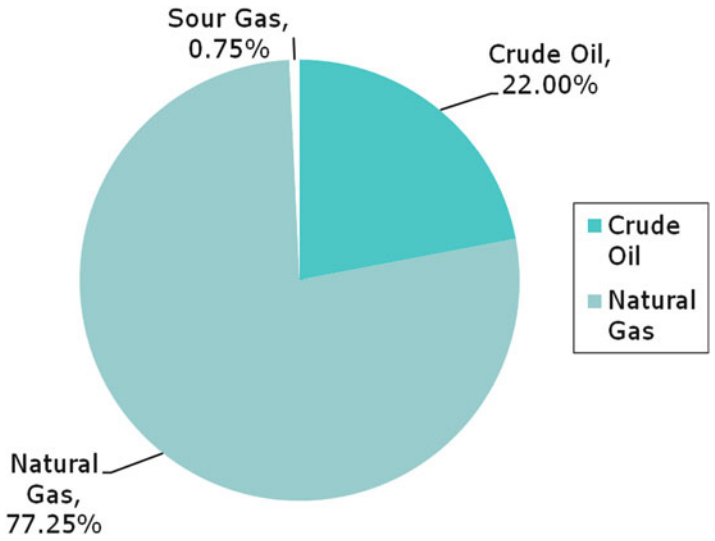


**Fig. 2** Proportion of products transported on the 71,000 km of NEB regulated pipelines

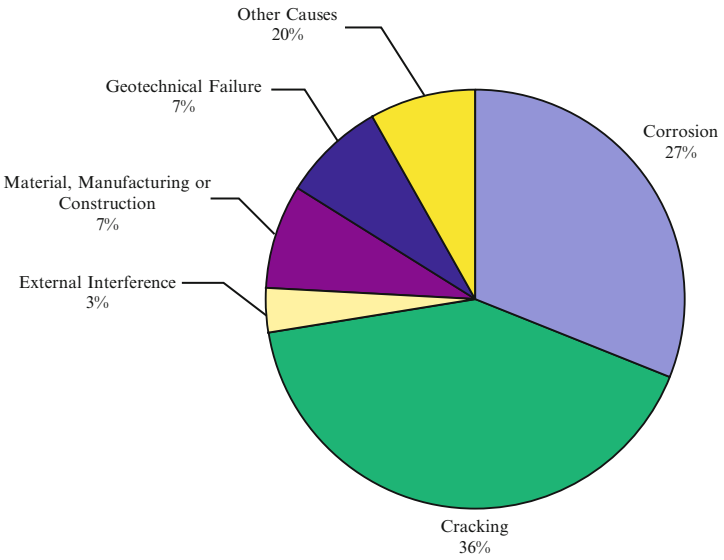


**Fig. 3** Causes of pipeline failure on NEB regulated pipelines

workers died as a result of poor maintenance practices and emergency response procedures. This resulted in a significant change to the requirement for Emergency Procedures and to in-service welding procedures in both the NEB Pipeline regulations and the CSA pipeline standards of the time. Similarly a spate of gas pipeline ruptures in the early 1990s, caused by stress corrosion cracking, resulted in an

inquiry conducted by the NEB [2] and had a significant influence on the Board's regulatory thinking at the time. In fact the requirements for an integrity management system in both the NEB Onshore Pipeline Regulations [3] and the Z662 standard are traceable to the recommendations from that Inquiry.

Sometimes the regulator initiates change, such as in the use of performance or goal based requirements rather than prescriptive requirements. With the latter there is no latitude for the use of alternative approaches, whereas performance based regulations establishes the required end result (which could be a goal or a prescribed performance target) and leaves the means of its achievement to the regulated entity. Goal *oriented* regulation, which will be discussed more fully later, is a mix of prescriptive and goal based requirements. This is probably the major differentiation in how pipelines are currently regulated in Canada, the NEB adopting a goal oriented approach, and the Provinces invariably retaining a more prescriptive approach. This difference may largely be explicable in terms of the mandates of the various regulators as well as the capability or sophistication of the companies they regulate and the nature of their facilities. The vast majority of the 71,000 km of transmission pipeline which the NEB regulates is operated by a small number of sizeable companies who have considerable in house technical staff resources. By comparison, for the most part, the Provinces regulate a very large number of companies whose secondary business is operating gathering systems and whose primary business is exploration and production.

## 4 The National Energy Board Approach to Pipeline Regulation

The Board has responsibilities to the Parliament of Canada for physical and financial regulation of inter provincial and international pipelines as well as international power lines and in 2009 celebrated its 50th anniversary. It is quasi judicial in nature, its current 9 member Board selected for their independence of thought and their individual expertise in one, or several aspects of the Board's remit. As a pipeline regulator the National Energy Board is defined by its hearing processes, its "full- lifecycle regulation" or "cradle to grave" regulatory scheme and its increasing use of goal-oriented regulations. Figure 4 shows in some detail the various elements comprising the full life cycle approach to pipeline regulation.

The advantage of such a scheme is that the Board can utilise its ability as a single regulator to oversee and influence all aspects of a pipeline's design, construction, operation and abandonment. The Board's current On Shore Pipeline Regulations, promulgated in 1999 [3], combined with the conditions of approval in awarding a certificate to operate a pipeline, set out the requirements and compliance activities and give meaning to them by ensuring that they are followed. Inspections and Audits are the respective means for monitoring compliance in the construction and operations phases and have the most potential to minimise safety and environmental incidents.

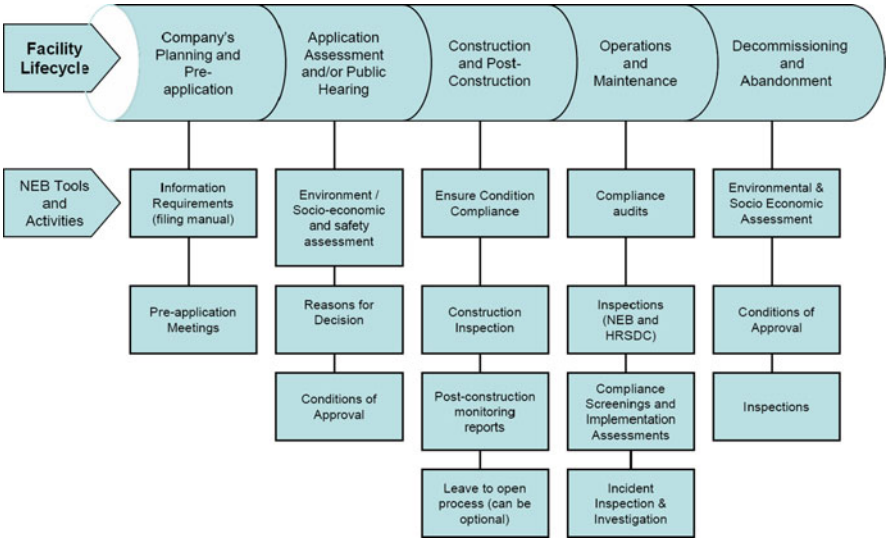


**Fig. 4** Full Life cycle approach to pipeline regulation

## 5 Some History on the NEB's Road to Goal Oriented Regulation

The Board's first two pipeline regulatory instruments were very prescriptive and specified the filing requirements for the design, construction, testing and repair of pipelines. The Board decided what constituted a hazard and what needed to be protected, while the regulations specified how these were to be addressed. As noted earlier, Regulations are influenced by the issues and problems facing regulators at the time of their creation. For example, as a result of difficulties with first generation electric resistance welding (ERW) pipes the *Oil Pipeline Regulations* of 1978 contained a clause limiting ERW pipe larger than 457 mm to a pressure no greater than 20% of SMYS. Compliance was monitored by requiring the filing/approval of documents and through inspections.

In 1988, the Board issued the *Onshore Pipeline Regulations* (OPR) which were more flexible than those they replaced. The level of detail required for submissions was decreased and some requirements were eliminated. The regulations became more aligned with accepted industry standards by choosing to use the CSA standards as their technical basis. Environmental protection was also becoming increasingly important so a requirement for environmental protection procedures and measures for construction, based on an issues list, was introduced into the OPR. Compliance was monitored by reviewing the specifications and procedures sub mitted by the proponent in its Application, auditing their records, and performing inspections of the pipeline facilities during construction and its subsequent operating life. It was observed that some companies would produce

"compliant manuals" but did not implement them. The Board developed enforcement procedures using administrative tools such as assurances of voluntary compliance.

As a general observation, most companies at the time were reactive rather than proactive regarding environmental and integrity issues and the prevailing regulations were unsuccessful in dealing with this reality [4].

As a consequence, the Board revised its pipeline regulations in 1999 choosing to use a goal oriented approach, and this was followed 3 years later by the issuance of its Processing Plant regulations, again using a goal oriented approach. As with previous regulations, the CSA standards were incorporated by reference and this provides the source of the majority of the prescriptive requirements within the Board's regulations.

Goal-oriented regulations were inspired by Lord Cullen's report on the Piper Alpha explosion of July 1988, wherein the fully prescriptive approach was rejected in favour of a goal-oriented approach to offshore oil and gas operations. Cullen went beyond determining the causes of the deadliest disaster in offshore oil industry history to make 106 specific recommendations, initiating a new pro-active and improved approach to safety involving goal setting. Further his report reassured all stakeholders – the oil industry, the government and the public that offshore oil and gas operations could be conducted safely if a rational goal oriented approach was implemented, together with the effective use of technology and stringent inspection procedures. Influenced by this approach, as well as findings from its own experience, the NEB developed its hybrid form of regulation. In taking this step, it was ahead of the recommendations made by an external advisory committee to the Canadian government, appointed to examine "Smart Regulation". On April, 2007 the federal Government issued a Directive on Streamlining Regulations with the objectives of "protecting and advancing the public interest by working with Canadians and other governments to ensure that its regulatory activities result in the greatest overall benefit to current and future generations of Canadians". To achieve this it set out the following objectives:

- protect public health, safety, security and environment,
- promote a fair and competitive market economy,
- make decisions based on scientific evidence using the precautionary principle as necessary,
- create accessible, understandable and responsive regulation,
- advance the efficiency and effectiveness of regulation,

In short the Board's goal oriented approach embodied these objectives, enabling companies to use their intimate knowledge of their individual systems and incorporate proven modern technologies in order to operate safely and remain competitive.

## 6 Experience with Goal Oriented Regulation

In the goal oriented regulatory approach a clear role for the regulator is to set out the framework for protection of the public and the environment, while the role of the regulated company is to develop and deliver protection programs. Overall, the

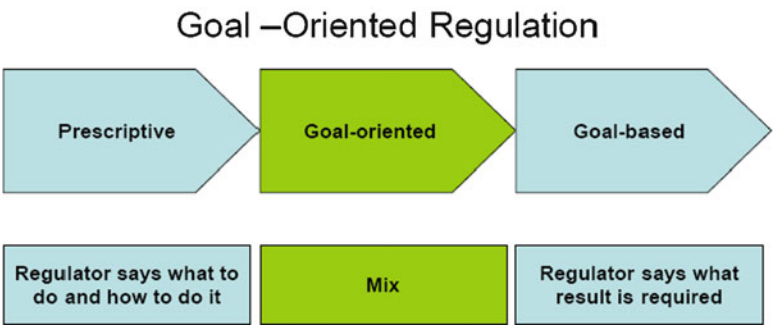


**Fig. 5** Regulatory spectrum

*Onshore Pipeline Regulations*, *1999* shifts more of the responsibility for identifying and managing risk from the regulator to the company, (Fig. 5). The Regulatory Impact Statement issued at the time the regulations came into effect, indicated that the Board intended to monitor compliance by conducting detailed audits of company specifications and management systems, assessing the skill level of personnel on staff and by performing inspections of pipeline facilities during their operational life. Since 1999, the Board has frequently re-iterated its expectation that effective management systems have been implemented by companies, most recently by the Board's Vice Chairman at the International Pipeline Conference 2008 [5].

> The use of management systems is necessary to achieve goals and effectively manage risks. Since the introduction of the OPR in 1999, the NEB has been consistent in its message that compliance with the OPR requires companies to develop, implement and maintain management programs for the design, construction, operation and maintenance of their infrastructure. These programs and the elements of a management system are mandated by the OPR and CSA.

While the Onshore Pipeline Regulations, 1999 does not contain an explicit requirement for management systems, the requirement is implicit and descriptions of what would constitute such a system can be found in the non-mandatory Guidance Notes to the Onshore Pipeline Regulations 1999. [6]. An explicit requirement for a management system, specifically a "Safety and Loss Management System", was recently introduced into the CSA Z662 standard 2007 edition and has been adopted by Provincial regulators.

So much for the theory, in determining the methods used to achieve compliance in practice, it is important to note that the regulations are intended to apply as a whole and not as a discrete set of individual elements. In the absence of the check list approach of prescription, there is a distinct need for experience and discernment on the part of the auditor in determining the adequacy and effectiveness of a given element in a company's program. Upon introduction of the new goal-oriented regulations, and to help audit staff conduct thorough audits and promote consistency and fairness, "expected elements" were developed as a tool to ensure nothing important was overlooked. These expected elements contained quite a detailed list of what was believed to be the essential components of a management system as espoused by ISO. When shared with the regulated companies however, their expressed concern was that they were being audited to these elements rather than their own programs! It was recognized that the Board itself needed a management

system to improve consistency and incorporate continual improvements to its compliance program. As a result the audit system was one of the first systems to be included in the Quality Management System developed at the Board. A written protocol for the audit process was developed, containing five elements and fifteen sub-elements which companies are legally required to meet, as well as commonly accepted elements of an ISO management system. Companies are assessed against the legal requirements identified in the NEB Act and associated regulations, other relevant provincial and federal acts and regulations, facility approval conditions *and the processes, procedures and standards identified by the company as comprising its programs*. In order to promote fairness, clarity and completeness, Board auditors have developed templates which have a logical management system flow and enable the findings of the audits to be assembled using a consistent approach.

The Board's expectation is that after 10 years of exposure to goal oriented regulation, companies should have robust documented programs in place that have benefited from internal audits and continual improvement to ensure their adequacy and effectiveness. The results of 30 audits conducted since Goal oriented regulation was introduced, indicates that the majority of regulated companies have most of the program elements in place to deal effectively and proactively with identified hazards and that many have instituted comprehensive management systems. Further an external independent review of the Board's approach to goal oriented regulation, conducted on behalf of the Internal Audit Committee, found a high degree of acceptance among all stakeholders.

## 7 Advantages of Goal Oriented Regulation

In common with pipeline companies, a Regulator has finite technical resources with varying capabilities and availability. The challenge is to make the most effective use of the resources available while still discharging its statutory duties. To do so the Board has been developing and using a risk based life cycle approach for use in planning and staffing compliance activities. As an example, information on company performance, collected during its construction and ongoing operational activities, forms the basis for assembling a risk profile. This is then used in assessing whether to, and when to conduct a full or focussed audit, or when to pursue in greater detail the technical content of a facilities application. This enables appropriate staff resources to be assigned accordingly. For companies, goal oriented regulation provides the ability to assess and take measured risks where appropriate. They can make effective use of their intimate knowledge of the construction and operating history of their pipeline system and avail themselves of the most recently available technology, to devise methods which meet regulatory requirements and create competitive advantage. The adequacy of these new methods is the responsibility of the company to assess and the regulator to determine, either as a result of an audit or a specific application.

It is in this area that the effects and importance of research to goal oriented regulation is most readily seen. Clearly if a company has either developed a proprietary technique, or become aware of pertinent new technology, it can start the process

of amending the existing pipeline standard to incorporate the new development. If after scrutiny, it is accepted and becomes a part of the newest version of the Standard, it is reasonable to expect, but by no means will it be certain, that will it be adopted by the appropriate regulators. (A regulator may choose to adopt all or portions of a Standard). In Canada the Z662 standard is produced on a 4 year cycle, hence that length of time could elapse before the technology is ratified. In contrast, with a goal oriented approach, if the proponent can demonstrate convincingly the technology meets the desired end goal, then he is given a waiver which, while maybe project specific, is still quicker than the alternative process.

## 8 The Future of Goal Oriented Regulation

While regulatory change occurs at seemingly glacial speed, it is not static and the intent at the NEB is to update the Onshore Pipeline Regulations. To persist with a goal oriented approach to regulation, it has to be seen to be mutually beneficial to all stakeholders. As noted earlier the Board did conduct an external audit with that finding and hence is committed to the evolution of the process. This resolve is strengthened by the recent inclusion of a formal requirement in CSA Z662 for management systems incorporating the full life cycle. The NEB consults regularly with its constituents and communication is a key factor in ensuring that there is no confusion as to where the bar has been set and what tools can be applied to meet and exceed the requirements. One of those constituents is our fellow regulators. We are aware of the fact that a number of our regulated companies fall under the ambit of other regulators and it can be burdensome to meet different regulatory requirements. We are confident though that the flexibility inherent in goal oriented regulation is such as to enable the requirements of others to also meet our compliance needs. Hopefully this will lead to a rationalisation that would enable company programs and management systems to be consistently applied across multiple jurisdictions. In conclusion an effective regulatory framework encourages advances to be made in pipeline technology and balances judicious direction when necessary, with freedom of action when appropriate. Thank you.

## References

1. Anon. CSA Z662, *Oil and Gas Pipeline Systems* (Canadian Standards Association, Mississauga, 2007)
2. Anon. National Energy Board Stress Corrosion Cracking on Canadian Oil and Gas Pipelines Report of the Inquiry. MH-2-95. (Calgary, Alberta, Canada, Dec 1996)
3. National Energy Board, *Onshore Pipeline Regulations* (National Energy Board, Calgary, 1999)
4. P. Trudel, (2009) Private communication
5. S. Leggett, Conference closing remarks. in *7th International Pipeline Conference*, Calgary Alberta, Canada, 3 Oct 2008
6. Anon. National Energy Board, *Guidance Notes for Onshore Pipeline Regulations 1999 Amendment 1* (National Energy Board, Calgary, 2003) (20th January)

# Fracture Mechanics Approach to Stress Corrosion Cracking of Pipeline Steels: When Hydrogen Is the Circumstance

**J. Toribio**

**Abstract** Stress corrosion cracking is a problem of major concern in pipeline steels. This paper deals with the fracture mechanics approach to the phenomenon. Paraphrasing the famous sentence by Ortega y Gasset "yo soy yo y mi circunstancia", one could say that the material is itself and its circumstance, the latter being the physico-chemical and mechanical environment. The paper analyzes situations in which the circumstance enhances hydrogen embrittlement. A theoretical study is provided of the validity of the fracture mechanics approach to hydrogen assisted cracking, analyzing the $K$-dominance condition to elucidate the role of the far field and the effect of history, the latter recalling the words of the Spanish poet Antonio Machado: "hoy es siempre todavía", and perhaps T. S. Eliot's "and all is always now".

## 1 Introduction

Paraphrasing the Spanish philosopher Ortega y Gasset, one could really say that *the material is itself and its circumstance*, which indicates, firstly, that the material is intrinsically imperfect, and therefore, that surface or internal defects are inherent in it; and secondly, that there is an evolution of its mechanical properties throughout the service life, due to the combined effect of mechanical load history and surrounding physico-chemical environment.

This consideration of the material as a live entity immersed in the surrounding environment has an important consequence: the concept of material is strongly linked with the existence of superficial or internal defects or geometrical flaws such as cracks or notches (from the macroscopical point of view) or imperfections in the microstructure such as lattice defects, dislocations, micro-voids, etc (from the microscopical point of view). Thus the classical approach in mechanical and

J. Toribio (✉)
Department of Materials Engineering, University of Salamanca, E. P. S.,
Campus Viriato, Avda. Requejo 33, 49022 Zamora, Spain
e-mail: toribio@usal.es

T. Boukharouba et al. (eds.), *Integrity of Pipelines Transporting Hydrocarbons*,
NATO Science for Peace and Security Series C: Environmental Security,
DOI 10.1007/978-94-007-0588-3_4, 

structural engineering in which the material is totally defined by its constitutive equation – or, even worse, merely by its elastic properties – turns to new approaches (materials science and fracture mechanics approaches) according to which material behaviour depends not only on the intrinsic characteristics of the material itself, but also on the circumstance, i.e., on extrinsic factors such as load history (load magnitude, kind of loading, loading rate, etc) and environment (temperature, humidity, corrosive agents, etc.) which make previous defects grow. It is important to notice, therefore, that a given material does not have a behaviour *per se*, but can exhibit one or another behaviour depending on the *circumstance*, i.e. on the specific working conditions (mechanical and physico-chemical environment). In this paper the hydrogen environment plays the role of circumstance.

In the case of pipeline steels having different microstructures as a consequence of the manufacture procedure [1–4], they can fracture provoking structural failure [5–8]. In addition, environmentally assisted cracking of pipeline steels is a problem of major technological concern, either in the form of pure stress corrosion cracking [9] or in the even more dangerous variety of environmental action: hydrogen assisted cracking, hydrogen degradation or hydrogen embrittlement [10, 11].

## 2 Fracture Mechanics Approach to Hydrogen Assisted Cracking: Analysis of the *K*-Dominance Condition

This section of the present review paper summarizes the achievements of a basic research line in the field of environmentally assisted cracking in general and of hydrogen degradation in particular. It deals with the meaning and significance of the fracture mechanics approach to hydrogen assisted cracking, analyzing the question of *K*-dominance not only over the purely mechanical aspects, but *also* over the environmental (physico-chemical) events influencing the whole coupled process of hydrogenation and failure.

Two key factors able to violate the uniqueness of the crack growth kinetics curve $v = v(K)$ are discussed: the role of *far field* (the stress-strain field which is not *K*-dominated) and the effect of the *history* of hydrogenation and crack growth. Stress-strain assisted diffusion of hydrogen is considered as the rate-controlling factor of hydrogen assisted cracking under sustained or quasi-static loading conditions. The far field is shown to have a minor effect on near-tip hydrogen diffusion. It can only widen the scatter band of crack growth rates in the near-threshold portion of the $v(K)$-curve.

With regard to the effect of history, the study reveals that hydrogenation and crack growth are coupled processes, one influencing the other, so the crack growth kinetics curve $v = v(K)$ is not unique as an intrinsic material property must be. However, a special regime of steady-state crack growth is seen to exist in which hydrogen assisted cracking turns out to be a *K*-dominated process, and the corresponding plot of the steady-state $v$ against $K$ acquires the uniqueness of a material's characteristic curve which may be used in engineering to provide more conservative evaluation of material resistance and structural integrity.

## 2.1 Problem Statement

Engineering design frequently involves problems of environmentally assisted cracking (EAC) in materials and structures, a phenomenon which appears in diverse forms such as stress corrosion cracking, hydrogen assisted cracking (HAC), liquid metal embrittlement, etc. In this framework, the fracture mechanics approach has proved to be effective for material evaluation and structural integrity assessment.

In the domain of linear elastic fracture mechanics under small scale yielding, the stress intensity factor $K$ is the only parameter governing the stress-strain state in the vicinity of the crack tip. The key of the fracture mechanics approach to EAC is the *crack growth kinetics curve* (Fig. 1): a plot of crack growth rate $v$ vs. stress intensity factor $K$, defined between the threshold $K_{th}$ (below which the crack growth rate $v$ is zero) and the fracture toughness $K_c$.

The idea of *uniqueness* of $v(K)$-curves and thresholds $K_{th}$ as intrinsic characteristics of {material-environment} systems forms the backbone of the approach and ensures the soundness of applications in engineering design. This uniqueness ensures the *similitude* of crack behaviour in test specimens and in structural components in service, thereby providing *transferability* of laboratory testing data to real engineering structures.

If the $v(K)$-curve including $K_{th}$ is indeed unique for a given {material-environment} couple, any discrepancy between predicted and real behaviour should be attributed to roughness in the analysis or experimental scatter but not to the concept. Otherwise, conceptual weakness makes the predictions less reliable and calls for more constraints on testing and evaluation to obtain data of the crack growth resistance parameters in an aggressive environment.

The reliability of the fracture mechanics approach to EAC in engineering design was reviewed by Toribio and Kharin [12], where an ample range of experimental evidence of uncertainty in the $v(K)$-curve and the threshold $K_{th}$ is presented. Although these items are supposed to depend solely on the material and the

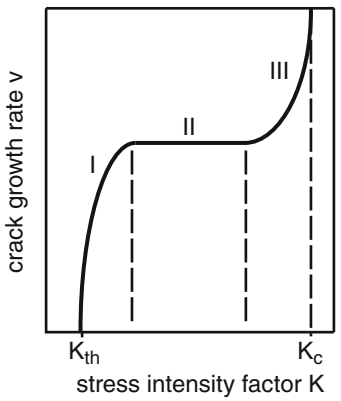


**Fig. 1** Scheme of a typical crack growth kinetics curve with three stages: near-threshold (*I*), plateau (*II*) and mechanical final fracture (*III*)

environment, they are notably sensitive to the influence of a wide family of test/service variables, namely the following:

(i) *pre-loading*: fatigue pre-cracking regime and overloads;
(ii) *geometry*: crack length, crack bluntness and stress intensity gradient;
(iii) *kinematics*: initial load, test interruption, rate of loading/straining.

The results quoted show that the same stress intensity factor does not always yield equal crack velocities in otherwise identical couples {material-environment}. The observed deviations cannot be related to imperfect testing and are systematic as distinct from obvious statistical scatter of test data. This uncertainty of the basic fracture mechanics characteristics of EAC produces loss of confidence in materials evaluation and structural integrity assessment.

In paper by Toribio and Kharin [13], a deal of uncertainty of EAC characterisation is eliminated in a strictly *local* fracture mechanics approach where both the mechanical and the environmental factors are treated in terms of local variables related to the crack tip. However, this local interpretation of the crack growth kinetics curve still remains incomplete and does not meet the essential requirements of an intrinsic material curve.

To solve the described problem, a procedure is proposed by Toribio and Kharin [13] for engineering safe design against EAC. For a given {material-environment} system, the aim is to find the *worst* crack tip situation producing the fastest crack growth rate $v_m$ attainable at each $K$. The corresponding master curve $v_m(K)$ is the envelope of all possible $v(K)$-curves for a {material-environment} couple and represents an intrinsic characteristic of the system: the weakest resistance to EAC.

However, the extent to which the $v(K)$-curve and the threshold $K_{th}$ are the properties of only the material and the environment becomes an open issue. This kind of uncertainty means that the process in general is not exclusively $K$-dominated, although no attempt has been made in the past to elucidate the matter of $K$-dominance over the whole family of contributing events as the check-point for the soundness of the fracture mechanics approach to EAC.

The present paper reviews some recent research work by the author on the meaning and significance of the fracture mechanics approach to the particular phenomenon of HAC (very important in engineering). The final aim is to elucidate the question of $K$-dominance not only over the mechanical aspects of the phenomenon but *also* over the environmental (physico-chemical) events affecting the coupled process of hydrogenation and failure.

## 2.2 Key Events and Modelling of HAC

The main events associated with HAC are described by Toribio and Kharin [14]:

(i) hydrogen supply to the prospective fracture places, involving hydrogen transport to metal, entry into it and transport within it;

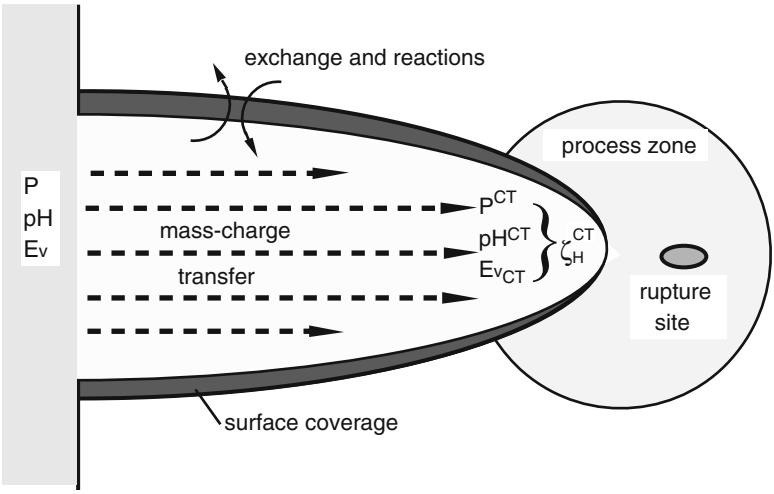


**Fig. 2** In-crack environmental currents and kinetic processes of mass-charge exchange and chemical reactions

(ii) stress-strain state as mechanical impetus for hydrogen assisted damage;
(iii) damage enhancement by hydrogen.

Crack tip hydrogen activity may be presented in terms of its partial pressure $P^{CT}$ in gaseous environments or the electrode potential $E_v^{CT}$ and the hydrogen ion exponent $pH^{CT}$ in corrosive conditions (all referred to the crack tip zone). They can significantly differ from $P$ or $E_v$ and pH (characteristics of the bulk environment). Relations of bulk and local environment parameters are governed by in-crack environmental currents and kinetic processes of mass-charge exchange and chemical reactions (Fig. 2). Thus, local environmental variables depend on the geometry of the crack and on time $t$:

$$P^{CT} = P^{CT}(P, a, \delta, t) \tag{1}$$

in gaseous environments, or

$$pH^{CT} = pH^{CT}(pH, E_v, a, \delta, t) \tag{2}$$

$$E_v^{CT} = E_v^{CT}(pH, E_v, a, \delta, t) \tag{3}$$

in corrosive ones, where the geometry parameters $a$ (crack depth) and $\delta$ (the height of an opened crack) represent the characteristic transportation distance from bulk environment to the crack tip (here only the crack depth is taken for the sake of simplicity) and crack opening displacement under load which gives the canal width

(variable along crack faces). The right hand parts of relations (1) and (2)–(3) in general are not plain functions of instantaneous values of displayed variables but functionals over their time histories depending, in particular, on the shapes of entire trajectories $a(\tau)$ and $\delta(\tau)$ in the time interval $0 \leq \tau \leq t$. This implies the influence of both loading/cracking history and crack geometry outside the $K$-controlled crack tip zone on the near tip environment, and therefore, on the value of $v$ at given $K$ under fixed bulk environment.

The phase of hydrogen entry into metal includes physical adsorption of hydrogen-containing species on metal surface; dissociative chemisorption of atomic hydrogen and its dissolution in the surface layer. The surface phase of sorption may be the rate determining step for HAC under relatively weak hydrogenation conditions at the crack tip, but this is unusual for most practical cases of gaseous or electrochemical (corrosive) hydrogenation when at entry sites elevated hydrogen activity is achieved.

Hydrogen promotes failure by different physical mechanisms, so that elementary fracture events are associated with a critical combination of hydrogen concentration $C$ and mechanical variables representing the stress-strain state. The latter determines the critical value of hydrogen concentration $C_{cr}$ to complete local fracture. Thus, the critical situation occurs when hydrogen concentration in prospective rupture sites reaches a critical value dependent on the mechanical action in the fracture process zone:

$$C = C_{cr} \tag{4}$$

The *critical* concentration of hydrogen is a function of the mechanical situation (stress-strain state) at a material point, i.e.:

$$C_{cr} = C_{cr}(\sigma, \varepsilon_p) \tag{5}$$

where $\sigma = \sigma(\boldsymbol{r}, t)$ and $\varepsilon_p = \varepsilon_p(\boldsymbol{r}, t)$ are respectively the tensors of stress and plastic strain, $\boldsymbol{r}$ being the spatial coordinate vector and $t$ the time. Throughout this section of the paper, a solid subjected to *sustained loading conditions* will be analyzed and in this case the tensors of stress and strain depend only on the spatial coordinate: $\sigma = \sigma(\boldsymbol{r})$ and $\varepsilon_p = \varepsilon_p(\boldsymbol{r})$.

The *actual* concentration, depending on the specific location of the material point and on time, is itself a function of the stress-strain state:

$$C = C(\boldsymbol{r}, t; \sigma, \varepsilon_p) \tag{6}$$

Hydrogen entry can be characterised by the equilibrium value $C_\Gamma$ of hydrogen concentration in stressed-strained metal at the entry surface $\Gamma$ (boundary between the metal and the environment):

$$C(\Gamma, t) = C_\Gamma \tag{7}$$

The driving force for diffusion $\mathbf{X}_D$ is determined by the gradient $\nabla$ of its chemical potential $\mu_H$:

$$\mathbf{X}_D = -\nabla\mu_H \tag{8}$$

which is related to the solubility coefficient $K_S$ (density of available sites) for hydrogen in metal:

$$\mu_H = RT \ln \frac{C}{K_S} \tag{9}$$

where $R$ is the ideal gas constant and $T$ the absolute temperature. The solubility $K_S$ depends on temperature; *hydrostatic stress* $\sigma$, alloy microstructure, chemical and phase composition of the alloy and hydrogen traps density (traps for hydrogen in metals are formed by lattice imperfections; dislocations are nearly the strongest kind of traps but not the only ones).

The overall density of traps depends on the plastic strain level which may be represented by the second invariant of the plastic strain tensor: the *effective or equivalent plastic strain* $\varepsilon_p$. In addition, plastic strain may affect the phase composition of an alloy, thereby causing variations of hydrogen solubility, as in austenitic steels through strain-induced $\gamma \rightarrow \alpha$ transformation. Thus, plastic strain is another variable affecting hydrogen solubility in metal, in addition to hydrostatic stress and temperature:

$$K_S = K_S(\sigma, \varepsilon_p, T) \tag{10}$$

The latter may be decomposed into its plastic strain dependent part $K_{S\varepsilon}$ and the hydrostatic stress related one:

$$K_S(\sigma, \varepsilon_p, T) = K_{S\varepsilon}(\varepsilon_p, T)\ \exp(\Omega\sigma) \qquad \text{with}\,\Omega = \frac{V_H}{RT} \tag{11}$$

where $V_H$ is the partial molar volume of hydrogen in metal.

The gradient (inhomogeneity) of any of the solubility-affecting factors can induce diffusion flux. On assuming *uniform temperature distribution* in the solid (a hypothesis maintained throughout this paper) the diffusion flux $\mathbf{J}$ may be expressed as follows:

$$\mathbf{J} = \frac{D}{RT} \quad C\,\mathbf{X}_D = -DC \quad \nabla \ln \frac{C}{K_S} \tag{12}$$

where $D$ is the diffusion coefficient of hydrogen in metal which characterises the specie mobility; the diffusivity should not be treated as a constant but considered to be dependent on plastic strain: $D = D(\varepsilon_p) \neq const$, to reflect the influence of the altered phase composition or trap density on the averaged (macroscopic) mobility

of diffusable species (cold work effect), apart from their effect on solubility reflected in Eqs. 10 and 11. Substitution of (11) into (12) yields:

$$\mathbf{J} = -D(\varepsilon_{\mathrm{p}})\left\{\nabla C - C\left[\nabla(\Omega\sigma) + \frac{\nabla K_{\mathrm{S}\varepsilon}(\varepsilon_{\mathrm{p}})}{K_{\mathrm{S}\varepsilon}(\varepsilon_{\mathrm{p}})}\right]\right\} \tag{13}$$

The condition of mass balance gives the diffusion equation in terms of concentration as:

$$\frac{\partial C}{\partial t} = -\mathrm{div}\ \mathbf{J} \tag{14}$$

which allows an evaluation of concentration evolution with time $t$. According to (13) and (14), the equation of stress-*and*-strain assisted diffusion in terms of concentration is:

$$\frac{\partial C}{\partial t} = D[\nabla^2 C - \mathbf{M} \bullet \nabla C - NC] + \nabla D \bullet [\nabla C - \mathbf{M}C] \tag{15}$$

where the dot • denotes scalar product and the coefficients $\mathbf{M}$ and $N$ are:

$$\mathbf{M} = \nabla \ln K_{\mathrm{S}}(\sigma,\ \varepsilon_{\mathrm{p}}); N = \nabla^2 \ln K_{\mathrm{S}}(\sigma,\ \varepsilon_{\mathrm{p}}) \tag{16}$$

The hydrogen entry into metal is characterised by the *boundary condition* for diffusion (7) with $C_\Gamma = C_0\, K_{\mathrm{S}}\,(\Gamma)$, where $C_0$ is the equilibrium hydrogen concentration provided by the environment in the bare metal (free of stress and plastic strain). Accounting for (11), it yields the following:

$$C_\Gamma = C_0\, K_{\mathrm{S}}(\Gamma) = C_0\, K_{\mathrm{S}\varepsilon}(\varepsilon_{\mathrm{p}}(\Gamma))\exp\left(\Omega\sigma(\Gamma)\right) \tag{17}$$

For solids under conditions of uniform environmental hydrogen activity characterised by an equilibrium concentration value $C_0 = const$, it is easy to get the exact *steady-state solution* of Eq. 15 of stress-strain assisted diffusion which is asymptotically attained at $t \to \infty$. This corresponds to the equilibrium state when the diffusion flux (12) is zero or, equivalently, when the diffusion driving force (8) is null. According to expression (12), this is provided when $C/K_{\mathrm{S}} = const$. Then, taking into account relation (11), the steady-state solution is the following:

$$C_\infty(r) = C_0\, K_{\mathrm{S}}(r) = C_0\, K_{\mathrm{S}\varepsilon}(\varepsilon_{\mathrm{p}}(r))\exp\left(\Omega\sigma(r)\right) \tag{18}$$

With $\varepsilon_{\mathrm{p}} = 0$, $K_{\mathrm{S}\varepsilon} = 1$ and the last expression coincides with the well known one for stress-only driven concentration.

## 2.3 *Meaning and Significance of the Fracture Mechanics Approach to HAC*

The basic concept of mechanical autonomy of the crack tip region ($K$-dominance) is the keystone of the linear elastic fracture mechanics approach [14]. It may be interpreted as follows: there is a region of characteristic size $R_{SIF}$ (Fig. 3) around the crack tip where the elastic stress-strain state is $K$-dominated, i.e., adequately represented *solely* by the universal $r^{-1/2}$ singular term of the complete series solution. This is the asymptotic term $\sigma_a$ of hydrostatic stress if one focuses on this component (the relevant one in hydrogen diffusion).

The whole inelastic zone (fracture process zone plus plastic region) may be so small that it does not sensibly disturb the linear elastic solution (*small scale yielding* condition). If this happens, the $K$-dominated annular elastic region still exists at distances from crack tip $R_Y < r \leq R_{SIF}$. Outside this annular domain (at $r > R_{SIF}$) the remote stress-strain field (*far field*) is not governed by $K$, nor is its hydrostatic component $\sigma_f$ in particular.

As far as this $K$-dominated ring shields completely the inelastic zone from any other external influence, except that provided by $K$, it means that the state of the whole inelastic near-tip region including the fracture process zone depends solely on $K$ and material, i.e., it is also autonomous and thus the stress intensity factor $K$ is the parameter governing the crack tip mechanical pre-damaged state, despite the lack of explicit treatment of nonlinear behaviour and microfracture events in the fracture process zone.

In the matter of HAC, when a crack of depth $a$ is present in the material, the hydrogen assisted fracture criterion (4) remains valid. Considering the $K$-dominance over the stress-strain state in the vicinity of the crack tip, the *critical* concentration (5) is a function of the stress intensity factor $K$ in this case:

$$C_{cr} = C_{cr}(\sigma(K, \boldsymbol{r}),\ \varepsilon_p(K, \boldsymbol{r})) \tag{19}$$

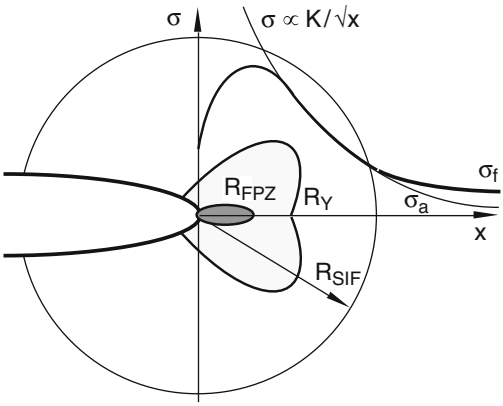


**Fig. 3** Specific zones and stress state in the vicinity of the crack tip. A nonlinear region (the fracture process zone of size $R_{FPZ}$) does exist in the vicinity of the crack tip where microscopic damage proceeds, and it is usually surrounded by the plastic region of size $R_Y$

and the *actual* concentration (6) yields:

$$C = C(\boldsymbol{r}, t; \sigma(K, \boldsymbol{r}),\ \varepsilon_{\mathrm{p}}(K, \boldsymbol{r})) \tag{20}$$

In terms of independent variables only and using the local coordinate $x$ with origin at the crack tip (Fig. 3):

$$C_{\mathrm{cr}} = C_{\mathrm{cr}}(K, x) \tag{21}$$

$$C = C(x, t; K) \tag{22}$$

Thus, to have $K$-dominance over the whole HAC process, and thus uniqueness of the $v(K)$ curve as an attribute of a given {material-hydrogen} system, two preconditions must be fulfilled:

/1/ K-controlled uniqueness of critical hydrogen concentration Ccr which must be reached at some point of the fracture process zone to cause local fracture and crack advance;

/2/ K-dominance over the process of hydrogenation in the fracture process zone ahead of the crack tip, i.e., uniqueness of the evolution of the distribution of hydrogen concentration $C(x,t)$.

According to criterion (4) the curves given by the right-hand parts of Eqs. 21 and 22 should meet at some point to cause crack extension. Achievement of exclusive $K$-dominance over the solution of this problem of contact between two curves (of *critical* and *actual* hydrogen concentrations) requires $K$-control over the curves themselves in the close vicinity of the instantaneous crack tip.

Since the critical concentration $C_{\mathrm{cr}}$ in the vicinity of the crack tip inherits the property of $K$-dominance from the stress-strain fields, the two preconditions /1/ and /2/ formulated above are equivalent to the following ones:

/1*/ $K$ is the only variable which controls the near-tip stress-strain fields (i.e., $\sigma = \sigma(K, \boldsymbol{r})$ and $\varepsilon_{\mathrm{p}} = \varepsilon_{\mathrm{p}}(K, \boldsymbol{r})$) in a domain embracing the physical process zone, thus dominating the mechanical aspects of both pre-damage and stress-strain affected hydrogenation;

/2*/ in addition, $K$ also governs the environment parameters which control hydrogenation in the very close vicinity of the crack tip (*local* environment parameters) which determine the hydrogen concentration evolutions $C(x,t)$ in the fracture process zone.

Finally, the two preconditions may be formulated in terms of fracture mechanics concepts as follows:

/1**/ $K$-controlled *mechanical autonomy* of the crack tip region, i.e., $K$-dominance over the stress-strain field, which is the keystone of linear elastic fracture mechanics under small scale yielding;

/2**/ $K$-controlled *environmental autonomy* of the crack tip region, i.e., $K$-dominance over the physico-chemical events, namely the boundary conditions and the hydrogen diffusion in the vicinity of the crack tip.

While the first precondition is always fulfilled in the framework of linear elastic fracture mechanic analyses under small scale yielding, the achievement of the second one is not guaranteed in all cases, because many causes may destroy the $K$-dominance in HAC and thus the uniqueness of the crack growth kinetics curve $v = v(K)$. In further sections of this paper, the effects of far field and history are discussed in depth.

However, in spite of the fact that the $v(K)$-curve is not always $K$-dominated (the second precondition could fail), on assuming sustained loading conditions (as in the approach presented in this paper) the threshold $K_{th}$ always meets the two preconditions of $K$-dominance, because the limit of crack non-propagation is associated with the unique steady-state distribution of concentration $C_\infty(\boldsymbol{r})$ near a tip of a stationary crack reached at $t \to \infty$. This stationary solution of the equation of stress-strain assisted diffusion was given in (18) and it has the same self-similitude properties as the stress-strain field. Therefore, only the first precondition (mechanical autonomy) is necessary to guarantee the uniqueness of the threshold state which is always $K$-dominated when linear elastic fracture mechanics, small scale yielding and sustained loading are considered.

## 3 The Effect of Far Field on $K$-Dominance in Hydrogen Assisted Cracking

The matter of $K$-dominance with regard to hydrogen diffusion in the near-tip region is addressed by Toribio and Kharin [15]. It is the question of the accuracy of the approximate hydrogen concentration distribution $C_a$ governed by the $K$-dominated component of the near-tip stress-strain field (i.e., by the *asymptotic* term $\sigma_a$) to represent the actual concentration $C_f$ being driven by the complete mechanical field containing the whole series expansion (i.e., influenced by the non-autonomous *far field* $\sigma_f$). To this end, the discrepancy $E = C_a - C_f$ between the two concentration distributions is the subject of interest to estimate the effect of the far field (the remote stress-strain field which is not $K$-controlled) on hydrogenation of the fracture process zone.

In accordance with the general form of the equation of stress-strain assisted diffusion (15), the equations to obtain the far-field affected concentration $C_f$ (exact) and the near-tip asymptotically driven one $C_a$ (approximate) are the following:

$$\frac{\partial C_f}{\partial t} = D\left[\nabla^2 C_f - \mathbf{M}_f \bullet \nabla C_f - N_f C_f\right] + \nabla D \bullet \left[\nabla C_f - \mathbf{M}_f C_f\right] \tag{23}$$

$$\frac{\partial C_a}{\partial t} = D\left[\nabla^2 C_a - \mathbf{M}_a \bullet \nabla C_a - N_a C_a\right] + \nabla D \bullet \left[\nabla C_a - \mathbf{M}_a C_a\right] \tag{24}$$

where the coefficients **M** and $N$ with subindices $f$ and $a$ are determined according to formulae (16) by their corresponding mechanical fields (the complete and the asymptotic ones).

Accounting for the small scale yielding condition, near the crack tip there is a $K$-dominated region ($r < R_{SIF}$) where both elastoplastic stress-strain fields coincide. In addition, plasticity is assumed to be associated solely with the crack tip region and no other plastic zones exist. Correspondingly, inelastic behaviour is always $K$-governed and plastic strain $\varepsilon_p$ does not participate in Eqs. 23–24 as a matter of distinction. Thus, the difference is related to the discrepancy between the two hydrostatic stress fields: the far field $\sigma_f$ and the asymptotic one $\sigma_a$ at $r > R_{SIF}$.

Subtracting one of the above equations from another the following equation can be derived with regard to discrepancy:

$$\frac{\partial E}{\partial t} = D\left[\nabla^2 E - \mathbf{M}_f \bullet \nabla E - N_f E\right] + \nabla D \bullet \left[\nabla E - \mathbf{M}_f E\right] + Q \tag{25}$$

where an additional source-type term arises:

$$Q = \begin{cases} D\Omega\, \nabla(\sigma_f - \sigma_a)\Sigma\, \nabla C_a \neq 0 & \text{at } r > R_{SIF} \\ 0 & \text{at } r \leqslant R_{SIF} \end{cases} \tag{26}$$

This expression represents the source term for diffusion of discrepancy $E$ which is the difference between the approximate $K$-driven concentration distribution and the exact far-field affected one. With nil initial and boundary conditions for $E$, its absolute value increases from zero with time since the source $Q$ produces this imaginable "diffusable substance" in the solid. This "error" is generated by the source $Q$ operative at $r > R_{SIF}$, and it diffuses from there towards the fracture process zone. The effect of the far field on $K$-dominance over hydrogen accumulation in the fracture process zone becomes more severe when a greater amount of "error" $E$ can reach the region $r < R_{FPZ}$ by "virtual" diffusion from the distant source (26) situated at $r > R_{SIF}$.

After estimation of the sizes of the crack tip zones represented in Fig. 3, and theoretical analysis of the near-tip hydrogen diffusion [15], it was possible to obtain the time evolution of the asymptotic ($K$-driven) concentration $C_a$ at the outer border of the fracture process zone where the effect from the source $Q$ appears first, i.e., at $x = R_{FPZ}$ as:

$$C_a(x = R_{FPZ},\, t) = C_a(\tau) = C_\infty(R_{FPZ})\ \text{erfc}\left(\frac{1}{2\sqrt{\tau}}\right) \tag{27}$$

where *erfc*(•) is the complementary error function and $\tau$ the dimensionless time defined as $\tau = Dt/R_{FPZ}^2$.

Figure 4 shows a plot of this function $C_a\,(\tau)$ (solid line). Approximately for $\tau \geq 130$, the concentration $C_a$ in the fracture process zone (i.e., for $x \leq R_{FPZ}$)

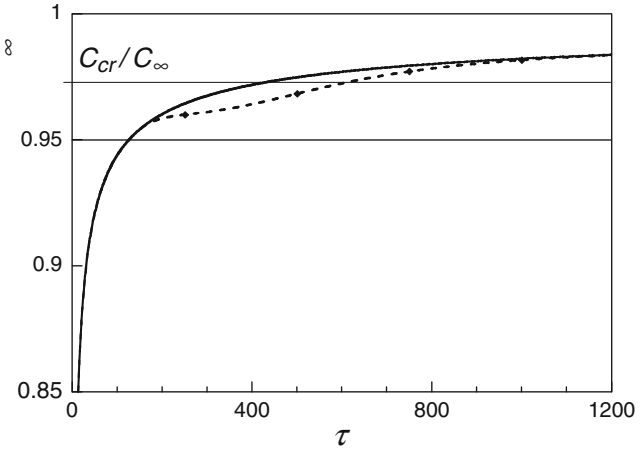


**Fig. 4** Plot of hydrogen concentration evolutions with time: asymptotically-driven (*K*-controlled) concentration $C_a$ (solid line) and a representative of the family of far-field affected concentration $C_f$ (dashed line). An example of near-threshold critical concentration level $C_{cr}$ below the steady-state one $C_\infty$ at $K_{th}$ is also shown

exceeds 95% of the steady-state level $C_\infty$. From then on, its further variation lies within a 5%-scatter band near this hydrogenation limit, i.e., the increase of *K*-driven concentration in the fracture process zone falls into this 5% strip from the time moment $t_{SS}$ (where *ss* indicates steady-state) given by:

$$t_{SS} = 130\frac{R_{FPZ}^2}{D} \tag{28}$$

The time $t_Q^*$ at which the source $Q$ becomes noticeable is [15]:

$$t_Q^* \geqslant t_{SS}\left(\frac{1}{16.1}\frac{R_{SIF}}{R_{FPZ}}\right)^2 \tag{29}$$

Estimating the ratio $R_{SIF}/R_{FPZ}$ from fracture mechanics assumptions, it yields:

$$t_Q^* > t_{SS} \quad \text{if} \quad E/\sigma_Y > 161 \tag{30}$$

where $E$ is the Young modulus and $\sigma_Y$ the yield stress of the material.

Thus the far field can affect the *K*-driven hydrogenation of the fracture process zone well after the transient concentration falls within a 5% scatter band near the steady-state hydrogen distribution in that area. Within the narrow 5%-width strip in the vicinity of the steady-state limit $C_\infty$ which defines $K_{th}$ by criterion (4) the supposition about *K*-control over hydrogen diffusion may be erroneous, as shown in Fig. 4 where the dashed line represents schematically one of the possible $C_f$-curves.

This fact can affect the $v(K)$-curve only in its near-threshold part, but without affecting the threshold itself which remains $K$-controlled, as demonstrated by Toribio and Kharin [15].

## 4 The Effect of History on $K$-Dominance in Hydrogen Assisted Cracking

Neither of the two processes of crack propagation and hydrogen diffusion should be considered separated from the other, since the movement of a crack tip is relevant to hydrogen accumulation in the fracture process zone. In terms of the theory of boundary value problems this situation is qualified as diffusion with moving boundary. Thus the crack growth *history* appears as a factor capable of affecting near tip diffusion and consequently the kinetics of HAC, apart from the stress-strain field represented by $K$. This again questions the idea of exclusive $K$-dominance over HAC.

The effect of history of the coupled hydrogenation-cracking process on $K$-dominance during HAC is addressed in previous research work [16, 17]. The first paper [16] develops theoretical bases and a qualitative analysis demonstrating the coupling between hydrogenation and crack growth, so that the crack growth rate in HAC generally is not governed solely by $K$. The quantitative consideration is given in the second paper [17] where the $K$-dominance condition is analyzed, showing the significance of the history effect which destroys $K$-control over crack growth rate, although a special regime of steady-state crack growth is seen to exist for which hydrogen assisted cracking becomes a $K$-dominated process.

In this section, the HAC process is analyzed in a *moving crack*. As in the rest of this paper, the analysis is focussed on sustained or quasi-static loading. The small scale yielding condition near the crack tip is assumed to be valid for the whole cracking process, so that the $K$-controlled mechanical autonomy of the near-tip region is supposed to be constantly preserved during crack growth. Adopting the framework of the diffusional theory of HAC outlined in previous sections, the analysis is confined to the *stress-strain* assisted diffusion as the responsible factor of HAC.

With regard to cracking, two approaches can be considered. According to one of them, crack growth proceeds discontinuously by a series of jump-like steps. The time intervals $\Delta t$ between discrete crack increments $\Delta a$ are just the periods of accumulation in the fracture process zone of the amount of hydrogen necessary to satisfy criterion (4). The crack growth rate is defined as:

$$v = \Delta a / \Delta t \tag{31}$$

Following the other approach, crack growth is assumed to go on continuously provided that criterion (4) is constantly fulfilled at a distance $x_c$. The instantaneous crack growth rate is defined here as:

$$v = \mathrm{d}a / \mathrm{d}t \tag{32}$$

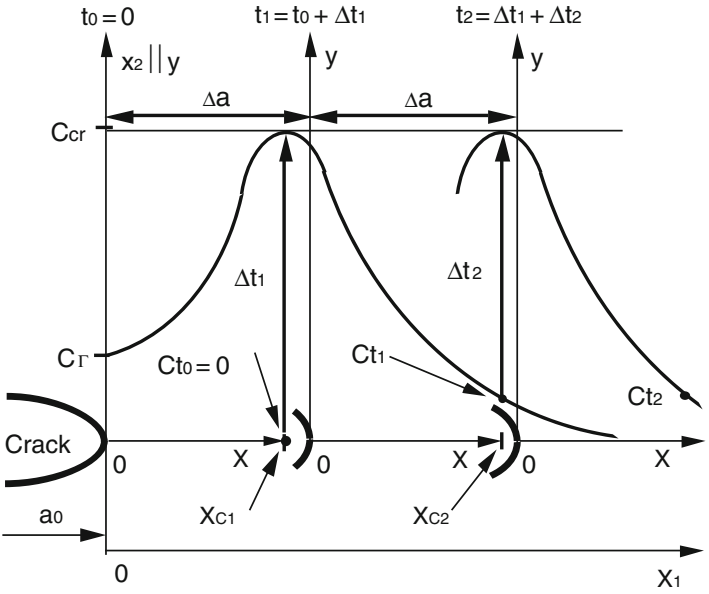


**Fig. 5** Sketch of metal hydrogenation in the vicinity of the crack tip which shows coupling of hydrogenation and crack growth processes

These approaches (jump-like and continuous) are usually considered to be essentially different with respect to background physics. Despite numerous speculations trying to support one or other on the basis of physical reasoning, none is generally accepted as adequate to represent the crack growth process.

*Jump-like (discontinuous) modelling of crack growth* is employed in Fig. 5 which shows schematically the hydrogen concentration curves near the crack tip after successive crack increments. The critical point $x_c$ is supposed for definiteness to coincide with the location at which hydrogen concentration and stress are maxima. Critical concentration must be attained at this point to produce a local rupture event causing jump-like crack increment. All the variables are supposed to be determined *solely* by material properties and $K$, i.e., they remain constant if $K = const$. Crack propagation consists of a series of loops (cycles) "hydrogen accumulation–local rupture–crack advance".

During each hydrogenation-fracturing cycle some amounts of hydrogen reach sites of possible subsequent fracture process zones. Thus, initial conditions for hydrogen diffusion within each particular loop are, in general, different from the preceding and subsequent cycles (see Fig. 5). This shows the coupling of hydrogen diffusion and crack growth processes which mutually influence on each other. Near tip hydrogen diffusion depends on the whole HAC history, and in particular on increase of crack size $a = a(t)$ and alterations of stress intensity factor $K = K(t)$. Thus, $K$-dominance in HAC fails because near-tip diffusion at a instantaneous $K$ proceeds along its specific way starting at the beginning of a particular HAC run.

*Smooth (continuous) modelling of crack growth* is useful for analytical consideration of the role of history of the coupled hydrogenation-cracking process in maintaining $K$-control over all crack tip events. Crack size is assumed to be a smooth function $a = a(t)$, the crack growth rate being its ordinary derivative (32).

Hydrogen concentration throughout the fracture process zone $C(x, y, t)$ is determined by stress-strain assisted diffusion. In an arbitrary fixed coordinate system $(x_1, x_2)$ *attached to the solid* it proceeds according to the equation:

$$\frac{\partial C}{\partial t} = -\nabla \bullet \left( \frac{D}{RT} \ \mathbf{X}_{\mathrm{D}} C \right) \tag{33}$$

which derives from (12) and (14), with the vector of diffusion driving force obtained from (8) and (9):

$$\mathbf{X}_{\mathrm{D}} = -RT \nabla \ln \frac{C}{K_{\mathrm{S}}} \tag{34}$$

When a moving crack is considered, the diffusion problem may suitably be considered in a movable coordinate system $(x, y)$ *attached to the crack tip* so that $x = x_1 - a(t)$, $y = x_2$. This will cause transformation of the diffusion equation (33) associated with the coordinate system $(x_1, x_2)$ pinned to the solid. Then the total time derivation of concentration is:

$$\dot{C} = \frac{\partial C}{\partial t} - \frac{\mathrm{d}a}{\mathrm{d}t} \frac{\partial C}{\partial x} = \frac{\partial C}{\partial t} - v \frac{\partial C}{\partial x} \tag{35}$$

After substitution of (35) into the left-hand part of (33), the modified equation of stress-strain assisted diffusion in moving coordinates can be obtained in a form which slightly differs from the initial one (33):

$$\frac{\partial C}{\partial t} = -\nabla \bullet \left[ \left( \frac{D}{RT} \ \mathbf{X}_{\mathrm{D}} - v \right) C \right] \tag{36}$$

where the vector $\boldsymbol{v} = v \, \boldsymbol{j}_x$ is independent of spatial coordinates and collinear with $x$-axis whose unit vector is $\boldsymbol{j}_x$ (then $\nabla \bullet (\boldsymbol{v} C) = \boldsymbol{v} \bullet \nabla C = v \ \partial C / \partial x$).

By analogy with the actual thermodynamic one, the *fictitious driving force* for diffusion may be formally introduced into Eq. 36:

$$\mathbf{X}_{\mathrm{D}}^{*} = \mathbf{X}_{\mathrm{D}} - \frac{RT}{D} \ v \tag{37}$$

With the use of expression (34) it yields:

$$\mathbf{X}_{\mathrm{D}}^{*} = -RT \nabla \left[ \ln \frac{C}{K_{\mathrm{S}}} + \frac{v}{D} \ x \right] = -RT \nabla \ln \frac{C}{K_{\mathrm{S}}^{*}} \tag{38}$$

where the formal solubility-like term is

$$K_S^* = K_S^*(\sigma,\ \varepsilon_p,\ v) = K_S(\sigma,\ \varepsilon_p)\exp\left(-\frac{v}{D}\ \ x\right) \tag{39}$$

To obtain some closed-form solutions useful to analyze the effect of history, the matter is simplified here by *neglecting the spatial variability of the hydrogen diffusion coefficient* $D = D(\varepsilon_p)$, i.e., taking $D$ as a constant averaged value of $D(\varepsilon_p)$ over the zone of interest. Following this way, the terms with $\nabla D$ do not appear in the diffusion equation:

$$\frac{\partial C}{\partial t} = D[\nabla^2 C - \mathbf{M}^* \bullet \nabla C - N^* C] \tag{40}$$

where vector and scalar coefficients, correspondingly, are the following:

$$\mathbf{M}^* = \nabla \ln K_S^*(\sigma,\ \varepsilon_p,\ v) \tag{41a}$$

$$N^* = \nabla^2 \ln K_S^*(\sigma,\ \varepsilon_p,\ v) \tag{41b}$$

Since near-tip stress-strain field components are controlled by $K$, these equation coefficients, apart from spatial coordinates, depend parametrically on $K$ and $v$:

$$\mathbf{M}^* = \mathbf{M}^*(K, v); N^* = N^*(K, v) \tag{42}$$

Therefore, the solution of this problem depends not only on $K$, but also on crack growth rate $v$: $C = C(x, t\,; K, v)$. Hydrogen concentration in the vicinity of the crack tip is determined by stress-strain assisted diffusion equation (40) with the following *boundary condition*:

$$C(x,t)|_{x=0} = C_\Gamma \tag{43}$$

where surface concentration $C_\Gamma = C_0 K_{slx=0} = const$. In addition, the *initial condition* is:

$$C(x,t)|_{t=0} = C_{t0}(x) \tag{44}$$

Crack growth rate $v$ becomes one more unknown variable which must be found from the solution of the *coupled* problem of hydrogen diffusion and crack growth. To close the system of equations for this coupled diffusion-cracking process, the criterion of crack growth (4) is employed. Using the distance $x_c$, the *critical* and *actual* concentrations (21) and (22) become:

$$C_{cr} = C_{cr}(K, x_c) \tag{45}$$

$$C = C(x_c, t; K, v) \tag{46}$$

and the crack growth criterion:

$$C(x_c, t; K, v) = C_{cr}(K, x_c) \tag{47}$$

This formulation of the diffusion-cracking problem is completely closed provided the stress intensity factor $K$ is somehow known. For such a case, if $C$ is a solution of the diffusion equation (40) parametrically dependent on crack growth rate $v$, the latter can be found from Eq. 47 as:

$$v = v(K, t) \tag{48}$$

Therefore, the crack growth rate must not be the same at equal values of $K$, but varies with the total HAC process time $t$.

However, in most practical situations, $K$ depends on both applied load and crack length, $K = K(a)$, and consequently, the coefficients (42) of Eq. 40 do too. The crack length $a$ turns out to be the additional unknown variable to be determined from the solution of the coupled problem. Differential equation (32) concerning crack size has the obvious solution:

$$a(t) = a_0 + \int_0^t v \, \mathrm{d}t \tag{49}$$

The problem is reduced to the same as for $K = const$, but now Eq. 47 to determine the crack growth rate with $K = K(\mathrm{a})$ becomes not a function parametrically dependent on v, but a functional over the whole *history* of the process. Correspondingly, crack growth rate as a solution of this coupled diffusion-cracking problem also becomes a functional dependent on a certain process history with its individual $K(a)$-variation. The variability of crack growth rate at the same $K$ is thus inevitable.

Using the same formalism as for a stationary crack under sustained load and taking the form of this solution in terms of the solubility coefficient $K_S$, substituting this by its analogue $K_S^*[\sigma(x; K),\ \varepsilon_p(x; K), v] = K_S^*(x; K, v)$, an approximate solution for diffusion near a moving crack tip may be built as:

$$C(x, t; K, v) = C_0 K_S^*(x; K, v) \operatorname{erfc}\left(\frac{x}{2\sqrt{Dt}}\right) \tag{50}$$

Taking into account the expression (39) this renders:

$$C(x, t; K, v) = C_0 K_S(x; K) \exp\left(-\frac{v}{D}\ x\right) \operatorname{erfc}\left(\frac{x}{2\sqrt{Dt}}\right) \tag{51}$$

Using the crack growth criterion (47), it yields an equation which can be solved to obtain the crack growth rate $v$ for a given $K$:

$$v(K,t) = -\frac{D}{x_c} \ln\left[\frac{C_{cr}(K,x_c)}{C_0 K_S(x_c,K)\,\mathrm{erfc}\left(\frac{x_c}{2\sqrt{Dt}}\right)}\right] \tag{52}$$

which has physical sense only after some incubation period $t_{in}$ has elapsed, i.e., at $t \geq t_{in}$. For earlier times $t < t_{in}$ it gives negative values of the crack growth rate when the expression in square brackets in formula (52) exceeds unity. This happens for:

$$t_{in} = \frac{1}{4D}\left[\frac{x_c}{\mathrm{erfc}^{-1}(C_{cr}/C_\infty)}\right]^2 \tag{53}$$

where the function $\mathrm{erfc}-^1(\bullet)$ is the one inverse to erfc $(\bullet)$ and $C_\infty = C_0\, K_S\,(x_c, K)$ is the exact steady-state solution for hydrogen diffusion near a stationary crack attained at long time $t \to \infty$.

For the range $K_{th} \leq K < K_c$ in the $v(K)$-curve (cf. Fig. 1), the inequality $C_{cr}(K) \leq C_\infty(K)$ is valid, i.e., the argument of the function $\mathrm{erfc}-^1(\bullet)$ in (53) always lies between 0 and 1 where the function is defined. This is because for HAC to occur, the critical hydrogen concentration $C_{cr}$ must be achieved sooner or later, and the steady-state one $C_\infty$ is just the maximum concentration which can ever be asymptotically reached at fixed $K$ near a stationary crack.

Figure 6 gives the time evolution of hydrogen concentration (51) for an initially stationary crack ($v = 0$). After applying the criterion (4), or (47) with $v = 0$, to obtain the instant at which it must start to grow, one obtains exactly the same result as given above in (53) for $t_{in}$. Thus the meaning of the time limit at which a solution exists for the crack growth rate in the coupled diffusion-cracking problem is just the incubation period before HAC starts.

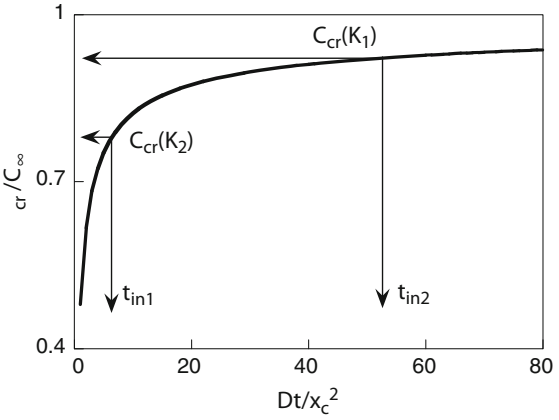


**Fig. 6** Accumulation of hydrogen in a near-tip fracture site according to the solution of the diffusion problem for a stationary crack and a sketch to explain the tendency of change of the values of $C_{cr}$ and $t_{in}$ with variation of $K$ (here $K_2 > K_1$)

From relation (52) it follows that the crack growth rate at fixed $K$ is a rising function of time which starts to increase from $v = 0$ at $t = t_{in}$ and asymptotically approaches some *steady-state* value $v_{SS}$ as $t \to \infty$:

$$v_{SS} = -\frac{D}{x_c} \ln\left[\frac{C_{cr}(K)}{C_0 K_S(K)}\right] = \frac{D}{x_c} \ln\left[\frac{C_\infty(K)}{C_{cr}(K)}\right] \tag{54}$$

The analysis clearly proves the intrinsic variability of crack growth rate values at a fixed $K$ level, as shown in Eq. 52. Hence, in general, crack growth rate is not a single-value function of $K$, and the $v(K)$-curve is not unique in a given {material-environment} system.

With regard to the *steady-state* regime of crack growth, all near-tip processes are time independent when viewed by an observer fixed to the moving crack tip. This obviously happens in HAC due to the existence of the steady-state solution (with $\partial C/\partial t = 0$ and $\partial v/\partial t = 0$) of the above considered coupled diffusion-cracking problem at constant $K$. The exact steady-state solution of Eq. 40 for a moving crack may be obtained using the same method as in the case of a stationary crack merely by nullifying the "fictitious driving force" (37), which yields the following:

$$C_{SS}(x_c; K, v) = C_0 K_S^*(x_c; K, v) \tag{55}$$

Comparing this with the estimate (50) of the non steady-state solution of the same equation, one concludes that the approximate solution (50), at least, approaches at $t \to \infty$ the exact steady-state concentration distribution in the vicinity of a moving crack tip. That is, the formal approximation of the non steady-state solution (52) has the right asymptotic behaviour.

For a given {material-environment (hydrogen)} couple, the steady-state crack growth rate (54) is a single-value function of $K$, and thus the crack growth kinetics curve as a plot of $v_{SS}$ vs. $K$ possesses the uniqueness of a material's characteristic curve. This stage of the HAC process, the steady-state crack growth, appears to be really $K$-dominated.

## 5 Conclusions

### 5.1 *Fracture Mechanics Approach to Hydrogen Assisted Cracking*

The meaning and significance of the linear elastic fracture mechanics approach to hydrogen assisted cracking was revised for small scale yielding and stationary cracks under sustained or quasi-static loading.

The role of *far field* on near-tip diffusion of hydrogen is of minor importance and can affect the $v(K)$-curve only in its near-threshold part, but it has no effect on the threshold itself which is still governed by $K$.

The effect of *history* appears in the form of coupling between hydrogen diffusion and crack growth and loss of $K$-dominance over the crack growth rate $v$, although a $K$-controlled steady-state value $v_{SS}$ does exist.

## 5.2 Final Conclusion

Since *material is itself and its circumstance*, when the latter is a hydrogenating environment, both far field and history (and especially the latter) could influence the coupled process of hydrogenation-cracking.

Therefore, in the matter of hydrogen assisted cracking, "the dream of yesterday is the hope of today and the reality of tomorrow" (R. H. Goddard), i.e., the yesterday affects the today, and the today influences the tomorrow.

In the latter case, it is possible to say, with the Spanish poet Antonio Machado, that "hoy es siempre todavía".

**Acknowledgements** Many results summarized in this paper are taken from previous works reported in the list of references. Special acknowledgement is gratefully given to the co-author of such papers: Dr. Viktor Kharin (formerly with the Pidstryhach Institute for Applied Mechanics and Mathematics of Lvov, now Associate Professor at the University of Salamanca).

Previous research works in which this paper is based were funded by the Spanish Institutions CICYT (Grant MAT97-0442), DGICYT (Grants UE94-0001 and SAB95-0122), and Xunta de Galicia (Grants XUGA 11801A93, 11801B95 and 11802B97) and the European Institutions CEE (*Human Capital and Mobility*) and NATO (*Scientific Programme*).

In addition, the author wishes to thank the financial support of his research at the University of Salamanca provided by the Spanish Institutions MCYT (Grant MAT2002-01831), MEC (Grant BIA2005-08965), MCINN (Grant BIA2008-06810), JCyL (Grants SA067A05, SA111A07 and SA039A08).

## References

1. W. Wang, Y.Y. Shan, K. Yang, Study of high strength pipeline steels with different microstructures. Mater. Sci. Eng. **A502**, 38–44 (2009)
2. W. Wang, W. Yan, L. Zhu, P. Hu, Y.Y. Shan, K. Yang, Relation among rolling parameters, microstructures and mechanical properties in an acicular ferrite pipeline steel. Mater. Des. **30**, 3436–3443 (2009)
3. F.R. Xiao, B. Liao, Y.Y. Shan, G.Y. Qiao, Y. Zhong, C. Zhang, K. Yang, Challenge of mechanical properties of an acicular ferrite pipeline steel. Mater. Sci. Eng. **A431**, 41–52 (2006)
4. M.C. Zhao, K. Yang, Y.Y. Shan, The effects of thermo-mechanical control process on microstructures and mechanical properties of a commercial pipeline steel. Mater. Sci. Eng. **A335**, 14–20 (2002)
5. J.E. Hood, Fracture of steel pipelines. Int. J. Pres. Ves. Piping **2**, 165–178 (1974)

6. S.O. Kotrechko, A.Y. Krasowsky, Y.Y. Meshkov, V.M. Torop, Effect of long-term service on the tensile properties and capability of pipeline steel 17GS to resist cleavage fracture. Int. J. Pres. Ves. Piping **81**, 337–344 (2004)
7. M.S. Kumar, M. Sujata, M.A. Venkataswamy, S.K. Bhaumik, Failure analysis of a stainless steel pipeline. Eng. Fail. Anal. **15**, 497–504 (2008)
8. V.D. Makarenko, M.Y. Mukhin, I.O. Makarenko, S.Y. Safronova, Crack resistance of pipe steels in industrial oil pipelines. Chem. Petrol. Eng. **44**, 672–675 (2008)
9. E. Gamboa, V. Linton, M. Law, Fatigue of stress corrosion cracks in X65 pipeline steels. Int. J. Fatigue **30**, 850–860 (2008)
10. D. Hardie, E.A. Charles, A.H. López, Hydrogen embrittlement of high strength pipeline steels. Corros. Sci. **48**, 4378–4385 (2006)
11. A. Torres-Islas, V.M. Salinas-Bravo, J.L. Albarrán, J.G. González-Rodríguez, Effect of hydrogen on the mechanical properties of X-70 pipeline steel in diluted $NaHCO_3$ solutions at different heat treatments. Int. J. Hydrogen Energy **30**, 1317–1322 (2005)
12. J. Toribio, V. Kharin, The reliability of the fracture mechanics approach to environmentally assisted cracking: 1. Uniqueness of the $v(K)$-curve. Mater. Des. **18**, 87–94 (1997a)
13. J. Toribio, V. Kharin, The reliability of the fracture mechanics approach to environmentally assisted cracking: 2. Engineering safe design. Mater. Des. **18**, 95–101 (1997b)
14. J. Toribio, V. Kharin, Evaluation of hydrogen assisted cracking: the meaning and significance of the fracture mechanics approach. Nucl. Eng. Des. **182**, 149–163 (1998)
15. J. Toribio, V. Kharin, *K*-Dominance condition in hydrogen assisted cracking: the role of the far field. Fatigue Fract. Eng. Mater. Struct. **20**, 729–745 (1997c)
16. J. Toribio, V. Kharin, The effect of history on hydrogen assisted cracking: 1. Coupling of hydrogenation and crack growth. Int. J. Fracture **88**, 233–245 (1997d)
17. J. Toribio, V. Kharin, The effect of history on hydrogen assisted cracking: 2. A revision of *K*-dominance. Int. J. Fracture **88**, 247–258 (1997e)

# Degradation of Properties of Long Term Exploited Main Oil and Gas Pipelines Steels and Role of Environment in This Process

**H.M. Nykyforchyn, E. Lunarska, and P. Zonta**

**Abstract** Comparison of mechanical (characteristics of strength, reduction of area and elongation, impact strength, hardness, fracture toughness), corrosion (corrosion rate and electrochemical parameters), corrosion-mechanical (stress corrosion cracking and hydrogen embrittlement) properties and parameters of hydrogen behaviour in the oil and gas pipelines steels in the as-received state and after 28–40 years of service are presented in the paper. Transported hydrocarbons serve as a hydrogen source and the hydrogen accumulates in the pipe metal during its use. This cause's in-bulk material diffused damage due to the presence of hydrogen traps created during service. The analysis of a change of the mentioned characteristics together with the results of hydrogen permeation and vacuum hydrogen extraction measurements indicate considerable "in-bulk" material degradation of main pipeline steels after long term service and the essential role of hydrogen in these processes. Therefore the monitoring of surface defects induced by corrosion and mechanical damage is insufficient for safe service if one does not take into account possible degradation of in-bulk material properties. It is possible to monitor in-bulk material property changes by measurements of electrochemical characteristics and it opens up possibilities for an application of electrochemical methods for diagnostics of in-service degradation.

H.M. Nykyforchyn (✉)
Karpenko Physico-Mechanical Institute of the NAS of Ukraine,
Naukova str. 5, 79601 Lviv, Ukraine
e-mail: nykyfor@ipm.Iviv.ua

E. Lunarska
Institute of Physical Chemistry of the Polish Academy of Sciences,
Kasprzaka str. 44/52, 01-224 Warszawa, Poland
e-mail: elunarska@ichf.edu.pl

P. Zonta
Venezia Tecnologie S.p.A., Via Delle Industrie, 39 – 30175 Porto Marghera,
Venezia, Italy
e-mail: pzonta@veneziatecnologie.it

T. Boukharouba et al. (eds.), *Integrity of Pipelines Transporting Hydrocarbons*,
NATO Science for Peace and Security Series C: Environmental Security,
DOI 10.1007/978-94-007-0588-3_5, 

## 1 Introduction

Main oil and gas pipelines are designed for long-term service, exceeding 30 years. Despite such a long planned in-service time, further life extention constitutes a great economic interest. However extension of the in-service time beyond the initially scheduled period is neither automatic nor always possible. This is because of the degradation processes taking place in the materials exposed to long-term working loads and environments. In this situation, evaluation of the remaining life time of main pipelines must take into account degradation processes taking place not only on the surface (defects of mechanical and corrosion nature), but also in the volume of the pipe wall. The aim of the paper is to present results obtained in the investigations of the in-bulk degradation of oil and gas pipeline and large volume oil storage tank steels. The analysis consists of a comparison of properties, in the as-received state and after a period of 28–40 years of service. The complex hydrogen permeation and vacuum hydrogen extraction measurements were used for the analysis of damage development during long-term service. A possibility of monitoring in-bulk material properties degradation by measurements of electrochemical characteristics is shown.

## 2 Main Oil Pipeline

Specimens of 0.10C-1.6Mn-0.30Si steel in as-received state and cut from the upper *up* and lower *bottom* parts of pipe being in service for 28 years were tested [1, 2]. Residual water, deposited from oil on the pipe bottom, was considered an aggressive environment causing possible in-bulk pipe wall hydrogenation from the internal surface of the pipe. It is confirmed by more intensive internal corrosion

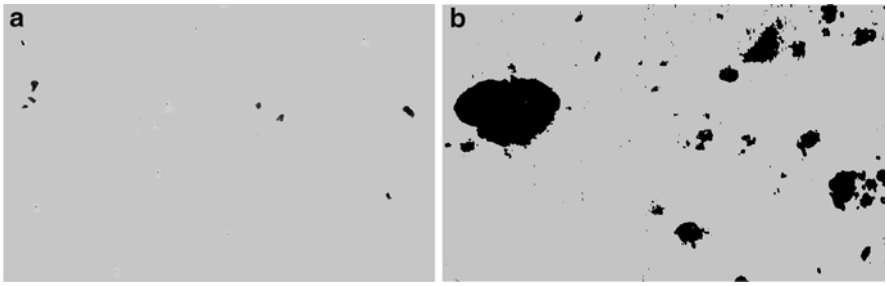


**Fig. 1** Appearance of the inner surface of the *up* (**a**) and *bottom* (**b**) parts of the pipe after 28 years of service

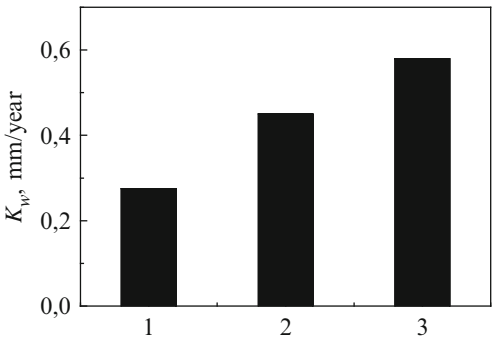


**Fig. 2** Corrosion rate of as received steel (*1*), *top* (*2*) and *bottom* (*3*) exploited pipe parts

**Fig. 3** Typical appearance of the impact tests fracture of specimens cut from (*left*) the top and (*right*) *bottom* parts of the exploited pipe

damaging of *bottom* part of the pipe (Fig. 1). The tests in simulated residual water showed that the corrosion rate was 200% higher for the *bottom* and 170% higher for the *top* part than for a virgin material (Fig. 2). Thus, the results provided evidence that the changes in the properties of material occur due to long time contact with the residual water as a source of hydrogen absorbed by the exploited metal.

The results of Charpy tests showed that the steel in as-received state exhibits the highest value of *KCV* (180 J/cm$^2$). The toughness of the material from the *up* part is about half of it (95 J/cm$^2$). Such a dramatic drop in the toughness agrees with what reported in [3] and indicates the degradation of mechanical properties, especially a lower resistance to brittle fracture, of the steels in oil transport lines. In the case of the *bottom* part of the pipe being in operation, it was not possible to evaluate the impact toughness, because of the formation of cracks parallel to the pipe axis (Fig. 3). This hydrogen induced stratification is a well known phenomenon observed in industrial pipe lines transporting crude oil containing a high amount of hydrogen sulfide and sulfide reduced bacteria.

Sensitivity of the pipe materials to stress corrosion cracking (SCC) was evaluated by slow strain rate ($10^{-7}$ s$^{-1}$) tensile tests under moderate cathodic polarization (0.5 A/m$^2$) in water deposited in the oil storage tank. The relative change of

**Table 1** The properties of plasticity of tensile tested 0.10C-1.6Mn-0.30Si

| Material | Test environment | ε (%) | RA (%) | $K_ε$ (%) | $K_{RA}$ (%) |
|---|---|---|---|---|---|
| As-received | Air | 36 | 77 | 39 | 55 |
| | Residual water | 14 | 42 | | |
| Being in service | Air | 28 | 56 | 25 | 5 |
| | Residual water | 7 | 3 | | |

elongation ε ($K_ε = ε^c/ε$ 100%) and relative reduction in area *RA* ($K_{RA} = RA^c/RA$ 100%) of specimens tested in air (ε, *RA*) and tested in the corrosion environment ($ε^c$, $RA^c$) were compared. As seen in Table 1, the *bottom* part of the exploited material exhibited lower strength and elongation than the as-received steel, either tested in air or in the aggressive environment. As seen in Table 1, the values of $K_{RA}$ are 55% and 5% for the virgin specimens and for specimens cut out from the *bottom* part of the exploited pipe respectively. The drastic decrease in the $K_{RA}$ and *RA* indicates the possibility of a drastic decrease in plasticity of metal in a course of exploitation.

## 3 Oil Storage Tank

The low carbon steel St.3sp (0.2C) was used for manufacturing the oil large volume tank which was dismantled after the long-term service [2, 4]. Oil-water level and the range of oil-levels are presented in Fig. 4. Taking it into account, four characteristic zones were chosen from the point of view of the working environment of the material: (a) zone I – upper part of the wall, absence of contact of steel with oil but with water condensed from oil surface; (b) zone II – lower part of the wall, constant contact of steel with oil; (c) zone III – tank wall closer to the bottom – constant contact of steel with residual water; (d) zone IV – bottom, constant contact of steel with the residual water. Experiments were carried out in the residual water, taken from the exploited storage tank.

No significant differences in the values of stress yield of material of different tank fragments were observed. However, there is a scatter of values of other strength indicators (Table 2). It concerns mainly material of zone II, which is characterized by the lowest hardness and the highest impact strength. The material of zone III is characterized by the lowest impact strength *KCV*. Thus, the metal in contact during the service with residual water, condensed on the bottom (zones III and IV) or on upper part of storage wall (zone I), showed the lowest levels of brittle fracture resistance.

## 4 Main Gas Pipeline

Steels 17G1S (0.17C-Mn-Si) and API 5L X52 in as-received state (spare pipes) and after service during 28–40 years were studied [5–8]. API 5L X52 steel (code X52 for as-received state) was in service for 30 years (code X52-10 and X52-12

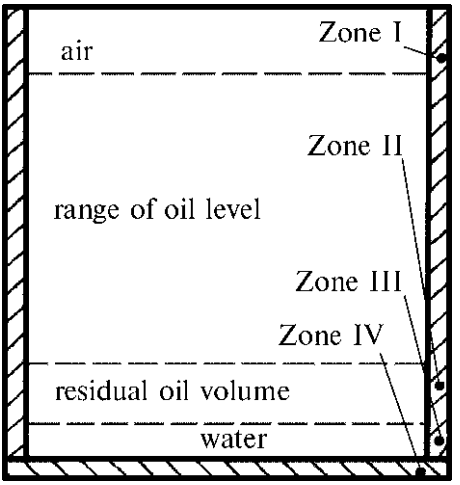


**Fig. 4** A storage tank with marked places, where specimens for tests were cut out (schematically)

**Table 2** Mechanical properties of the different zones of the exploited storage tank steel

| Indicator | Zone | | | |
|---|---|---|---|---|
| | I | II | III | IV |
| Hardness, [HV] | 126 | 108 | 130 | 123 |
| $\sigma_{UTS}$, [MPa] | 488 | 440 | 478 | 435 |
| $\sigma_y$, [MPa] | 278 | 263 | 273 | 266 |
| KCV, [J/cm$^2$] | 72 | 153 | 62 | 84 |

respectively to wall thickness 10 and 12 mm). Upper *up* and lower *down* parts of the exploited pipes were distinguished and in some cases specimens were cut out closer to inside *in* and outside *out* parts of the pipe wall. Such separateness of the different parts of exploited pipe is explained by the view that in the case of wet gas pipelines, the condensed water accumulates at pipe bottom [9].

As seen in Fig. 5 the internal surface of the pipes removed from service revealed the deposits of corrosion products. In the case of the *down* surface, non uniform and pitting corrosion was observed (Fig. 5b).

Long term service changes essentially the mechanical properties of the steels (Table 3). In the exploited pipes, the tensile stress–displacement curves exhibited an apparent yield plateau not observed for as-received material (Fig. 6) and strain-hardening coefficient $n$ increased. One should note a sharp decrease of yield strength for 17G1S steel and a decrease of $RA$ for both steels. However, the effect of service on elongation ε is specific: its increase was revealed for X52-10 and 17G1S steels. Such changes in the elongation may be incorrectly interpreted as an indication that exposure to in-service conditions improves plasticity of the materials. Hardness of the exploited steels was lower in comparison with as-received state, and a stronger effect was peculiar to the *bottom* parts of the pipes.

Essential decrease of impact strength $KCV$ is peculiar to the all exploited steels, more evident for *in* layers of pipe and also for specimens cut across pipe axis.

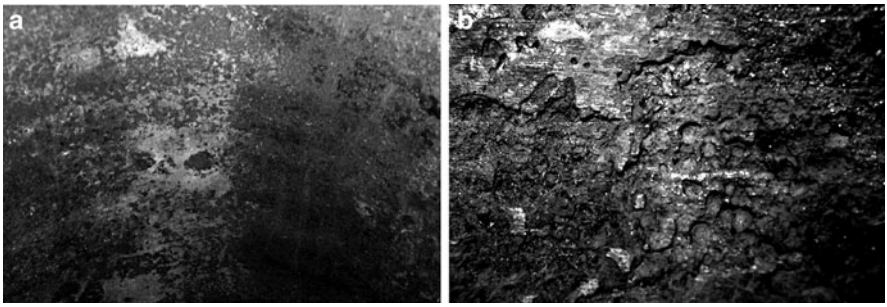


**Fig. 5** Appearance of the inner surface of pipe X52-10-*up* (**a**) and X52-10-*down* (**b**)

**Table 3** Mechanical properties of the studied gas pipeline steels

| Steel code | Service time, years | Pipe part | $\sigma_y$ MPa | $\sigma_{UTS}$ MPa | RA % | ε % | n | $J_i$ /$J_{0.2}$ kN/m |
|---|---|---|---|---|---|---|---|---|
| X52 | 0 | – | 355 | 475 | 72.9 | 22.7 | 0.59 | 86/412 |
| X52-12 | 30 | Bottom | 268 | 451 | 64.4 | 20.8 | 0.74 | 50/127 |
| | | Up | 255 | 460 | 62.5 | 22.9 | | |
| X52-10 | | Bottom | 362 | 536 | 54.6 | 29.7 | 0.82 | 37/79 |
| | | Up | 335 | 538 | 55.0 | 28.8 | | |
| 17G1S | 0 | – | 378 | 595 | 79.0 | 20.2 | 0.58 | 203/315 |
| | 28 | | 403 | 590 | 68.2 | 20.5 | | |
| | 29 | | 345 | 547 | 71.1 | 19.6 | 0.76 | |
| | 31 | | 419 | 574 | 73.8 | 21.8 | | 87/201 |
| | 38 | | 357 | 520 | 73.1 | 25.4 | 0.97 | |
| | 40 | | 302 | 515 | 69.2 | 26.3 | 0.75 | |

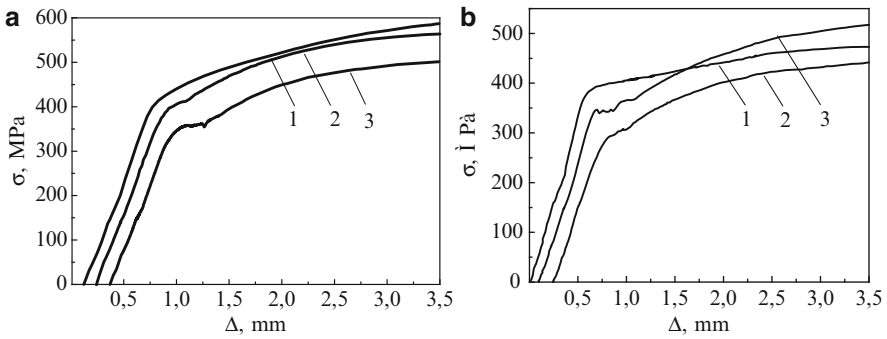


**Fig. 6** Typical tensile curves of (**a**) 17G1S steel in as-received state (*1*), after 31 (*2*) and 40 (*3*) years of service and (**b**) X52 steel in as-received state (*1*) and bottom parts of X52-12 (*2*) and X52-10 (*3*) steels after 30 years of service

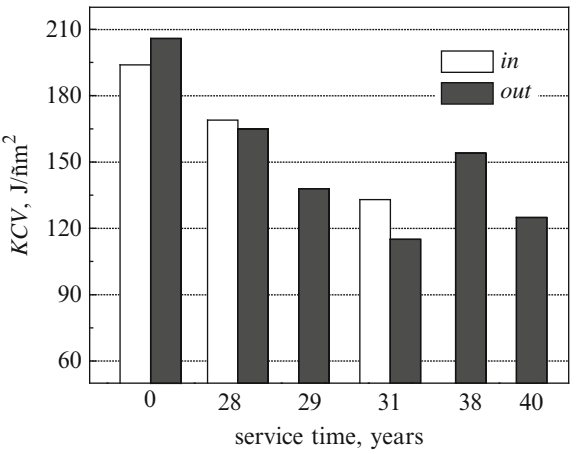


**Fig. 7** Impact strength of 17G1S steel in as-received state and after different duration of service

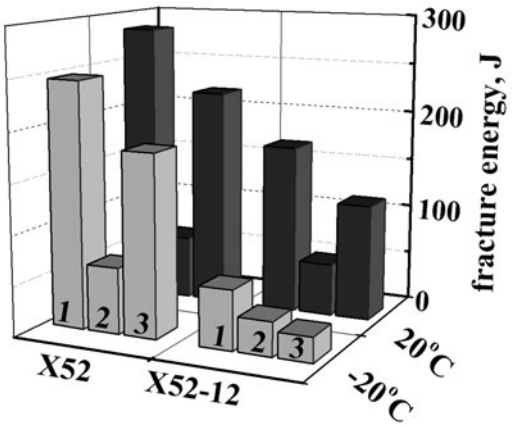


**Fig. 8** Total fracture energy (*1*) and its components of crack initiations (*2*) and crack propagation (*3*) during Charpy tests of X52 steel

Fig. 7 demonstrates the relationship between *KCV* levels and time of service for 17G1S steel.

A decrease of test temperature causes a slight decrease (15–20%) of *KCV* of X52 steel in the as-received state, due to the crack propagation component change (Fig. 8). At the same time low temperature impact strength of the exploited steel is three times lower for as-received steel and crack propagation component – is four times lower.

Long term service of pipe also causes a decrease of fracture toughness which was observed in all the studied steels. Figure 9 shows that for 17G1S steel, the effect is stronger for metal closer to the internal surface of the pipe.

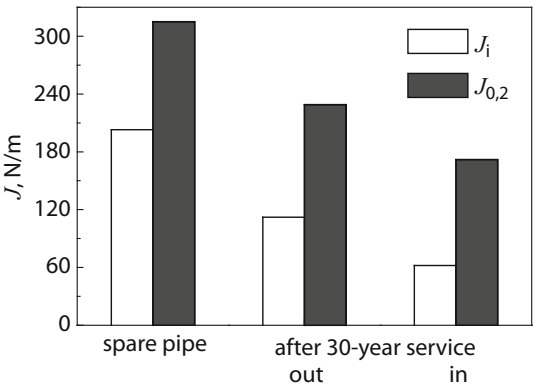


**Fig. 9** *J*-integral levels for crack initiation $J_i$ and 0.2 mm of crack increment $J_{0.2}$ for 17G1S steel in as received state and after 31 years of service

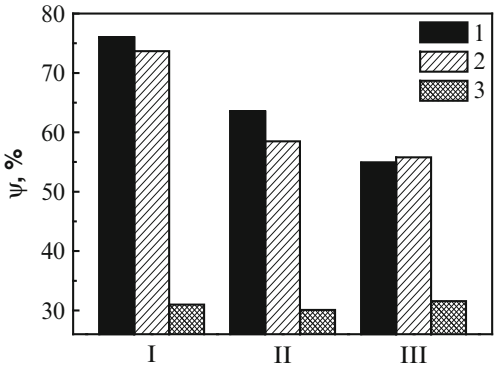


**Fig. 10** Averaged values of RA for steels X52 (I), X52-12 (II), X52-10 (III) as measured in air (*1*), in corrosive environment at corrosion potential (*2*) and at cathodic polarization (*3*)

SCC tests of smooth and compact tension specimens of X52 steel were performed by the slow strain tension method in an artificial environment, which simulates aqueous condensate in a gas pipe (brine) [9]. Some experiments were carried out at a moderate (0.1 A/m$^2$) cathodic polarization for hydrogen charging of specimens. Tests of smooth specimens at corrosion potential did not show SCC.

Show SCC sensitivity of the steel in as-received state and after service, using parameter *RA* (Fig. 10). However noticeable effect was produced by cathodic polarization that indicated the sensitivity of the steel in as-received state and after service, using parameter *RA* (Fig. 10). However noticeable effect was produced by cathodic polarization that indicated the sensitivity of exploited steel, especially the part *down*, to hydrogen embrittlement (Fig. 11).

Tests on pre-cracked specimens, in disagreement with tests on smooth specimens, indicated (Fig. 12) the susceptibility of investigated steels to SCC in the model environment under open circuit conditions. The application of cathodic

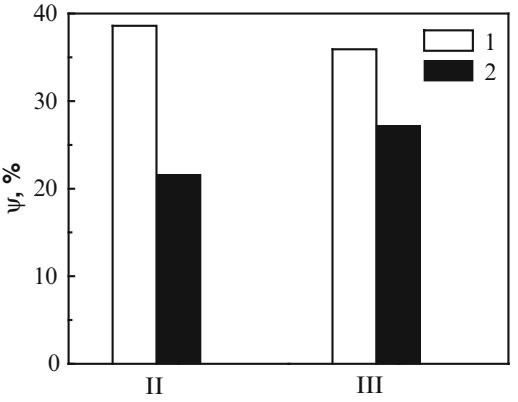


**Fig. 11** Susceptibility to HE of *up* (*1*) and *down* (*2*) parts of exploited steels X52-12 (II) and X52-10 (III) at cathodic polarization

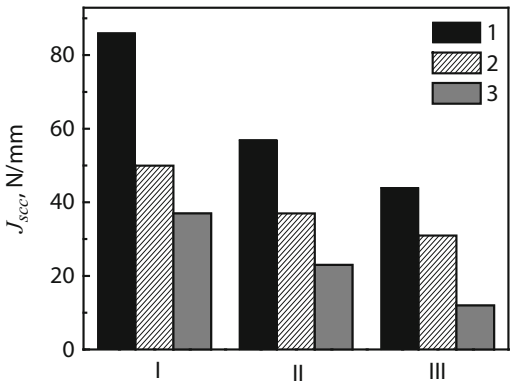


**Fig. 12** Crack growth resistance of X52 (*I*), X52-12 (*II*) and X52-10 (*III*) steels in air ($J_i$, *1*), in corrosion environment at corrosion potential (*2*) and at cathodic polarisation (*3*)

polarization additionally decreased the threshold $J_{scc}$ levels of steels. The as-received steel exhibited the maximum resistance to SCC, whereas X52-10 steel was characterized by the lowest $J_{scc}$ level.

## 5 Study of Hydrogen Behavior in Metal to Evaluate Damage

Concentration of hydrogen and its coefficient of diffusion in metal are often used to predict hydrogen damage mechanisms which cause a decrease of structural strength, since hydrogen concentration and its mobility define a possibility of hydrogen accumulation in pre-fracture zone and, correspondingly, an easing of fracture [10]. The known methods of investigating hydrogen behavior in metals have been used recently for an evaluation of material damage; taking into account

that hydrogen accumulates in a metal, mainly in defects, which are considered as hydrogen traps [11].

The known method of assessing hydrogen amount in a metal by vacuum extraction at elevated temperature was developed by increasing the temperature step by step and holding the temperature for a certain time on every level. Then only "low energy hydrogen" (hydrogen present at low energy, with respect to interaction with defects, traps) leaves the metal during holding at comparatively low temperature. Dislocations are an example of such defects. At the same time "high energy" hydrogen exists in "deeper" traps like pores and nano- and micro-cracks, therefore it can leave the metal only at higher temperatures. This base for an analysis of metal defectiveness was used for X52 steel. Table 4 shows the amount of hydrogen content extracted at different temperature ($V^n_H$) and the total hydrogen content ($V_H$). Exploited steels contained a higher total hydrogen amount than the as-received steels. It should be emphasized that in exploited materials the portion of hydrogen extracted at the highest temperature was higher than in the as-received steel.

Electrochemical method to assess hydrogen diffusion coefficient in metal requires the use of a specimen-membrane between two electrochemical cells [10, 11]. Then the ingress cell is cathodically charged and the opposite is anodically polarisated in a potentiostatic regime. In general the method allows to evaluate physical (lattice) $D$ and effective $D$*, taking into account hydrogen trapping,

**Table 4** Amount of hydrogen desorbed gradually at increased temperature ($V_H{}^n$, ppm) and total amount of extracted hydrogen ($V_H$, ppm)

| | $V_H{}^n$, ppm | | $V_H$, ppm | |
|---|---|---|---|---|
| Steel code and pipe part | 500 K | 700 K | 900 K | |
| X52 | 1.4 | 0.07 | 0.04 | 1.51 |
| X52-12 down-in | 0.01 | 1.00 | 0.41 | 1.42 |
| X52-12 up-out | 0.10 | 0.51 | 0.60 | 1.21 |
| X52-10 down-in | 0.15 | 0.80 | 4.15 | 5.10 |
| X52-10 up-out | 0.30 | 0.60 | 0.81 | 1.71 |

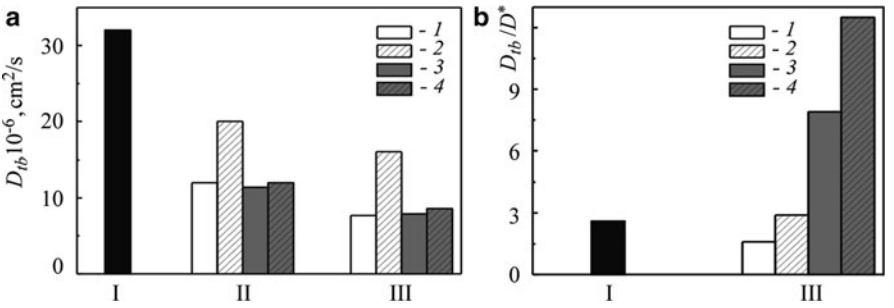


**Fig. 13** The calculated values of lattice hydrogen diffusivity (**a**) and the ratio of the lattice diffusivity to the apparent diffusivity (**b**) for steels X52 (*I*), X52-12 (*II*) and X52-10 (*III*) in different sections: *1*, *up-out*; *2*, *up-in*; *3* – *down-out*; *4* – *down-in*

**Table 5** Critical cathodic current density $i_c$

| Steel code and pipe part | X52 | X52-12 | | | | X52-10 | | | |
|---|---|---|---|---|---|---|---|---|---|
| $i_c$, mA/cm$^2$ | 40 | Down-in 7 | Down-out 15 | Up-in 40 | Up-out 35 | Down-in 6 | Down-out 12 | Up-in 20 | Up-out 20 |

hydrogen diffusion coefficients and, correspondingly, a relation $D/D^* = 1 + N\,(k/p)$, where $N$ = density of traps; $k$ i $p$ = kinetic constants of falling and extraction of hydrogen from traps; $N(k/p)$ = effectiveness of takeover of hydrogen by traps. Using this method, the highest lattice diffusivity was measured in the as-received X52 steel and the diffusivity decreased for metal being in service (Fig. 13a).

To some extent, the diffusivity calculated for the *down* parts of exploited pipes was slightly lower than that for the *up* parts, especially in the case of pipe X52-10. The efficiency of hydrogen trapping was higher in the exploited than in the as-received pipes. As seen in Fig. 13b, the trapping efficiency was higher in the case of *down* and especially *down-in* parts of the pipe.

This method was developed to increase step by step cathodic polarization in the ingress cell, holding for a fixed time cathodic current during every step. Correspondingly at the external side of the membrane an increase of ionization current (hydrogen flow) is observed. The current increase is regularity observed until the process of damage development begins to simultaneously influence hydrogen and residual stresses, caused by intensive cathodic charging. Then a sharp drop appears on the ionization current curve of membrane external side. It is a result of hydrogen trapping by new created defects that is a development of damage caused by cathodic charging. The current of cathodic hydrogenation corresponding to this situation is called critical $i_c$. It is possible to evaluate the metal sensitivity to hydrogen cracking: the higher $i_c$, the lower sensitivity to hydrogen cracking. Such evaluation was made for X52 steel (Table 5): the steel in as-received state is characterized by the lowest sensitivity to hydrogen cracking ($i_c = 40$ mA/cm$^2$) and on the contrary, the *down-in* part of X52-10 steel – shows the highest sensitivity ($i_c = 6$ mA/cm$^2$).

## 6 Two Stages of In-Service Degradation and the Role of Corrosive/Hydrogen Enriched Environments

Degradation of main pipeline steels in general is related to deformation aging, which brings about an increase in strength at the expense of plasticity [12]. However, our results strongly suggest that in principle, the degradation should be considered as a two stage process, with deformation aging stage (I) followed by diffused damage development (II) (Fig. 14). The time of stage (I) indicated in Fig. 14 is somewhat arbitrary. On the other hand it agrees with the results obtained in studies of degradation in main pipelines, exploited in the range of 28–40 years.

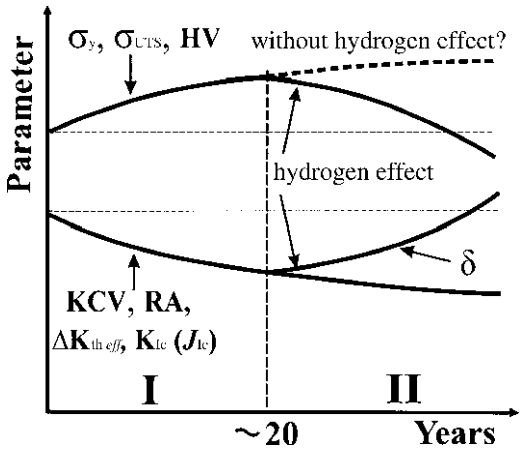


**Fig. 14** Schematic explanation of the changes in the parameters used to describe properties of materials exposed to a long time service

There are direct and indirect symptoms of the in-service damaging of pipeline steels. First, there is contradictive tendency in the changes of *RA*, which decreases, and an increase in elongation ε, related to diffused damage of the materials (the effect of diffused micro-cracks opening). Secondly, there is a decrease in tensile strength and hardness accompanied by a decrease in toughness. Usually the opposite tendency was observed, if a change of material state produced by heat treatment, alloying, deformation etc. Thirdly, the complex of comparative investigation of hydrogen behaviour in steels in as-received state and after service (hydrogen extraction and permeation tests) supports the hypothesis that damage develops during service.

One should deduce that deformation aging and damage development result in ambiguous, and a sometimes opposite effect on the mechanical properties of the degraded material. The above situation might be modelled by the composite "metal matrix – pores". Deformation aging strengthens and embrittles the metal matrix, as shown by the increase in strain-hardening coefficient *n* and by the decrease in *RA*.

Porosity causes a decrease of strength and hardness but at the same time causes metal embrittlement. On the other hand, strength is sensitive to both processes and may increase or decrease, depending on the balance between the deformations strengthening and defects accumulation in the matrix. Since deformation strengthening and damage act in the opposite directions, a service exposure should have different impact on the plasticity: deformation decreases the *RA*, while the defect increases the elongation, as schematically shown in Fig. 14.

The role of hydrogen in the second stage of degradation is not yet fully recognized. Hydrogen induced changes that can be illustrated as examples of non-uniform in-service degradation, which results in some components being far more deteriorated that the rest (which can be used for reference). For example, degradation of the oil storage tank zones in contact during service only with residual water is stronger in comparison with the zone II that was in contact only

with oil. Similar results were obtained for the steels of oil and gas pipelines, in which residual water also accumulates at the bottom of the pipe. This water induces significant changes in the properties of *bottom* and *up* parts of pipe. This again shows that a corrosive environment speeds up the degradation as the metal absorbs hydrogen, which intensifies the second stage of corrosion damage.

## 7 Evaluation of In-Service Degradation by Monitoring Electrochemical Properties Change

The change of properties which define material workability during long term service is caused by the change of metal state. Electrochemical parameters should be, in principle, sensitive to such changes. The following parameters were investigated as possible indicators for monitoring electrochemical properties of oil and gas main pipeline steels: corrosion potential $E_{cor}$, Tafel coefficients $b_a$ and $b_c$, corrosion current $i_{cor}$, current at certain anodic potential $j_a$, and polarization resistance $R_p$ [13]. Examples of the changes in the values of these parameters are presented in Fig. 15, which shows that polarization resistance and corrosion current

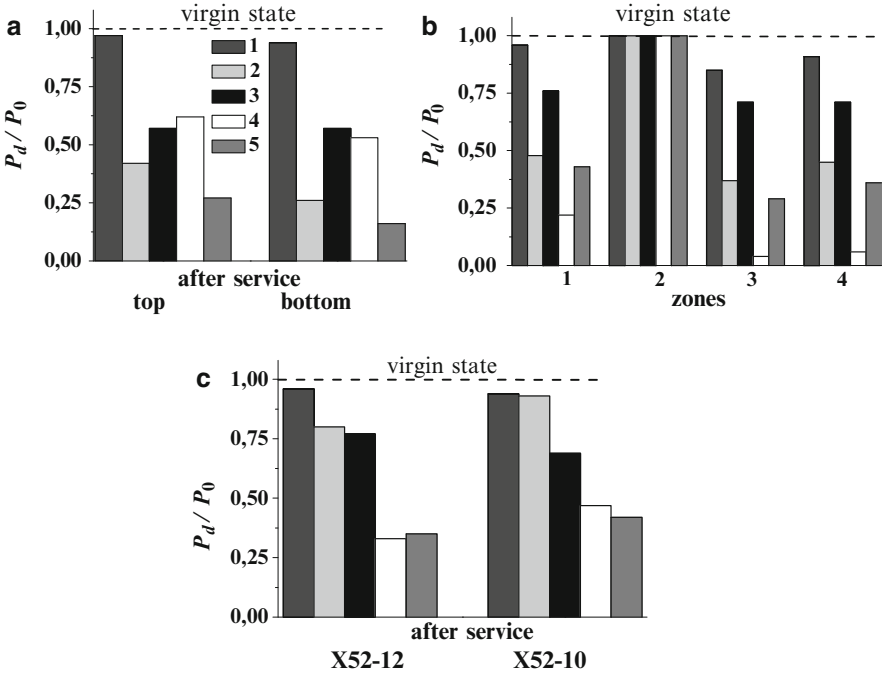


**Fig. 15** The effect of in-service time on electrochemical characteristics (parameter $P_d$) of (**a**) 10GS steel, (**b**) St.3sp and (**c**) API 5 L X52 in comparison to data from reference materials (parameter $P_0$): *1* – $E_{cor}$, *2* – $b_a$, *3* – $j_{cor}$, *4* – $j_a$, *5* – $R_p$

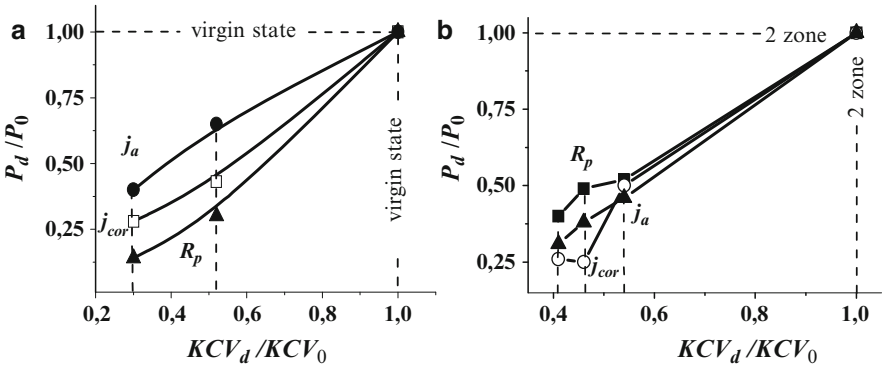


**Fig. 16** Correlation between relative changes in the ($P_d/P_0$) after long exposure to in-service conditions and degradation sensitive properties of metals: (**a**) 10GS steel; (**b**) St.3sp steel

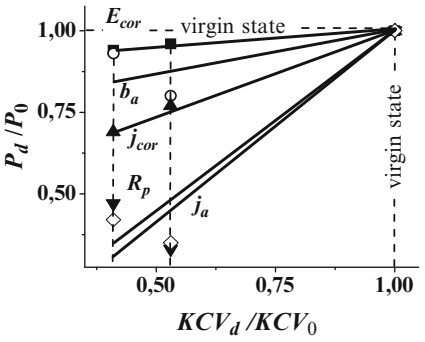


**Fig. 17** Correlation between relative changes in the ($P_d/P_0$) after long exposure to in-service conditions and degradation sensitive properties of API 5 L X52 steel

are the most sensitive indicators of the degradation. This approach can be used to monitor in-service degradation of materials exposed to benign environments (where the state of material is changed due the action of mechanical stresses only). If the material is exploited in aggressive environment, there is no evidence that only this environment should be used to investigate changes in electrochemical parameters. A clear correlation between the changes of the mechanical and electrochemical properties is demonstrated in Figs. 16 and 17.

Such a correlation can be used for a development of NDT methods for monitoring of degradation of mechanical properties. Those methods should take into account in-bulk material degradation due to the hydrogen intake. As a result, the material near the internal surface of pipeline can have different properties that the one near to the external. In field conditions, electrochemical properties are usually measured at the external surface. In such situation, it is recommended the estimation of the trough-the-wall-thickness structural gradients.

## 8 Conclusions

1. The following in-bulk material degradation modifying the mechanical and corrosion-mechanical properties of oil and gas main pipeline and storage tank steels exploited for 28–40 years was observed:
   - decrease in resistance to brittle fracture, revealed by a drop of impact strength, reduction of area, fracture toughness and resistance to stress corrosion cracking and hydrogen embrittlement,
   - anomalies of mechanical behaviour, specific of in-service embrittlement of metal: decrease in the resistance to brittle fracture simultaneously with decrease in hardness; opposite change of the plasticity parameters, decrease in the $R_A$ accompanied by increase in elongation,
   - special sensitivity of crack growth resistance characteristics of the in-service metal degradation; high sensitivity of impact toughness *KCV,* mainly caused by the decrease in the crack propagation energy component, i.e. by fracture mechanics parameters.
2. Metal degradation might be detected more efficiently under conditions promoting metal embrittlement, such as low temperature, tests in corrosion environments, and under action of hydrogen (application of cathodic polarization or tests on precracked specimens).
3. Generally, the degradation was higher in the *down* and especially *down-in* parts of the pipe, thus proving the negative effect of transported medium (due to the condensation of its aggressive components at the pipe bottom) and confirming the important role of hydrogen, absorbed by metal, in bulk material degradation.
4. The main factor of pipe degradation in the long-term service has been assumed to be the microdamage, which was indirectly confirmed by the improved efficiency of hydrogen trapping, increased ratio of deep hydrogen traps, increase in uniform elongation and decreased hardness. Two stages of the process due to long term service of main pipelines are considered: deformation aging and defects accumulation.
5. Monitoring of surface defects induced by corrosion and mechanical damage is insufficient for increase service life if one does not take into account possible degradation of the in-bulk material properties. It is possible to monitor in-bulk material properties changes by measurements of electrochemical characteristics. That opens up possibilities for the application of electrochemical methods for diagnostics of in-service degradation.

## References

1. Z.V. Slobodyan, H.M. Nykyforchyn, O.I. Petrushchak, Corrosion resistance of pipe steel in oil-water media. Mater. Sci. **N3**, 424–429 (2002)

2. H.M. Nykyforchyn, K.-J. Kurzydlowski, E. Lunarska, Hydrogen degradation of steels in long term service conditions, in *Environment-Induced Cracking of Materials*, ed. by S.A. Shipilov, R.H. Jones, J.-M. Olive, R.B. Rebak. Prediction, Industrial Developments and Evaluations, vol. 2 (Elsevier, Amsterdam, 2008), pp. 349–361
3. A.Y. Krasowsky, A.A. Dolgiy, V.M. Torop, Charpy testing to estimate pipeline steel degradation after 30 years of operation, in *Proceedings of Charpy Centary Conference*, vol. 1, Poitiers, 2001, pp. 489–495
4. A. Zagórski, H. Matysiak, O. Tsyrulnyk, O. Zvirko, H. Nykyforchyn, K. Kurzydlowski, Corrosion and stress corrosion cracking of exploited storage tank steel. Mater. Sci. **N3**, 113–117 (2004)
5. O.T. Tsyrulnyk, H.M. Nykyforchyn, YuD Petryna, M.I. Hredil, I.M. Dzioba, Hydrogen degradation of steels in gas mains after long period of operation. Mater. Sci. **N5**, 708–717 (2007)
6. H. Nykyforchyn, E. Lunarska, O. Tsyrulnyk, K. Nikiforov, G. Gabetta, Effect of the long-term service of the gas pipeline on the properties of the ferrite–pearlite steel. Mater. Corros. **N9**, 716–725 (2009)
7. H. Nykyforchyn, E. Lunarska, O.T. Tsyrulnyk, K. Nikiforov, M.E. Gennaro, G. Gabetta, Environmentally assisted "in-bulk" steel degradation of long term service gas trunkline. Eng. Fail. Anal. **17**, 624–632 (2010)
8. G. Gabetta, H.M. Nykyforchyn, E. Lunarska, P.P. Zonta, O.T. Tsyrulnyk, K. Nikiforov, M.I. Hredil, DYu Petryna, T. Vuherer, In-service degradation of gas trunk pipeline X52 steel. Mater. Sci. **N 1**, 104–119 (2008)
9. G. Gabetta, M. Margarone, Corrosion and flow models predictions compared using case histories, in *NACE Corrosion Conference Expo Paper 07522*, Nashville, Apr 2007, p. 13
10. V.M.A. Devanathan, Z. Stachurski, The mechanism of hydrogen evolution on iron in acid solutions by determination of permeation rates. J. Electrochem. Soc. **11**, 619–623 (1964)
11. E. Łunarska, Application of hydrogen permeation technique for estimation of gradual hydrogen induced degradation of steel, in *Proceedings of International Conference on Environmental Degradation of Engineering Materials*, ed. by A. Zieliński, D. Desjardins, vol. 1 (Gdańsk-Jurata, Gdańskie Towarzystwo Naukowe, 1999), pp. 32–37
12. Nechaev YuS, Metallic materials for the hydrogen energy industry and main gas pipelines: complex physical problems of aging, embrittlement, and failure. Usp. Fiz. Nauk Russ. Acad. Sci **N7**, 681–697 (2008)
13. H.M. Nykyforchyn, O.T. Tsyrulnyk, In-service degradation diagnostics of low-alloyed steels and aluminium alloys properties by electrochemical methods. Ultrasound **N1**, 46–49 (2009)

# Assessment Methodologies for Girth Weld Defects in Pipelines

**W.R. Tyson, S. Xu, and D.-M. Duan**

**Abstract** Imperfections such as lack-of-fusion and undercut are inevitable in field welding of pipelines. Also, small defects can grow in service by corrosion or fatigue. Above a certain size, such defects must be removed or repaired. In the present state of the art, determination of allowable defect size is done by Engineering Critical Assessment (ECA). ECA methods used in current international pipeline standards are reviewed and compared.

## 1 Introduction

Two common types of planar imperfection are found in pipelines: axial, and circumferential. Long axial cracks can develop from stress-corrosion cracking, and methods to assess the effects of such flaws are well developed and standardized in documents such as ASME B31G [1]. Circumferential flaws most commonly result from problems with field welding. The traditional approach to dealing with such flaws identified at the time of welding is to assess them against performance expected of good workmanship, and to repair them if they exceed this standard. However, occasionally flaws are detected by inspection after the normal construction period, when repairs are difficult and costly. Indeed, it is often the case that flaws larger than the workmanship standards are not a threat to the integrity of the pipe, and in such cases repairs are not only unnecessary but could lead to more problems than they solve. Since the early 1980s it has been possible to assess the effect of flaws on integrity using the concept of "fitness-for-purpose" and the methods of Engineering Critical Assessment (ECA). Various ECA methodologies have been developed, and codified in a plethora of standards in use around the world, such as FITNET [2].

W.R. Tyson (✉) and S. Xu
MTL/CANMET, Natural Resources Canada, Ottawa, Canada
e-mail: Bill.Tyson@nrcan-rncan.gc.ca; Su.Xu@nrcan-rncan.gc.ca

D.-M. Duan
TransCanada PipeLines Ltd., Calgary, Canada
e-mail: da-ming_duan@transcanada.com

T. Boukharouba et al. (eds.), *Integrity of Pipelines Transporting Hydrocarbons*,
NATO Science for Peace and Security Series C: Environmental Security,
DOI 10.1007/978-94-007-0588-3_6, 

For pipelines, ECA methods are provided as informative (non-mandatory) annexes to the pipeline standards of the Canadian Standards Association (CSA) [3] and the American Petroleum Institute (API) [4].

The current trend is to provide assessment at various levels of accuracy with, of course, the complexity and expense increasing with the level of accuracy, as exemplified by the various levels of analysis offered in the British Standards Institution document BS 7910 [5] on assessment of flaws in metallic structures. The "normal assessment route" recommended in BS 7910 is based on the Failure Assessment Diagram (FAD). This procedure has been adopted recently by the API, and is being evaluated by a work group of the CSA for possible incorporation in CSA Z662.

It is the objective of this paper to review the principles that form the foundation for ECA, and to discuss their application to assessment of girth weld defects in pipelines.

**Principles**: ECA is based on fracture mechanics, and it is first necessary to summarize the concepts used in this discipline. Fracture mechanics deals with the effect of a crack in a material on the conditions for structural failure, i.e. the load to extend the crack. The basic information required is: defect geometry, loads, and material properties. At its simplest level, the material is considered as a linear elastic solid which leads to "Linear Elastic Fracture Mechanics" (LEFM). More realistic results are obtained by treating the material as an elastic/plastic solid, in the framework of "Elastic Plastic Fracture Mechanics" (EPFM). Fracture mechanics is a well developed discipline and has been presented in a number of excellent textbooks such as, for example, Anderson [6] (from which many of the illustrations in this review have been drawn). The core concepts of fracture mechanics and of ECA are summarized below.

## 2 Fundamentals of Fracture Mechanics

### *2.1 LEFM*

Consider a planar crack in a solid with a tensile stress ($\sigma = \sigma_{yy}$) applied normal to the crack. The stress is concentrated at the crack tip, and if the solid deformed in a perfectly linear elastic fashion there would be a "$1/\sqrt{r}$ stress singularity" of stress as a function of distance r in front of the tip in the "singularity dominated zone" near the tip as shown in Fig. 1. The magnitude of the singularity is governed by a parameter called the "stress intensity factor" K, which for a "Mode I" crack (in which the tensile stress is normal to the crack plane) is called "$K_I$". $K_I$ is a function of geometry and applied stress.

For a "through" crack (with straight crack front) of length 2a centrally located in a very large plate, $K_I$ is given by the relation: $K_I = \sigma\sqrt{\pi a}$.

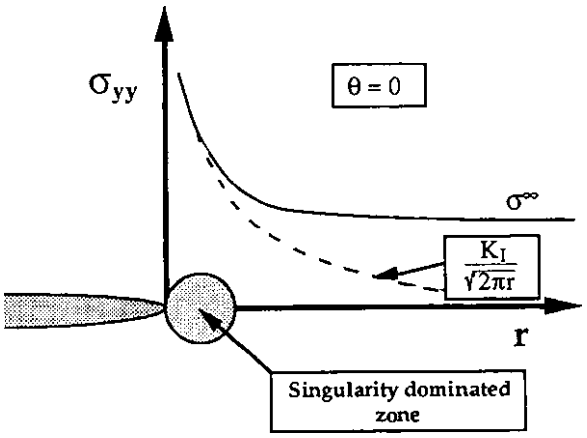


**Fig. 1** Stress distribution ahead of crack tip [6]

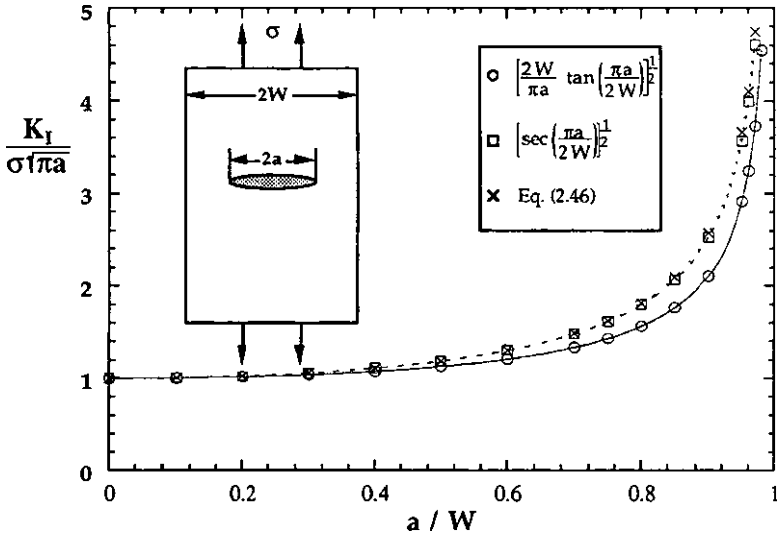


**Fig. 2** Stress intensity factor for central through crack in a plate [6]

For more complicated geometries, $K_I$ is still proportional to stress and can be written in the form $K_I = Y\ \sigma\sqrt{\pi a}$ where Y is a function of the geometry. For example, in a finite-width plate containing a central through crack, $Y = K_I/\ \sigma\sqrt{\pi a}$ is shown in Fig. 2. The increase in K as a/W approaches 1 results from the increase in the stress in the ligament between the crack and the plate edge above the level that would obtain in an infinite plate because of the reduction of load-bearing area. Various functional forms have been suggested to approximate the level of increase of K, as shown in the figure.

For other geometries of interest, such as surface semi-elliptical flaws in plates or circumferential surface flaws in pipes, stress distributions have been determined – usually by finite element analysis (FEA) – and results for the geometry factor Y have been widely published. The key factor is that K varies in proportion to the applied stress.

## 2.2 EPFM

In actuality, of course, engineering solids are not linear elastic; they are chosen specifically for their ability to dissipate stress by plastic deformation or other means. Pipe steels have been engineered to display a high level of both strength and toughness; the latter property depends on the ability of the material to deform plastically and show a high degree of ductility. The stress-strain properties of such steels can be adequately described by three parameters: the elastic modulus E, the yield stress σy, and the work hardening rate n (or N). Although there are complicating factors in many cases such as the presence of a "yield elongation" (sometimes called discontinuous yielding), in FEA the elastic-plastic stress-strain curve is generally described by a linear initial portion followed by a power-law work hardening region. The strength level of pipe steels has increased typically from X42 ($\sigma_y = 290$ MPa) in the 1950s to X100 and even X120 ($\sigma_y = 690$ and 830 MPa) currently under development. Work hardening coefficients are typically in the range n = 10–30. The key property of engineering steels is their ability to reduce the stress at the crack tip by plastic deformation, and thereby decrease the probability of fracture. The effect of this is shown in Fig. 3. The stress in the plastic zone is limited by the yield stress (shown as a constant value in Fig. 3; the effect of work hardening on increasing the stress within the plastic zone will be considered below). This redistributes the load in front of the crack, and in effect the elastic region is displaced away from the crack tip by a distance $r_y$ approximately equal to

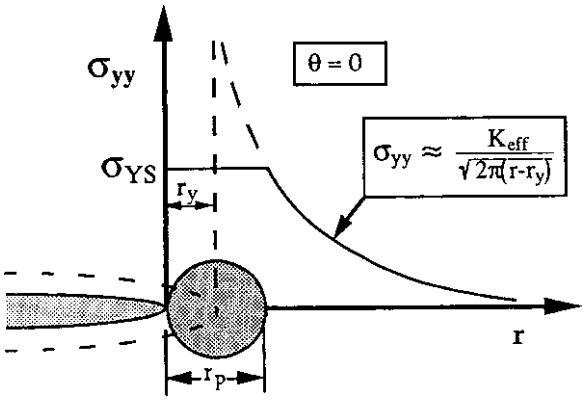


**Fig. 3** Irwin plastic zone correction [6]

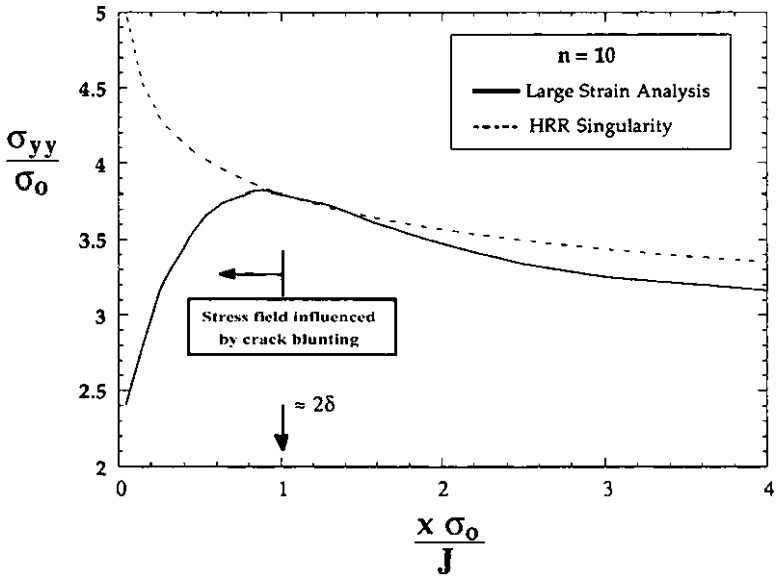


**Fig. 4** Stress distribution at crack tip in an elastic-plastic solid with strain hardening coefficient n = 10 [6]

half the plastic zone size $r_p$. This has the effect of increasing the magnitude of the stress intensity factor; Irwin has suggested that the effective stress intensity factor may be written as $K_{eff} = Y \cdot \sigma\sqrt{\pi(a + r_y)}$. The result is that the effect of plasticity at the crack tip is to increase K above the value it would have in a strictly elastic solid. This has important results on flaw analysis, as we shall see.

Actually, the stress in the plastic zone is not constant but increases with work hardening as the strain increases near the tip. The effect of this has been dealt with in EPFM. Figure 4 shows the so-called "HRR singularity" (after Hutchinson, Rice and Rosengren who first analysed the problem) as a dashed line. The mathematical form of the singularity is:

Given in Eq. 1 . The singularity is of much lower "strength" than the linear elastic singularity, with strength 1/(n + 1) compared with ½. The singularity results from the neglect of blunting as a result of plastic flow at the crack tip; this blunting has the effect of reducing the stress concentration. Large-deformation FEA can be used to account for the geometry change at the crack tip, with the results shown in Fig. 4 by the solid line. In any case, the HRR field well represents the stress at the crack tip within the plastic zone beyond a distance of about twice the CTOD δ (defined in Fig. 6), which includes the critical "process zone" within which the fracture micromechanisms of cleavage and microvoid coalescence occur.

The magnitude of the HRR singularity is controlled by the "J-integral" defined by Eq. 1. J is evaluated as a line integral taken around the crack tip. The details of the evaluation need not concern us here; they are described at length in standard textbooks. The key feature is that J increases as the stresses and strains within the

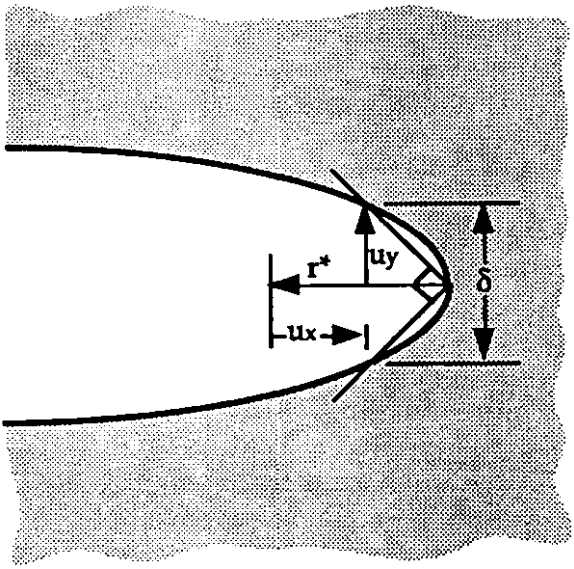


**Fig. 5** Definition of CTOD δ [6]

plastic zone increase in a way that can be expressed mathematically, evaluated for any geometry by FEA, and measured experimentally for simple geometries.

$$\sigma_{ij} = \sigma_0 \left( \frac{EJ}{\alpha\, \sigma_0^2 I_n\, r} \right)^{\frac{1}{n+1}} \cdot \tilde{\sigma}_{ij(n,\theta)} \tag{1}$$

With: $J = \int_{\Gamma} \left( W dy - T_i \frac{\partial u_i}{\partial X} ds \right)$

A driving force parameter complementary to J is δ, the crack-tip opening displacement (CTOD) defined in Fig. 5. The CTOD develops as a result of blunting in response to the high stresses and strains at the crack tip. There is a close correspondence between J and δ, as shown by the relationships in Eq. 2. Both J and δ can be divided into elastic and plastic components. The first relation, between J and K, holds only for the elastic component of J (note that E' is the "effective modulus": E in plane stress or $E/(1-\nu^2)$ in plane strain, where ν is Poisson's ratio). The second relation, between J and δ, is general, with m a parameter that depends on geometry and work hardening coefficient.

As noted in Eq. 2, m varies with constraint (notably plane stress or plane strain). The "constraint", essentially the hydrostatic component of the stress which inhibits plastic flow and consequent stress relief, is smaller in plane stress than in plane strain and so the deformation and blunting is larger in plane stress. That is, for a given crack driving force J the CTOD δ is larger for plane stress and so the value of m in the relation $J = m\sigma_y\delta$ must be smaller in this case. Note also that the relation between J and δ can be expressed in the form $J = (1/d_n)\sigma_o\delta$ where $\sigma_o$ is the yield stress in the power-law (Ramberg-Osgood) stress-strain relation. Hence, $m = (1/d_n)$ and so $d_n$ depends on constraint and work hardening coefficient as does m.

$$J = \frac{K^2}{E'} \tag{2a}$$

and:

$$J = m\ \sigma_{YS} \cdot \delta \tag{2b}$$

with: $m \approx 1$ (pl. stress) or $\approx 2$ (pl. strain); or,

$$J = \left(\frac{1}{d_n}\right) \cdot\ \sigma_0\, \delta$$

with: $d_n$ dependent on $\sigma_0$, n, and contraint

Either J or δ may be used as the crack driving force, and these parameters are inter-related by Eq. 2. As the applied load increases, the driving force increases as well. The linear elastic portion of J is given by $J = K^2/E'$, and so increases quadratically with stress since K is proportional to stress. However, as the applied load increases, the plastic zone size increases, and the total driving force (elastic + plastic) increases more rapidly than the linear elastic component. This may be understood from Fig. 3; the effective crack size increases as the plastic zone grows.

The result is that J varies with applied load as shown in Fig. 6. The linear elastic component increases quadratically (proportionally to (applied load)$^2$) and the

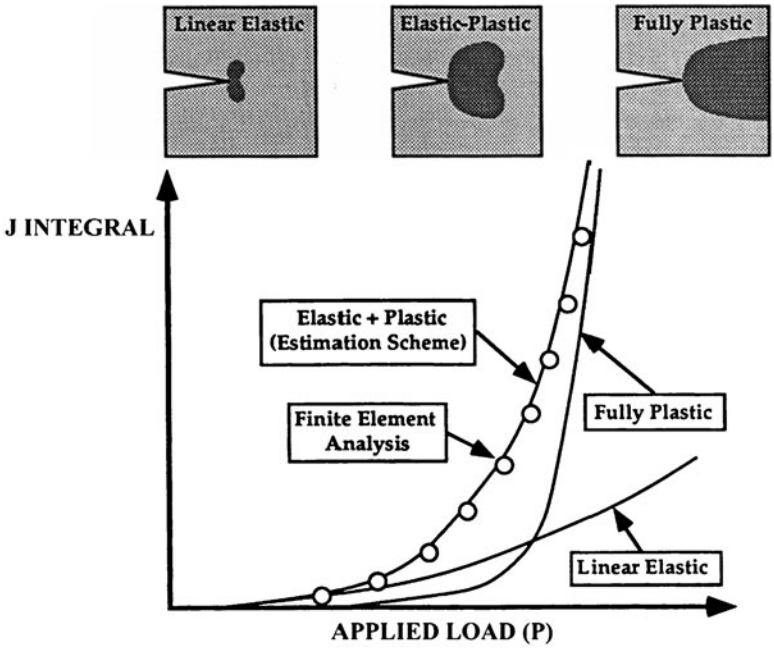


**Fig. 6** Evolution of J-integral with applied load [6]

plastic component grows rapidly as the extent of plasticity increases. $J_{plastic}$ is very large as the limit load is reached, where the "limit load" is the load at which plasticity spreads across the remaining ligament. The applied stress at limit load is commonly termed the "collapse stress" $\sigma_c$; care must be taken in noting whether the context implies that this should be calculated when the ligament stress reaches the yield stress $\sigma_y$ or the "flow stress" $\sigma_f = (\sigma_y + \sigma_{UTS})$ where $\sigma_{UTS}$ is the ultimate tensile strength.

## 3 Fundamentals of ECA

When the crack-tip driving force reaches a critical value dependent on the material (the "toughness"), then crack propagation occurs. This occurs in LEFM at $K = K_{IC}$, and in EPFM at $J = J_{IC}$ or $\delta = \delta_{IC}$. ECA involves the estimation of the crack driving force for a given crack geometry and load, and comparison of driving force with material toughness. J and δ may be expressed as functions of remote σ (stress-based design) or ε (strain-based design, SBD).

The simplest situation is one in which it is possible to define a "critical toughness" at which failure occurs, i.e. in LEFM at $K = K_{IC}$. Then ECA may be performed using the FAD of Fig. 7, in which the proximity to fracture is estimated (at the "assessment point") using $K_r = K/K_{IC}$ and the proximity to collapse is estimated using $\sigma_r = \sigma/\sigma_c$ where σ is the applied stress and $\sigma_c$ is the collapse

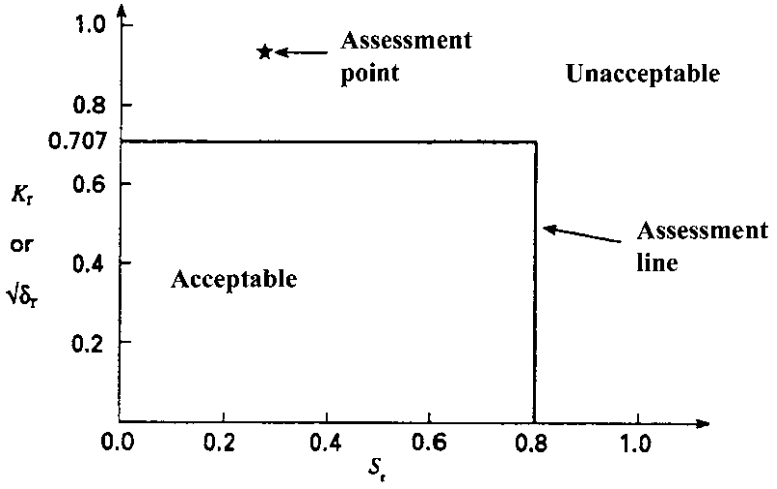


**Fig. 7** "Level 1" FAD [6]

stress defined above. If the stress is low enough, then the assessment point will lie below both the fracture condition and the collapse condition and will be in the "Acceptable" part of the FAD. However, as the stress increases, the assessment point moves linearly away from the origin (note that both K and σ are proportional to applied load) and eventually crosses into the "Unacceptable" region, where failure either by fracture or plastic collapse is predicted.

If there is substantial plastic deformation, EPFM must be used. In this case, there will be an increase in J with applied stress above the elastic value as described above. Then, using as axes $K_r = \sqrt{J_e/J}$ and $L_r$ or $\sigma_r = \sigma/\sigma_c$ (where the collapse stress is usually defined as the limit load in which the ligament reaches the yield stress rather than the flow stress), we may derive an elastic-plastic FAD as shown in Fig. 8. This FAD reflects the fact that the total J increases more rapidly than the elastic J as the applied stress increases, and becomes very large at the limit load. In other words, $K_r$ begins at $K_r = 1$ and drops rapidly near the limit load. The FAD of Fig. 8 is used in the same way as that in Fig. 7, with the assessment point lying either in "Acceptable" or "Unacceptable" portions of the diagram.

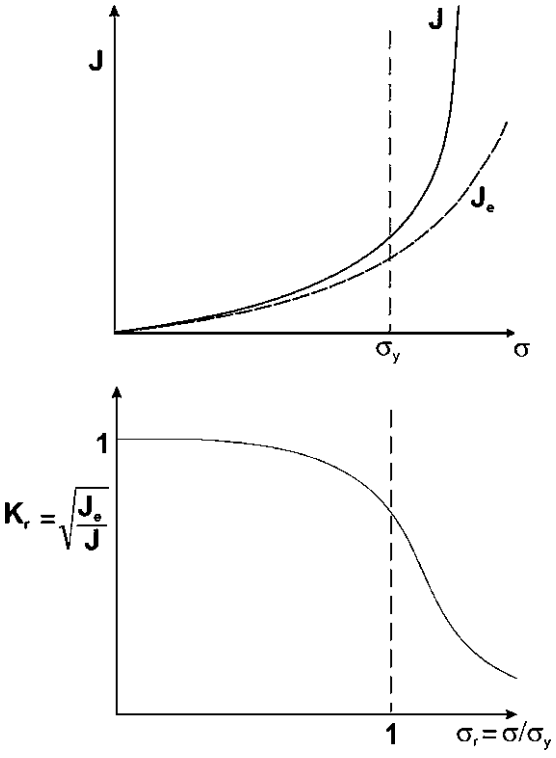


**Fig. 8** Construction of FAD using EPFM

## 4 Toughness Testing

In order to perform an ECA, it is necessary to measure the toughness of the material. This is commonly done using bend bar specimens, as shown in Fig. 11, from ASTM E 1820 [7].

The load and crack mouth opening displacement (CMOD) are monitored during the test, and the CMOD compliance is measured by periodic unloading of the specimen. The J-integral is calculated from the area under the load-CMOD curve, using equations developed using FEA in combination with the J-integral definition in Fig. 3. The crack length is deduced from the CMOD compliance, again from equations developed using FEA. The result is a curve of J-integral as a function of crack growth Δa, the so-called "Resistance curve" (R-curve). From the R-curve, critical values of toughness may be derived, such as values at a particular amount of crack extension or at maximum load of the test specimen. Similarly, CTOD values may be calculated from J using equations similar to those of Fig. 5, using values of the parameter m (given in the test standard) estimated from FEA as a function of work hardening coefficient and specimen geometry (i.e a/W for the bend bar, where a is crack length, and W is specimen width as shown in Fig. 9).

For weld testing, the commonly used standard is Part 2 of the British Standards Institution toughness testing standard BS 7448 [8]. This document gives details for dealing with residual stresses in pre-cracking, control of notch placement in the desired microstructure, etc.

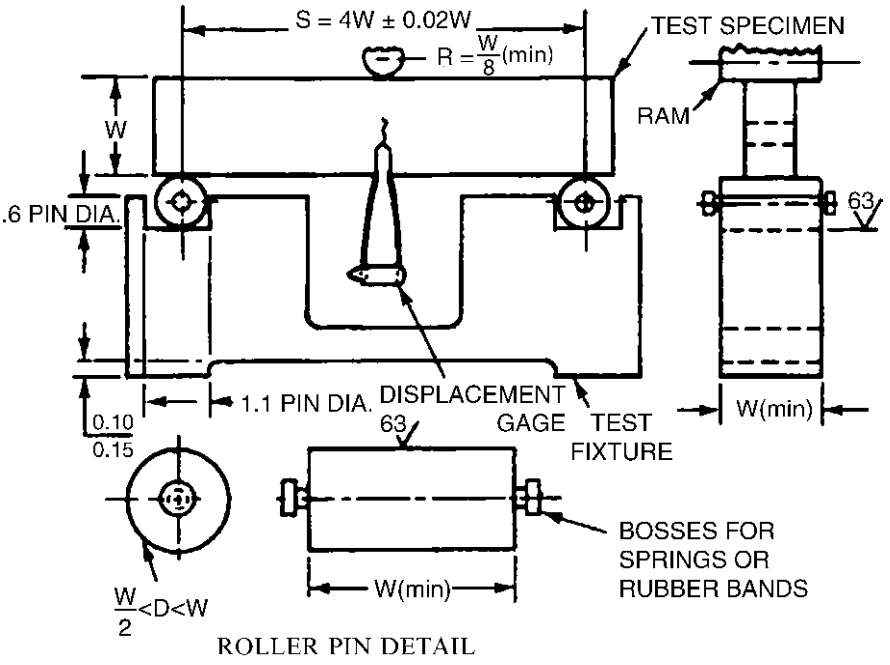


**Fig. 9** Test specimen set-up, from ASTM E 1820 [7]

## 5 Current Standards

The focus in this paper is on girth weld flaws in pipelines, as shown in Fig. 10. These are typically semi-elliptical surface flaws, of length 2c and height (depth) a.

In North America, the pipeline standards in use are those of the Canadian Standards Association (CSA Z662, "Oil and Gas Pipeline Systems") [3], and the American Petroleum Institute (API Standard 1104, "Welding of Pipelines and Related Facilities") [4] as mentioned in the Introduction. Internationally, the British standard BS 7910, "Guide to methods for assessing the acceptability of flaws in metallic structures", [5] is commonly referred to.

The ECA methodology used in the CSA standard is based on the first methodology to be developed for assessing weld defects, the so-called "COD design curve". This curve enables the derivation of a lower-bound fracture prediction by comparing a plasticity-corrected CTOD driving force with the toughness measured at brittle fracture or maximum load. It is similar to the "Level 1" FAD of BS 7910 shown in Fig. 7. The collapse stress is derived from the "Miller equation" [9] modified to fit experimental data on failure of pipes containing circumferential (girth) flaws.

In the API standard [4], two levels of analysis are offered. The first is a simplified procedure requiring a minimum amount of data. The second is based on an FAD similar to that of Level 2 of BS 7910. The stress intensity factors are estimated from an analytic fit to FEA results of Chapuliot et al. [10].

In a project currently under way at CANMET, a comparison is being made of acceptable flaw sizes using ECA based on the different standards. In addition to the "COD design curve" approach of the CSA standard, FAD methodologies as represented by Level 2 of BS 7910 (Fig. 11) are being compared. The normal assessment route of Level 2A (the dotted curve) uses a generalized lower-bound failure curve requiring no detailed stress-strain data, and Level 2B allows calculation of a less conservative material-dependent failure curve dependent on the work hardening coefficient.

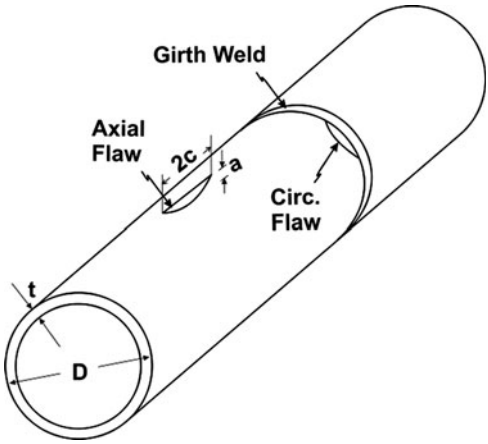


**Fig. 10** Typical flaws in pipe

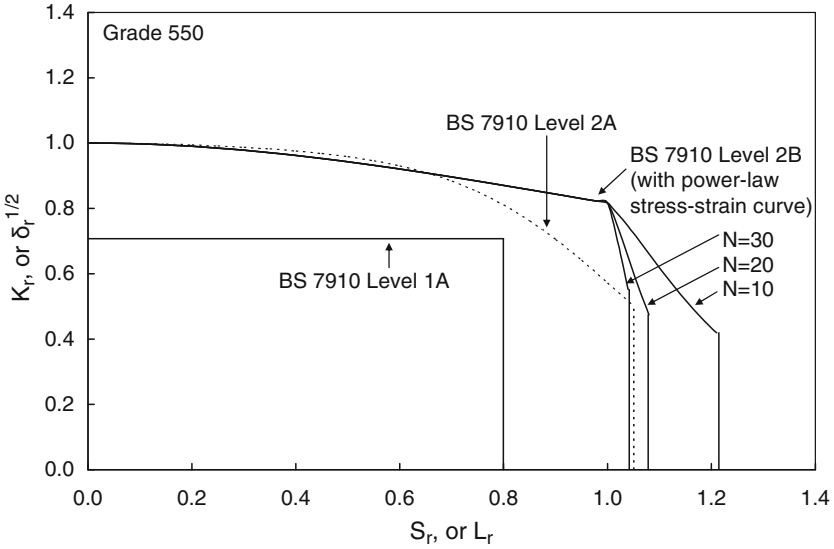


**Fig. 11** FAD (*Level 2*) of BS 7910

A useful format to show the results is that of a graph of an "allowable flaw size" in which flaw sizes deduced from assessment points lying on the failure curve with subsequent application of safety factors are shown. Figure 14 is such a graph, in which the allowable length of a surface semi-elliptical flaw is shown as a function of the flaw depth (height) of the flaw according to the three different standards. Note that there is a maximum length of allowable flaw according to CSA and API, of 10% and 12.5% of the pipe circumference. Similarly, in both standards there is a maximum allowable depth of 50% of wall thickness for gas pipelines. Different segments of the curves in Fig. 12 correspond to different failure mechanisms of fracture (crack propagation) or ductile overload (plastic collapse). There is not a great deal of difference between the "Level 1" assessments of the three standards for the particular case in Fig. 12 (details of pipe, material, and stress are given in the figure). The FAD methodologies are represented by BS 7910 Level 2A and API Append. A Option 2. The BSI curve is less conservative than the API curve, although both are based on the same FAD. The difference is due largely to a difference in collapse stress; BSI uses an equation proposed by Kastner, while API uses a conservatively modified Miller equation. The Miller equation predicts collapse at a significantly lower stress than that of Kastner.

There would be obvious practical and economic benefits in using the less conservative approach, provided that it could be demonstrated that there is an adequate "failure reserve factor" that can be defined as the actual failure stress divided by the predicted failure stress. Such factors can be calculated from experimental data such as that shown in Fig. 13.

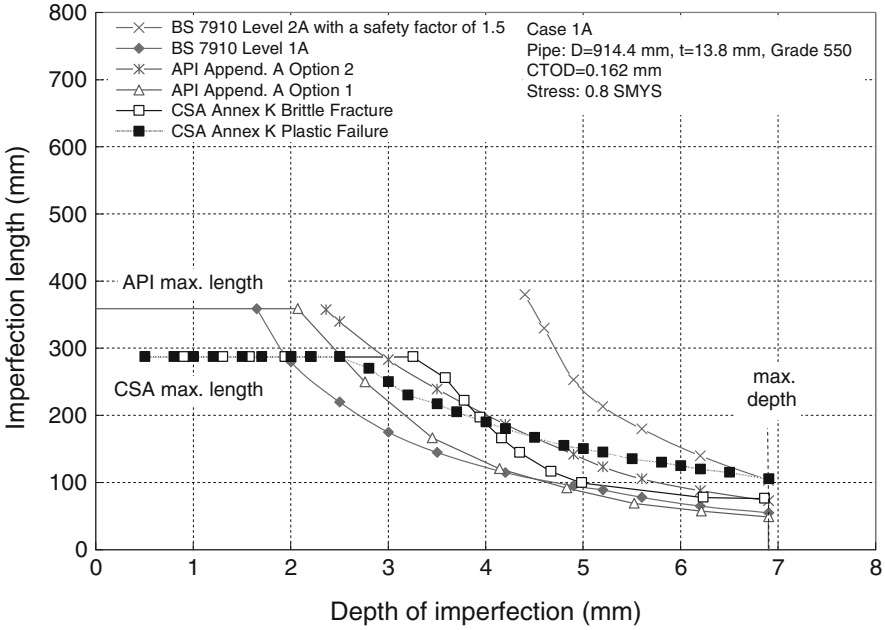


**Fig. 12** Allowable flaw size according to various standards

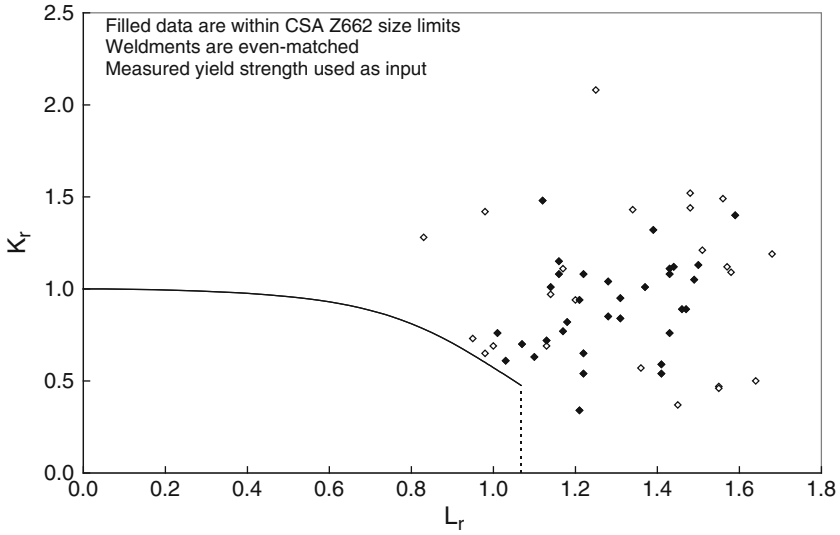


**Fig. 13** Full-scale pipe experimental failure data compared with FAD of BS 7910 Level 2A; no explicit safety factor

All the results in the figure are conservatively predicted, in the sense that failure occurred at stresses larger than those on the failure curve.

Note that the failure reserve factor defined above can be calculated from the ratio of (length of a line from the origin to the failure point)/(length from the origin to the FAD failure curve), since the variables on both axes vary linearly with applied stress. The data shown in Fig. 13 have an average reserve factor of about 1.5. At first sight, it is surprising that the data are all above the failure curve rather than scattered about it, since the failure curve purports to predict the conditions at failure. However, there are a number of conservatisms built into the methodology as follows:

- the failure curve is a lower bound for a wide variety of geometries,
- the critical CTOD values are conservatively estimated, since most standards require three separate tests with the critical CTOD taken as the lowest of the three,
- no allowance is made for differences in constraint between test specimen and full-scale pipe; since the former is in bending and the latter is in tension, the toughness relevant to the pipe is higher than measured in the test owing to the lower constraint,
- the applied tensile stress is overestimated for pipe in bending owing to use of the elastic formula for the outer fibre stress [11],
- the equation used for the collapse stress is conservative, as shown by a number of experimental results.

These conservatisms accumulate to provide a substantial reserve factor. There are countervailing factors however, such as the neglect of residual stresses, neglect of geometrical stress concentrations such as high-low offset of the two sides of the weld, and neglect of the effects of yield discontinuities which can generate large crack driving forces near the limit load. Nevertheless, there are no failures at stresses below the failure curve in Fig. 13 even though all these countervailing influences could be present and no explicit safety factor has been imposed (such as requiring the maximum flaw size to be half the critical size, which is equivalent to shrinking the FAD toward the origin). For application to pipelines currently being constructed, there are a number of factors that add to conservatism. The measurement of CTOD is currently more conservative than in the past, since values measured by older standards, based on specimen rotation about an axis in the ligament, can be significantly larger than values measured from FEA and J as now incorporated, for example, in ASTM E 1820 [7]. For assessment purposes the specified minimum yield stress (SMYS) is used rather than the actual yield stress, and since actual yields are typically 10–20% higher than SMYS this adds a significant reserve to the collapse stress. The "worst-case" scenario is used to estimate applied stress.

Location of the flaw is seldom at the point of maximum tensile stress. However, in the final analysis, decisions on the optimum degree of conservatism are matters of engineering judgment. In particular, not only the average failure reserve factor but also its standard deviation need to be considered.

## 6 Conclusions

Flaws are inevitably encountered in girth welds in pipelines. Every precaution should be taken to ensure that the size of such flaws do not exceed workmanship standards, because this would imply sub-standard workmanship that could be associated with even worse problems. Modern methods of flaw detection are increasingly reliable, and when flaws are detected a decision must be made to accept them or take remedial measures. ECA has been developed to assist engineers to make this decision. Using simplified or more sophisticated methods such as those described in this paper enables a judgement to be made on whether flaws are structurally significantly or not. It is especially important to ensure adequate mechanical testing of samples representative of construction welds to ensure that toughness properties are well characterized.

**Acknowledgment** This paper provides background material that has been acquired by the authors over many years of experience in the field of fracture mechanics applied to pipelines. The authors are grateful to their employers (MTL/CANMET and TransCanada PipeLines Ltd., TCPL) for providing the opportunity to obtain this knowledge. The authors are grateful to TCPL for supporting the work on application of the Failure Assessment Diagram to pipeline girth welds.

## References

1. ASME B31G, *Manual for Determining the Remaining Strength of Corroded Pipelines* (ASME, New York, 2009)
2. FITNET, M. Kocak, *FITNET Fitness-for-Service (FFS) Procedure, Revision MK8, 2008* (GKSS Research Centre, Geestacht, 2008)
3. CSA Standard Z662-07, *Oil and Gas Pipeline Systems*. Annex K: Standards of Aceptability for Circumferential Pipe Butt Welds Based Upon Fracture Mechanics Principles (Canadian Standards Association, Mississauga, 2007)
4. API Standard 1104, *Welding of Pipelines and Related Facilities*, 20th edn. (API Publishing Services, Washington, 2005). Errata July 2007, December 2008
5. BS 7910:2005, *Guide to Methods for Assessing the Acceptability of Flaws in Metallic Structures* (British Standards Institution, London, 2005). Amended September 2007
6. Ted L. Anderson, *Fracture Mechanics: Fundamentals and Applications*, 2nd edn. (CRC Press, Boca Raton, 1994). 3rd edn. 2005
7. ASTM E 1820, *Standard Test Method for Measurement of Fracture Toughness* (ASTM International, West Conshohocken, 2009)
8. BS 7448, *Fracture Mechanics Toughness Tests*, Part 1 (for Homogeneous Materials) and Part 2 (for Welds) (British Standards Institution, London, 1991)
9. A.G. Miller, Review of limit loads of structures containing defects. Int. J. Pres. Ves. Piping **32**, 197–327 (1988)
10. S. Chapuliot, M.H. Lacire, P. Le Delliou, Stress intensity factors for internal circumferential cracks in tubes over a wide range of radius over thickness ratios. ASME **365**, 95–106 (1998)
11. G. Wilkowski, D.J. Shim, F.W. Brust, P. Krishnaswamy, Inherent safety factors in the API girth weld defect tolerance analysis – Part II, *Proceedings of Pipeline Technology Conference*, Ostend, 12–14 Oct 2009, Paper no. 2009-006

# Weldability of a Supermartensitic Stainless Steel 12Cr4Ni1Mo Pipeline and the Effect of Welding Current on Precipitated Ferrite δ in the HAZ

**A. Nouri and M. Bouabdallah**

**Abstract** The weldability of the recently introduced supermartensitic stainless steel (SMSS) 12.5Cr4Ni1Mo is investigated by observing the emerging phases resulting from the weld in the heat affected zone and the melted zone as well. We noticed a practically similar martensitic structure to be dominant in the melted zone of TIG autogenous welds after normal cooling conditions. Some ferrite δ phase was observed to precipitate in the heat affected zone. This emerging ferrite δ phase was observed to precipitate according to a specific pattern localized in the heat affected zone. This pattern was found to be closely related to the welding parameters, especially the welding current. We attempted to establish experimentally a correlation between the welding current and the percentage of precipitated ferrite δ phase in the heat affected zone. The study presents as well an experimental evaluation of some mechanical properties of TIG autogenous welds on (SMSS) stainless steel 12.5Cr4Ni1Mo simulating the use of matching welding consumable. The obtained results, so far, lead to an interesting convenience of investigating the use of matching welding consumable with such steel.

## 1 Introduction

The (SMSS) with a high tensile strength associated to a much better corrosion resistance against $CO_2$ and $H_2S$ in sweet and mildly sour environments [1] is reported to have a remarkable improved weldability with a much softer martensite structure compared to conventional martensitic stainless steels [2]. Because of this combination of qualities, in addition to a fairly low cost, this new class of stainless

A. Nouri (✉) and M. Bouabdallah
National Polytechnic School of Algeria, 10, Avenue Hassen Badi,
BP 182, El Harrach 16200, Algeria
e-mail: ahmed.nouri@ymail.com; mabrouk.bouabdallah@enp.edu.dz

T. Boukharouba et al. (eds.), *Integrity of Pipelines Transporting Hydrocarbons*,
NATO Science for Peace and Security Series C: Environmental Security,
DOI 10.1007/978-94-007-0588-3_7, 

steels presents an economical alternative in several industrial applications requiring high class materials especially pipeline applications.

The weldability of such (SMSS) stainless steels is a major gain observed practically in all the different types of (SMSS) [3, 4] as classified by Marshall&Al (lean, medium and high). The improved weldability of this new emerging class of stainless steels was subject to numerous experimentations and studies including the use of different welding processes using different welding consumables [1]. In the early stages, satisfactory results were obtained for the weld of SMSS using superduplex stainless steels consumables under TIG and MIG processes. More lately, many research studies suggested different welding consumables as a more suitable choice especially matching consumables for the welding of SMSS [5]. However, because of the variation in the percentage of alloying elements, each type of (SMSS) reacts differently to welding operation on a microstructural level. In general, tow major welding effects are frequently mentioned to occur in the heat affected zone of (SMSS): firstly a martensite coarsening in the HAZ progressing toward the adjacent region to the weld [6, 7] and secondly the emergence of ferrite δ [3, 4, 7]. The latest outcome is of particular interest since the substantial affect that ferrite δ can have on the mechanical and the chemical properties of the weld joint [8, 9].

## 2 Experimental

Controlled TIG welding operations were carried out using different welding current intensities under Gas shield protection on several identical samples of the medium (SMSS) 12.5Cr4Ni1Mo taken from a 15 Cm pipe. Tow welding cases have been subject to our investigation: A first case with an autogenous TIG weld without using any consumable and a second case using a low Carbone austenitic stainless steel consumable (0.019C, 18Cr, 12Ni, 2.8Mo). All welding operations were done at a constant speed of 15 cm/min using direct current. The weld joints were investigated with metallographic examination by optical microscopy, and X-ray diffraction examination. The martensitic structure was revealed by immersion etching in aqueous Kalling's reagent. The ferrite δ was revealed by electrolytic etching in sodium hydroxide.

In the welded specimens, the X-ray examination was carried out as much restricted as possible to the adjacent region around the weld joint frontier, that's to say an area about 4 mm large around the frontier line between the melted zone and the base metal (Fig. 1).

All the samples subject to X-ray examination where polished aggressively using electrolytic etching several times prior to examination.

Charpy testing was performed on samples taken in the longitudinal axe of the pipe. The samples were prepared with a **U** notch. The tests were carried out at a temperature of 20°C.

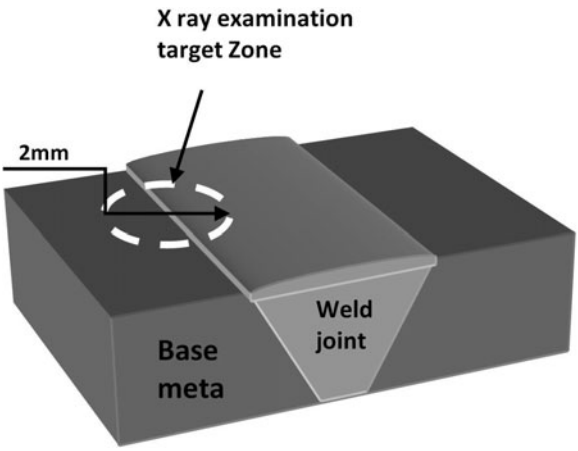


**Fig. 1** Area subject to X-ray examination in the welded specimen

## 3 Results and Discussion

### *3.1 Mechanical Study*

Because of the gradient nature of heat transfer, we have observed a certain gradual grow of martensite grains in the HAZ zone that might affect some mechanical properties (Fig. 2).

Compared to the base metal, the most affected HAZ region by the heat presents a higher hardness value. It is to be noticed that the melted zone of the (SMSS) have a softer martensite than the one of the HAZ region according to hardness testing.

The impact value was tested in different cases including base metal in received state as a reference. A comparison between the base metal and the autogenous weld shows a good continuity of the toughness impact value between the autogenous weld joint and the base metal. The tow prior results were higher compared to the impact value for an austenitic weld joint carried out by TIG on the same SMSS with the austenitic stainless steel consumable (0.019C, 18Cr, 12Ni, 2.8Mo).

### *3.2 Microstructural Study*

The microstructure of the base metal at the obtained state was investigated first to reveal the microstructure. According to optical observation, the microstructure is practically constituted of martensite.

The X-ray examination of the base metal at the received state confirms a mostly martensitic microstructure. A small amount of austenite is revealed as well, invisible under optical microscopy observation, and estimated to about 4% against 96% of martensite according to the collected X-ray data.

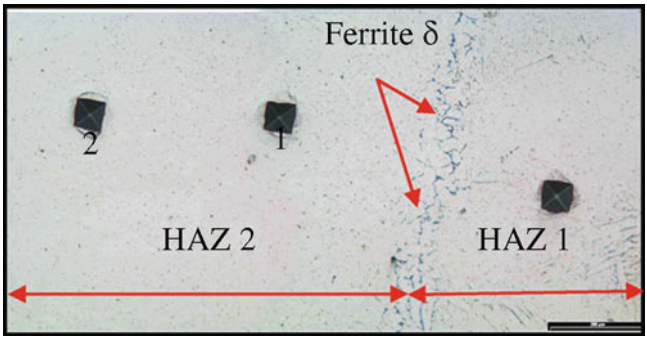


**Fig. 2** Microhardness variation in the HAZ zone

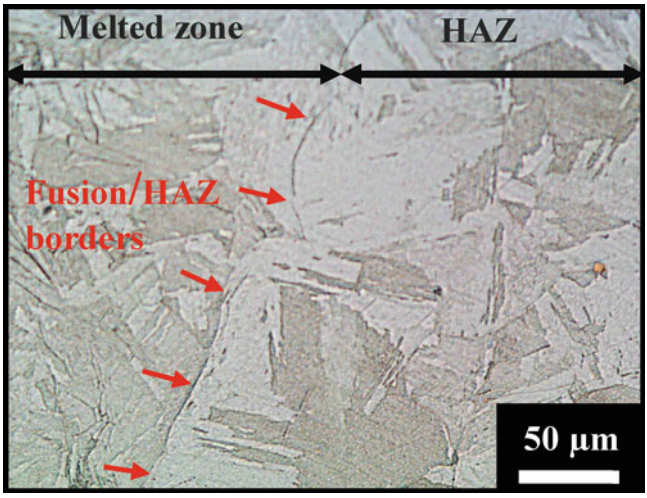


**Fig. 3** Autogenous TIG weldement microstructure

The autogenous TIG weld was found to outcome some characteristic results both in the melted zone and the heat affected zone as well. In the melted zone, the microstructure was still practically martensitic.

The matensite grains in the melted zone were consequently larger compared to the base metal at the initial state. No new phases are observed in the melted zone under natural cooling in one pass weld (Figs. 3 and 4).

In the heat affected zone, we observed a martensite coarsening in the HAZ growing toward the fusion frontiers of the weld to become consequently bulky (Fig. 4).

Some ferrite δ was observed to precipitate in the heat affected zone. This ferrite δ was noticed to precipitate according to a specific pattern localized exactly between tow distinguished regions of the HAZ presenting clearly tow different martensite grains size (Fig. 5).

According to optical microscope observation and X-ray diffraction data, there are no other new precipitated phases beside ferrite δ in the HAZ zone.

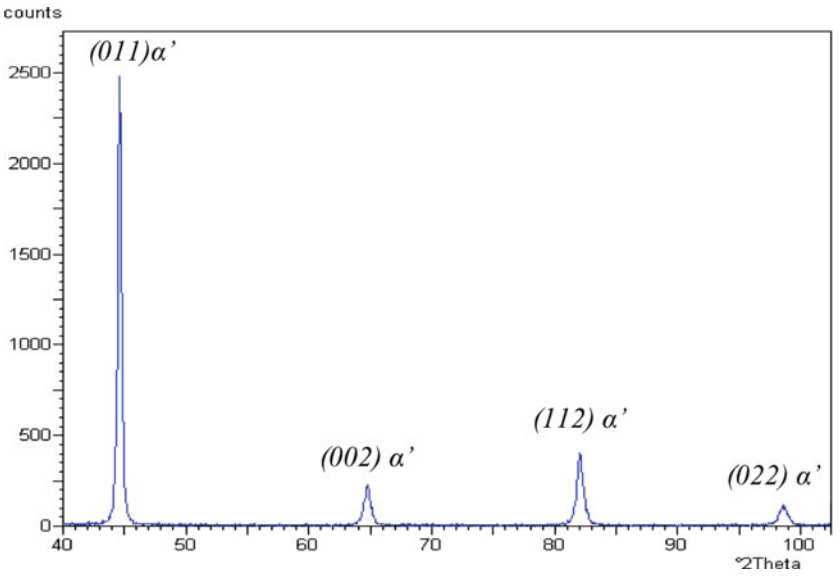


**Fig. 4** Autogenous TIG weldement X-ray examination

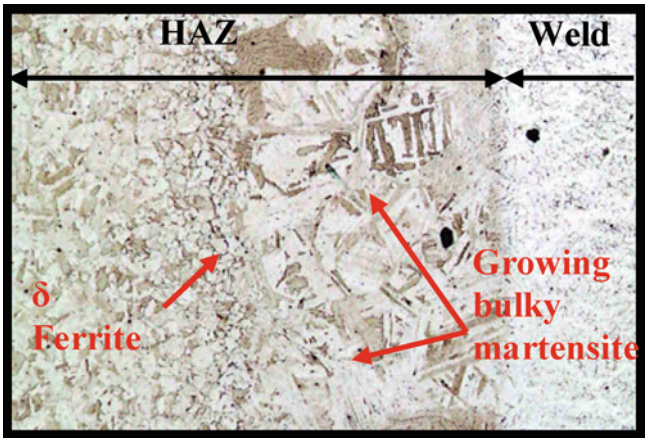


**Fig. 5** HAZ zone in the SMSS

The ferrite δ precipitates into a formation of a strip parallel with the frontier of the melted zone (Fig. 6).

It has been noticed that this strip of precipitated ferrite δ separates the HAZ into tow distinguished zones according to the size of the martensite. The HAZ region located to the side of the melted zone presents a significant larger coarsening effect of the martensite grains. On the other side, the HAZ region located toward the base metal presents a gradually much smaller matensite grains (Fig. 5). The precipitation pattern of ferrite δ was found to be closely related to the welding parameters, especially the welding current. Higher welding currents induced larger percentage of precipitated ferrite δ in the HAZ (Fig. 7).

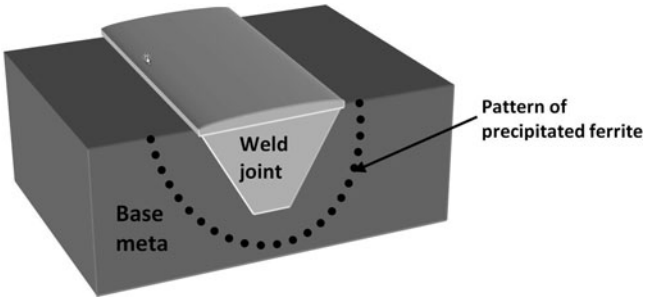


**Fig. 6** The observed characteristic pattern of precipitated ferrite δ

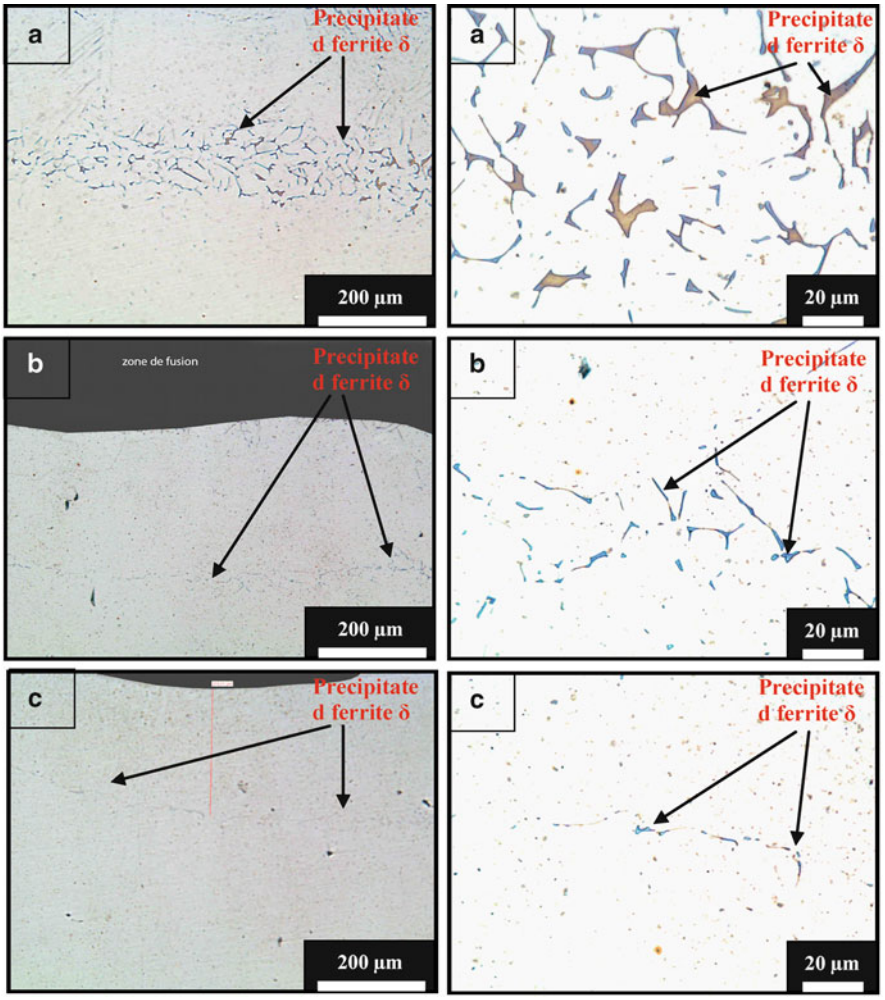


**Fig. 7** Morphology of precipitated ferrite δ in the HAZ of SMSS TIG weldements corresponding to different welding current intensities, a1&a2 at 200A; c1&c2 at 120A; b1&b2 at 65A

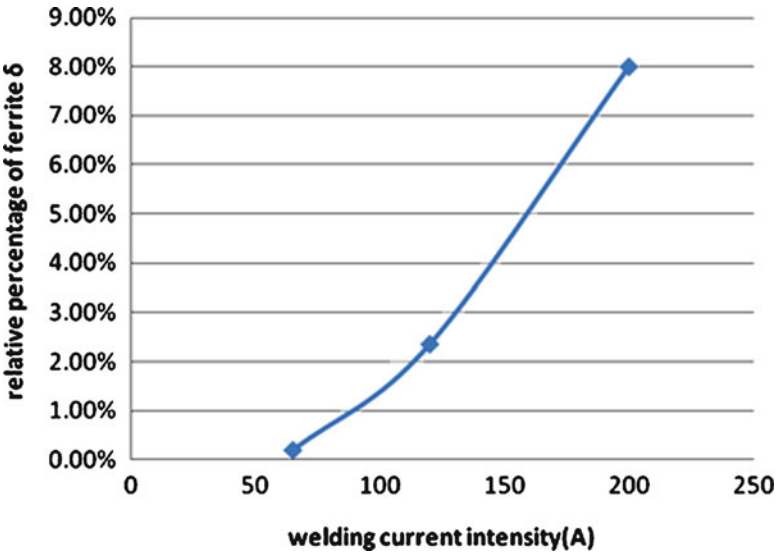


**Fig. 8** Effect of Welding Current on the volumetric percentage of precipitated ferrite δ in the HAZ of 12.5Cr4Ni1Mo (SMSS)

The morphology of ferrite strip was observed to change according to three major parameters when changing the welding current intensity:

- firstly, the global fraction of the precipitated ferrite that increases with the increase of the welding current intensity,
- secondly, the width of the precipitated ferrite strip that increases with the increase of the welding current intensity and thirdly, the distance between the ferrite strip and the welding frontier that increases with the increase of the welding current intensity.

The obtained results led us to establish experimentally a quantification of the influence of welding current intensity on the amount of precipitated ferrite δ in the HAZ (Fig. 8). It is clear that increasing the welding current causes excess heat, which increases the rate of ferrite δ precipitation in the HAZ.

## 4 Conclusion

We have concluded in this work the possibility to establish experimentally a relationship between the welding current intensity and the volume of precipitated ferrite δ in the (SMSS) 12.5Cr4Ni1Mo. It has been deducted that the amount of precipitated ferrite δ increases with the increase of the welding current intensity. The prediction of such parameter allows an important optimization of the welding operation.

During this work, we noticed the interesting possibility of using a matching welding consumable in the case of the investigated steel and giving a highly homogenous continuity of the martensitic structure between the melted zone and the base metal without a critical need for an after welding heat treatment.

**Acknowledgments** We are grateful to the organizing team of the NATO workshop, especialy Pr BOUKHAROUBA, for making such valuable opportunity possible. We are thankful to the team of DML, SONATRACH, ALGERIA for allowing us to use their facility. We are thankful to Dr Abdallah Nouri in SIMAP, INP, France for helping to provide the samples. We wish to thank all the members of the Advisory Committee for their valuable advice and review. We are deeply grateful to who ever contributed in achieving and improving this work.

## References

1. M. Ueda, H. Amaya, K. Ogawa, Kunio Kondo, T. Mori, Corrosion resistance of weldable super 13Cr stainless steel in H2S containing CO2 environments, in *Corrosion 96*, NACE International, Denver, 1996, 24–29 March 1996
2. K. Kondo, K. Ogawa, H. Amaya, M. Ueda, H. Ohtani, Development of weldable super 13Cr martensitic stainless steel for flowline, in *International Offshore and Polar Engineering Conference*, Kitakyushu, 2002
3. T.G. Gooch, P. Woollin, A.G. Haynes, Welding metallurgy of low carbon 13% chromium martensitic steels, *Supermartensitic Stainless Steels 99*, Brussels, 1999
4. J.C. Lippold, D.J. Kotecki, *Welding Metallurgy and Weldability of Stainless Steels*, A John Wiley & Sons, Inc. Publication, 2005, *ISBN 0-471-47379-0*. P80;82
5. M. Goldschmitz, L. Carlsson, R. Pedersen, S. Rigdal, J. Vandenbroek, Developments in the welding of supermartensitic stainless steels: recent developments and applications, in *Welding International* 2004, Houston, 2004
6. J.K. Solberg, E.V. Ladanova, G. Rorvik, Post weld heat treatment response of coarse grained heat affected zone in a supermartensitic stainless steel, in *Supermartensitic Stainless Steels 99*, Brussel, 1999
7. P. Woollin, D. Carrouge, Heat affected zone microstructures in supermartensitic stainless steels, in *Supermartensitic Stainless Steels 2002*, Brussels, 2002
8. J. Zaayman, G.T. Van Rooyen, The toughness of the heat affected zone of welds in 11.5 percent chromium steels, in *1st International Chromium Steels and Alloys Congress*, vol. 2, SAIMM, Johannesburg, 1992
9. G. Cumino, A. Poli, T. Ono, S. Hashizume, K. Yamazaki, L. Scoppio, Supermartensitique 13% cr large diameter seamless pipes: mechanical corrosion and weldability properties. Latin Am. Appl. Res. **32**, 215–219 (2002)

# "Canadian Experience in SCC of Pipelines and Its Remedies" Recent Progress in SCC of Pipelines in Near-Neutral pH Environment

**Mimoun Elboujdaini, Binyang Fang, and Reg Eadie**

**Abstract** Evidence from a failure pipeline that had been in-service for 34 years showed that there are often quantities of tiny blunt cracks, frequently in crack colonies, in the pipeline. The vast majorities of these small cracks are seen to be dormant and hence tend to be innocuous. However, if the small cracks can surpass a threshold depth, around 0.5–0.6 mm, these cracks can be activated and begin to grow and may eventually lead to pipeline rupture if not detected and removed. The mechanisms are far from being understood. This paper is to review pipeline stress corrosion cracking (SCC) to help understand the mechanisms on pit-to-crack transition and early growth to contribute to pipeline integrity management so that rupture can be avoid or reduced. Specimens were pitted using two different techniques and then cyclically loaded in near-neutral pH environment sparred with 5% $CO_2$/balance $N_2$ gas mixture at high stress ratios (minimum stress/maximum stress), low strain rates and low frequencies which are close to those experienced during pipeline operations. The crack morphologies produced in laboratory with these techniques were found to be very similar to those from the failed pipeline in the field, which has never been reported before. It was proposed that two different mechanisms were responsible for the early-stage crack growth. For cracks less than 0.5–0.6 mm deep, they were blunt, engendered by anodic dissolution (localized corrosion), which was facilitated by stresses. So it was called stress-facilitated dissolution crack growth. Once crack depth was larger than the critical value,

M. Elboujdaini (✉)
CANMET Materials Technology Laboratory, Natural Resources Canada,
Ottawa K1A 0G1, Canada
e-mail: melboujdaini@nrcan-rncan.gc.ca

B. Fang
Ross Energy Services Ltd., Calgary, Alberta T2P 1A1, Canada
e-mail: bingyan.fang@rintegrity.ca

R. Eadie
Professor of Materials Engineering, Department of Chemical and Materials Engineering,
University of Alberta, Edmonton, Alberta T6G 2V4, Canada
e-mail: reg.eadie@ualberta.ca

T. Boukharouba et al. (eds.), *Integrity of Pipelines Transporting Hydrocarbons*,
NATO Science for Peace and Security Series C: Environmental Security,
DOI 10.1007/978-94-007-0588-3_8, 

around 0.5–0.6 mm, the cracks would be reactivated and more hydrogen would be trapped in the plastic zones. Thus, hydrogen would play an important role in crack propagation. So in this stage, cracks tended to become sharp and the mechanism was referred to hydrogen assisted cracking. The observations from the field can be interpreted very well by using the proposed models. It was suggested that cracks deeper than 0.5–0.6 mm in the field should be removed to reduce or avoid the threat of rupture. If active corrosion and hydrogen related Stage II growth can be prevented then smaller cracks are innocuous.

## 1 Introduction

Near-neutral pH stress corrosion cracking (NNpHSCC) has been a big concern for oil and gas pipeline integrity assessment since the first failure was documented as having occurred in 1985 [1]. Although NNpHSCC has been investigated extensively, it is still not completely understood. It has been found that pits can facilitate crack development by acting as stress concentrations and by modifying the local environment chemistry to be more susceptible to cracking [2]. In laboratory investigations, it has also been found that the earliest cracks appeared to initiate at corrosion pits that formed around non-metallic inclusions and that later cracks grew from corrosion pits that formed randomly on the surface [3–6]. So SCC of pipeline steels commonly originates from corrosion pits. Sometimes, cracks can also be nucleated around other types of discontinuities. Wang [7] indicated that some cracks could be formed preferentially along the heavily deformed metal in scratches on the surface. It was also reported that preferential corrosion occurred at the boundaries of pearlite colonies, and transgranular crack-like features could grow from such surface attack [8].

The damage process of NNpHSCC in pipelines induced by pitting corrosion, after near-neutral pH (NNpH) solution (ground water in anaerobic soil) has penetrated disbonded coating and reached the pipe surface, may be composed of the following sequence: first pit nucleation and growth, then transition from pits to microstructurally short cracks, then transition from microstructurally short cracks to physically short cracks and finally transition from physically short cracks to long cracks, whose subsequent growth leads to the final failure. Generally, the long crack growth and fracture only amount to a small part of the total life, whereas, a significant part of the total life is consumed at stages before the long crack growth threshold is exceeded. At the same time, limited studies about pitting corrosion, NNpHSCC crack initiation and short crack growth [5, 8, 9] have been carried out, compared to long crack growth [10–13]. So it is important to investigate the processes occurring before the long crack growth threshold, and these are important to life prediction and assessment of pipelines.

Pit nucleation is related to the electrochemical processes occurring during corrosion. The time for pit nucleation is dependent on the electrolytes (as influenced by the soil and the presence of carbon dioxide in the soil), the electrochemical potential, the temperature, the pipeline materials properties, the loading parameters

and other variables, which are not well understood yet, although there has been much progress in the rational description and modeling of pit nucleation and early pit growth [14–16]. Pit nucleation has been reported to follow lognormal and Weibull distributions [17]. Maximum pit depth in mild steel was found to be fitted to a bi-modal probability distribution [18, 19]. To date, there have been a few models concerning pit growth [20, 21], and these are mainly empirical. Pit growth in service may proceed under intermittent exposure conditions and it may take years to initiate cracks [22], making it difficult to study NNpHSCC on smooth samples under conditions close to those in in-service pipelines. So an accelerating technique to generate pits was employed in this study, the details of which have been reported in another paper [23]. Basically it consists of an acid-immersion treatment to passivate the surface and then a second immersion in dilute hydrochloric acid, which leads to rapid pitting growth at sites where the passive layer is either removed with a needle or at innate weaknesses in the film where pits grow spontaneously. Another pit growing method by using electrochemical technique was also reported before [24].

After the transition from pits to cracks has occurred in the field, tiny, elongated blunt cracks, frequently in crack colonies, are often seen in very large numbers [25]. The vast majorities of these small cracks are found to become dormant and hence tend to be innocuous. However, if the small cracks can surpass a threshold depth, around 0.5–0.6 mm [26], these cracks can be activated and begin to propagate and may eventually lead to pipeline rupture if not detected and removed. So studies concerning the growth of these small cracks and how potential growth can be identified and avoided will contribute significantly to an understanding of NNpHSCC initiation and help in pipeline integrity management.

## 2 Experimental

### *2.1 Specimens*

X-52 line pipe steel from Enbridge Pipelines Inc. that had exhibited NNpHSCC crack colonies after 34 years of service was used in this project. The pipe was 34″ (864 mm) in external diameter and 7.9 mm in measured wall thickness. The chemical composition can be seen in Table 1. The microstructure consisted of pearlite and ferrite. It was found that there were very few, if any, inclusions on the axial transverse (A-T) surface, while there were a lot of inclusions on the radial transverse (R-T) and the axial radial (A-R) surfaces (Fig. 1a–c). In addition, the inclusions on the R-T surface were relatively smaller than those on the A-R surface. Energy dispersive X-ray spectroscopy (EDS) analysis showed that the non-metallic inclusions on the A-R surface were mainly MnS (Fig. 1d). And these inclusions were more abundant on the axial-radial section at mid-wall (shown in Fig. 1c). Hence, it was likely that the inclusions were elongated along the axial direction during the rolling processes.

**Table 1** Chemical composition of X-52 pipeline steel (wt.%)

| Elements | X-52 | Elements | X-52 |
|---|---|---|---|
| C (Carbon) | 0.261 | Cr (Chromium) | 0.027 |
| Mn (Manganese) | 1.150 | Mo (Molybdenum) | 0.013 |
| P (Phosphorus) | 0.008 | Al (Aluminum) | 0.002 |
| S (Sulfur) | 0.019 | V (Vanadium) | 0.003 |
| Si (Silicon) | 0.036 | Nb (Niobium) | 0.003 |
| Cu (Copper) | 0.033 | Ti (Titanium) | 0.002 |
| Sn (Tin) | 0.002 | Co (Cobalt) | 0.006 |
| Ni (Nickel) | 0.032 | Fe (Iron) | Balance |

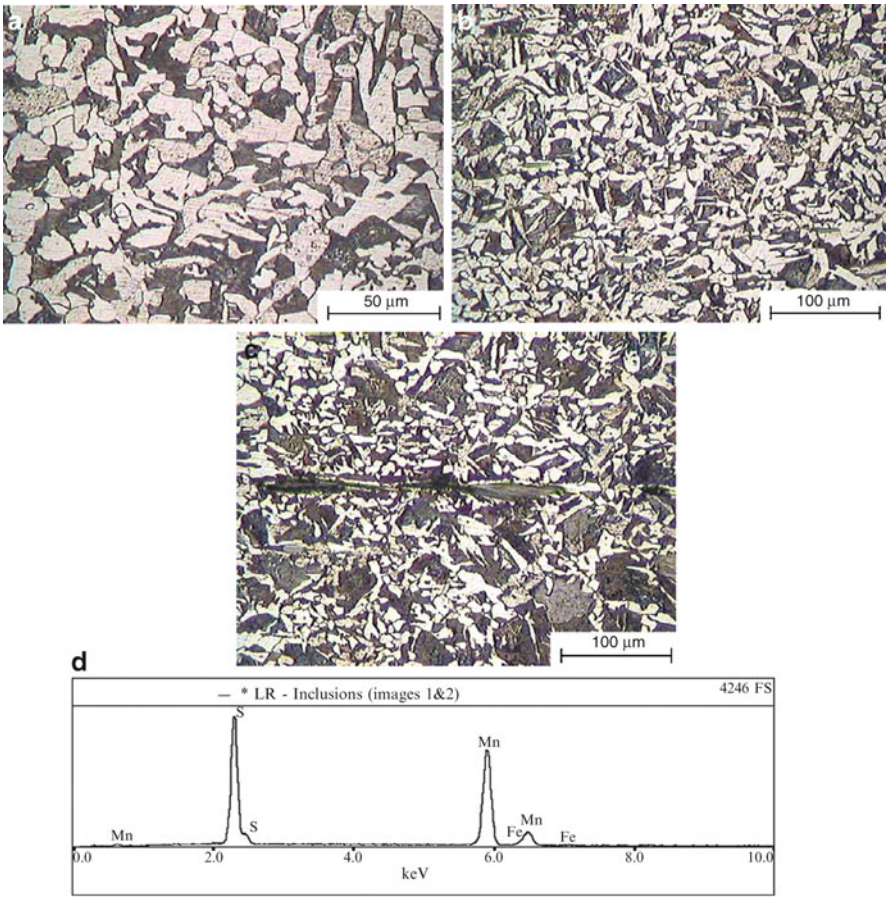


**Fig. 1** Microstructure of X-52 pipeline steel. (**a**) A-T surface; (**b**) R-T surface; (**c**) A-R surface; (**d**) EDS of the inclusions on A-R surface

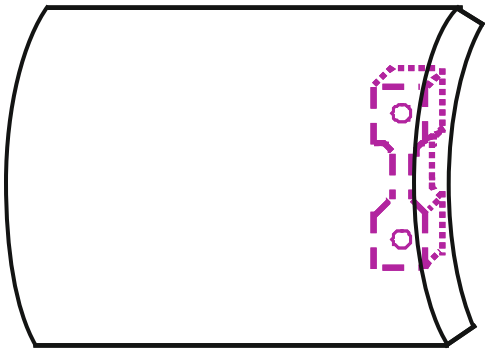

**Fig. 2** Schematic of the sample with orientations in the pipe

Dog-bone specimens with dimension of 36 × 7 × 3.5 mm in reduced section were machined from pipe with the length of the specimens along the transverse direction of the pipe so that the crack-advance plane (radial-axial) was the same as for NNpHSCC in the field (see Fig. 2 for a schematic of the orientations). After the sample surfaces had been ground to 1,200 grit in accordance with the standard metallographic procedure, they were degreased and cleaned using acetone and ethanol.

## 2.2 *Pitting the Surfaces*

After the surfaces were masked using PTFE tape leaving the gauge section exposed, the samples were put in concentrated $H_2SO_4$ solution to passivate the surfaces and then exposed to dilute HCl solution (the ratio of HCl to distilled water was 1:10) to grow pits, as reported by Fang et al. [23]. After 135 h, the pitted samples were taken out and washed using tap water. Then they were cleaned using EDTA and then ethanol in an ultrasonic cleaner to ensure that the passive films on the surfaces had been almost removed.

## 2.3 *SCC Tests*

The pitted specimens were cyclically loaded under a balanced triangular waveform as shown in Table 2 in a soil solution (ratio of soil to water is 1:5) and a NNpH inorganic test solution identified as C2 solution, both sparged with 5% $CO_2$/balance $N_2$ gas mixture. C2 solution is made with the following ingredients 0.0274 g/L $MgSO_4{\cdot}7H_2O$, 0.0255 g/L $CaCl_2$, 0.0035 g/L KCl, 0.0195 g/L $NaHCO_3$, and

**Table 2** Loading conditions in NNpH solutions (all were sparged with 5% $CO_2$)

| Condition | Peak stress | Stress ratio | Frequency (Hz) | No. of cycles |
|---|---|---|---|---|
| A | 100% SMYS | 0.8 | $1 \times 10^{-4}$ | 1,345 |
| B-1 | 100% SMYS | 0.63 | $7.6 \times 10^{-5}$ | 1,394 |
| B-2 | 106% SMYS | 0.63 | $7.6 \times 10^{-5}$ | 1,394 |

0.0606 g/L $CaCO_3$ dissolved in high purity water. The pH after sparging was close to 6.2 for the C2 solution and near 7.0 in the soil solution.

After testing in the solution for the desired number of cycles, the tests were stopped and the samples were taken out. After cleaning using EDTA and ethanol in the ultrasonic cleaner, the samples were rinsed and dried with warm air and the sample surface observations were made using optical microscopy (OM) and scanning electron microscope (SEM). Thereafter, the sample surfaces were sectioned step by step to examine crack and pit depths, and crack and pit shapes. The sectioning was perpendicular to the cracked and pitted surfaces, and the sectioning progressed perpendicular to the loading direction. After each grinding and polishing step, measurements were made using OM and SEM to reveal the crack and pit dimensions.

## 3 Results and Discussion

### *3.1 Blunt Crack Emanation and Characteristics*

The corrosion pits had acted as stress concentrations (micro-notches) and served to initiate the blunt flaws. The stress and deformation fields in the immediate vicinity of the corrosion pits had a strong bearing on how the NNpHSCC cracks nucleated and propagated. In the mean time, the existing pits would continue to grow during exposure by anodic dissolution. When the stress concentrations at the roots of the corrosion pits were large enough, plastic deformation would occur. Slip irreversibility was enhanced, because of the dissolution of slip steps (the anodic corrosion reaction). At the same time, the iron atoms at the surface of the plastic zone had higher energy, acting as anodes in solution compared to the relatively less deformed surrounding regions serving as cathodes. Thus, galvanic cells would form driven partly by the higher dislocation density. So preferential electrochemical attack would focus on the regions at the pits where plastic deformation was localized. Hence, dissolution in plastic zones around the corrosion pits was accelerated. This dissolution, in turn, could enhance stress concentrations. In the end, blunt cracks were initiated, as shown in Fig. 3. These NNpHSCC cracks were mainly formed by stress-facilitated dissolution localized in plastic zones. Consequently, this type of crack was quite wide.

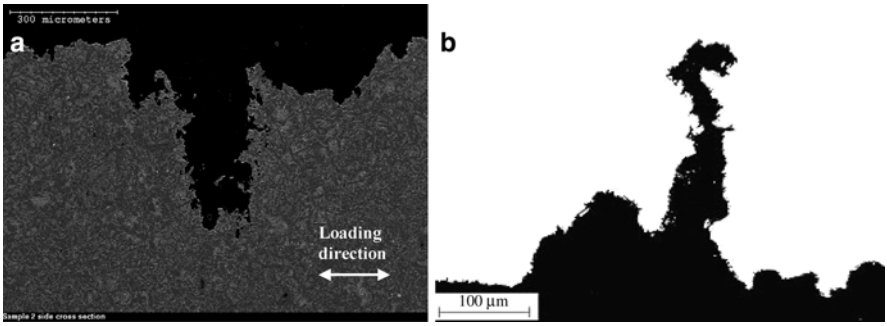


**Fig. 3** Photomicrographs of NNpHSCC crack cross-section features on the R-T surface cycled in NNpH solution sparged with 5% $CO_2$/balance $N_2$ gas mixture (**a**) in soil solution under load condition A [27]; (**b**) in C2 solution under load condition A [28]

In addition, it was also found that not all of the pits were cracked. For most of non-cracking pits, the pit aspect ratios (the ratio of pit depth $a$ to pit surface width $w$ on that section) were below 0.6 (Fig. 4a). However, many of cracking-pits were seen to have pit aspect ratios of over 0.5 (Fig. 4b). This indicated that for $a/w > 0.5$, pits would likely tend to become cracks. Considering that stress concentration factor for an elliptical corrosion pit is related to $w/2a$, where $w/2$ is the semi-axis which is perpendicular to the tensile loading, and $a$ is the bottom radius of the corrosion pit [29], the deeper the pits, the larger the stress concentration factor. Thus, the plastic zone and the extent of surface plasticity in the corrosion pit were also larger, which would promote the dissolution of the Fe atoms within the plastic zone. When the dissolution progressed to a certain degree, the pit had become a crack. Again in Fig. 4b, for the pits with aspect ratio below 0.5, the bottoms could be irregular, and the cracking locations had smaller curvature radii. Thus, the stress concentrations would be higher and cracks still tended to have initiated at the regions with higher curvature. In addition, this type of cracking is consistently found in regions of high tensile residual stress in the pipelines, where the total stress would be significantly higher than the stress just from the internal pressure in the pipeline [3, 30]. Since this was an API X-52 steel after yielding there would be some stress increase with increasing strain. Consequently, the higher degree of corrosion or cracking was believed to be primarily related to higher plastic strain. The increased plastic strain would explain the blunt cracks versus sharp cracks. This indicated that the presence of higher plastic strains ahead of the pits increased the corrosion rate. Blunt cracks initiated around many corrosion pits, which were acting as stress concentrators (micro-notches) and were the principal sites for initiation.

The ratios of crack tip width to crack mouth width for the majority of these blunt cracks were seen to be around 0.1 (Fig. 4c). Thus, blunt cracks could have survived. However, this also indicated that there was significant corrosion along the crack walls. The amount of lateral corrosion significantly increased as the crack mouth

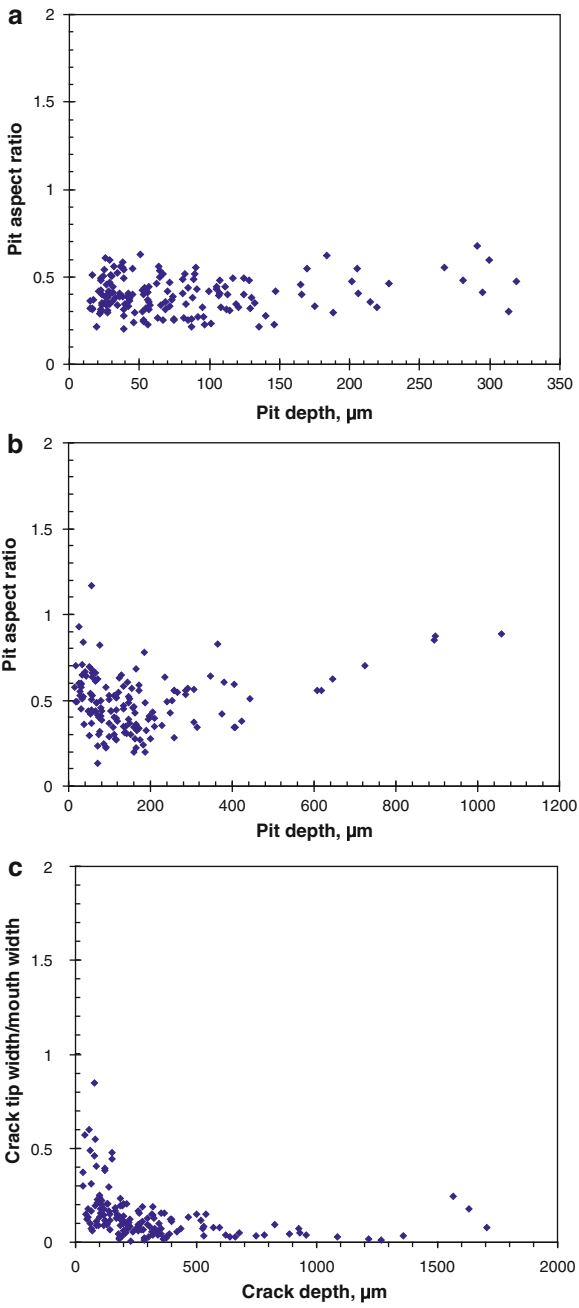


**Fig. 4** Geometry of pits and cracks. The aspect ratio distribution on the sample cyclically loaded at 100% of SMYS, 0.0001 Hz and R of 0.8 in NNpH solution sparged with 5% $CO_2$ of (**a**) non-cracking pits and (**b**) cracking pits. (**c**) the crack tip width/crack mouth width for cracks

was approached. It was also noted that the ratio of crack tip width/mouth width in Fig. 4c was close to values seen on the same steel pipe in the field. In addition, most of cracks were found to be less than 0.5–0.6 mm in depth, which was consistent with the observations in the field [7]. The crack morphologies observed in the tests on the samples (Fig. 3) were found to be very similar to NNpHSCC cracks found in the field [7, 26] in this pipe, as shown in Fig. 5. So it was reasonable to say the conditions in this study could represent NNpHSCC initiation conditions encountered in the field where clusters of SCC cracks were less than 0.5–0.6 mm in depth, although the peak normal stress in this study was somewhat higher highlighting the need for high residual tensile stresses.

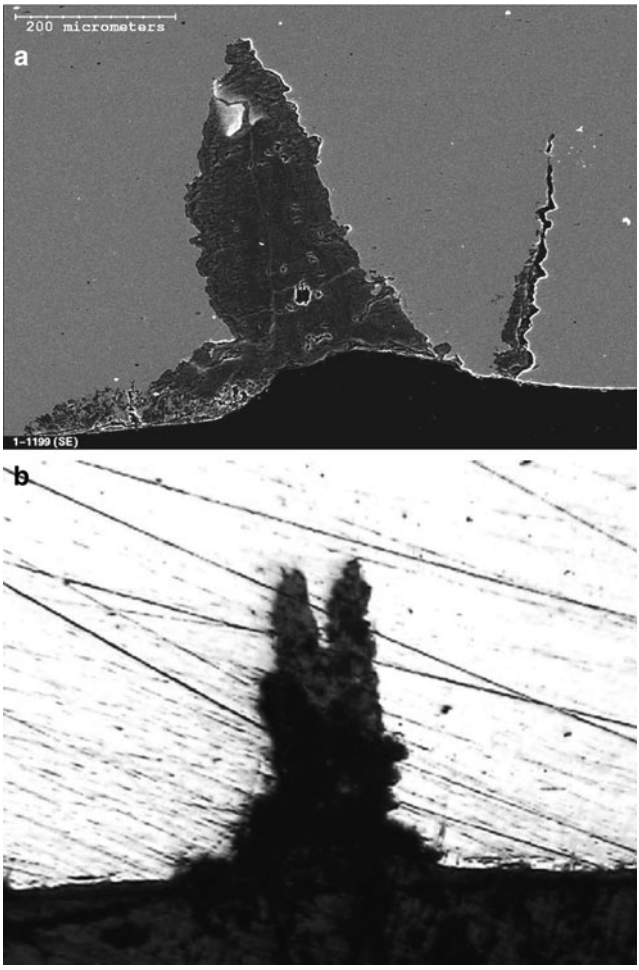


**Fig. 5** Photomicrograph of NNpHSCC cracks on an oil pipeline [26]

### 3.2 *Blunt Crack Growth*

After blunt cracks had initiated, they might grow under benign conditions. It was clearly seen that most of cracks were distributed between 30 and 390 μm in depth, as shown in Fig. 6a, and the most probable crack depth was around 30–90 μm. Figure 6b shows that the median of crack depth was at 140 μm, and the lower and upper box values (quartiles) were 86 and 245 μm, respectively. The whisker was from 24 to 456 μm with a few outliers shown with asterisks. All the evidence once again reflected that the majority of crack depths were below 0.5–0.6 mm, consistent with the field observations as shown in Fig. 7.

Once the blunt crack growth rate was higher than the pit growth rate, the stress facilitated corrosion dissolution rate would be dominant and thus, dissolution would

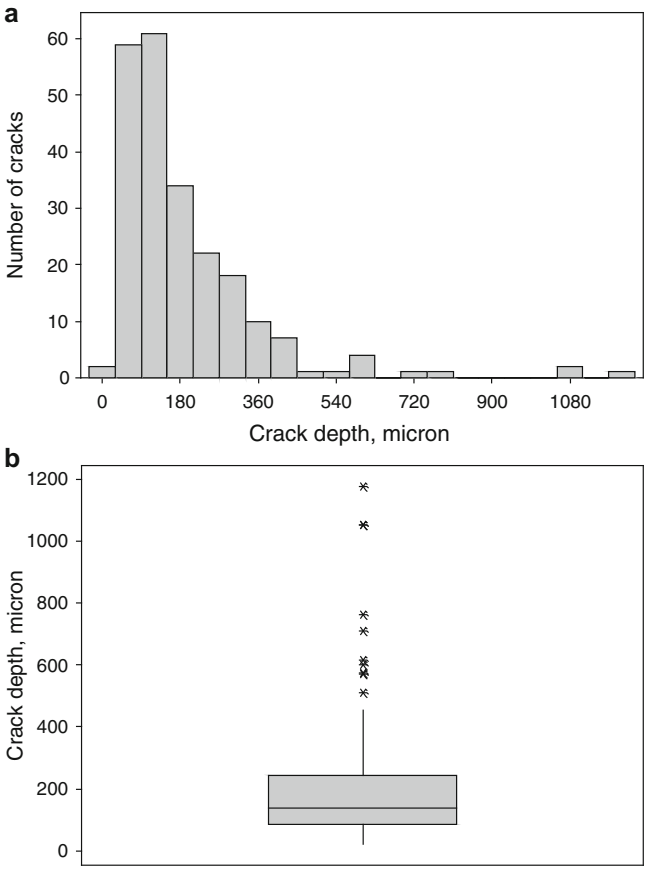


**Fig. 6** Distribution of crack depth on the sample cyclically loaded at 100% of SMYS, 0.0001 Hz and R of 0.8 in NNpH environment after 1,345 cycles; (**a**) number of cracks versus crack depth; (**b**) boxplot of crack depth

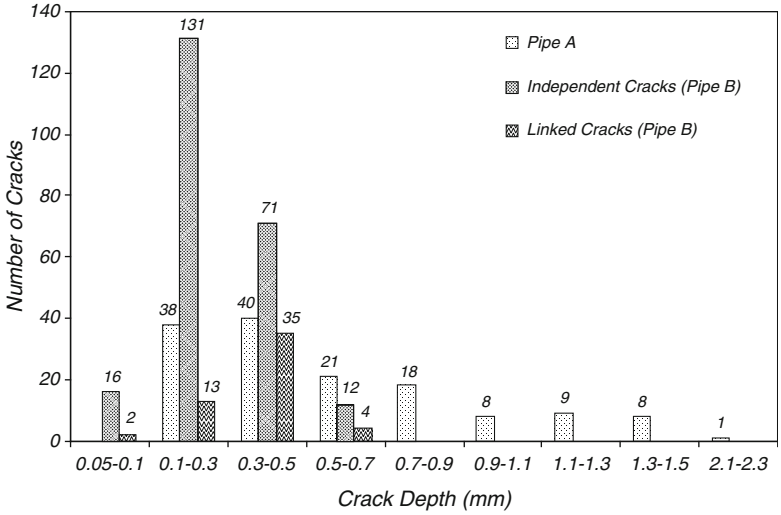


**Fig. 7** Number of cracks vs. maximum crack depth in pipe B and pipe A [26]

be localized and localized corrosion around the corrosion pits would be accelerated and blunt cracks would grow. In the end, dissolution formed blunt crack would survive and might grow under intermittent conditions.

It was sometimes seen that non-metallic inclusions (mainly MnS as revealed by EDS) were located ahead of the cracks on the crack advancement plane, as shown in Fig. 8. When the blunt cracks grew and reached these non-metallic inclusions, the solution in the blunt crack enclaves could get to these inclusions and electrochemically react with the inclusions [3–6, 31]. The inclusions would then be corroded and eaten away since the non-metallic inclusions (MnS) acted as an anode and the base steel nearby acted a cathode. The relative area ratio of the base steel to the non-metallic inclusion was huge, thus, galvanic corrosion would be accelerated and corrosion attack would be localized on the inclusions, which, in return, increased stress concentrations and plastic deformation. Thus, blunt crack growth because of inclusions enhancing stress facilitated dissolution would be maintained, as reported previously [32]. When the inclusions were completely eaten away, the blunt crack would advance as stress facilitated dissolution reported previous. In addition, at this time, the stress concentration would be much higher, which might further enhance the stress riser and plastic deformation. All of these, in turn, would contribute to the blunt crack growth.

Still in Fig. 8, there were few non-metallic inclusions ahead of the blunt crack tip and these aligned inclusions could contribute to significant crack growth.

Considering the microstructure differences on the different surfaces as reported in a previous paper [32], the nonmetallic inclusions were elongated along the longitudinal direction, and some inclusions were about 0.5 mm long, which would have facilitated pit nucleation, if the R-T surface was exposed to the

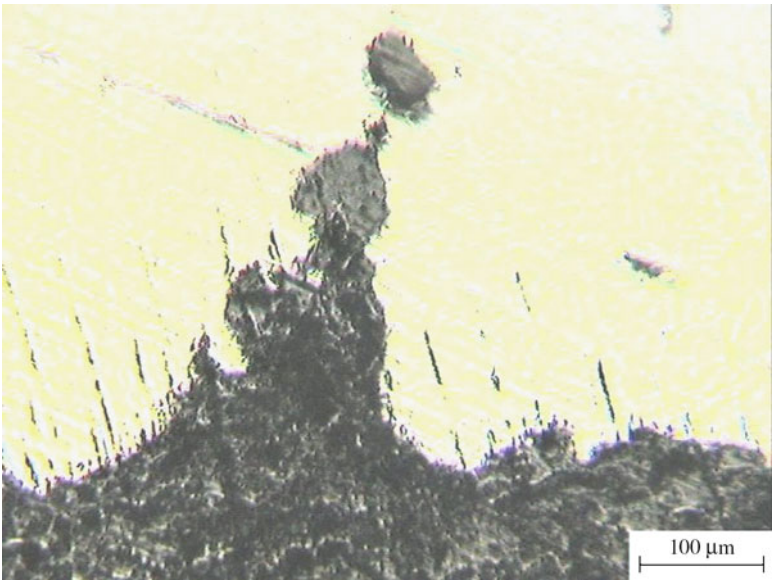


**Fig. 8** Photograph of a crack initiation from a corrosion pit and non-metallic inclusions located ahead of the crack tip

NNpH solution, and promoted pit-to-crack transition and blunt crack growth. As the crack growth direction in depth was the same as the elongated inclusions, the latter would also have assisted crack growth.

However, if the orientation of the inclusions was approximately perpendicular to the pit growth direction or blunt cracks, the blunt cracks might grow and touch the inclusions under appropriate conditions. Also once the blunt cracks encountered the inclusions, the dissolution and growth would be localized on the inclusions. However, since the inclusions were approximately perpendicular to the blunt cracks, when the inclusions were corroded completely, the blunt crack tips would become much blunter, which therefore reduced stress concentrations and stress intensity factors, and hence lowered the crack growth driving forces. Thus, the cracks might stop growing and became dormant. This type of crack was also observed in this report, as shown in Fig. 9 where a balloon-like morphology was seen. The cracks observed in this case might not threaten pipeline integrity from a management point of view.

Since inclusions were elongated in the longitudinal direction, especially in the mid-wall, the crack growth in the longitudinal direction would be significantly influenced by the coalescence with inclusions. These cracks, if not detected and removed, might put a pipeline at a risk to cracking or failure. It would be helpful and important if some tools could be employed to monitor the existence of this type of crack and inclusion, and some measures could be taken to prevent the cracks from growing.


**Fig. 9** Photograph of a blunt crack and the blunt crack tip on R-T surface for a specimen cyclically loaded in C2 solution under condition B-1

## *3.3 Crack Transition*

Figure 3 shows a blunt crack that had initiated from the bottom of a big pit. The blunt crack initiation and growth mechanism has been addressed above as being caused by plastic-deformation-facilitated dissolution. When blunt cracks grew deep enough, they could surpass a threshold, around 0.5–0.6 mm. Thereafter, the apparent dormant blunt cracks would be reactivated, and tend to start to grow. However, the morphologies of the crack tips exceeding the critical depth were significantly different from the blunt cracks. Crack tips in this stage looked very sharp. Thus, anodic dissolution would not be the dominant process in this stage. When the blunt cracks grew deep enough, the plastic deformation would be larger. Thus, the corresponding plastic zones would be bigger accordingly, which would produce larger hydrostatic stress zones ahead of the deeper cracks. Hence, more hydrogen would be trapped in the larger plastic zones and could play an important role in crack growth. So, for this stage, the crack growth mechanism was hydrogen assisted cracking (HAC) instead of dissolution. In a word, there were two different mechanisms for early crack growth in NNpHSCC. Before the threshold, around 0.5–0.6 mm deep, referred to as "Stage I", it was plastic-deformation-facilitated dissolution that made wide blunt crack initiation from corrosion pits and growth. After the threshold, called "Stage II", hydrogen was responsible for the subsequent

sharp crack growth. This is the first time these two different crack types have been observed and reproduced in the laboratory. These two different mechanisms are necessary for NNpHSCC crack initiation and early growth. These are quite consistent with the observations in the field. The sharp cracks in Stage II can create a significant risk to pipeline integrity. If they can't be detected and removed, they will likely keep growing and eventually once the long crack corrosion fatigue threshold is surpassed, cracks will grow much faster, even leading to pipeline rupture or leakage. Compared to the long crack growth stage, the blunt crack growth in Stage I and the sharp crack growth in Stage II consume a majority of pipeline life. So Stages I and II cracks are very important for pipeline integrity management and should be addressed intensively. Unfortunately, so far no research has touched Stage I blunt cracks and little has paid attention to Stage II sharp cracks, while most has focused on long crack growth. For in-service pipelines, removing Stage II cracks that are deeper than 0.5–0.6 mm would benefit the pipeline integrity and enhance the remaining life. If Stage I crack growth can be repaired, that would significantly extend the remaining life. If active corrosion can be prevented such as by cathodic protection then smaller stress facilitated dissolution cracks are innocuous. More hydrogen, however, would be generated on the sample surfaces and in the crack enclaves, which might enhance the amounts of hydrogen, trapped on Stage II cracks and accelerate Stage II crack growth. Thus, cathodic protection might impair one type of crack growth but assist another type of crack propagation. So a better way is to reduce both the active corrosion and hydrogen generation simultaneously, such as with an inhibitor, if it can be found, that can prevent free corrosion by forming a film or surface layer (shifting anodic and cathodic polarization curves to the left). Then this would significantly benefit pipeline life.

## 4 Conclusions

Based on the results and discussion above, the following conclusions were made. The depth and the depth aspect ratio for non-cracking pits were seen to be smaller than for cracking pits. For cracking pits, generally when the pit depth aspect ratios were higher than 0.5, cracks would be likely to initiate. The deeper the pit and the higher the ratio the higher the probability for pit-to-crack transition. Blunt cracks were seen to have initiated from the corrosion pits on the pitted samples cyclically loaded in near-neutral pH environment and these blunt cracks were generally less than 0.5–0.6 mm deep, consistent with the observations from the field. These blunt cracks were transgranular and believed not to put pipelines at a risk from integrity management point of view. Most of cracks were found to be shallow and wide because they tend to be dormant and not to propagate to failures. Hence, they were innocuous. Once these shallow blunt cracks exceeded a critical depth, these cracks could be activated and continue to propagate which was related to hydrogen effect. All the evidence was consistent with the field observations. Thus, the conditions employed in this research can represent the operational ones in the field, which is

one of the reasons why NNpHSCC cracks have been so difficult to initiate and have not been successfully reproduced in laboratory. If active corrosion and hydrogen generation can be prevented such as with a corrosion inhibitor, then smaller cracks are innocuous.

**Acknowledgments** The authors would like to acknowledge an NSERC Strategic Grant and Enbridge Pipelines Inc. for financial support, and an NSERC/AUAF facility access grant at CANMET Materials Technology Laboratory. The authors thank Scott Ironside of Enbridge for the experimental pipeline material.

## References

1. NEB, Stress corrosion cracking on canadian oil and gas pipelines. Report of the Inquiry. National Energy Board. MH-2-95, Dec 1996
2. M. Baker Jr., Inc., Stress corrosion cracking study, TTO Number 8, Integrity Management Program Delivery Order DTRS56-020D-70036, Final Report, Jan 2005
3. Y.-Z. Wang, R.W. Revie, M.R. Shehata, R.N. Parkins, K. Krist, Initiation of environment induced cracking in pipeline steel: microstructural correlations, in *Proceedings of International Pipeline Conference/1998*, vol. 1, ASTM, Calgary, 1998, pp. 529–542
4. M. Elboujdaini, Y.-Z. Wang, R.W. Revie, Initiation of stress corrosion cracking on X-65 linepipe steels in near-neutral pH environment, in *Proceedings of International Pipeline Conference/2000*, vol. 2, ASTM, Calgary, 2000, pp. 967–978
5. M. Elboujdaini, Y.-Z. Wang, R.W. Revie, R.N. Parkins, M.T. Shehata, Stress corrosion crack initiation processes: pitting and microcrack coalescence, *Corrosion/2000*, Paper no. 00379, NACE International, Houston, 2000
6. Y.-Z. Wang, R.W. Revie, R.N. Parkins, Mechanistic aspects of stress corrosion crack initiation and early propagation, *Corrosion/99*, Paper no. 143, NACE International, Houston, 1999
7. S.H. Wang, W. Chen, T. Jack, F. King, R.R. Fessler, K. Krist, Role of prior cyclic loading in the initiation of stress-corrosion cracks in pipeline steels exposed to near-neutral pH environment, in 2000 IPC, Calgary, 2000, pp. 1005–1009
8. R. Chu, W. Chen, S.-H. Wang, F. King, T.R. Jack, R.R. Fessler, Microstructure dependence of SCC initiation in X-65 pipeline steel exposed to a near-neutral pH soil environment, Corrosion, **60**(3), 275–283 (2004)
9. F. King, T. Jack, W. Chen, S.H. Wang, M. Elboujdaini, W. Revie, R. Worthingham, P. Dusek, Development of predictive model for the initiation and early-stage growth of near-neutral pH SCC of pipeline steels, *Corrosion/2001*, Paper no. 01214, NACE, Houston, 2001
10. S.B. Lambert, J.A. Beavers, B. Delanty, R. Sutherby, A. Plumstree, Mechanical factors affecting stress corrosion crack growth rates in buried pipelines, *IPC/2000*, ASME, Calgary, 2000, pp. 961–966
11. X.Y. Zhang, S.B. Lambert, R. Sutherby, A. Plumtree, Transgranular stress corrosion cracking of X-60 pipeline steel in simulated ground water. Corrosion **55**, 297–305 (1999)
12. B.A. Kim, N. Oguchi, Y. Hosokawa, W. Zheng, G. Williams, M. Laronde, J.A. Gianetto, G. Shen, W.R. Tyson, Experimental study on SCC susceptibility of X60 steel using full pipe sections in near-neutral pH environment, IPC/2004, ASME, Calgary, 2004, pp. 133–141
13. W. Chen, R. Sutherby, Environmental effect of crack growth rate of pipeline steel in near-neutral pH soil environments, IPC/2004, ASME, Calgary, 2004, pp. 123–132
14. G. Engelhardt, D.D. MacDonald, Corrosion **54**, 469–479 (1998)
15. A. Turnbull, Br. Corros. J. **28**, 297–308 (1993)
16. Z. Szklarska-Smialowska, D. Grimes, J. Park, The kinetics of pit growth on alloy 600 in chloride solutions at high temperatures. Corros. Sci. **27**, 859–867 (1987)

17. P. Shi, S. Madhadevan, Damage tolerance approach for probabilistic pitting corrosion fatigue life prediction. Eng. Fract. Mech. **68**, 1493–1507 (2001)
18. R.E. Melchers, Statistical characterization of pitting corrosion – Part 1: Data analysis. Corrosion **61**, 655–664 (2005)
19. R.E. Melchers, Statistical characterization of pitting corrosion – Part 2: Probabilistic modeling for maximum pit depth. Corrosion **61**, 766–777 (2005)
20. D.G. Harlow, R.P. Wei, A probability model for the growth of corrosion pits in aluminium alloys induced by constituent particles. Eng. Fract. Mech. **59**, 305–325 (1998)
21. Y. Kondo, Prediction of fatigue crack initiation life based on pit growth. Corrosion **45**, 7–11 (1989)
22. A. Turnbull, Issues in modelling of environment assisted cracking, in *Environmentally Assisted Cracking: Predictive Methods for Risk Assessment and Evaluation of Materials, Equipment, and Structures*, ed. by R.D. Kane (ASTM STP 1401, West Conshohocken, 2000), pp. 23–39
23. B. Fang, R. Eadie, W. Chen, M. Elboujdaini, Passivation/immersion method to grow pits in pipeline steel and a study of pit nucleation and growth resulting from the method. Corros. Eng. Sci. Technol. **44**(1), 32–42 (2009)
24. B. Fang, R.L. Eadie, W. Chen, M. Elboujdaini, Electrochemical method pits generation and its application in crack initiation in pipeline steel in near-neutral pH environment, in *NACE Northern Area Western Conference*, Edmonton, 11–14 Feb 2008
25. W. Chen, F. King, E. Vokes, Characteristics of near-neutral pH stress corrosion cracks in an X-65 pipeline. Corrosion **58**, 267–275 (2002)
26. W. Bouaeshi, S. Ironside, R. Eadie, Research and cracking implications from an assessment of two variants of near-neutral pH crack colonies in liquid pipelines. Corrosion **63**(7), 648–660 (2007)
27. B. Fang, R. Eadie, W. Chen, M. Elboujdaini, Passivation/acid-immersion method to grow in pipeline steel and a study of pit nucleation and growth resulting from the method, Corros. Eng. Sci. Technol. **44**, 32–42 (2009)
28. B. Fang, R.L. Eadie, M. Elboujdaini, W. Chen, Transition from pits to cracks in pipeline steel in near-neutral pH solution, in *12th International Conference on Fracture*, Paper no. ICF2009-290, Ottawa, 12–17 July 2009
29. W.D. Pilkey, *Peterson's Stress Concentration Factors*, 2nd edn. (Wiley, New York, 1997), pp. 62–69
30. J.A. Beavers, J.T. Johnson, R.L. Sutherby, Materials factors influencing the initiation of near-neutral pH SCC on underground pipelines, 2000 International Pipeline Conference, vol. 2 (ASME, New York, 2000), pp. 979–988.
31. B. Fang, E.-H. Han, J. Wang, W. Ke, Mechanical and environmental influences on stress corrosion cracking of an X-70 pipeline steel in dilute near-neutral pH solutions. Corrosion **63**, 419–432 (2007)
32. B. Fang, R. Eadie, W. Chen, M. Elboujdaini, E.-H. Han, The effect of microstructure on pit-to-crack transition and crack growth in an X-52 pipeline steel in near-neutral pH environment, International Pipeline Conference, IPC 2008-64112, Calgary, 29 Sept – 3 Oct 2008

# Hydrogen Embrittlement of Steels – Testing and Modelling as a Joint Effort

**Wolfgang Dietzel**

**Abstract** To study the phenomenon of stress corrosion cracking (SCC) and hydrogen embrittlement (HE) of metallic materials, and in particular of high strength steels, fracture mechanics based techniques are well suited. Experiments using a rising displacement test technique and pre-cracked specimens were employed for experimental characterisation of the susceptibility of these materials to environmentally assisted cracking and to study the mechanisms of failure caused by the uptake of atomic hydrogen from a corrosive environment. This work was complemented by simulating the degradation process caused by HE. The experimental work was partly performed in conjunction with the Technical Committee 10, Environmentally Assisted Cracking, of the European Structural Integrity Society, ESIS, in the context of two European research projects. As a result, a new ISO standard on EAC testing, ISO 7339 – Part 9, was established. The work is now focused on the development of suitable modelling approaches to HE. Such models can either be used in addition to experimental testing or, to some extent, can replace traditional SCC testing.

## 1 Introduction

It is important to prevent stress corrosion cracking (SCC) in service and to reduce the likelihood of consequent unexpected fast fracture without being unnecessarily conservative. Since there is no generalized analytical approach which allows prediction of combinations of material and environment that result in SCC, the avoidance of SCC has to be based either on past experience and/or on SCC testing in the laboratory. The current design approaches presume that short-term laboratory-scale experimental data can be extrapolated to predict long-term structural

W. Dietzel (✉)
Institut für Werkstoffforschung, Helmholtz-Zentrum Geesthacht,
Max-Planck-Str. 1, Geesthacht D-21502, Germany
e-mail: wolfgang.dietzel@hzg.de

T. Boukharouba et al. (eds.), *Integrity of Pipelines Transporting Hydrocarbons*,
NATO Science for Peace and Security Series C: Environmental Security,
DOI 10.1007/978-94-007-0588-3_9, 

performance. In principle, these tests consist of stressed pieces of the material exposed to a corrosive environment, and the aim of the tests is to determine if and how SCC occurs in the material during the test period.

SCC test methodologies follow the two basic philosophies underlying structural design [1], i.e.:

– the safe-life approach,
– the damage-tolerance approach.

The older safe-life approach undertakes to design the structure for a finite service life during which there is no significant damage, viz. there is no critical crack. Consequently, this approach does not include in-service inspection. The damage-tolerance approach, which evolved later, includes designing for an adequate service life without significant damage, but also enables operation beyond the actual life at which damage begins to occur. It must be shown that damage, and in particular cracks, are detected by routine inspection before the cracks propagate to the extent that they decrease the residual strength of the structure below a safe level.

The damage-tolerance philosophy goes beyond the safe-life approach by including the possibility that cracks or flaws already exist in new structures. Either in-service inspection has to ensure structural integrity during the service life, or it has to be ensured that any initial cracks grow sufficiently slowly during the design service life, so that they do not reach a critical crack size which would cause failure.

## 2 The Fracture Mechanics Approach to SCC

In the damage-tolerant design practice fracture mechanics concepts are utilised to characterize the initiation and growth of cracks from initial flaws. This approach is also applied to cracks which are caused or enhanced by the presence of a corrosive environment. Typically, linear elastic fracture mechanics, LEFM, concepts are employed, and the plane-strain stress intensity factor in the opening mode, $K_I$, is used to quantify the stress situation at the crack tip controlling the onset of cracking and the subsequent crack extension. Fracture mechanics based SCC testing is then performed with the primary aim of determining the threshold, $K_{ISCC}$, and the crack growth velocity, da/dt. Since the specimens used already contain initial cracks, the stage of crack formation from an initially smooth surface is precluded and the problem of separating the environmental influence on both crack initiation and extension is thus avoided.

Experience has shown that the results obtained from the different types of SCC tests and on various specimen configurations are identical if all specific requirements are carefully met. Data obtained on part through-cracked specimens can, for example, be used to predict crack initiation and growth in plates containing small semi-elliptical surface flaws which simulate defects in large structures [2]. This underlines the capability of the fracture mechanics approach to transfer stress

corrosion data from small-scale laboratory specimens to real components and structures.

The test technique used to determine $K_{ISCC}$ is expected to yield reliable and reproducible results which only depend on the material/environment combination under test, but not on the method of testing. Since only reliable and relevant laboratory test data enable an appropriate risk assessment with respect to stress corrosion cracking, the choice of a suitable test methodology is essential to predict the likelihood of crack initiation and propagation but to avoid unnecessary conservatism.

A number of test standards exist which provide guidance for performing fracture mechanics SCC tests, issued by ASTM (ASTM E 1681-95), ISO (ISO 7539), and NACE (NACE TM 0177-90). According to the older ones of these standards, $K_{ISCC}$ was in the past evaluated either using constant load or constant deflection experiments, and the duration of the tests was often "left open to the parties concerned". Test times recommended for constant load tests ranged from 100 h for titanium alloys to 10,000 h for aluminium alloys and steels (ASTM E 1681-95, ISO 7539-6). A major advantage of static tests using constant load or constant deflection experiments is their moderate requirements regarding the experimental set-up. On the other hand, they have some inherent shortcomings:

1. the duration of a static test can be quite long and/or the test is terminated after an arbitrary test time. It sometimes remains uncertain whether the measured K-value really represents the threshold of the material/environment combination under investigation,
2. discrepancy can exist between laboratory tests performed under static conditions (constant load, constant deflection) and practical situations where dynamic loading and increasing plastic deformation can occur and may be prerequisite for SCC [3],
3. the specimens must satisfy the minimum size requirements imposed by the linear elastic fracture mechanics concept; for lower strength and/or more ductile materials this can lead to large specimen dimensions, particularly the specimen thickness may exceed the thickness of the actual component.

## 3 Rising Load/Rising Displacement SCC Testing

The first two of the above problems can be overcome by using dynamic test techniques like the slow strain rate test in which constant extension rates are applied [4]. Because of their accelerating nature these tests usually yield results within an acceptable amount of time, and they can reveal cases of susceptibility to SCC which remain undetected in static tests. The slow strain rate test is typically performed on smooth or notched specimens; although this type of testing has also been in use for fracture mechanics based SCC investigations on pre-cracked specimens for many years [5, 6]. Until recently, no SCC test standard existed which specified

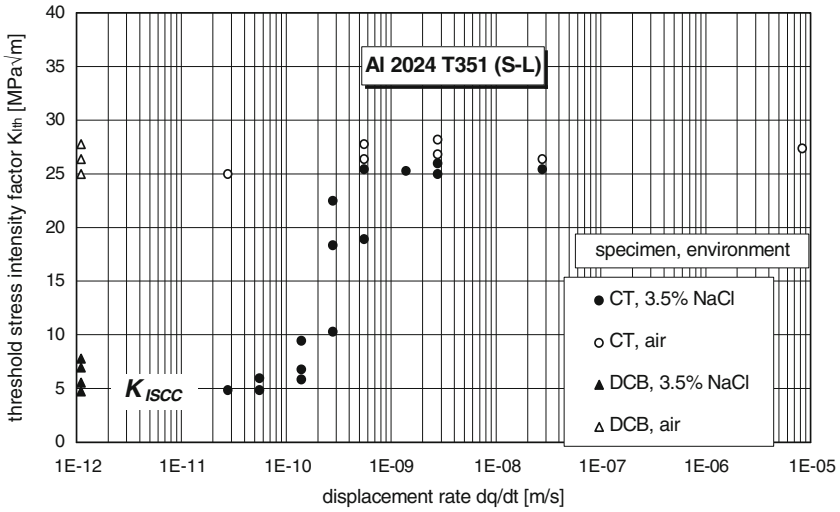


**Fig. 1** Influence of the displacement rate, dq/dt, on the stress intensity factor at crack initiation, $K_{Ith}$, measured in rising displacement tests on CT specimens (*circles*); the results of long term constant displacement tests (10,000 h) on DCB specimens are shown for comparison (*triangles*) [2]

a procedure for fracture mechanics based rising load/rising displacement tests on pre-cracked specimens. As Fig. 1 illustrates for the case of the high-strength aluminium alloy AA 2024 T351, the major problem encountered in such tests is the selection of a suitable loading or displacement rate to be applied in order to obtain "reliable" $K_{ISCC}$ values. "Reliable" in this context means that the $K_{ISCC}$ values should be in agreement with the results of long term constant displacement tests on DCB specimens which in this case had lasted approximately 10,000 h.

In 1992 the Technical Committee 10, *Environmentally Assisted Cracking*, of the European Structural Integrity Society, ESIS, issued "Recommendations for Stress Corrosion Testing Using Pre-Cracked Specimens" (ESIS P4-92 D) related to rising displacement SCC testing of pre-cracked specimens. This document formed the basis for two research projects funded by the European Commission and involving more than 30 laboratories and in which the approach taken in ESIS P4-92 D was experimentally verified [7]. The results led to a new ISO standard on SCC testing, i.e., ISO 7339 – Part 9: Preparation and Use of Pre-cracked Specimens for Tests Under Rising Load or Rising Displacement (ISO/DIS 7539-9), which was finally issued by ISO in 2003.

The main feature of this standard is the establishment of a curve of the type shown schematically in Fig. 2. Here it is assumed that the lower shelf region of this curve corresponds to the looked-for threshold value $K_{ISCC}$ for the onset of subcritical cracking caused by SCC/HE. In practice, it can be fairly difficult to decide whether the displacement rate selected for determining $K_{ISCC}$ is low enough to ensure that this lower shelf has really been reached. New approaches of simulating HE seem to offer a solution to this problem (see further below).

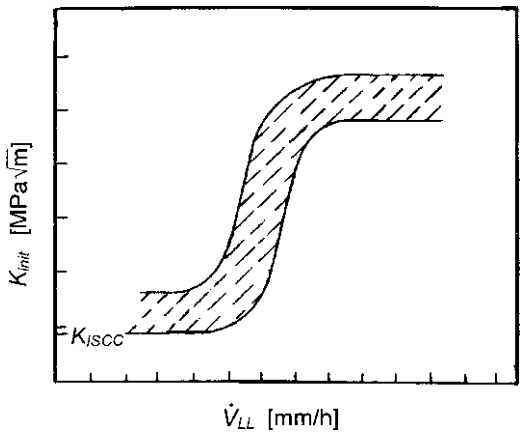


**Fig. 2** Initiation value of stress intensity factor as a function of the applied displacement rate (*schematic*)

## 4 The Elastic–Plastic Fracture Mechanics Approach to SCC

The applicability of linear elastic fracture mechanics to SCC and the use of $K_I$ as driving force parameter build on the assumption of limited plasticity and of predominant plane-strain conditions. In cases of SCC in which there is not a higher amount of plasticity, neither plane-strain nor linear elastic conditions are satisfied.

As mentioned above, a pre-requisite for the applicability of LEFM is that the specimens must satisfy the minimum size requirements imposed by the linear elastic fracture mechanics concept, as presented in Eq. 1. For lower strength and/or more ductile materials this may result in large specimen dimensions, particularly with respect to thickness:

$$a,\ B,\ (W - a) \geq 2.5\left(\frac{K_I}{\sigma_y}\right)^2 \tag{1}$$

## 5 The J Integral

This led to the application of elastic–plastic fracture mechanics concepts also to problems of SCC, and the J integral methodology has been employed by a number of authors [8–10]. Figure 3 demonstrates the effect of hydrogen embrittlement on J-R curves measured in rising displacement tests at C(T) specimens of a high strength steel [11]. The difference between the two curves shown in this figure is that one was obtained in air and the second one under cathodic protection in a corrosive environment (substitute ocean water according to ASTM D1141).

Figure 3 indicates that the value of the J integral at crack initiation, $J_{0.2}$, significantly decreased due to the environmental degradation caused by the ingress

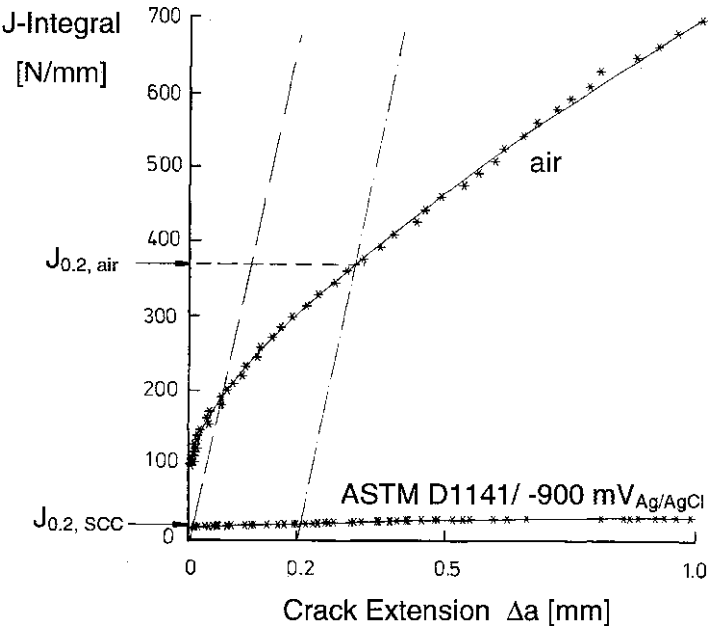


**Fig. 3** J-R curves determined on pre-cracked compact specimens of the low-alloyed structural steel FeE 690T [11]

of atomic hydrogen and leading to hydrogen embrittlement. The slope of the crack growth resistance curve measured in the corrosive environment becomes almost negligible, indicating that only little mechanical energy is needed in this case to achieve further crack extension. It should, however, be pointed out that the test in the corrosive environment was carried out at a very low displacement rate (1 μm/h, measured in the crack mouth of the specimen, CMOD) to allow for sufficient time of the hydrogen to enter into the material, to diffuse within the material and to accumulate in the vicinity of the crack tip.

## 6 The Crack Tip Opening Displacement, CTOD

In addition to the J-integral concept other elastic–plastic fracture parameters, i.e., the crack tip opening angle, CTOA, and the crack tip opening displacement, CTOD, are successfully applied to study SCC. These two parameters are particularly suited for fracture toughness assessments of thin-walled structures including the initiation and growth of stress corrosion cracks in such structures.

The crack tip opening displacement, CTOD, often designated "δ", is specified as the relative displacement of the crack surfaces normal to the original, un-deformed crack plane at the tip of the fatigue pre-crack. Experimentally, this parameter can be determined at the surface of a specimen or a component, e.g., by using a specially

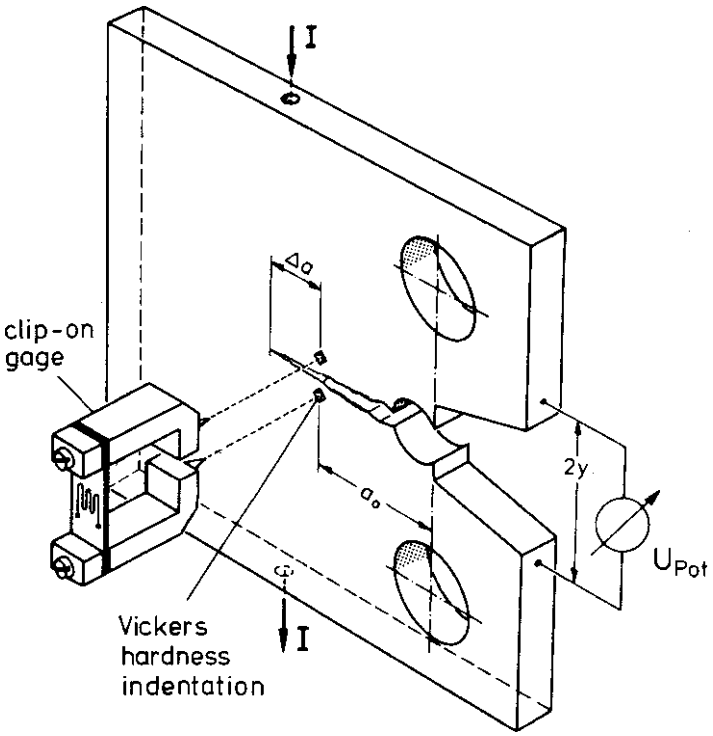


**Fig. 4** Clip-on gauge for measuring the CTOD over a gauge length of 5 mm ("$\delta_5$"); the figure also illustrates the position of the current leads ("I") and the measuring location for the potential drop across the crack when using the DCPD [12, 13]

designed clip-on gauge which measures the CTOD over a gauge length of 5 mm ($\delta_5$), as is demonstrated in Fig. 4 [12].

This figure also illustrates the position of the current leads ("I") and the measuring location for the potential drop across the crack when using the potential drop method for measuring crack lengths [13]. In SCC experiments performed in a corrosive environment, a direct measurement of the variable $\delta_5$ is difficult, since the clip-on gauge would have to be immersed in the corrosive environment during the test, and hence needed careful protection against corrosion. Calibration experiments performed on a number of materials and under various environmental conditions have confirmed that an excellent agreement exists between directly measured $\delta_5$ data and values which are calculated from the load and the crack mouth opening displacement, CMOD.

The expression correlating $\delta_5$ and the CMOD is derived from the British Standard 5762 and modified with respect to crack extension [14]:

$$\delta_{BS}^{M} = \frac{K^2}{2\,\sigma_y\,E'} + \frac{0.6\Delta a + 0.4(W - a_0)}{0.6(a_0 + \Delta a) - 0.4W + z} \cdot v_{pl} \tag{2}$$

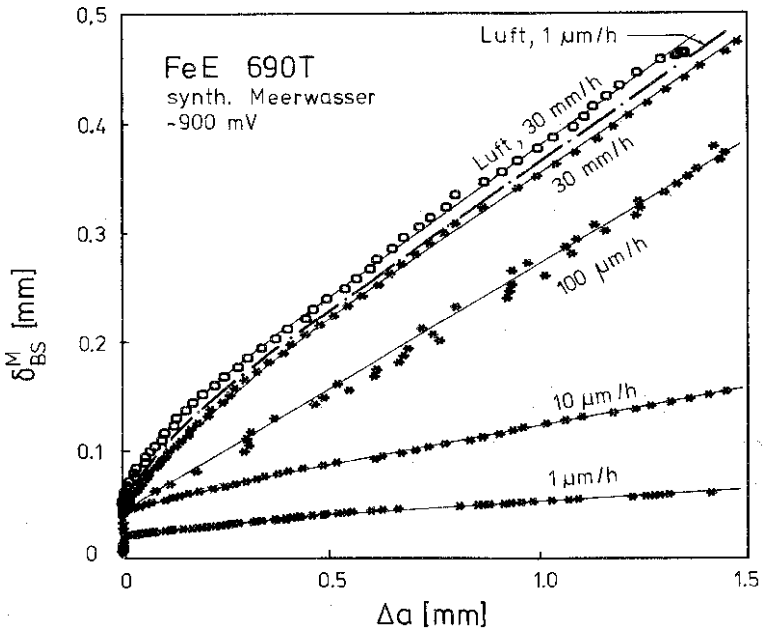


**Fig. 5** CTOD R-curves under hydrogen charging conditions and in laboratory air, determined at displacement rates between 1 µm/h and 30 mm/h [2]

In this modified CTOD the motion of the rotation centre of the specimen due to crack extension is taken into account. In Eq. 2, $v_{pl}$ is the plastic portion of the crack mouth opening displacement, (CMOD), E′ the Young's modulus for plane strain, and z is the distance between the load line and the actual measuring position for v. Figure 5 shows a set of CTOD R-curves which was generated for the same combination of material and environment leading to Fig. 3 and applying CMOD displacement rates between 1 µm/h and 30 mm/h [2].

Another feature which is associated with this type of rising displacement tests is the fact that the crack growth rate, da/dt, measured in such a displacement-controlled test, becomes essentially constant once the initiation stage is passed [11]. In Fig. 6 the plateau or steady-state values of these crack growth rates are plotted as a function of the applied deformation rates, the latter measured as the increase of the parameter $\delta_5$ with time, $d\delta_5/dt$. The data were obtained for the same material/environment combination as was investigated in Fig. 3. It can be seen that at deformation rates $d\delta_5/dt$ below $10^{-5}$ mm/s the crack growth rates measured in the corrosive environment started to deviate from the straight line relationship that in this log-log presentation is characteristic of tests in air, and form a second branch of the curve towards higher crack growth velocities.

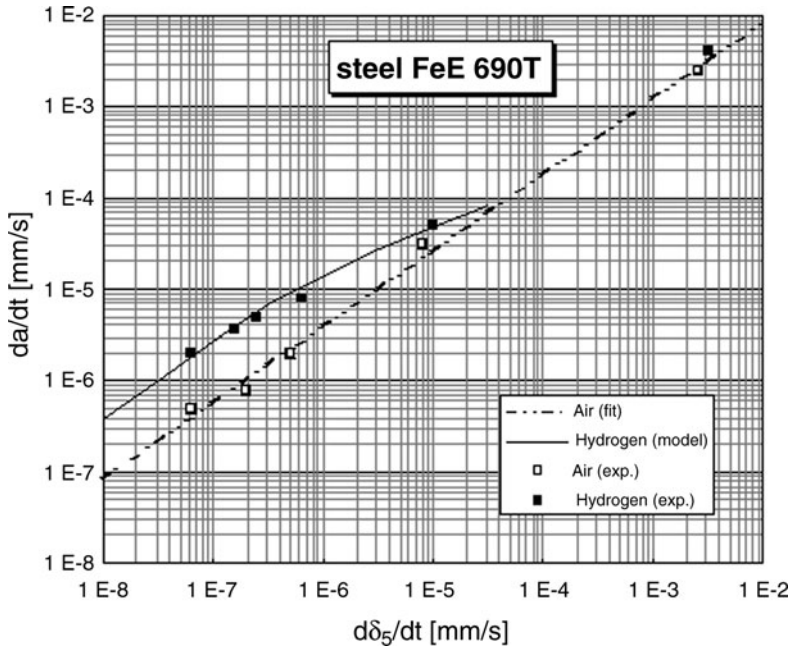


**Fig. 6** Relationship between the applied deformation rate, $d\delta_5/dt$, and the crack growth rate, da/dt, measured for the material/environment combination of Figs. 3 and 5 [11]

## 7 Modelling of Hydrogen Assisted Crack Growth

In recent years, increased computer power has made modelling a useful tool for simulating mechanisms of SCC and hydrogen embrittlement. This has not only improved the understanding of the micro-mechanisms involved in environment-assisted failure but can also be complementary to laboratory SCC testing. Multi-scale modelling describing the influence of a corrosive environment on crack susceptibility of components and structures may allow prediction of deformation behaviour and crack initiation in different material configurations under different external loads and environmental conditions. It can give predictions of critical flaws and fracture toughness of existing components and structures and may suggest the optimal microstructure configuration of new constructions with respect to withstanding environmentally-assisted cracking. Figure 6 indicates that the relative increase in crack growth velocity at low deformation rates caused by hydrogen embrittlement can be rationalized by a theoretical model. According to this superposition model the total crack growth velocity consists of a component due to ductile failure and a second one caused by hydrogen embrittlement [15, 16]. The model assumes that the hydrogen enters the specimen through the freshly created surface at the crack tip and that the diffusion inside the material is impeded by traps resulting from plastic deformation in the plastic zone ahead of the tip [17].

To mimic the experimental findings using this model, information about the impact of plastic deformation on the effective hydrogen diffusion coefficient was acquired from permeation experiments on thin plastically deformed membranes of the same material, and this information served as input parameter for predicting the acceleration of the crack growth velocities by hydrogen embrittlement [18, 19].

In another approach, the effect of hydrogen diffusion and of hydrogen embrittlement on stable crack propagation was assessed by a finite element simulation based on a cohesive model [20]. In the specific version of this model in which hydrogen enhanced crack extension was taken into consideration, two parameters characterizing the effect of hydrogen, i.e., the effective diffusivity, $D_{eff}$, and a reduction factor for the cohesive strength, μ, were introduced in addition to the two commonly used parameters cohesive strength, $T_0$, and critical separation, $\delta_0$ [21].

This way, it could be shown that a thus extended cohesive model could mimic the effect of HE on CTOD-R curves measured at various displacement rates for the steel FeE 690 T, as is displayed in Fig. 5. A comparison between model and experiment and the obtained good agreement is demonstrated in Fig. 7 [22]. The use of this model can also help to assess whether the displacement rate applied in a particular SCC test for determining $K_{ISCC}$ has been chosen sufficiently low enough to reach the lower shelf area indicated in Fig. 2.

In Fig. 8, a prediction is made regarding the influence of the displacement rate on the value of $K_{ISCC}$ determined in rising displacement tests [23]. The prediction is related to the same combination of material (steel FeE690T) and environment (hydrogen charging in ASTM D 1141) which was investigated in Figs. 3, 5 and 6, and the parameters were taken from cohesive modelling leading to Fig. 7.

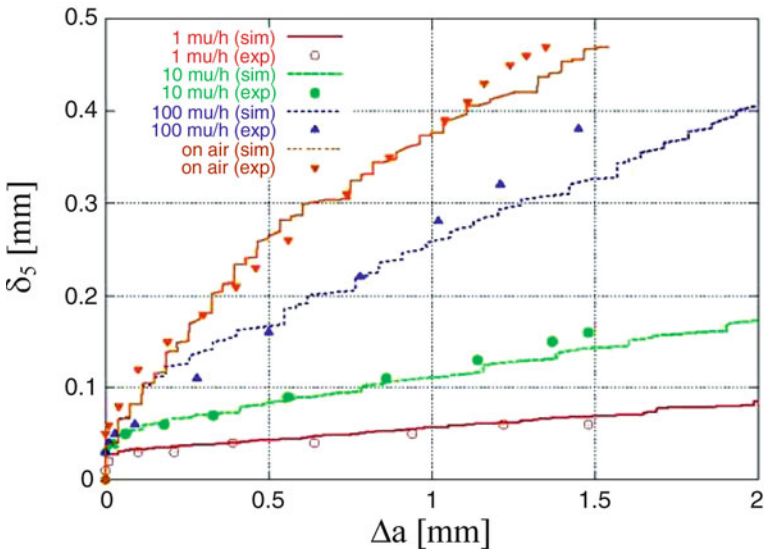


**Fig. 7** Comparison of experimental and simulated CTOD R-curves under hydrogen charging conditions and in laboratory air (displacement rates: 1, 10 and 100 μm/h, cf. Fig. 5) [21, 22]

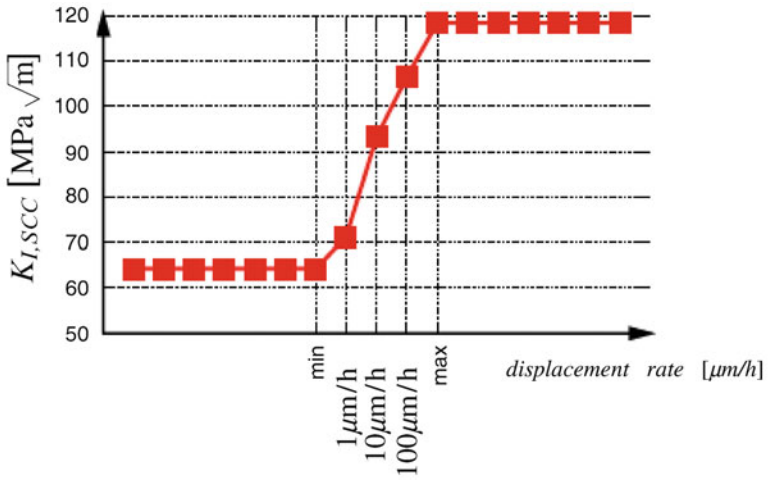


**Fig. 8** Model prediction for the influence of the applied displacement rate on the initiation value of stress intensity factor $K_{ISCC}$ according to Fig. 2 [23]

## 8 Conclusions

Rising displacement tests on pre-cracked specimens are in combination with elastic–plastic fracture mechanics methodology well suited to study the mechanisms of hydrogen embrittlement. Measurements of the relationship between crack growth velocity and the applied deformation rate and of CTOD based crack growth resistance curves can be used for a comparison with model calculations in which the hydrogen embrittlement is simulated. This way it is possible to mimic the influence of hydrogen embrittlement on both the crack growth velocity and on the crack growth resistance. It is expected that in the future suitable modelling can, at least to some extent, replace expensive and time consuming testing of hydrogen embrittlement. New nano-mechanical test methods which are under development can validate and provide information obtained from such models and can thus provide a safe basis for avoiding cases of SCC and to assess the criticality of existing components and structures with respect to SCC.

## References

1. R.J.H. Wanhill, Fracture control guidelines for stress corrosion cracking of high strength alloys, NLR Technical Publication TP 91006 L, 1991
2. W. Dietzel, Zur Anwendung bruchmechanischer Methoden bei der Untersuchung des Umgebungseinflusses auf die Rißausbreitung bei zügiger Beanspruchung, Report GKSS 91/E/27, Geesthacht, 1991 (in German)
3. J.G. Erlings, H.W. de Groot, J. Nauta, The effect of slow plastic straining on sulphide stress cracking and hydrogen embrittlement of 3.5% Ni steel and API 5L X60 pipeline steel. Corros. Sci. **27**, 1153–1167 (1987)

4. R.N. Parkins, Development of strain-rate testing and its implications, in *Stress Corrosion Cracking – The Slow Strain-Rate Technique*, ed. by G.M. Ugiansky, J.H. Payer (American Society for Testing and Materials, West Conshohocken, 1979), pp. 5–25
5. P. McIntyre, A.H. Priest, Accelerated test technique for the determination of KISCC in steels, British Steel Corporation Report MG/31/71, London, 1972
6. W.G. Clark Jr., J.D. Landes, An evaluation of rising load KISCC testing, in *Stress Corrosion – New Approaches*, ed. by H.L. Craig Jr. (American Society for Testing and Materials, West Conshohocken, 1976), pp. 108–127
7. W. Dietzel, Characterization of susceptibility of metallic materials to environmentally assisted cracking, Report GKSS 99/E/24, GKSS-Forschungszentrum Geesthacht GmbH, Geesthacht, 1999
8. D.R. Anderson, J.P. Gudas, Stress corrosion evaluation of titanium alloys using ductile fracture mechanics technology, in *Environment Sensitive Fracture, Evaluation and Comparison of Tests Methods*, ed. by S.W. Dean, E.N. Pugh, G.M. Ugiansky. ASTM STP 821 (American Society for Testing and Materials, West Conshohocken, 1984), pp. 98–113
9. G. Abramson, J.T. Evans, R.N. Parkins, Investigation of stress corrosion crack growth in Mg alloys using J-integral estimations. Metall. Trans. **16 A**, 101–108 (1985)
10. W. Dietzel, K.-H. Schwalbe, D. Wu, Application of fracture mechanics techniques to the environmentally assisted cracking of aluminium 2024. Fat. Fract. Eng. Mater. Struct. **12**(6), 495–510 (1989)
11. W. Dietzel, K.-H. Schwalbe, A study of the hydrogen induced stress corrosion cracking of a low alloy steel using fracture mechanics techniques, in *Hydrogen Effects on Material Behaviour*, N.R. Moody, A.W. Thompson (Hrsg.), The Minerals, Metals & Materials Society, 1990, pp. 975–983
12. D. Hellmann, K.-H. Schwalbe, On the experimental determination of CTOD based R-curves, in *The Crack Tip Opening Displacement in Elastic-Plastic Fracture Mechanics, Workshop on CTOD Metodology*, ed. by K.-H. Schwalbe (Springer-Verlag, Berlin/Heidelberg, 1986), pp. 115–132
13. W. Dietzel, K.-H. Schwalbe, Monitoring stable crack growth using a combined AC/DC potential drop technique. Z. Materialprüfung/Mater. Testing **28**(11), 368–372 (1986)
14. K.-H. Schwalbe, Introduction of $\delta_5$ as an operational definition of the CTOD and its practical use, in *Fracture Mechanics*, ed. by W.G. Reuter, J.H. Underwood, J.C. Newman. ASTM STP 1256, vol. 26 (American Society for Testing and Materials, Philadelphia, 1995), pp. 763–778
15. W. Dietzel, M. Pfuff, *The Effects of Hydrogen on Material Behavior*, ed. by N.R. Moody, A.W. Thompson (The Minerals, Metals & Materials Society, Warrendale, 1996), pp. 303–311
16. H. Vehoff, H.-K. Klameth, Acta. Metal **33**(6), 955–966 (1985)
17. A.H.M. Krom, R.W.J. Koers, A. Bakker, Hydrogen transport near a blunting crack. J. Mech. Phys. Solids **47**, 971–992 (1999)
18. W. Dietzel, M. Pfuff, G.G. Juilfs, Studies of SCC and hydrogen embrittlement of high strength alloys using fracture mechanics methods. Mater. Sci. Forum **482**, 11–16 (2005)
19. W. Dietzel, M. Pfuff, G.G. Juilfs, Investigations of hydrogen transport in plastically deformed steel membranes, in *Proceedings of 2nd International Conference on Environmental Degradation of Engineering Materials*, EDEM'2003, Bordeaux (FR) (ISBN 1-904350-07-0)
20. I. Scheider, Simulation of cup-cone fracture in round bars using the cohesive zone model, in *First M.I.T. Conference on Computational Fluid and Solid Mechanics*, ed. by K.J. Bathe (Elsevier, Amsterdam, 2001), pp. 460–462
21. I. Scheider, M. Pfuff, W. Dietzel, Simulation of hydrogen assisted stress corrosion cracking using the cohesive mode. Eng. Fract. Mech. **75**(15), 4283–4291 (2008)
22. R. Falkenberg, W. Brocks, W. Dietzel, I. Scheider, Simulation of stress-corrosion cracking by the cohesive model. Key Eng. Mater. **417–418**, 329–332 (2010)
23. R. Falkenberg, Simulation von Wasserstofftransport und Rißwachstum infolge wasserstoffinduzierter Spannungsrißkorrosion mit einer Analyse der Kopplungsphänomenologie, Ph.D. thesis, Christian-Albrechts-Universität zu Kiel, Kiel, 2010

# The Role of Material and Corrosion Engineering in Managing the Service-Life Integrity of Flow and Export Lines

**Manuela Gentile, Roberta Vichi, Roberto Bruschi, and Furio Marchesani**

**Abstract** Material and corrosion assessment are crucial engineering tasks that can deeply influence the satisfactory performance of interfield and export lines over the design lifespan. The project conditions to be pursued, can be different, and the field of engineering investigations needed and technical solutions developed, vast. The selection of line pipe material at design stage, in relation to the transported products and flow rate, relevant temperature and pressure profiles along the route and external environment as well, is a factor for a successful project. To be noticed that there are significant differences in the relevant engineering tests for the final selection, whether dealing with a short small diameter multi-phase flow line or a long strategic large diameter treated gas trunk line. On the other hand, the integrity management of a line over the operating time span, when the variation of transported product composition or inlet temperature and pressure as well, may occur, is a very specific process, to be assessed case by case, far different from the management of a strategic gas trunk line the performance of which over time is not subject to significant variation of transport conditions and the integrity of which may affect the vital activities of a district. In most circumstances the relevant project decisions regarding material and corrosion management are to be taken at a very early design stage, deeply influencing the future project development and operation as well. It shall be a very expert and safe decision. In this paper we will provide a brief overview of a few topics regarding strategic pipeline material selection and integrity management of interfield network, referring to recent outstanding R&D and project experiences.

M. Gentile (✉), R. Vichi, R. Bruschi, and F. Marchesani
Saipem Energy Services S.p.A., Fano, Italy
e-mail: Manuela.Gentile@saipem.com; Roberta.Vichi@saipem.com;
Roberto.Bruschi@saipem.com; Furio.Marchesani@saipem.com

T. Boukharouba et al. (eds.), *Integrity of Pipelines Transporting Hydrocarbons*,
NATO Science for Peace and Security Series C: Environmental Security,
DOI 10.1007/978-94-007-0588-3_10, 

# 1 Introduction

The last three decades saw the satisfactory accomplishment of some 10,000 km of strategic submarine and cross country pipelines, in increasingly deep and difficult waters, as well as across remote and harsh regions. Applied research provided a new technological background. Dedicated conferences and publish hundreds research notes dedicated to the structural integrity of pipelines, presented and discussed in specific international symposia. Loading regimes, interaction with soil and sediments, linear and non linear response in static and dynamic conditions, strength capacity, material and welding technology, stress and strain based design criteria, new equipment for installation, experiences in inspection and maintenance technology, repair, corrosion and strength degradation, rehabilitation have been studied and are still occupying plenty of joint industry research programmes. Relevant findings are currently embodied into design codes and are the basis for some challenging project perspectives envisaged in the coming years in increasingly harsh environments.

Pipeline technology is still topical for both operators and contractors due to the new challenges of the coming decade. A reason for this can be found in the increasingly difficult environments new pipelines are expected to sustain and in the complexity encountered in merging different disciplines: from environmental issues to fracture mechanics passing through geotechnics, ocean and coastal engineering, fluid dynamics and structural mechanics, etc., the objective is the structural integrity of each section of the pipeline (1,200 Km mean 100.000 fiels welds, and the failure of one jeopardizes the entire system) that has to tackle actions from both external – permanent, environmental, accidental – and internal – operational – media interacting with it. Further there are pipeline networks in operation, e.g. offshore field under development or at the end of the production cycle, that require particular care for minimizing environment threats still maintaining their operating target.

Pipeline systems include trunk lines (rigid, steel), long (~$10^2$ km) and generally large diameter (>16″ OD) pipelines transporting treated hydrocarbons mostly sweet gas at high pressure (>10 MPa), interfield (rigid or flexible) pipelines (flow lines), short (~$10^1$ km) and in general small diameter (<16″ OD) pipelines transporting single or multiphase often untreated and sour hydrocarbons. Actually this separation shall be reflected in design codes. Different design criteria in relation to the different roles that trunk lines and interfiled pipelines generally fulfil should be established. As an example, the Transmediterranean pipeline system supplies approximately 30% of gas used in Italy, 27 billion $m^3$/year. The first three lines (20″ OD) were laid in deep waters (more than 600 m) in 1979 and 1980, the second two (26″ OD) in the early Nineties. The availability of this gas, actually strategic, provides quite different arguments for the integrity and carrying capacity over the years with respect to those related to the productivity of an offshore field and, therefore, to the well being of an interfiled pipeline sometimes in service for a short lifetime!

For both types of pipeline systems whether trunk lines or interfield lines, the adopted technology provided an excellent performance over the past 30 years, as shown by the lack of significant incidents implying shut down or, at worst, loss of

containment. A thorough analysis of available failure statistics sometimes has shown a weak correlation between adopted design criteria and experienced failures. Therefore a general consensus has arisen over recent years on the introduction of the limit state approach as a way to rationalize the design phase, particularly from the perspective of reducing costs of new transportation networks and documenting the pipeline reliability of new ventures in ultra deep waters and harsh or sensitive environments.

"External Interference" appears to be the most likely cause of pipeline failure, in general 30–60% according to the different sources [1]. Corrosion is the second cause, 50–20% as a complement to the external interference. In addition, corrosion is reported mainly in the near platform zone, probably indicating a correlation between external impact causing coating damage and development of corrosion attack but also due to more severe operating conditions, particularly high temperature. In the Gulf of Mexico a higher incidence of corrosion failure is evident with respect to North Sea pipelines. This can be attributed to the higher average age of such lines which were built in compliance with older design and corrosion protection standards. The corrosion protection design in new pipelines is such that the corrosion failure rate should be decreased to negligible figures. Material failures are reported to represent a minor contribution to the overall failure probability. Again, this is expected to be even more evident for new pipelines complying with modern material specifications and very restrictive criteria for weldability and toughness.

For a pipeline, the selection of the most appropriate material is a crucial step and is usually performed since the preliminary phases of a project, in relation to the project parameters foreseeable at the time and taking into account the management of the line over time (i.e. variation of product composition, inlet temperature and pressure, vertical profile of the laying bed/burial configuration, etc.). This selection is significantly different when dealing with a short small diameter multi-phase flow line with respect to a long strategic large diameter treated gas trunk line. Aggressive fluids in multi-phase flow line can be faced utilizing inhibitors, Corrosion Resistance Alloy. As an example, plenty of efforts are dedicated to field development in difficult conditions, from both external environment and product aggressiveness. As an example, the Kashagan Oil Fields Development is the most challenging project currently undertaken by Oil&Gas Industry. External environment (arctic conditions) as well as considerable present of $H_2S$, in the extracted products, are the key issues. As for trunk lines, current research is looking into long distance gas transportation and deep water profile. Long distance transportation of large volumes of natural gas requires high pressure and large diameter-thick wall line pipe. High grade steels (equivalent X100 and X120) are proposed by industry to meet technical-economical feasibility targets. ENI comprehensively worked on X100, particularly looking into the sensitivity to environment of new high grade carbon steels.

Moving from design to operation, an appropriate maintenance and monitoring program can significantly help ensuring its safety during the life time. In operating a pipeline it shall be taken into account that pipelines are subjected to loads and environmental effects which may cause them to become degraded with the passage of time. Degradation has a variety of causes, including corrosion, mechanical damage, fatigue, and stress corrosion cracking. In particular, a huge work has

been made by Majors, on the modelling of the corrosion phenomenon. In the application, a remarkable uncertainty on the previsions is evident. We are currently developing an engineering procedure that analyzes fluid dynamics, production, geometry, transported fluids, etc. along lifetime, to identify critical locations where different corrosion mechanisms might be relevant, applies advanced engineering tools (artificial neural networks) across the specific locations previously identified, using the experiences maturated in the industry (e.g. the model proposed) and calibrating the previsions on the basis of detailed and qualified field measures as well, and provides an assessment of corrosion rate with a measure of confidence linked to both model uncertainty and uncertainty of the input parameters.

## 2 Material Selection for HG.HP.HC for Long Distance Gas Pipeline

Current research is looking into long distance transportation of large volumes of natural gas. In order to improve the economics of the pipeline transport system, industry is proposing high pressure and large diameter-thick wall line pipe in link with high grade steels (equivalent X100 and X120).

Trunk line usually experience negligible corrosion phenomenon due to the sweet and dry internal fluid and only minor issues arise from external corrosion.

However, exploiting new, high grade steels, potential risks can occur, mainly related to the uncertainties of the safety of such pipelines in the long term, as in field experience are practically absent. The huge investments required for these transport systems push for specific investigations and qualifications.

ENI comprehensively worked on X100, particularly looking into the sensitivity to environment of new high grade carbon steels. In the last years a relevant effort was paid to qualify the application of X100 steel line pipes for a long distance gas transportation [2].

The usage factors for pressure containment, as well as line pipe capacity to sustain global and local deformations, are closely linked to investment costs and reliability in operation. A series of studies confirms the major role of steel on costs, and such a new material can be adopted only when full confidence on satisfactory performance in operation, is achieved.

Further concerns are related to the susceptibility of high grade steels to hydrogen embrittlement and environmental aggression, in case of severe local deformations or pipe wall surface damages, as those caused by third party interference, and under the sustained action of the internal pressure.

The pipe integrity (EAC and EAC + Mechanical Damage) evaluation is a paramount important aspect to be evaluated in order to perform “economical risk evaluation”, particularly high EAC susceptibility could vanish the economical benefit of the high grade steel save as it could affect long pipeline section.

A pilot section in X100 line pipes was built to assess the fabrication, constructability and in service behaviour of a X100 pipeline. The line was put in (simulated) service to test (and monitor) a realistic realization of X100 gas pipeline over the time.

**Fig. 1** Samples of in field tests, (*on the left*) in field cells where artificial low pH environment is reproduced and strain gauges on mechanical damage, (*on the right*)

Specific issues tested are the in service behaviour of special components (hot bends, tees, dielectric joints and other fittings), coupled to X100 line pipes and field bends.

The test section included different wall thicknesses, as a major was the investigation of the safe working factors for X100 line pipes, in relation to local steel deformability and environmental assisted fracture behaviour on damaged pipe in realistic operation condition. The effect of the working factor, that is the level of the circumferential stress mobilized to resist the internal pressure (in relation to the steel characteristic strength), both in integer pipes in presence of sweet environment and in damaged pipes in presence of normal and aggressive environment, on the safe life operability of a high pressure pipeline crossing harsh environments, see Fig. 1.

At the end of the simulated operation, line pipe and crack stopper capacity to arrest running shear fracture was tested (burst test).

In parallel to the pilot section testing, full scale and laboratory tests were purpose designed and performed to extend the qualification of the X100 steel grade and define the limits and the weak points for its applicability.

The susceptibility to environmental cracking was assessed also through laboratory tests investigating slow strain rate and slow bending (SB) tests. The SB tests evidenced a potential critical role by the longitudinal welding: some steels showed a very high HE resistance, other high HE susceptibility and a final brittle propagation of the cracks. The possibility of insurgence of HE phenomena in the longitudinal welding was also confirmed by the ISSR tests.

The SSR tests carried out in the NN-SCC environment focused the increasing of the SCC susceptibility with the Actual Strength. The NN-SCC cracks are always initiated from localized attacks. An electrochemical procedure to obtain localized attacks on the surface was developed.

Finally, both in field and laboratory tests evidenced the strong effect of the third part mechanical damage on the HE behaviour of the X100 steels.

Specific full scale tests were designed to further investigate the combined effect of working factors, cyclic pressure loads, mechanical damage and different level of cathodic protection. Traditional X65 carbon steel pipes were also involved in order to assess the high grade resistance/criticality on a comparative basis too.

## 3 Material Selection for Deep Water Pipeline

The traditional view of subsea crossings, which three decades ago were considered as merely belonging to offshore operation i.e., export lines from offshore fields, is definitely changed. Offshore trunklines in service or in construction exceed 1,000 km, the longest ones stretching across the North Sea (Langeled, 44 in. pipeline between Norway and England, in operation) and the Baltic Sea (Nord Stream 2 × 48 in., 1,200 km pipelines between Russia and Germany, soon to be under construction). Currently, a few 1,000–2,000 km subsea pipeline ventures (in deep waters and hostile environments) are being planned. Subsea pipelines between continents can now be conceived, and a series of new projects are currently on the desk, to transport gas from, for example, Oman or Iran to India (in more than 3,000 m water depth) and across the Black Sea, the latter to create an offshore permanent link from the Caspian and Middle East regions to central Europe. The Mediterranean basin provides a relevant development framework for strategic submarine crossings.

Line pipe material specification is an important issue for deepwater projects, and this is reflected in the efforts of certification bodies to get consensus on international guidelines. The stringent requirements on weld-ability and toughness, as well as on geometric tolerances and resistance characterisation of the line pipe are currently met by a significant number of pipe mills worldwide. There is certainly room for overcoming the traditional reluctance of pipeline operators to use high strength steel such as X80 or even X100. X70 line pipe has been laid offshore relatively recently (Europipe II in the mid-1990s, Langeled in 2004, and next up, Nord Stream), and X120 is already on the line.

For increasing steel grades, the higher material proportionality limit allows for higher working stresses, for both installation and operation, assuming the pipeline is specified to work within the elastic field i.e., fully recoverable deformation after unloading. The adoption of limit states-based design, as proposed in some new projects, allows the pipeline to work beyond the proportionality limit. The actual stress-strain curve of steel and the performance of girth welds therefore becomes a more important factor for pipeline integrity.

One crucial aspect of working with high strength steels concerns welding technology, as well as acceptance criteria for maximum weld defects and weld toughness. Advanced and more precise non-destructive control of welds, and engineering criticality assessment methods, have been introduced in the last 10 years to qualify weld strength vs. defect acceptance criteria. For increasingly high grade steels, it is difficult to get a tough weld stronger than the parent

pipe and, considering the thick wall, the heat affected zone of the longitudinal seam weld is a concern. Overmatching and tearing capacity of the as-weld material – key factors in the assessment of the strength capacity of a weld in operation under large strains, as well as the softening of the heat affected zones – become critical issues.

For shallow, long distance pipelines, the reduction of a few millimetres of wall thickness, thick due to the high pressure and large diameter of the lines, would have a significant cost impact without impacting on the overall safety, strictly linked to the wall thickness. When it is the internal pressure that dictates the MWTR, there is proportionality between the required thickness and the characteristic strength, so for the same diameter and internal pressure, the required wall thickness for X60 is two times the one for X120.

For ultra deepwater pipelines, the steel grade is not a priority. The relationship between the strength characteristic and wall thickness for collapse strength is not direct as per internal pressure containment. There is a parameter, the fabrication factor, which significantly affects the minimum wall thickness requirements for external pressure containment, the subject of a series of investigation after it was first introduced in design guidelines. It is related to the fabrication process of creating a round pipe by using cold bending thick plates. For collapse strength, the proportionality limit in compression is relevant, which may be significantly lower than the one in tension. There may also be a further difference between samples taken at the inner wall from samples taken at the outer wall (across the large thickness). Pipe mills must demonstrate that at the end of the fabrication cycle, after the coating and particularly the associated thermal processes, the fabrication factor is partially recovered.

## 4 A Crucial Issue of Deep Water and Closed Sea Gas Pipeline

Deep water and closed seas may be characterised by anoxic conditions with the proliferation of anaerobic bacteria, i.e. Sulphate Reducing Bacteria (SRB), which generate a significant amounts of $H_2S$ in the sediments that may cause Sulphide Stress Cracking mechanism as the consequence of hydrogen-uptake in the steel, and it depends on number of parameters of which the most important are hydrogen sulphide concentration and pH. Briefly, atomic hydrogen migrates into the steel and concentrates at inclusions and voids in the steel. Voids are fault in the crystal lattice that can be filled by small interstitial atoms. Most voids occur at points of high stress, where slippage of metal atoms has concentrated the dislocation in the crystal lattice, as a result of yielding of the steel. The steel becomes embrittled because the hydrogen acts in a way similar to an alloying element and prevents further stress relaxation by movement of the dislocations.

This may be particularly relevant for UOE cold formed pipes, which undergoes significant plastic strain during fabrication (Thermo-Mechanical Controlled

cooling Process plates – TMCP). The susceptibility to SCC generated by the external environment is related of the following conditions:

- the probability to have a "sour environment" (pH value and $H_2S$ concentration),
- the probability that a material can be exposed to a sour environment coupled with the coating breakdown,
- the steel material susceptibility to this corrosion phenomena.

Normally the application of external anticorrosion coating provides the main protection for the steel. Nevertheless steel exposure may occur in those locations where the coating has been damaged by natural degradation or by external interferences. A methodology is proposed to quantify the risk of external SCC during engineering phase. A case study exemplification [3], is presented using the Baltic Sea sediments environmental data recovered by bibliographic sources.

In order to assess the most reliable design value of $H_2S$ concentration and pH for pipeline design, representative distribution functions for both pH and $H_2S$ concentration in seabed mud are found. On this basis, the external environment seen by an hypothetical pipeline as been classified following the NACE/ISO15156 [4], approach as "susceptible to sulphide stress cracking". In this code the critical level of hydrogen sulphide for SSC is defined in terms of concentration or partial pressure of hydrogen sulphide and pH.

The application of the proposed methodology leads to "a ready to use" considerations for a pipeline project. In detail, using the collected literature data characterizing the sediment mud of major areas in the Baltic Sea, $H_2S$ concentration and pH were used to construct a cumulative distributions of $H_2S$ concentrations and pH. A 2-parameter (for $H_2S$ concentrations) and a 3-parameter (for pH), Weibull distributions show a reasonably good fit with the available data points.

From the selected Weibull distributions is possible to evaluate the probability that the pipe will actually see an external environment able to promote SSC phenomena. The approach is to apply a Monte Carlo statistical method to calculate the probability of having a sour environment. Once the steel material has been tested and proven resistant to such environment it is possible to state that SSC susceptibility is related to the probability of an external environment to exceed the target test condition. Following the NACE/ISO 15156 framework, which correlated the severity of the sour conditions on a pH – $H_2S$ partial pressure plot, see Fig. 2, it is possible to measure the exceeding probability of an environment worst than the target point using the following criteria:

- rectangular criteria,
- SSC bound translation criteria.

"Rectangular criteria" takes into account the probability that the case study environment shows a pH or a $H_2S$ partial pressure "worse" than the "target test point". This criteria consider pH and $H_2S$ critical concentration independently to each other: if single parameter exceeds the target test point the environment condition is assumed more severe of target point (Fig. 1).

Following the physical meaning of SSC Region Classification NACE/ISO 15156 [4], "SSC bound translation criteria" defines a new reference line parallel to the

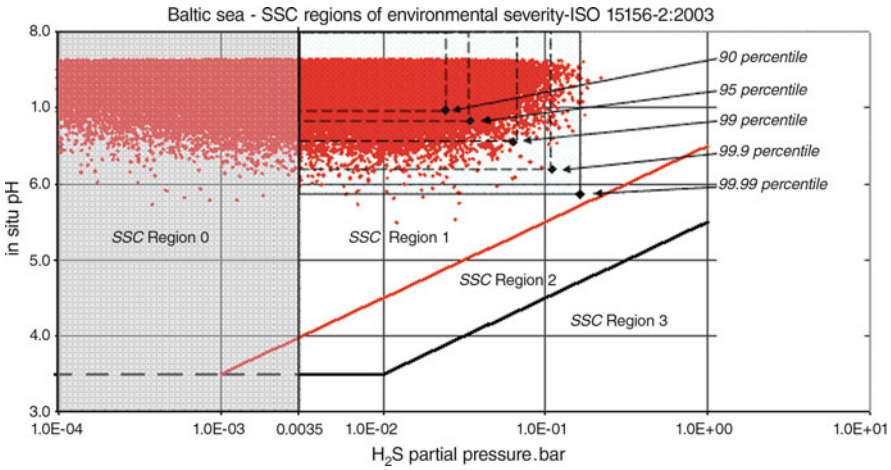


**Fig. 2** SSC environment severity – rectangular criteria

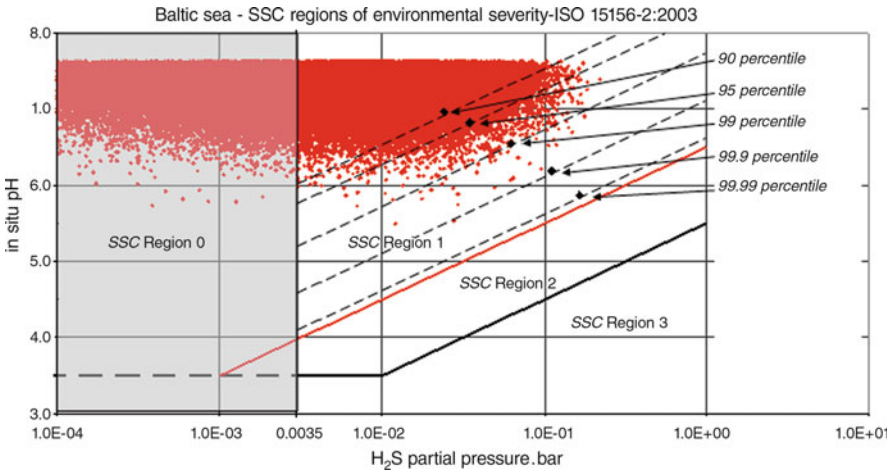


**Fig. 3** SSC environment severity – SCC region bound translation criteria

SSC Region 1/SSC Region 2 bound-line for each target test point. Considering the new reference line, the probability that the case study environment is worst than the target point is calculated by counting point (the couple of pH and $H_2S$ partial pressure) "worse" than i.e. under the new reference line, see Fig. 3.

The "SSC bound translation criteria" is considered more rational because its link the physics of the problem (being based also on the experimental evidence) and also still conservative.

Randomization analyses with a classical Monte Carlo approach was used. Statistical uncorrelated sampling of $H_2S$ concentration and pH data from their statistical distributions were made and then plotted in the ISO framework.

On these bases the case study environment shall be considered as "mild sour" (i.e. Region 1 of ISO15156 framework) with a frequency of 56%, and therefore it is necessary to qualify the steel material for Region 1. At the same time, the "target test points" have been assumed as the same percentile value for pH and $H_2S$ concentration distributions, i.e. 90, 95, 99, 99.9 and 99.99. Note that it is a conservative approach, because the minimum percentile value of pH is linked to the maximum value of $H_2S$.

The application of a "SSC region bound translation criteria" unless the more conservative "rectangular criteria" presented above, leads to the following results.

A conservative target test conditions can be assumed (Table 1): i.e. a $H_2S$ concentration of 850 ppm and pH of 5.9, safely representative of 99.99% percentile of the Baltic Sea environment, see Fig. 4.

If a pipeline steel material is tested and proven resistant to such environment, the residual probability of SSC susceptibility is equal to the joined probability for a pipeline of a bare metal surface exposed to a seabed mud with a "sour condition" worse than the test condition. In this case study the calculated probability is only $10^{-6}$ to $10^{-7}$. This means that the frequency to find a bare steel surface exposed to sour environment able to active SSC phenomena is less than $10^{-5}$ events/pipeline/year, acceptable for DNV rules [5].

**Table 1** Target test point

| Target test points | | | | | | |
|---|---|---|---|---|---|---|
| Percentile | 90 | 95 | 99 | 99.57 | 99.9 | 99.99 |
| $H_2S$ (ppm) | 123 | 177 | 320 | 405 | 562 | 837 |
| pH | 6.97 | 6.83 | 6.55 | 6.41 | 6.19 | 5.87 |
| Out of range probability ("SSC region bound translation criteria") | 3.7E-02 | 1.0E-02 | 4.7E-04 | 1.0E-04 | 1.0E-05 | <1.0E-6 |

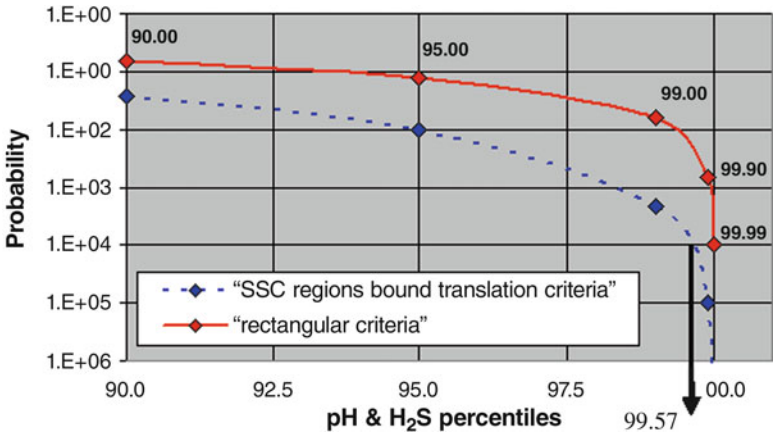


**Fig. 4** Comparison between different criteria for SSC Baltic Sea environment severity

## 5 Operation of Interfield Networks

Operating a pipeline requires an understanding of the purpose of the pipeline, how the pipeline was designed and constructed, the codes and standards that govern the operation, the operational history of the pipeline, and the pipeline's current status. It also requires a good knowledge of pipeline engineering and many other related fields, such as corrosion control, automatic control, fluid mechanics, structural engineering, machine maintenance, etc.

Therefore, it takes engineers and technicians of different disciplines and training working together as a team in order to keep a modern pipeline system running and maintained in good condition. Unqualified operators and/or inadequate training often result in improper operation of the pipeline and damage to the system, or frequent unscheduled shutdown. The use of modern computers and automatic control system has greatly decreased the number of technical personnel needed to run a pipeline system; however the knowledge and training required by the technical personnel who run a pipeline have been increasing steadily.

How to operate a given pipeline system depends on the purpose of the pipeline. All the operational strategies and details must be designed to achieve this purpose. The strategy is normally planned around a set of operational parameters such as the discharge through the pipe, mean velocity, temperature range of the fluid transported, maximum and minimum pressures at various locations along the pipe, pump speed and head, valve closing speed, etc. These operational parameters are determined not only by the original design but also by the changing pipeline condition e.g. production and market demand. This shows that the operational strategy and parameters that govern a pipeline may change with time, and the current situation governs the ongoing operation of the pipeline.

The set of operational parameters and their relevant allowable ranges are the results of multidisciplinary complex studies designed to ensure safe, uninterrupted and optimum productivity in oil and gas streams. For an export line, these studies ensure system integrity and transport capacity under both routine (steady and transient states) and emergency conditions. For a flow line, another issue has to be considered i.e. to prevent pipe blockage.

Flow assurance is a multidisciplinary process to guarantee successful and economical flow of hydrocarbon stream from reservoir to the point of sale along the complete operating life of the production system and considering all the potential operating conditions (steady state, transients and possibly emergency). Understanding the concept helps to ensure that any development plan, from exploration through abandonment, is technically viable and designed for optimal operations throughout the field's life. Besides network modelling and transient multiphase simulation, flow assurance involves effectively handling many solid deposits, such as, gas hydrates, asphaltene, wax, scale, and naphthenates.

Bespoke software and commercial multiphase packages are available to execute flow assurance projects and engineering the flow of oil, water and gas in pipelines and receiving facilities. These include PVT packages for fluid modelling and

characterization (e.g. reservoir fluid phase behaviour, hydrate, wax, and asphaltene precipitation and deposition, water chemistry and inorganic scales, rheology of produced fluids and rock-fluid interactions), as well as simulation software for steady and transient multiphase flow simulation.

Internal corrosion processes depend on the service of the pipeline. The main mechanisms are sweet corrosion caused by the presence of carbon dioxide, sour corrosion caused by hydrogen sulphide, and microbiological corrosion resulting from the activity and growth of sulphate-reducing bacteria (SRB) in the pipeline. A detailed description of each mechanism is provided in [6]. The prevention of corrosion requires attention throughout the life cycle of the pipeline, from design (selection of materials adequate to the transported fluid and/or the definition of a corrosion allowance thickness, and treatment of transported fluid for an export-line only) to operation (corrosion status monitoring). Due to the huge economic impact of corrosion, recent studies indicate a cost of corrosion of about 3–4% of PIL in the more industrialized countries [7], a huge work has been made by Majors, on the modelling of the internal corrosion phenomenon to provide a reliable corrosion rate prediction.

The leakage or rupture of a petroleum-product pipeline poses a threat to both the environment and public health due to the pollution of surface water, ground water, and/or soil. For natural gas pipelines, the greatest threat is property and life lost from explosion and fire resulting from pipeline leaks or rupture due to the highly flammable nature of natural gas.

## *5.1 Corrosion Management*

Different oil companies and research institutions have developed a large number of prediction models, mainly focusing on $CO_2$ corrosion of carbon steel in oil and gas wells and pipelines fully or partially described in the literature. Several models have been developed mainly based on empirical correlations with laboratory or field data. Some other models were built based on a strict mechanistic analysis of the various processes involved in the corrosion mechanism. Commonly used $CO_2$ corrosion models are the De Waard and Milliams [8] and [9], the De Waard et al. [10] and the Norsok M-506 [11].

It is seen that different parameters are used as inputs and the number of the required ones varies considerably from model to model [12]. An overview of the parameters treated in the various prediction models includes operating temperature and pressure, flow rates, $CO_2$ and/or $H_2S$ mole fraction in the gas phase, measured or calculated pH of condensed and/or formation water, bicarbonate concentration in the water phase, total ionic strength in the water, inhibitor efficiency, glycol concentration in the aqueous phase and so on.

As an example, the De Waard et al., [9], predicts corrosion rate due to $CO_2$ as a function of operating conditions and acid gas molar fraction:

$$\mathrm{Log}(\mathrm{CR}) = 5.8 - \frac{1710}{\mathrm{t} + 273} + 0.67 \cdot \mathrm{Log}(\mathrm{pCO_2}) \tag{1}$$

Where $pCO_2$is the $CO_2$ partial pressure and t the fluid operating temperature. Several corrective factors have subsequently been added to the former equation to take into account the effect of the total system pressure, high temperature, pH, glycol and/or inhibition and water wetting.

For multiphase pipelines the variation in flow regime, liquid flow velocity, water wetting and temperature along the pipeline will have a large effect on the prediction of pipeline corrosion. Most of the models take limited account for multiphase flow effects, and some of the models require separate fluid flow calculations. Many of these models take flow-related parameters like liquid velocity or water, oil and gas production rates into account. However, most of the models are point models, i.e. they can only be used to predict the corrosion rate at a given location in a well or pipeline where the temperature, pressure, water chemistry and flow conditions are specified. The models either take liquid velocity as input or assess the flow effect on corrosion by a simplified fluid flow calculation in a point.

In the application of the internal corrosion models, a remarkable uncertainty on the previsions is evident, see Fig. 5, due to the complexity of the phenomenon as pipelines are usually afflicted by a combination of degradation modes (microbially induced corrosion, oxygen corrosion, etc.), the difficulty in modelling the interactions among different corrosive species such as $CO_2$ and $H_2S$, and the difficulty in obtaining reliable input parameters. The high spread in previsions also reflects the different philosophies used in models development [13, 14].

In details, different prediction models for $CO_2$ corrosion of carbon steel have been evaluated in two Joint Industry Projects, JIP, carried out at the Institute for Energy Technology, IFE, in Norway [13, 14]. The corrosion models have been run with a series of test cases in order to examine the sensitivity of the different models to input parameters such as temperature, water chemistry and flow velocity. Field data with actual corrosion measurements have been gathered from the companies

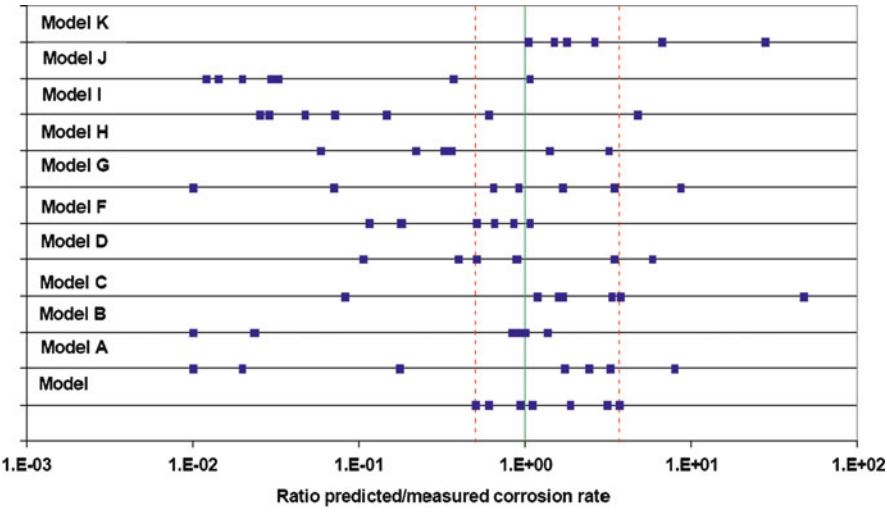


**Fig. 5** Previsions (*discouraging*) of corrosion rate (mm/year) [15]

participating in the projects. The corrosion models have been run for the actual field cases and the predicted corrosion rates have been compared with the actual measured corrosion rates.

The projects have demonstrated that it requires much time, effort and patience to collect reliable corrosion field data from oil and gas production systems, and that the chances of obtaining good field data are increased if the required parameters are not over-specified. Moreover, very different results are obtained when the models are run for the same test cases. The corrosion models have very different approaches in accounting for oil wetting and the effect of protective corrosion films, and this seems to account for much of the differences in behaviour.

### *5.2 New Engineering Approach*

We are currently developing an engineering procedure covering internal corrosion of flow lines containing $CO_2$, $H_2S$ and/or $O_2$ together with liquid water containing corrosive species, microorganisms that may influence corrosion and solids such as deposits or scale. The aim is to obtain an assessment of corrosion rate associated to a measure of variance that considers the uncertainty on the input parameters.

The prediction of corrosion rate resulting from this new engineering approach, involves to combine fluid flow models and corrosion models into a single package as fluid dynamics i.e. flow regime, liquid flow velocity, water or oil wetting, governs the initialization and development of the corrosion phenomenon. In order to perform a corrosion evaluation for a specific well or pipeline it is therefore necessary to first perform a fluid flow simulation with a separate fluid flow model and then use the results from this simulation as input for running corrosion models in the well or pipeline.

The procedure consists of three separate phases:

- flow assurance analysis to locate where it is most likely corrosion problems may occur and relevant corrosion mechanisms identification,
- use of advanced engineering tools to manage parameters and models uncertainties,
- use of corrosion model prediction in the integrity assessment.

## 6 Flow Assurance and Relevant Corrosion Mechanisms in Critical Locations

In the first phase, it is required to collect and then organize in as detailed of manner as possible, all existing, relevant, essential, historic and current operating data about the pipeline segments and/or regions relevant to corrosion distribution.

The types of data collected are typically available in design and construction records (e.g. routes, material, flow rates, design pressures and temperatures, and

microstructure), operating and maintenance histories, corrosion survey records, gas and liquid analysis reports, and inspection reports from prior integrity evaluations or maintenance actions.

Then, calculations are performed using steady and transient multiphase flow simulation software, such as OLGA®, to determine flow regimes and hold-ups in order to prioritize locations along a pipeline for susceptibility to and severity of corrosion damage. In fact as the operating conditions vary along the route, the engineering of the fluid flow has the benefit to predict the flow regime along the pipeline which is used for the prediction of oil or water wetting of the pipe wall moreover, pressure, temperature, liquid flow velocity, wall shear stress an so on, are used in the corrosion rate calculations i.e. as input parameters of the available corrosion models. The factors contributing to the distribution of corrosion within each flow regime are identified and the locations of different corrosion damage severity are predicted (e.g. deposits of formation and/or condensed water, high flow velocities, etc.).

As corrosion rate conditions are variables not only in space but also in time, significant variations in time of main input parameters are identified and simulations are repeated for each time interval, see Fig. 6. Samples of in field tests, (on the left) in field cells where artificial low pH environment is reproduced and strain gauges on mechanical damage, (on the right)

In each identified point, the conditions, corrosion rate depends on, can be different. A probability of occurrence is calculated for each corrosion mode in each critical location and point in time. The most probable development mode is selected as input, as well as other potential (second in ranking). For the corrosion mode identified as most likely to occur in each location and point in time, corrosion rate is predicted by relevant openly available models considered not as deterministic correlations but as probabilistic functions since despite what we often think, the input parameters are not deterministic quantities i.e. quantities which are perfectly known but are random variables with an associated probability mass function and cumulative distribution function. So corrosion rate itself, CR, as a function of random variables, $X_1$, $X_2$, ... $X_k$ can be described as a random variable:

$$CR = f(X_1, X_2, ..., X_k) \tag{2}$$

In applying the developed/available formulas, a preliminary assessment is carried out to evaluate the sensitivity of the different models to input parameters such as operating pressure and temperature, water chemistry and flow velocity in order to identify the most critical ones i.e. to show the ones for which obtaining reliable values is most important. A multivariable regression technique is applied to rank the input parameters and establish which have a greater influence on the prediction of the corrosion phenomenon i.e. to assess the weight to be associated to an input change. As the accuracy of the corrosion rate predictions is limited by the quality of the input data, the most critical input parameters are considered as random variable with an associated probability mass function in order to consider the uncertainty relevant to their true value.

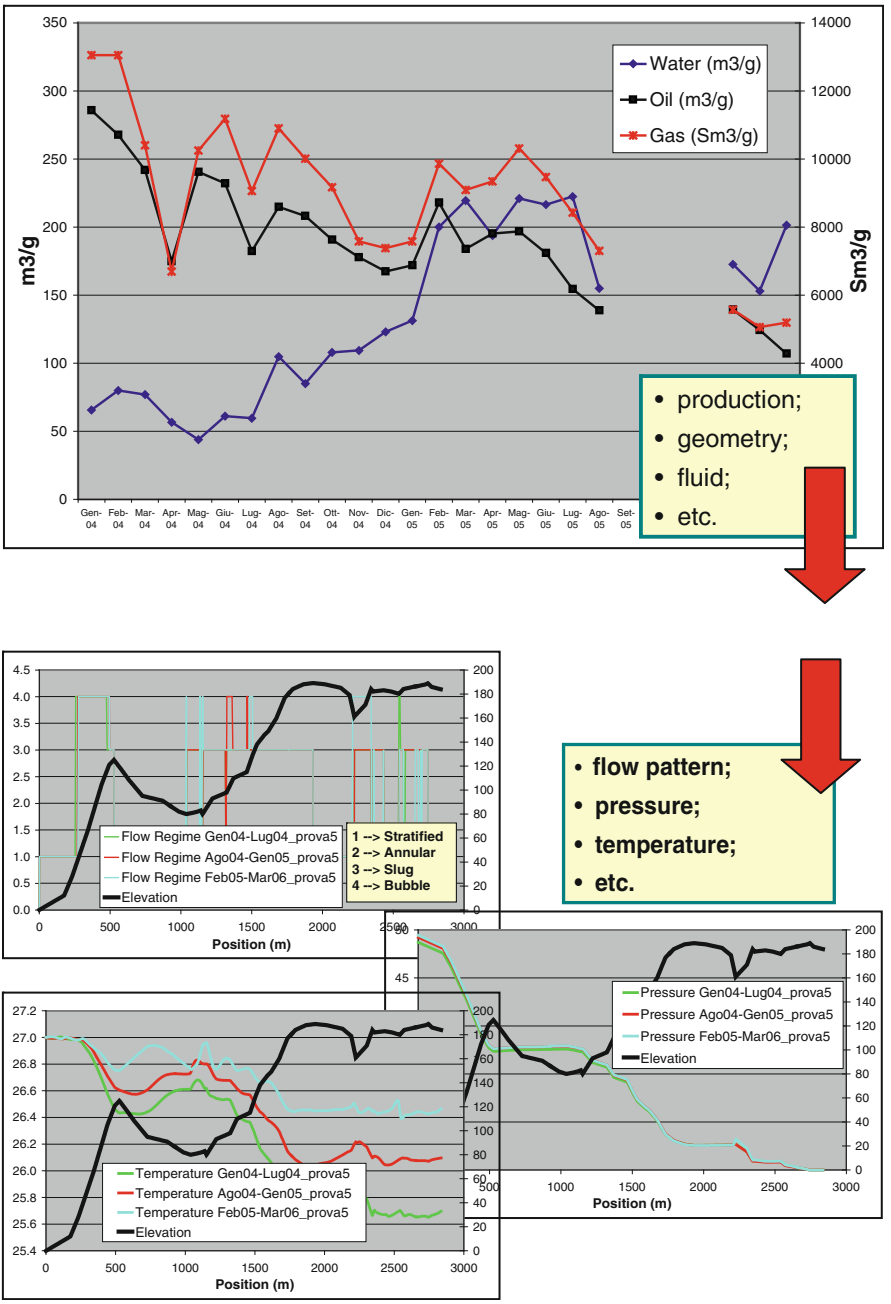


**Fig. 6** Analysis of fluid dynamics, production, geometry, transported fluids, etc. along lifetime

Moreover, in order to estimate how corrosion predictions vary as a function of input changes i.e. to assess the uncertainty of the previsions, a statistical analysis is carried out by means of Monte Carlo and Rosenblueth methods [16].

The Monte Carlo method is a simulation technique used to generate some results numerically without actually doing any physical testing. Defined the probability distributions of the main parameters, the simulation technique generates samples of numerical data which allow to assess the cumulative distribution function, CDF, of the function of random variables as indicated in Fig. 7.

The Rosenblueth's 2k + 1 point estimate method provides an estimate of the mean, $\overline{Y}$, and coefficient of variation, $V_Y$, of a function of random variables $Y = f(X_1,X_2,...,X_k)$ by evaluating the function at 2k + 1 key points where k is the number of the input parameters, as indicated below:

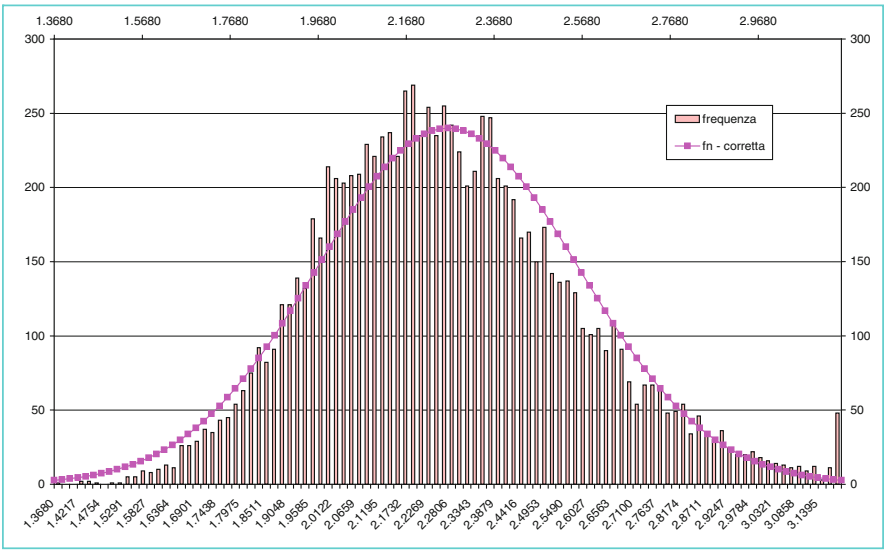


**Random Variable:**

- pressure (normal);
- temperature (normal);
- $CO_2$% (normal);
- $HCO_3^-$ (normal).

**10000 samples**

| | |
|---|---|
| average (mm/year) | 2.26 |
| standard deviation | 0.30 |
| coefficient of variation | 13.2% |

**Fig. 7** Assessment of the cumulative distribution function of a function of random variable

$$\bar{Y} = y_0 \cdot \prod_{i=1}^{k} \left( \frac{\bar{y}_i}{y_0} \right) \tag{3}$$

$$V_Y = \sqrt{\left[ \prod_{i=1}^{k} \left( 1 + V_{Y,i}^2 \right) \right] - 1} \tag{4}$$

## 7 Corrosion Prediction Vs. Parameters and Models Uncertainties

The second phase of the procedure applies advanced engineering tools i.e. artificial neural networks, ANN, with the aim of obtaining an improved prediction of the internal damage along the pipeline route.

The artificial neural network is a parallel distributed process, PDP. It consists of a pool of simple processing units which communicate by sending signals to each other over a large number of weighted connections. Commonly, neural networks are adjusted, or trained, so that a particular input leads to a specific target output, see Fig. 8.

Designing a neural network consists of arranging neurons in various layers, deciding the type of connections among neurons for different layers, as well as among the neurons within a layer, deciding the way a neuron receives input and produces output and determining the strength of connection within the network by allowing the network to learn the appropriate values of connection weights by using a training data set. The process of designing a neural network is an iterative process. The developer must go through a period of trial and error in the design decisions before coming up with a satisfactory design. The design issues in neural networks are complex and are the major concerns of system developers [17, 18].

Neural networks are sometimes called machine learning algorithms, because changing of its connection weights (training) causes the network to learn the solution to a problem. The strength of connection between the neurons is stored as a weight-value for the specific connection. The system learns new knowledge by adjusting these connection weights.

The learning ability of a neural network is determined by its architecture and by the algorithmic method chosen for training. The training method usually consists of unsupervised learning (the hidden neurons must find a way to organize themselves without help from the outside) or reinforcement learning (the connections among the neurons in the hidden layer are randomly arranged, then reshuffled as the network is told how close it is to solving the problem) or back propagation. The last one method is proven highly successful in training of multilayered neural nets. The network is not just given reinforcement for how it is doing on a task. Information about errors is also filtered back through the system and is used to adjust the connections between the layers, thus improving performance [19].

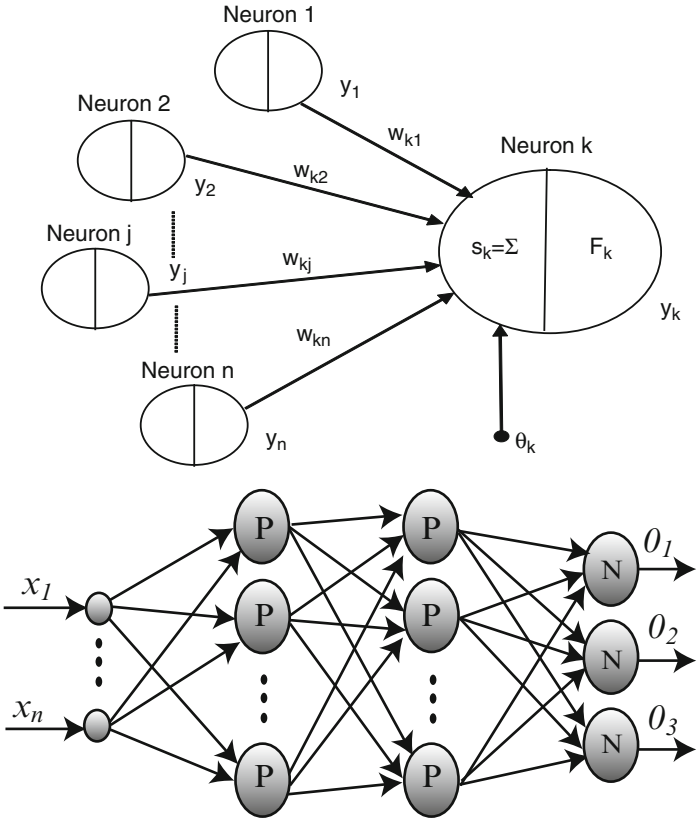


**Fig. 8** The basic components of an articial neural network (*on the left*) and the parallel distributed processing (*on the right*)

In this proposed engineering procedure, the ANN is a feed forward network with a single hidden layer of sigmoid neurons followed by an output layer of linear neurons as multiple layers of neurons with non linear transfer functions allow the network to learn non linear and linear relationship between input and output vectors. The linear output layer let the network produce values outside the range 0 to +1.

A back propagation rule has been chosen to train the ANN based model. The network weights and biases are updated in the direction in which the performance function decreases most rapidly. One iteration of this algorithm can be written:

$$w_{n+1} = w_n - \beta_n \cdot g_n \tag{5}$$

Where $w_n$ is the vector of current weights and biases, $g_n$ is the current gradient and $\beta_n$ is the learning rate. A batch training mode has been chosen i.e. the weights and biases of the network are updated only after the entire training set has been applied

to the network and a mean squared error, mse, as performance function. To avoid the network memorizes the training example i.e. for improving generalization, a regularization technique is applied as well as preprocessing of the network inputs and targets.

In details, the artificial neural network is trained by field data and experiences made by competent groups, introduced using developed/available formulas (models). The predictions provided by the learned models are combined with the aim of forming an improved estimator:

$$f(X) = \sum_i \alpha_i \cdot f_i(X) \tag{6}$$

where $\alpha_i$ is the coefficient or weight of the prediction provided by the ith learned model, $f_i$.

A combining strategy must be able to robustly handle the inherent correlation, or multicollinearity, of the models while identifying the unique contributions of each. A high degree of correlation is expected because the available formulas are attempting to perform the same prediction task i.e. an assessment of the corrosion rate. Correlation reflects the amount of agreement or linear dependence between models when making a set of predictions. The more the models agree, the more correlation, or redundancy, is present. Another issue in combining the predictions of learned models is detecting each model's unique contribution to predicting the target outcome. Models generated using different learning algorithms are more likely to make such contributions. A good combining strategy must be able to weight each model according to its unique contribution. An approach based on Principal Components Regression, PCA, is applied to find weights for the developed/available formulas with low prediction error, without discarding any of the original models, and without being subject to the multicollinearity problem [20].

The incorporation of prior knowledge into neural networks can improve neural network learning in several respects, for example, a faster learning speed and best generalization ability. However, neural network learning is data driven and there is no general way to exploit knowledge which is not in the form of data input-output pairs. A technique, which integrates a priori knowledge and ANN modelling, is applied to generate augmented training data set from the field data measurements and to impose correct behaviour on the ANN model i.e. to condition the ANN model [21]. The calibration of the previsions on the basis of detailed and qualified field measures as well, is necessary as, the models, in general, have a built-in conservatism and they probably over-predict the corrosion attack significantly for many cases.

At the end of the training phase, the ANN based model is applied to assess corrosion rate applied across the specific locations previously identified, using the experiences maturated in the industry (e.g. the proposed models) and calibrating the previsions on the basis of detailed and qualified field data, as well.

To sum up, as the quality of the input data has a major impact on the reliability of the predicted corrosion rates, and the complexity of acquiring good field data

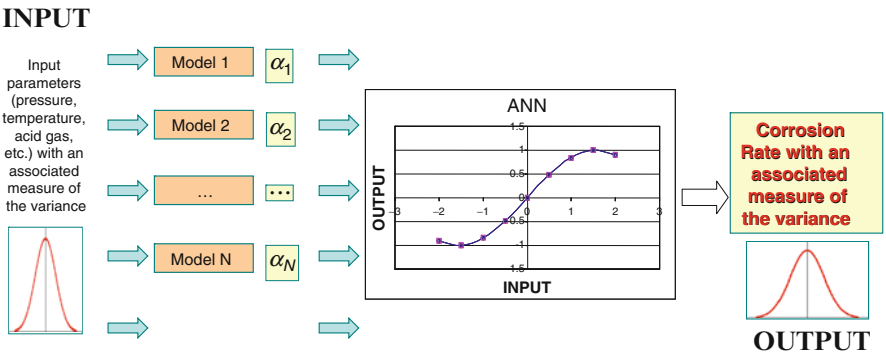


**Fig. 9** Application of an Artificial Neural Network based model

is often not fully appreciated, a measure of the variance is associated to input parameters such as pressure, temperature, acid gas, etc., in assessing the corrosion rate by the openly available $CO_2$ models, both during the training and application phases of the ANN base model, providing in output a prediction of corrosion rate with an associated measure of variance, applying an ANN based model, see Figs. 9 and 10.

## 8 Rationale Use of Corrosion Model Prediction

Finally, in the third phase an analysis of results and a prevision of corrosion rate along lifetime is carried out adding up in each identified critical point, the partial corrosion rate due to certain operating and morphology conditions, see Fig. 11.

Along a pipeline temperature, pressure, flow velocity and flow regime vary. Predicting the behaviour of the fluid flow allows to identify the locations, along the transport system, where it is most likely that corrosion problems may occur. Moreover, the flow regime prediction from a flow model is used for the prediction of oil or water wetting of the pipe wall whilst pressure, temperature, liquid flow velocity, wall shear stress an so on, are used in the corrosion rate calculations. In operating a pipeline it shall be taken into account that pipelines are subjected to loads and environmental effects which may cause them to become degraded with the passage of time. Degradation has a variety of causes, including corrosion, mechanical damage, fatigue, and stress corrosion cracking. All pipeline operators are well aware of this, and the prudent operators have active programs to mitigate deterioration and to remediate defective pipe.

Moreover, the procedure has the benefit to identify the most probable mechanism of internal damage in each critical location along the pipeline route and point in time.

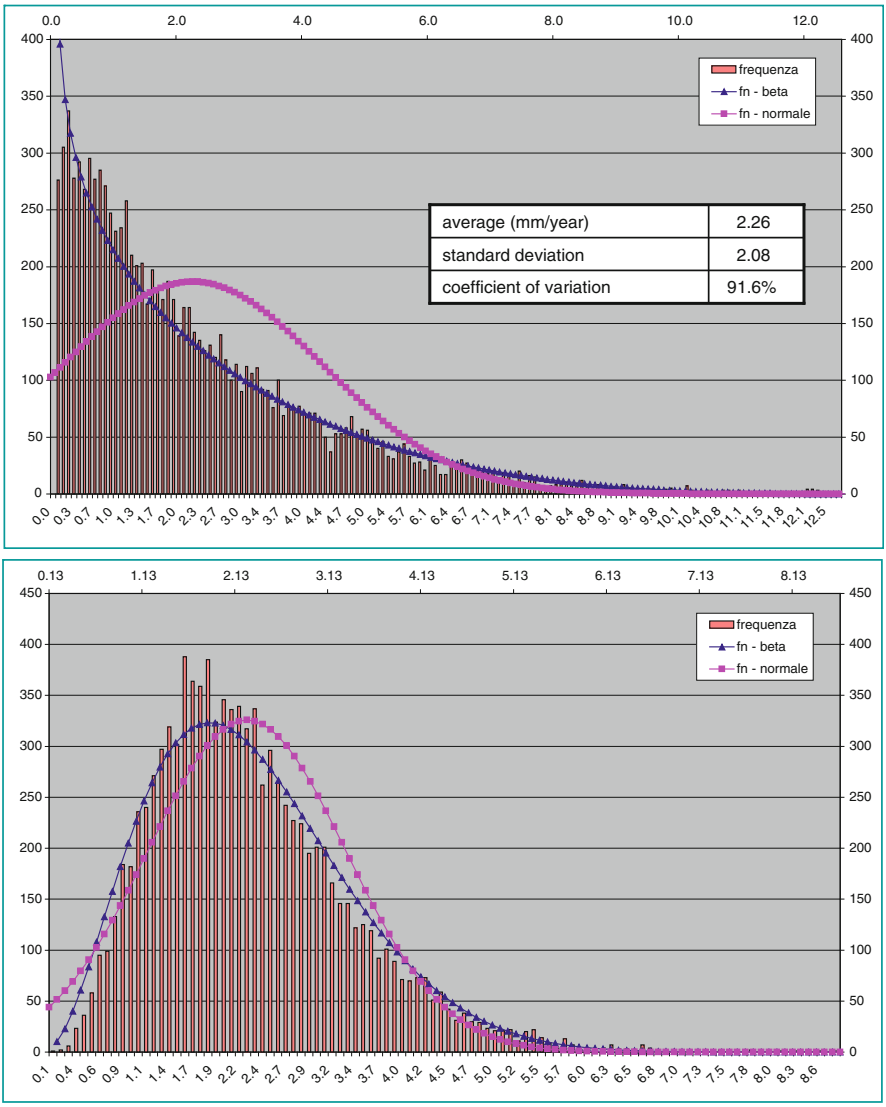


**Fig. 10** Statistical analysis of the ANN prediction

Summarizing, the suggested procedure provides an assessment of corrosion rate with a measure of confidence linked to both model the input parameters uncertainties along lifetime that allows to:

- identify corrosion mechanisms with their probability of occurrence in each critical location and point in time,
- assess the development of corrosion along the pipeline over time.

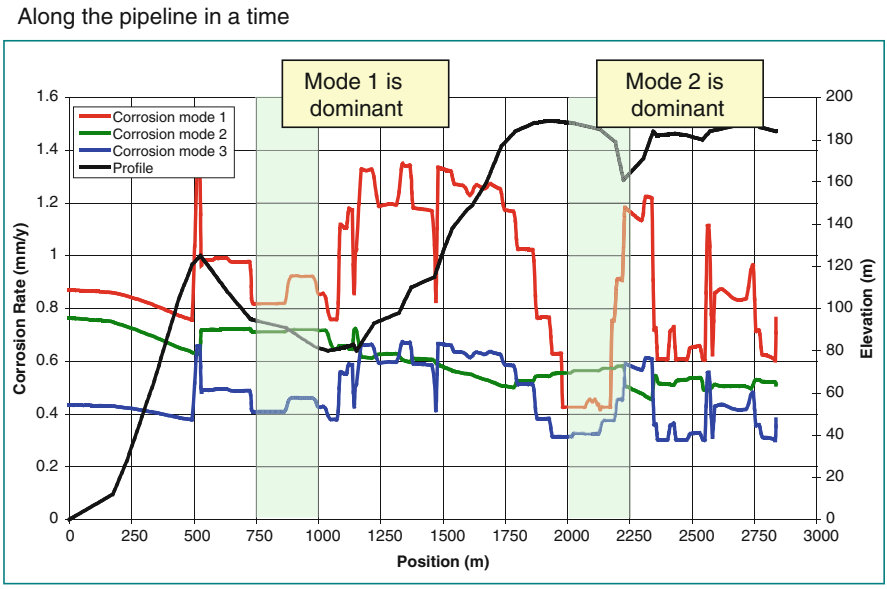


**Fig. 11** Analysis of results and prevision of corrosion rate along lifetime

In this way, the significant uncertainty in the models for corrosion prediction is in some way mitigated and an assessment of the extent of corrosion, defect depth and length, provided. As the wall thickness of a steel pipe is the most relevant parameter affecting the pipe capacity to withstand the combined loads imposed during installation and under operating conditions i.e. internal (bursting-pressure containment failure mode) and/or external pressure (collapse) pipeline, the results provided by the suggested engineering procedure may be applied in the integrity assessment, detailed described in the next paragraph.

## 9 The Integrity Assessment

The corrosion rate prediction is a difficult task due to significant uncertainties and variability's in flow characteristics, pre-existing conditions, corrosion resistance. . . . Usually a reliability analysis is the most appropriate approach to rationally investigate the matter, allowing to also considering the uncertainties in the applied pressure/loads and material resistance parameters.

Pipeline integrity monitoring includes a variety of measures taken to monitor the condition of the pipeline including its immediate environment, in order to determine or head off damage to the pipe and its associated equipment, maximize the efficiency and safety of the pipeline, minimize potential accidents and service interruptions due to pipeline neglect, and safeguard company and public interests.

A partial list of measures that should be involved in pipeline integrity monitoring includes leak detection, inspection pigs, visual and underwater inspection of pipe exterior, and checking of pressure regulators and pressure-relief valves.

In the analyses, the extent of corrosion, defect depth and length, is the major variable. The first step is to perform a screening on the criticality of the line to corrosion, utilizing the most accurate model for corrosion available. In this way, the significant uncertainty in the models for corrosion prediction are in some way mitigated, getting a preliminary screening on the attention it has to be paid to the pipeline. The various operating condition occurred (or expected) in the pipeline life are considered and the corrosion rate can be calculated along the pipeline, defining the location of the most critical points.

Unfortunately, the uncertainties in the models for the prediction of corrosion rate do not allow to be enough confident on the obtained results. The scatter in the models often cover all other sources of uncertainty, e.g. internal pressure, wall thickness, temperature, steel yield strength, fluid composition. In order to improve the prediction accuracy of the models, experimental checks and comparisons are necessary. Two different ways can be used:

- intelligent Pig Run, in the pipelines where this is feasible, and when the safety resulting from the reliability analysis results lower than target allowable values. Uncertainties related to measurements of remaining wall thickness in an intelligent Pig run are low, allowing to accurately estimate the corrosion rate along the specific pipeline. On this basis, the models for corrosion estimate can be calibrated and, hopefully, extending the gained know how on the phenomenon to similar pipelines (may be not piggable). A Pig run along a single pipeline provide a huge amount of data that can be used to train ANN avoiding un necessary inspection activities. For the pipeline effectively suffering of relevant corrosion phenomenon, at the end the Pig run it is possible to calculate the safety level of the pipeline at any required location, identifying any location of the threatening corrosion defect. Then it is possible to intervening, restore the required safety level for the pipeline,
- check the extent of corrosion in some specific location, the worst according to the prediction model, in order to improve model accuracy. This approach is usually applied in the not-piggable pipeline, as the definition of the worst location for corrosion is quite difficult and rarely it is possible to obtain a definitive answer on the safety of the pipeline. More reliable failure estimate are obtained in case similar pipelines have been inspected with intelligent pig, obtaining the corrosion rate for operating conditions close to the ones under analysis. In any case, for not piggable pipelines, risk analyses are performed, combining the failure estimations with the consequences of any leak or failure. These analyses give the ultimate word upon the operability of the pipelines.

A first requirement for the definition of minimum wall thickness is the containment of internal pressure. Onshore and shallow water pipeline have to be designed to resist against bursting, internal pressure is the most important load. In these cases several pipeline standards give recommendations and criteria for assessing the

serviceability and integrity of corroded steel pipe sections [22–25]. In particular, in [5], partial safety factors have been calibrated to ensure a target safety level.

Actually, for ultra-deep water conditions, failure modes related to the external pressure, the predominant load, are more relevant than bursting: design checks against cross section collapse and propagation buckling under external pressure alone, and ovalisation buckling under combined bending, axial and external pressure loads, are the relevant ones. Study on the behaviour of corroded pipelines under external pressure and/or combined loads are not so readily available neither standardized.

The failure mechanisms of pipes with corrosion defect subject to combined load condition i.e. internal pressure, axial force and bending moment, depend on several parameters i.e. steel pipe diameter, pipe diameter to thickness ratio, pipe segment length to diameter ratio, stress-strain relationship (yield stress, ultimate stress and uniform elongation), steel axial force (generally normalized with the yield axial force), internal pressure (generally normalized with the yield internal pressure), pipe initial ovalisation, pipe initial curvature, girth weld characteristics (residual stresses, pipe misalignment at the joint, change in material properties in the heat affected zone, HAZ, and pinching deformations that arise at the weld from the thermal contractions and contribute to the initial pipe deformations), corrosion defect location with respect to the loads, corrosion pattern (simple, multiple and interacting metal losses) and metal loss dimensions i.e. corrosion depth to pipe thickness ratio, corrosion length to pipe diameter ratio and corrosion width to pipe diameter ratio.

Numerical studies and experimental tests have been performed in the last 15 years aiming to investigate the failure mechanisms and quantify design criteria and equations for pipeline subject to external/internal pressure combined with steel axial force and bending moment.

FE models such as ABAQUS®, calibrated by experimental tests may be developed and used to quantify the strength and deformation capacity, to analyse the failure mechanisms and limit loads of pipe subjected to combined loads with single corrosion and interacting defects [26, 27].

Figure 12 shows the typical failure mechanisms/modes of intact and corroded pipes subject to internal pressure. An outward bulge failure mechanism develops for the intact pipe, see Fig. 12a. By contrast, for the corroded pipes, the localised bulge and tear developed in the region where failure occurs is less visible than for the intact pipe, mainly because of the lower strain energy level stored in this tube before failure, see Fig. 12b. The failure modes for intact and corroded pipes under external pressure are shown in Fig. 13. The corrosion patterns on the pipe surface (width, depth and location of the corrosion defect) affect the collapse behaviour and the deformation shape during and after failure.

The FEM analyses may be linked to a probabilistic assessment in order to determine the reliability of the pipeline system considering all the relevant uncertainties in the major parameters e.g. extent of corrosion defect due to the model used in the prediction (large scatter) and/or accuracy of the pig instrumentation tool (small scatter), yield stress, axial strain, bending moment, etc. To be noted that the

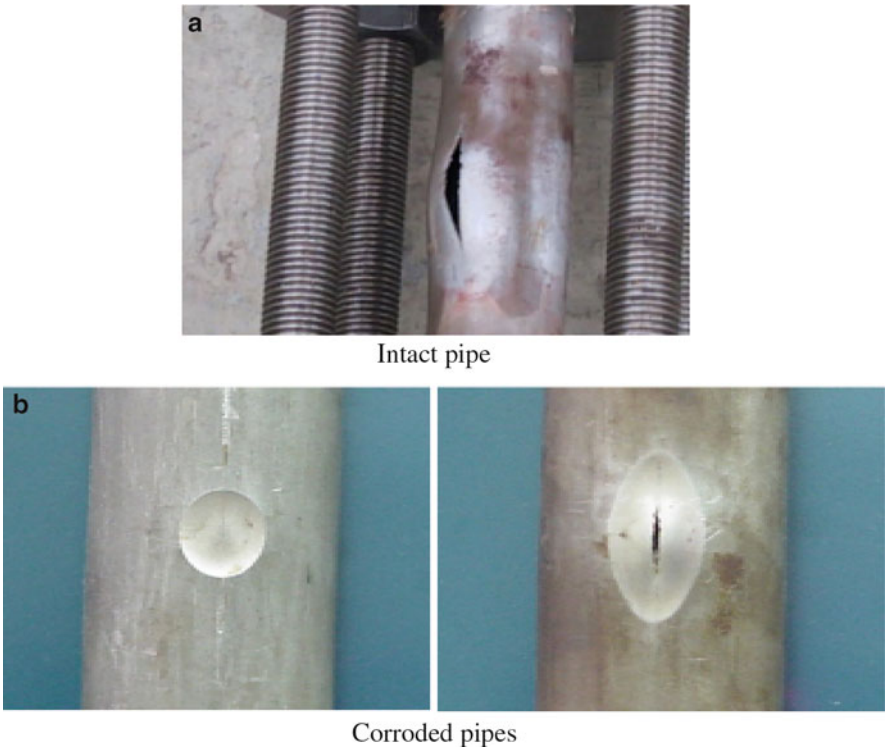


**Fig. 12** Typical failure mechanisms of intact (**a**) and corroded (**b**) pipes subject to internal pressure

accuracy relevant to FE models has to be included in the reliability assessment and that the probability functions associated to input parameters (random variables) can play a major role in the resulting failure probability.

## 10 Conclusions

High pressure transportation of large volumes of natural gas, i.e., with an inlet pressure greater than 10 MPa, makes the gas pipeline option competitive over long distances, both cross-country and offshore. The adoption of high grade steels can extend the breakeven distance, at which the cost per thermal unit is competitive in the end users' market. Cross-country pipeline operators, initially reluctant to high pressures, are presently planning large volumes of gas transportation over long distances, requiring large diameters; and thick pipe walls, met by increasing the steel grade. At present, offshore pipelines, whether in deep or shallow waters or across mild or rough sea beds, can pose an alternative to onshore projects, potentially reducing transit fees, a significant component of cost for end users. Offshore

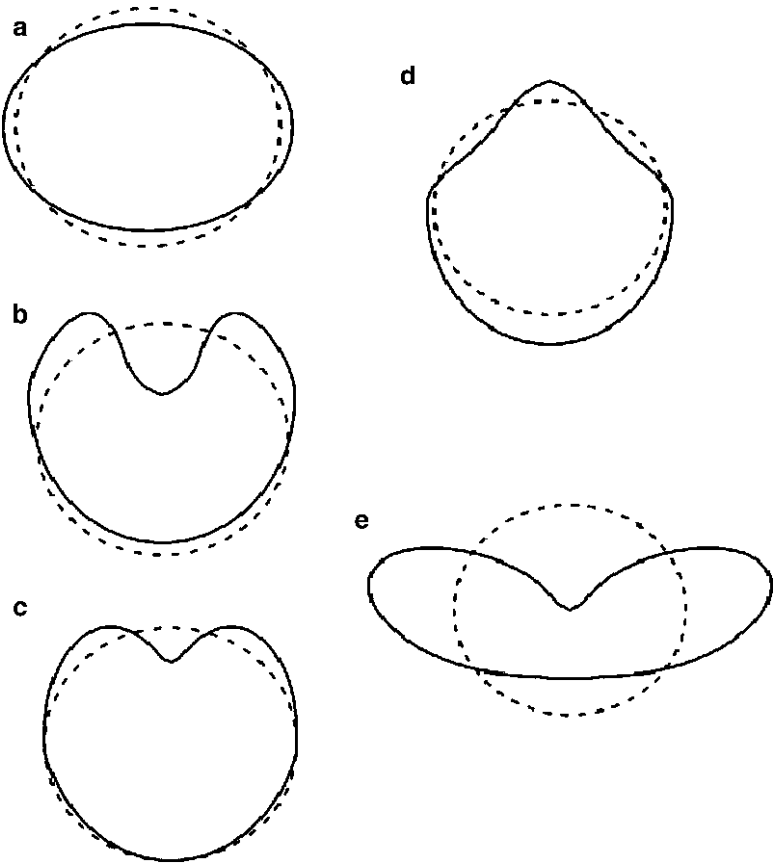


**Fig. 13** Typical failure mechanisms of intact and corroded pipes subject to external pressure. Symmetrical Collapse Modes: (**a**) Flat Mode; (**b**) U1-Mode; (**c**) U2-mode; (**d**) "Pear"-mode; (**e**) U3-mode

routes can also help strategically, ensuring the security of supply across politically unstable regions by reducing asset vulnerability. Projects in water depths of 3,000–3,500 m are now being considered and so the offshore industry is called to solve demanding material and line pipe challenges; develop new and reliable installation technologies for ultra deep waters and difficult seabeds; improve the engineering prediction of in-service behaviour over the entire design lifetime; identify the suitable technological measures to tackle environmental hazards typical to ultra deep waters; and to move the already advanced tools for inspection and integrity management technology to increasing water depths.

The relationship between the hydraulic regime of the basin and of the nature of seabed sediments, may be a factor in the selection of the steel proprieties (clean to sour) and field joint integrity as well.

The integrity of interfield network, throughout their operating lifetime, is an important area for operators to consider in maximizing reliability and serviceability for economic, contractual and environmental reasons. Many relevant improvements have been performed in years, but models for corrosion estimates still have many uncertainties and significant expertise is required to manage the issue. The proposed engineering procedure, introducing a measure of variance both in input parameters and corrosion rate prediction, may allow to mitigate, the significant uncertainty in the models for corrosion prediction and provide an assessment of the extent of corrosion, defect depth and length. Pipeline integrity monitoring includes a variety of measures taken to monitor the condition of the pipeline including its immediate environment, in order to determine or head off damage to the pipe and its associated equipment, maximize the efficiency and safety of the pipeline, minimize potential accidents and service interruptions due to pipeline neglect, and safeguard company and public interests. A partial list of measures that should be involved in pipeline integrity monitoring includes leak detection, inspection pigs, visual and underwater inspection of pipe exterior, and checking of pressure regulators and pressure-relief valves.

## References


1. R. Bruschi, F. Tura, Offshore pipeline safety, OMC 1995, Washington, DC, 1995
2. C.M. Spinelli, F. Marchesani, TAP project, IPC 2004, Calgary, 2004
3. M. Gentile, M. Fehervari, M. Drago, E. Torselletti, R. Bruschi, Il Rischio di Tensocorrosione da $H_2S$ all'Esterno di Condotte Sottomarine: una Metodologia di Valutazione Quantitativa, Giornate Nazionali sulla Corrosione e Protezione, 2009
4. ISO 15156, Sulphide stress cracking resistant metallic materials for oilfield equipment, 2003, 814 Corrosion, **2**, 8–10 (2005)
5. DNV OS-F 101, Submarine pipeline systems, Det Norske Veritas, 2007
6. A.C. Palmer, R.A. King, *Subsea Pipeline Engineering* (PennWell, Tulsa, 2004)
7. G. Gabetta, P. Cavassi, Il costo della Corrosione, Tpoint no. 3, 2001
8. C. De Waard, D.E. Milliams, Carbonic Acid Corrosion of Steel, *Corrosion1975*, Paper N°31, 1975
9. C. De Waard, U. Lotz, Prediction of $CO_2$ corrosion of carbon steel, *Corrosion93*, Paper no. 69, Houston, 1993
10. C. De Waard, U. Lotz, A. Dugstad, Influence of liquid flow velocity on corrosion: a semi-empirical model, *Corrosion 95*, Paper no. 128, NACE, Houston, 1995
11. NORSOK M-506, $CO_2$ corrosion rate calculation model, Norwegian Technology Standards Institution, Oslo, 2005 http://www.nts.no/norsok
12. R. Nyborg, P. Andersson, M. Nordsveen, Implementation of $CO_2$ corrosion models in a three-phase fluid flow model, *Corrosion2000*, Paper no. 48, Houston, 2000
13. R. Nyborg, Evaluation of $CO_2$ corrosion prediction models. Final Report Kjeller Field Data Project, IFE Institute for Energy Technology, No. 2000/135, 2000
14. R. Nyborg, Evaluation of $CO_2$ corrosion prediction models, IFE Institute for Energy Technology, No. 2003/170, 2003
15. T. Sotberg, A. Sjaastad, P.O. Gartland, T. Landmark, Pipeline operational safety by integrating flow modelling and risk reliability assessment, *Rio Pipeline Conference 2005*, Rio de Janeiro, 2005

16. A.S. Nowak, K.R. Collins, *Reliability of Structures* (McGraw-Hill, New York, 2000)
17. B. Krose, P. van der Smagt, *An Introduction to Neural Network* (University of Amsterdam, Amsterdam, 1996)
18. S. Haykin, *Neural Networks* (Prentice Hall, Upper Saddle River, 1994)
19. D. Klerfors, *Artificial Neural Networks* (Saint Louis University School of Business & Administration, St. Louis, 2001)
20. C. Merz, M. Pazzani, A principal components approach to combining regression estimates. Machine Learn. **0**, 211–218 (1997)
21. S. Milani, D. Šel, N. Hvala, S. Strmnik, R. Karba, Improving neural network models of a hydrolysis process by integration of a priori knowledge, *European Symposium on Intelligent Techniques*, Aachen, 1999
22. ASME B31G, *Manual for Determining the Remaining Strength of Corroded pipelines, Supplement to the ASME B31 Code for Pressure Piping* (American Society Of Mechanical Engineers, New York, 1991)
23. BS 7910, *Guidance on Methods for Assessing the Acceptability of Flaw in Fusion Welded Structures* (British Standard Institution, London, 2005)
24. API 579, *Fitness for Service*, API, 2000
25. ABS, *Submarine Pipeline Systems* (American Bureau of Shipping, New York, 2005)
26. L.M. Bartolini, A. Battistini, L. Marchionni, L. Vitali, Strength and Deformation Capacity of Corroded Pipes, *XIX Congress Italian Association for Theoretical and Applied Mechanics AIMETA*, Ancona, 2009
27. R. Bruschi, L. Vitali, E. Torselletti, A. Santicchia, Collapse capacity of corroded pipes design equation vs. 3D FE analyses, Italian ABAQUS Regional User's Meeting, Bari, 2006

# Protection for Natural Gas Installations Against the Corrosive Effect of Mercury by a Chemical Nickel Coating

**C. Fares, A. Merati, M.A. Belouchrani, and A. Britah**

**Abstract** Aluminium in contact with mercury is degraded by amalgamation. This phenomenon is of interest in LNG (Liquefaction of Natural Gas) operations. Where the mercury – either contained in natural gas or from other sources – may be introduced into the system and come into contact with equipment made of aluminium or aluminium alloys (for example, cryogenic exchangers, LNG storage tanks and cargo tanks). Various methods to remove mercury from gas streams are used to trap mercury upstream installations in question by the means of specific absorbers. However, this trapping is not total, and corrosion by mercury even with the state of traces always threatens. In this context, and for the intention of preserving these installations even in the presence of corrosive metal, we recommended a solution which consists in applying a metal chemical nickel coating using the sodium hypophosphite like reducer.

## 1 Introduction

Liquefied Natural Gas (LNG) is simply an alternative method to transport methane from the producer to the consumer. Methane ($CH_4$) gas is cooled to $-161.5°C$, converting its gaseous phase into an easily transportable liquid whose volume is

C. Fares (✉)
Laboratoire de Mécanique Avancée (LMA), Faculté GM&GP, l'USTHB, Alger, Algeria;
BP 32, 16111 Bab-Ezzouar, Alger, Algeria
e-mail: chahinezfares@yahoo.fr

A. Merati
Laboratoire d'Electrochimie et Corrosion, E.M.P, BP17C, Bordj El Bahri, Alger, Algeria
e-mail: meratiab@yahoo.fr

M.A. Belouchrani and A. Britah
Laboratoire de Génie des Matériaux, E.M.P, BP17C, Bordj El Bahri, Alger, Algeria
e-mail: mohamedelamine.belouchrani@hotmail.fr; malek.britah@gmail.com

T. Boukharouba et al. (eds.), *Integrity of Pipelines Transporting Hydrocarbons*,
NATO Science for Peace and Security Series C: Environmental Security,
DOI 10.1007/978-94-007-0588-3_11, 

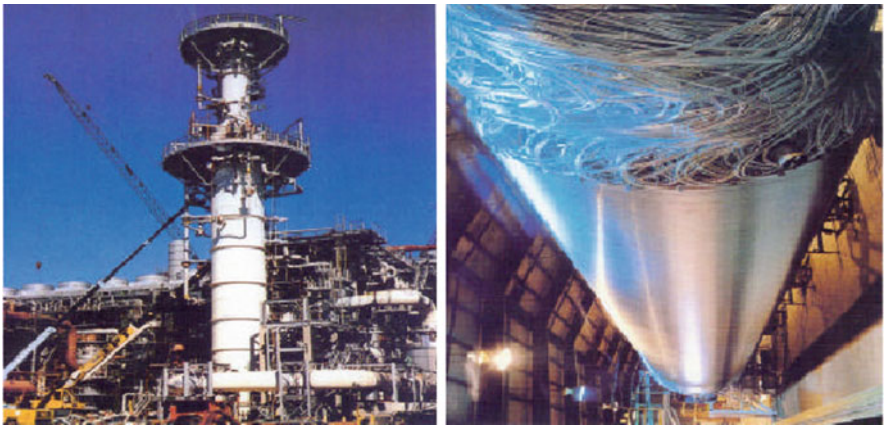

**Fig. 1** External and interior sight of the exchanger

approximately 600 times less than the equivalent volume of methane gas. It is usually stored and moved at cold temperatures and at low pressures.

The LNG plant in Algeria has adopted the Air Products Pre-Cooled Mixed Refrigerant (MCR) process that uses propane to pre-cool the processed gas, then a mixed refrigerant consisting of Nitrogen, Methane, Ethane and Propane to liquefy and sub-cool the processed gas into LNG. The second two stages use the Air Products (A-P) proprietary Main Cryogenic Heat Exchanger (MCHE) unit, which is built directly by A-P [1, 2]. It consists of aluminium tubing in a spiral wound configuration around a stainless steel core, they have a length of 60 m and diameters interior and out-side, respectively of 14 and 16 mm. A simple exchanger can include roughly 20,000 tubes. An example is shown in Fig. 1.

LNG operation requires gas to be cooled to very low temperatures; care must be taken to remove all impurities, water vapour, hydrogen sulphide, carbon dioxide, nitrogen and mercury from the gas stream at processing plants.

However, the quantity and the flow of the treated gas, which are about 277.000 $m^3/h$ cause the mercury not to be retained completely by the upstream installation absorbers containing activated carbon impregnated of sulphur [3]. If mercury is present in the liquid form (e.g. during process interruptions or plant shut down) it can do catastrophic damage to the aluminium heat exchangers in LNG plant [3–12].

In the natural gas, mercury at relatively low concentrations can concentrate in the cryogenic distillation process and can degrade the aluminium materials by three basic mechanisms [13]:

- Amalgamation: is the process by which mercury forms liquid solutions with aluminium metal. There is increased risk of mercury damage if under thermal, mechanical stress or some chemical environments, the $Al_2O_3$ protective surface oxide cracks.

- Amalgam corrosion: is the combined action of mercury and moisture producing a corrosion process that propagates with miniscule amounts of mercury. The reaction is:

$$Hg + Al \rightarrow Hg(Al)_{amalgam} \quad (1)$$

$$Hg(Al) + 6H_2O \rightarrow Al_2O_3 \cdot 3H_2O + H_2 + 3Hg \quad (2)$$

- Small amounts of aluminium can dissolve in liquid mercury, diffuse to the mercury–moist air interface, and then rapidly oxidize. Since, oxidation removes aluminium from the mercury, further aluminium can dissolve, and the process can continue until the aluminium is completely converted to oxide.
- Liquid metal embrittlement (LME): LME of Al alloys by mercury is one example of a generic phenomenon in which many metals are embrittled by certain liquid metals [14–20]. LME is generally much more severe than other embrittling processes, such as hydrogen embrittlement or stress-corrosion cracking, and once cracks have initiated, very rapid sub-critical cracking can occur even at low stresses (stress-intensity factors). Mercury induced LME in aluminium alloys leads to intergranular cracking and potentially very widespread damage in heat exchange manifolds.

The solution exposed in this work, to protect aluminium from mercury attack consists to operate directly on the aluminium tubes by the application of a metal coating. Several techniques are offered for the realization of metal coatings; the chemical method is characterized by its simplicity, the homogenous of deposit thickness and the possibility to cover complex parts [21–24]. In the preventive aim against corrosion, the autocatalytic coatings of chemical nickel are frequently used in the surface treatment field.

## 2 Experimental Procedure

The reaction which governs the deposition in chemical or electrolytic process is the same (reaction (3)). The difference lies in the source of electrons exchanged in this reaction.

In electrodeposits, these electrons are provided by a current external source, in the other case, their provisioning is ensured by the oxidation of chemical species introduced into the plating bath. When the substrate to be covered oxidizes, the method is said by displacement, whereas the oxidation of a form reduced in solution defines the method called by reduction (Fig. 2) [21–24].

The reducer used in this study is the sodium hypophosphite. The deposition of nickel directly on aluminium gives uniform but not adherent deposits, for this, the realization of intermediate fixing coat between the substrate and the nickel deposit was essential. After several test, nickel deposited by displacement technique was

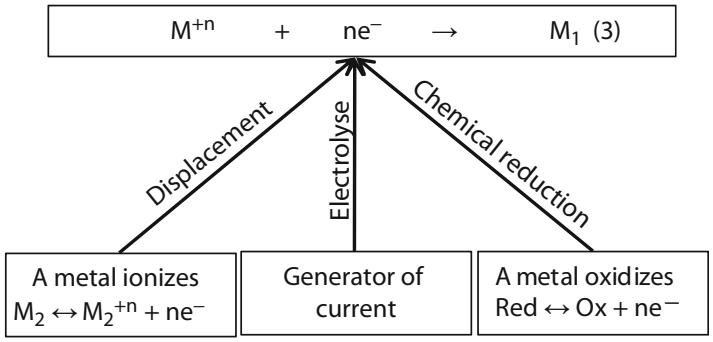


**Fig. 2** Diagrams of supply electron

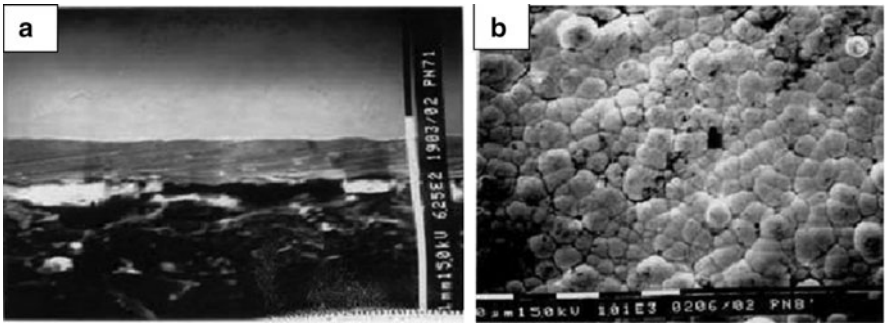


**Fig. 3** Metallographic cut of a nickel deposit (S.E.M.): (**a**) Thickness distribution, (**b**) Surface distribution of the grains

selected as under layer. The external coating of nickel was elaborated during 1 h at 80°C. In this case, the thickness is about 17 µm [24]. The microscopic observation shows that the deposits surfaces are marked by the presence of spherical grains, whereas, the thickness is dependent on a uniform distribution as shown in Fig. 3.

## 3 Behaviour Study Against the Mercury Corrosive Attack

The elaborated coatings improve generally the aluminium corrosion resistance in saline medium. In this case, the objective is to study the influence of mercury on the behaviour of substrates covered by autocatalytic nickel. The tests carried out consist to follow the free potential evolution according to time and to establish potentiodynamic curves after 1 h of immersion in acid solutions containing different mercury nitrate concentrations (300, 500, 700 and 1,000 mg/l). The results obtained, for immersions of about 30 min, indicate that the aluminium without deposit presents a strong sensitivity to the mercury corrosive attack (Fig. 4).

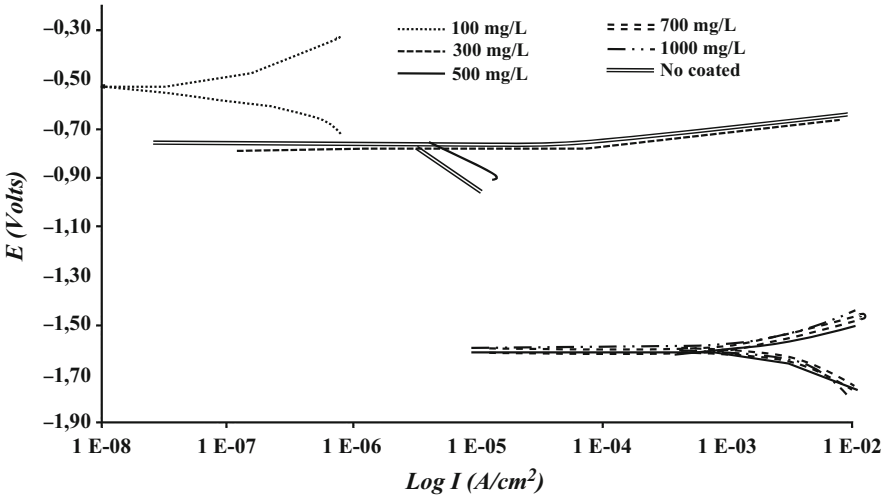


**Fig. 4** Potentiodynamic curves after 1 h of immersion of aluminium without deposit, in acid solutions containing different mercury nitrate concentrations

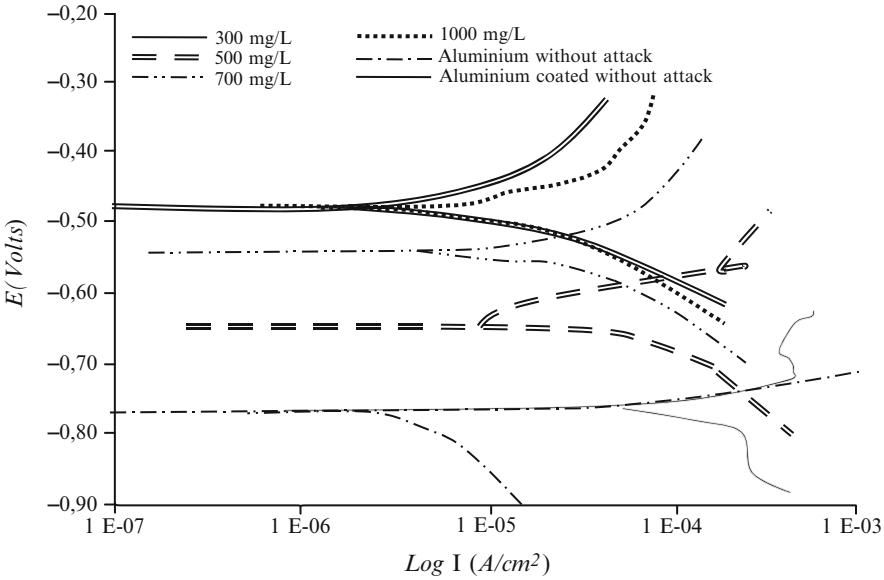


**Fig. 5** Potentiodynamic curves of coated aluminium, in acid solutions containing different mercury nitrate concentrations

Whereas, those obtained for coated samples show that the free potential rises with the mercury nitrate quantities and their behaviour becomes similar to the no coated one at the concentration of 1 g/l. the current densities decrease slightly with the concentration increase (Fig. 5).

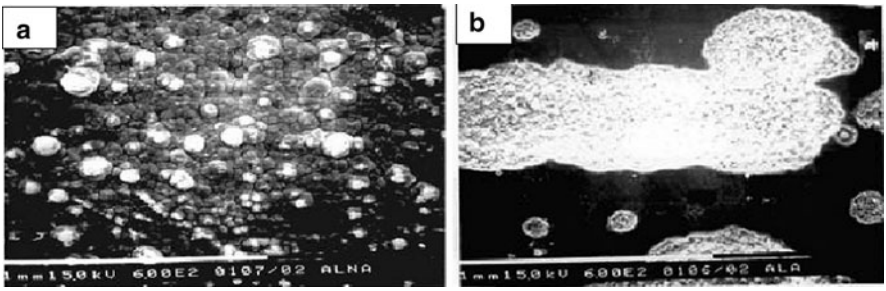


**Fig. 6** S.E.M. observations of: (**a**) coated aluminium after immersion in mercury nitrate solution (500 mg/l), (**b**) no coated aluminium attacked by nitrate mercury solution (300 mg/l) during 15 min

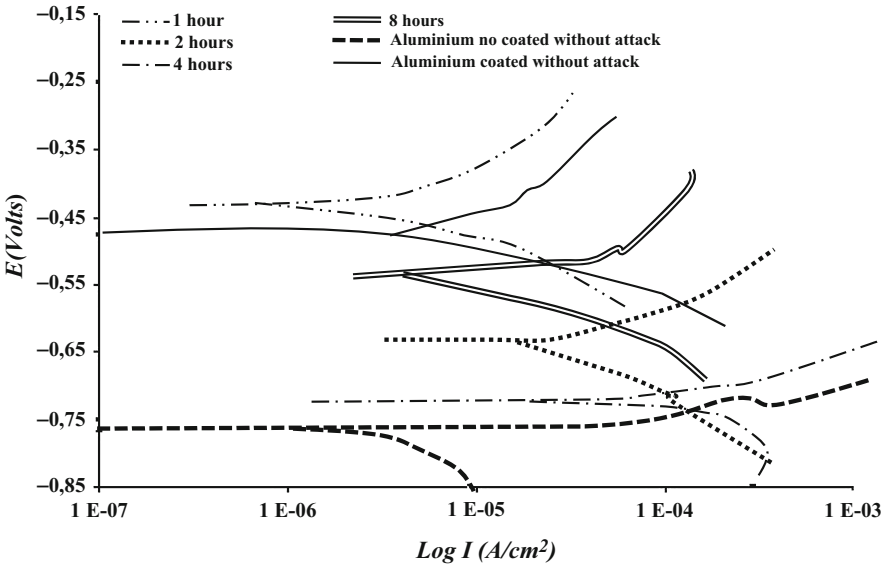


**Fig. 7** Potentiodynamic curves of the coated aluminium for different immersions

No pit or crack, observed on no coated aluminium after only 15 min (Fig. 6b), have been revealed by the SEM observation on the coated one (Fig. 6a). To simulate a real situation of this corrosion problem, the coated aluminium was immersed in humid liquid mercury. After 4 h, it was noted that the potential decreases to reach the aluminium potential value, and then becomes nobler after 8 h (Fig. 7).

These observations can be interpreted by corrosion product filling the pores, either by passivity due to the diminution of deposit activity or by a protector film created by this corrosion product. Knowing that the aim of this work is to protect the exchanger tubes against the mercury attack, nickel layers were elaborated on similar tubes. These layers were uniform and present the same characteristics that those elaborated initially on rectangular samples (Fig. 8).

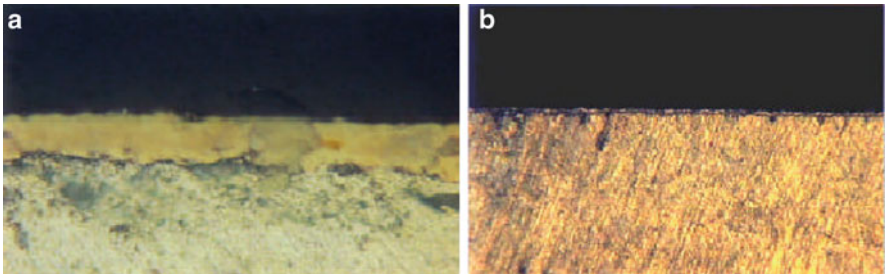


**Fig. 8** Metallographic cuts of a nickel deposit on an aluminium tube: (**a**) Transversal x500 and (**b**) Longitudinal x200


**Fig. 9** Comparison between the mercury corrosive attacks of: (**a**) no coated aluminium tube after 20 min and (**b**) the coated aluminium tube after 6 month

The Fig. 9b indicates that no mercury attack is observed on the tubes coated even after 6 months, whereas after only 10 min, the attack starts and the no treated tube is completely damaged 20 min later (Fig. 9a).

To complete this work and knowing that these tubes are used at cryogenic temperatures, layers elaborated were tested in this condition. Controls carried out after 16 h of immersion of these tubes in nitrogen liquid at temperature of −96°C, show that not only the surfaces and the deposit remain intact, but also the hardness improves.

## 4 Conclusions

The nickel autocatalytic coating obtained by treatment of 1 h at 80°C on fine nickel layer realized by displacement, improve the behaviour of aluminium substrates against mercury corrosion. In a mercury liquid solution, the not covered aluminium

corrosion start at the mercury concentration of 300 mg/l, whereas; the aluminium protected by chemical nickel presents a good resistance even to high concentrations. The deposits carried out inside the tubes are also characterized by an excellent resistance in contact with the metallic mercury and at low temperatures.

## References


1. P.Y. Martin, J. Pigourier, LNG process selection, no easy task, *Hydrocarbon Engineering*, Axens, 2004
2. J.M. Van de Graaf, P. Barend, Large-capacity LNG trains, the shell parallel mixed refrigerant process, *Business Briefing: Instrumentation & Processing*, LNG Review, 2005
3. T. Goto, A. Furuta, K. Sato, High efficiency mercury removal absorbent for natural gas liquefaction plant, in *10th international Conference Proceeding*, Kuala Lumpur, 1992
4. J.E. Leeper, Mercury corrosion in liquefied gas plants. *Energy Process*. Can. **73**, 46–51 (1981)
5. R. Coade, D. Coldham, The interaction of mercury and aluminium in heat exchangers in a natural gas plants. *Int. J. Press. Vessels Pip*. **83**, 336–342 (2006)
6. J.J. English, G. Kobrin, R. Serauskas, Liquid mercury embrittlement of aluminium. *Materials Selection and Design*, **28**, 62–63 (1989)
7. L. Lacourcelle, Nickelage chimique; Techniques de l'ingénieur. *Edition Technip*, traité Matériaux métalliques **M5** (M1565), 1–14 (1995)
8. C. Farés, Amélioration du comportement à la corrosion de l'aluminium en présence du mercure par un dépôt de nickel chimique, *Master thesis*, E.M.P, Alger, 2002
9. M.H. Brown, W.W. Binger, R.H. Brown, Mercury and its components, a corrosion hazard, in *8th Annual Conference of National Association of Corrosion Engineers*, Glaveston, 1952
10. F.M. Beard, R.A. Hine, The effect of allowing constituents in aluminium of corrosive attack by mercury. *Br. Corros. J*. **1**, 98–101 (1965)
11. R.C. Plumb, M.H. Brown, J.E. Lewis, A radiochemical tracer investigation of the role of mercury in the corrosion of aluminum, *Corrosion*, 11 (N°6) (1956), p. 277[t]
12. E.G. Meek, Aluminium corrosion, *Science Note SSR*, June 1987
13. M.R. Pinnel, J.E. Bennett, Reactions between mercury-wetted aluminum and water. *J. Mater. Sci*. **8**, 1189 (1973)
14. M.R. Pinnel, J.E. Bennett, Voluminous oxidation of aluminum by continuous dissolution in a wetting mercury film. *J. Mater. Sci*. **7**, 1016 (1972)
15. J.J. Krupowicz, D.S. Hampton, Cracking of aluminium alloy 5083 in mercuric salt solutions, 1989
16. W.B. Brooks, The hazards of mercury to metals and alloys in process industries and some little known sources of mercury contamination, *Corrosion*; 24 N° 10, (1968) p. 335
17. S.M. Wilhelm, A. McArthur, R.D. Kane, Methods to combat liquid metal embrittlement in cryogenic aluminum heat exchangers, in *Proceedings of the 73rd GPA Annual Convention*, New Orleans, March 1994, pp. 62–71
18. P.J.L. Fernandes, R.E. Clegg, D.R.H. Jones, Failure by liquid metal induced embrittlement. *Eng. Fail. Anal*. **1**(1), 51–63 (1994)
19. J.J. English, D.J Duquette, Mercury liquid embrittlement failure of 5083-0 aluminum alloy piping, *Handbook of Case Histories in Failure Analysis*, vol. 2, 1993, pp. 207–213
20. S.P. Lynch, Metal-induced embrittlement of materials. *Mater. Charact*. **28**, 279–289 (1992)
21. P. Gordon, Metal-induced embrittlement of metals-an evaluation of embrittler transport mechanisms. *Metall. Trans. A* **9A**, 267–273 (1978)

22. L. Lacourcelle, Revêtements métalliques par voie électrolytique. Techniques de l'Ingénieur **M5**, 1550 (1990). *Edition Technip*
23. Y. Badé, Revêtement métallique par voie électrolytique, Nickelage; Techniques de l'Ingénieur, *Edition Technip* **M5** (M1610), (2000) p. 1–14
24. J.W. Oswald, Dépôts électrolytiques de nickel épais, *Centre d'Information de Nickel*

# Corrosion Study of API 5L X60 Gas Pipelines Steels in $NS_4$ Simulated Soil

**A. Benmoussat and M. Traisnel**

**Abstract** External corrosion and cracking are the major threats and the principal mechanisms of buried pipelines deterioration. Indeed they reduce the structural integrity of the transmission system of gas pipelines. Investigations carried out on GZ1 site line, in Algeria, after about 30 years of exploitation under high pressure revealed that under certain conditions the not protected surfaces in contact with the ground developed many failures by corrosion and cracking: coating failure, reductions in thickness, pitting, etc. In this study the methodology was defined initially, by an expertise of the characteristic parameters of working GZ1 line which broke due to external corrosion, and then a simulation, in laboratory, of the conditions and the corrosion damage mechanisms. We were particularly interested in the corrosive electrolytic medium choice because it can simulate NS4 soil solution and the protection system by using corrosion inhibitors containing polyphosphates. Results showed that the corrosion potential is slightly moved towards the anodic values, when the pH of soil solution tends to a light acidity. This shift goes with a clear reduction of anodic and cathodic current densities and the polarization resistance Rp decreases. In the explored temperature range and simulating soil, corrosion current density increases with temperature increase. The corrosion activation energy increases with temperature according to the soil environment. Nyquist diagrams present the same general form for corrosion according to the slightly neutral pH for various immersion times in the steel/test solution interface.

A. Benmoussat (✉)
Corrosion Research Equip of LAEPO Laboratory, Abou Bekr Belkaid University of Tlemcen, Tlemcen, Algeria
e-mail: abbenmoussa@gmail.com

M. Traisnel
Unité de Matériaux Et Transformations (UMET) (UMR-CNRS 8207), Ecole Nationale Supérieure de Chimie de Lille, ENSCL, B.P. 108, Villeneuve d'Ascq Cedex F-59652, France
e-mail: michel.traisnel@ensc-lille.fr

T. Boukharouba et al. (eds.), *Integrity of Pipelines Transporting Hydrocarbons*, NATO Science for Peace and Security Series C: Environmental Security,
DOI 10.1007/978-94-007-0588-3_12, 

## 1 Introduction

The transport of oil and natural gas fossil resources from their geographical localization to their consumption centers usually located in industrialized zones takes place by the mean of buried pipelines networks. Since 40 years, an important buried tube network has been constructed and always develops through the world [1]. The search for always increasing pipeline profitability has led to the development of high-strength and high-toughness pipelines steels and to avoid any increase of tube thickness. The transport reliability depends on soil environment interaction and the choice of pipeline material and steel protection which will avoid damage. Corrosion risks are preoccupying phenomena in oil industry. External corrosion pits and cracking phenomena are the major threats and the main deterioration mechanism of buried pipelines under coating failure and cathodic protection (CP) that can reduce the structural integrity of buried pipelines transmission system. Corrosion behaviour of low carbon steel pipeline alloys in soil environment under protection failure motivates our research. The objective is to bring a better comprehension of damage mechanisms and to reduce steel failures in service.

Carbon steels of weakly C-Mn allied type as API 5L X60 of GZ1 pipeline in Algeria [2] are protected from the external soil aggressions by a bituminous coating whose action is coupled with a cathodic protection system (minimum potential specified −850 mV versus ($Cu/CuSO_4$)), which aims to maintain steel in its protection field and thus, to avoid any risk of external damage by corrosion or cracking during a possible rupture of the coating. Unfortunately, the investigations carried out on GZ1 site line [3], after about 30 years of exploitation under high pressure revealed many failures: coating failure, reductions in thickness, pitting, cracking. These chemical, biochemical or mechanical failures occurred particularly in clay soils, like montmorillonite type or saline underground waters subsoil.

Steel pipelines corrode in soil by complex electrochemical processes because of different nature of soil electrolytes. Corrosion phenomena in underground conditions are still unclear, because soil is a complex material, a porous, heterogeneous and discontinuous environment constituted by mineral or organic solid phase, water liquid phase, air and other gas phases. It is necessary to examine every particular site to explain the corrosion mechanisms models. The factors that influence corrosion in soil are numerous as soil type, moisture content and the position of the water table, soil resistivity and soluble ion content, soil pH, oxidation-reduction potential and the role of microbes in soil corrosion. Soil properties depend of soil particle size distribution, organic content, mineralogical composition and structure. Soil profiles are developed from parent materials in response to factors associated with the climate. Mineral composition is a key to understanding how a soil can influence the corrosion of buried steel. Clays are among the most common minerals on earth. Most clay has notable plasticity when wet and a marked ability to adhere to surfaces. Physically, clays of the montmorillonite group such as bentonite can radically change volume through dehydratation/rehydratation or ion exchange. This shrinking and swelling can exert forces on structures buried in montmorillonite rich soils

leading to potentially detrimental consequences. Coarse silica sands tend to be relatively permeable, well drained, and inert. Dissolved carbonate will buffer the solution in the neutral to alkaline pH range [4]. Exposure of this saturated solution to steel surfaces rendered alkaline by electrochemical reactions induced by an effective cathodic protection system will precipitate hard white carbonate scales on the metal surface which can involve corrosion problems. The physicochemical parameters of soil including resistivity (ρ), redox potential (E), pH, salt and moisture content can be determined quickly to estimate soil corrosivity. Weight loss measurements is the most important parameter for determining soil corrosivity, but it takes a long time to obtain weight loss data The electrochemical parameters such as corrosion current density (Icorr) and polarization resistance (Rp) can serve as parameters for evaluation of soil corrosivity with accuracy and ease. Electrochemical impedance spectroscopy (EIS) and potentiodynamic polarisation [5] were carried out to study the mechanism of pipeline steel soil corrosion. The likely rate of corrosion of underground corrosion can be assessed in terms of the soil pH, resistivity, temperature, and redox potential. However, the relationship between soil corrosivity and physicochemical parameters is very complex; therefore, the soil corrosivity appraised by these parameters is often unreliable. A number of probes have been developed for field measurements of these parameters. Li and Cao [6] reported the development of a new soil corrosivity probe that could be used to measure not only corrosion current density and corrosion potential of metals in soil, but also parameters of soil.

## 2 Materials and Methods

In this study the methodology was defined, initially, by an expertise of the characteristic parameters of working GZ1 line which broke due to external corrosion, and then a simulation, in laboratory, of the conditions and the corrosion damage mechanisms. We were particularly interested in the corrosive electrolytic medium choice because it can simulate NS4 soil solution and the protection system by using corrosion inhibitors containing polyphosphates.

### *2.1 Pipeline Steel*

In zones where GZ1 steel pipeline are damaged (from pK = 145 to pK = 226), (pK = kilometer point) samples of corroded X60 steel and not corroded ones have been studied by micro analytical techniques. These tubes from 40″ diameter are rolled and welded in spiral are posed in 1976 which the failures corrosion pits and cracks were detected. Micrographic analysis has been done by scanning electronic microscopy (SEM). Elemental composition of the samples was determined by spectrophotometric analysis type "SPECTRO RP 212" Measured values were compared to values quoted in the material test certificates [7]. Electrochemical

**Table 1** Elemental composition of API 5L X-60 steel pipeline

| C% | Si% | Mn% | P% | S% | Cr% | Mo% |
|---|---|---|---|---|---|---|
| 0.180 | 0.0364 | 1.4000 | 0.0175 | 0.0131 | 0.0284 | 0 |
| Ni% | Al% | Cu% | Ti% | V% | Sn% | Fe% |
| 0.0182 | 0.0493 | 0.0326 | 0.0058 | 0.0061 | 0.0031 | ≈97.880 |

measurements, potentiodynamic polarization and impedance spectroscopy (EIS) were carried out by means of potentiostat equipment. Soil simulating solution was chosen according to results obtained of the most aggressive GZ1 environment composition.

Steel pipeline of weakly C-Mn allied type as X60 for use in gas transmission is manufactured according to the specified chemical composition and mechanical parameters. It is manufactured from a variety of materials including carbon steel and corrosion resistant alloys (Table 1). Steel, although susceptible to corrosion, is widely used because of its low cost, high strength and the ease of field makeup by welding. The use relies on appropriate design allowances and corrosion controls. It is manufactured to the API-5L specification cover grade X60 and other grades [7]. It has a specific set of mechanical parameters including: yield strength, tensile strength and toughness that pipe must comply with. Chemical composition is specified as maximum limits of four elements, i.e. carbon, manganese, phosphorus and sulphur. Composition and microstructure can vary significantly between pipes. These variations result in substantial differences in corrosion performances of pipeline steel in a corrosion regime. GZ1 tube diameter of 40 in. and a fine pearlitic-ferritic microstructure have been manufactured in Algerian Annaba steel factory controlled lamination and accelerated cooling. The refinement of ferritic grain size has been obtained by different mechanisms of hardening and precipitation based on the dislocation movement that increases elasticity limit and steel tenacity. Hall-Petch laws [8] have since been verified experimentally and explain the hardening induced by a reduction in the ferritic grain size.

$$\sigma_y = \sigma_0 + \frac{K_y}{\sqrt{d}} \tag{1}$$

$\sigma_y$ – Elasticity limit
$\sigma_0$ – sum of hardening stresses based on the dislocation movement
$K_y$ – constant expressing the grain size effect

Samples cover grades X60 within the API-5 L specifications, were obtained from pipe Algerian gas producer's society SONATRACH. Materials have been chosen as representative of tubes posed on the line in 1974 where corrosion pits and corrosion cracks were detected. Samples were cut by flame-cut from the pipe walls and the test coupons were then cut from these sections by wet sawing. The cutting process was chosen as it does not alter the microstructure and corrosion test at the coupon surface, due to its low heat input and the absence of mechanical damage. The sections were polished by emery paper of 600–2,000 grit before being tested.

## 2.2 Soil Simulating Solution

The corrosion is related to soil conditions in which the structures are buried. The techniques available to determine the aggressiveness of the site may include laboratory tests based on a soil chemical analysis in a specific location. Several soil samplings have been taken from various Algerian sites from which we have chosen the most aggressive composition. Soil extract was prepared according to AFNOR French norm A–05.250 P. 278.

A mass of ground is taken, then mixed with distilled water and analyzed by spectrophotometer microanalysis. The chemical composition of soil is given in Table 2. The criterion of steel aggressiveness is principally the chloride, sulphate and bicarbonate content. However, the analysis should also include the concentration of sodium, potassium and calcium ions so that an ionic balance can be struck. The test solution is obtained by reconstitution of the chemical composition of soil in a solution called "soil simulating solution". Si is the considered site. The analogue soil excavations determined some synthetic solutions named NS1 to NS4 [9]. The chemical composition is described in Table 3.

The soil chemical composition shows that the principal electrolytes contained in pipe soil environment are variable proportions of carbonates and bicarbonates according to line sites and quantities of chlorides and sulphates. $NS_4$ synthetic electrolytic solution was selected as soil simulating solution and aggressive solution for electrochemical measurements. The pH of $NS_4$ synthetic electrolytic solution is ranged between 8 and 8.5. pH measurements raised on the line showed values ranging between 6.5 and 8.5. This low value for tubes submitted to a cathodic protection and generating alkalinity by hydroxyl ions is explained by $CO_2$ dissolved in the electrolyte. In laboratory, a bubbling of $CO_2$ gas in an aqueous solution would permit to adjust the pH of the medium to pH $\approx$ 6.7.

**Table 2** Chemical composition of corrosive soils solution

| | Mass (mg/l) | | | | | |
|---|---|---|---|---|---|---|
| Sites | $Ca^{2+}$ | $Mg^{2+}$ | $K^{+}$ | $Cl^{-}$ | $SO_4^{2-}$ | $HCO_3^{-}$ |
| S1 | 94.60 | 56 | 7.6 | 76.9 | 736 | 117 |
| S2 | 18.96 | 16.44 | 11.7 | 47.33 | 458.4 | 183 |
| S3 | – | – | 6 | 7.8 | 74 | 218 |

**Table 3** Composition of $NS_i$ synthetic electrolytic solution of soil [9]

| | Denomination | | | |
|---|---|---|---|---|
| Composition (mg/L) | $NS_1$ | $NS_2$ | $NS_3$ | $NS_4$ |
| KCl | 149 | 142 | 37 | 122 |
| $NaHCO_3$ | 504 | 1,031 | 559 | 483 |
| $CaCl_2{\cdot}2H_2O$ | 159 | 73 | 8 | 181 |
| $MgSO_4{\cdot}\ 7H_2O$ | 106 | 254 | 89 | 131 |

## 2.3 Electrochemical Measurements

Pre-treatment of steel samples surfaces was carried out by grinding with emery paper of 600–1,200 grit, rinsing with bidistilled water, and ultrasonic degreasing in ethanol and drying at room temperature before us. All tests have been performed at 30 ± 1°C. Electrochemical measurements were carried out by means of Tacussel – Radiometer PGZ 301 equipment. Polarization equipments were carried out in a conventional three electrodes glass cell with a platinum counter electrode and a saturated calomel electrode (SCE) as reference with luggin capillary bridge. All tests have been performed in de-aerated solutions under stirred conditions at room temperature. Electrochemical cell used and polarization measurements was the same as described in paper [10]. The potentiodynamic polarization curves were recorded by a constant sweep rate of 0.5 mV $s^{-1}$. Before recording the polarization curves, the open – circuit potential was stable within 30 min. The cathodic branch was always determined first, the open–circuit potential was then re–established and the anodic branch determined.

Electrochemical impedance spectroscopy (EIS) measurements were performed using Tacussel – Radiometer PGZ 301 frequency response analyser in a frequency range of $10^5$ to $10^{-2}$ Hz with 10 points per decade. Impedance equipment is controlled by Tacussel corrosion analysis software model voltamaster 4. Square sheet steel of size (5 × 5 × 0.06 $cm^3$), which exposed a 7.88 $cm^2$ surface to the test solution, were used as the working electrode.

## 2.4 Soil Resistivity

Soil resistivity (ρ) was determined according humidity values on line environment. The moisture content was determined by weight loss measurements. One weighs an earth sample is dried in a drying oven 105°C during 24 h. The weight difference between earth sample before and after evaporation is regarded the moisture content determined as the evaporated water mass. This method is not precise and does not give a constant weight after earth sample evaporation.

## 2.5 Corrosion Inhibitor Used

The corrosion inhibitor used is disodic Hydrogéno-monophosphate is an odourless hygroscopic white powder of chemical formula: $\mathbf{Na_2HPO_4}$

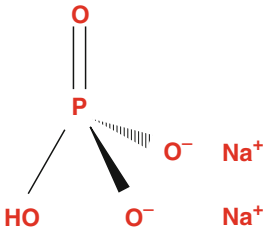

The inhibitors solutions containing polyphosphates were obtained by dissolution in distilled to obtain different concentrations ($10^{-3}$, $10^{-2}$, $10^{-1}$, $5.10^{-1}$ M).

## 3 Results and Discussions

### *3.1 Potentiodynamic Polarization*

The anodic and cathodic polarization curves are recorded on low carbon steel in de-aerated soil simulating solution at various pH and temperatures that simulates conditions of pipe soil environment.

#### 3.1.1 pH Influence

Polarization curves in the pH range 6–8 are shown in Fig. 1. The polarization parameters values of ($I_{corr}$), corrosion potential ($E_{corr}$), polarization resistance and cathodic and anodic Tafel slopes ($b_c$), ($b_a$) are given in Table 4. For corrosion potential value ($E_{corr} = -452.8$ mV/SCE), the corrosion of low carbon pipeline steel in acidic soil simulating solution is obtained.

Results of polarization curves show that the corrosion of iron as a function of pH increases considerably at acidic environments. If values of pH decrease toward the neutral or acidic pH in the range 6–8, steel corrosion increases and polarization

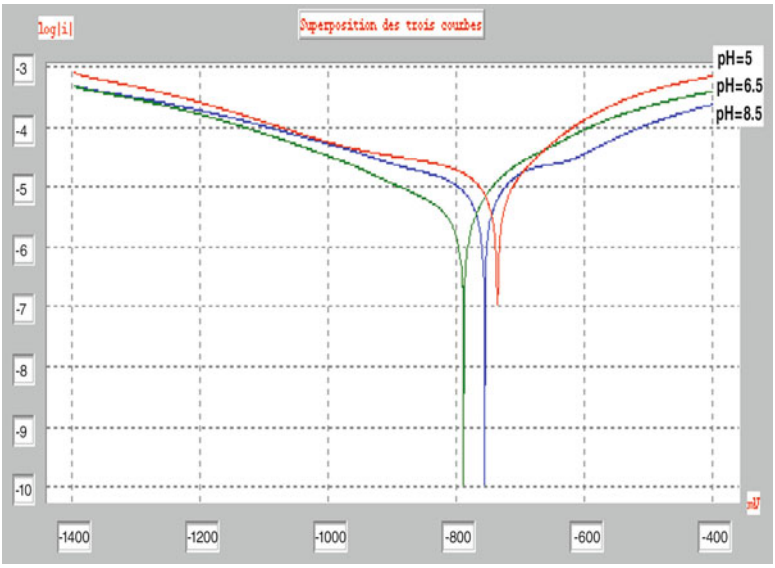


**Fig. 1** Potentiodynamic polarization curves of X60 carbon steel in NS4 simulating solution of corrosive soil environment at 30°C

**Table 4** Polarization parameters for the corrosion of carbon steel in soil simulating solution according to the pH variation in the range 6–8

| pH (mV) | $E_{corr}$/SCE ($\mu A.cm^{-2}$) | $I_{corr}$ ($mV.dec^{-1}$) | $b_c$ ($mV.dec^{-1}$) | $b_a$ ($mV.dec^{-1}$) | $R_p$ kohms.cm$^2$ |
|---|---|---|---|---|---|
| 6.7 | −452.8 | 3.137 | 177.0 | 190.4 | 6.87 |
| 7.5 | −704.4 | 26.686 | 475.5 | 168.5 | 1.51 |
| 8.0 | −759.3 | 5.715 | 231.7 | 87.2 | 3.54 |

resistance decreases. In alkaline pH from pH ≈ 8, the corrosion of steel decreases and polarization resistance increases.

The pH of soil will generally fall within the range 4–10. Soils containing well humidified organic matter tend to be acidic. Mineral soils can become acidic due to leaching of basic cations ($Ca^{2+}$, $Mg^{2+}$, $Na^{+}$, and $K^{+}$) by rainwater and as the result of dissolving of carbon dioxide into the groundwater. In the context of steel corrosion in soil, the passivity occurs at high pH values. In contrast to iron, amphoteric metals, such as aluminium, which are protected by oxide films, can be rapidly corroded in alkaline soils with high pH values as well as in acidic environments.

King [11] in a review of soil corrosiveness developed a monogram that combined the influence of resistivity and pH on the corrosion rate of steel pipe in soil but cautioned that the figure should only be used as a guide. The monogram ignores the influence of both oxidation-reduction potential and microbial activity, key parameters in underground corrosion. It may be applied to the prediction of corrosion rates in aerobic conditions.

### 3.1.2 Temperature Influence

Gas pipelines operation shows that the temperature vary between seasons, or the climatic changes and can modify the interactions between steel and the middle environment in soil. Temperature effect on the steel resistance corrosion was carried out using potentiodynamic measurements. Polarization curves in the temperature range 20–60°C are shown in Fig. 2. Polarization parameters values; corrosion current density ($I_{corr}$), corrosion potential ($E_{corr}$), cathodic Tafel slopes ($b_c$) and polarization resistance ($R_p$) are given in Table 5. The temperature can modify the interaction between steel electrode and the electrolytic medium. It modifies the electrochemical corrosion speed of metals. Steel corrosion is a function of pH and temperature. In neutral pH, oxygen reduction reaction and diffusion speed are favourable reaction with temperature and causes a reduction in solubility. In acidic pH, corrosion speed grows in an exponential form with the temperature because of the over tension reduction of hydrogen release.

In the studied temperature range, the corrosion current density increases with increasing temperature and the steel corrosion potential moves towards the negative values when the temperature increases in the studied solution. The anodic polarization curves present parallel Tafel straight lines indicating that the hydrogen

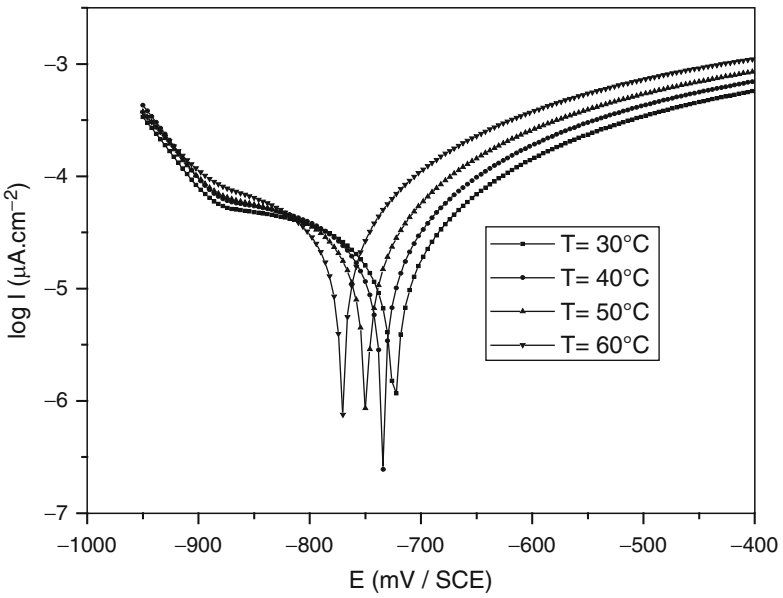


**Fig. 2** Temperature influence on polarization curves of C-Mn steel in NS4 simulating solution of corrosive soil environment (pH ≈ 6.7)

**Table 5** Polarization parameters for the corrosion of low carbon steel in $NS_4$ soil simulating solution according to the temperature (pH ≈ 6.7)

| Temperature [°K] | $E_{corr}$/SCE [mV] | $I_{corr}$ [μA.cm$^{-2}$] | $b_c$ [mV.dec$^{-1}$] | $R_p$ [kohms.cm$^2$] |
|---|---|---|---|---|
| 293 | −705.0 | 16.86 | 563.4 | 2.59 |
| 303 | −705.0 | 26.68 | 475.5 | 1.51 |
| 313 | −715.0 | 33.43 | 668.1 | 1.31 |
| 323 | −727.8 | 38.98 | 631.9 | 1.15 |
| 333 | −750.0 | 44.17 | 457.0 | 0.913 |

reduction reaction to steel surface is always done according to activation mechanism in all the temperature range studied. Results of temperature effect show that the corrosion current density increases with increasing temperature in corrosive test solution. The corrosion reaction can be regarded as an Arrhenius-type process, the rate is given by the following equation:

$$\log \text{Icorr} = -\text{Ea}/2.303\ \text{RT} + \text{k} \tag{2}$$

Where k is the Arrhenius pre-exponential constant, and $E_a$ is the activation corrosion energy for the corrosion process. Figure 3 present the Arrhenius plots of corrosion current logarithm density vs. 1/T. The Ea values were determined from the slopes of Arrhenius plots and are calculated to be Ea = 13.91 kJ mol$^{-1}$. This value is low compared to the value of steels corrosion activation energy in acidic

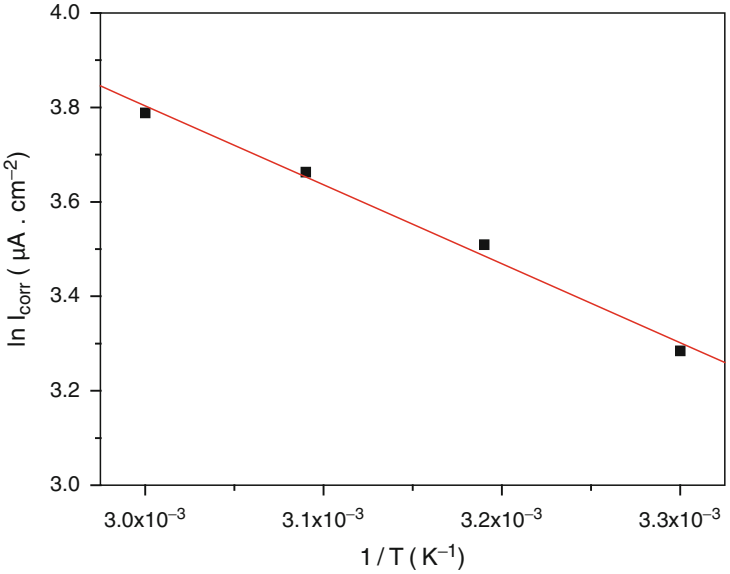


**Fig. 3** Arrhenius plot calculated from corrosion current density for steel in NS4 simulating solution of corrosive soil environment (pH $\approx$ 6.7)

environment which to reach a value of 60 kJ $mol^{-1}$ decreases in inhibitors presence. This reduction probably was attributed to inhibitors chemisorptions on the steel surface [11]. The activation corrosion energy increases with the temperature according to the pH soil environment. The protective efficiency of external coating is function of temperature and it protective properties and decreases the activation corrosion energy.

## *3.2 Electrochemical Impedance Spectroscopy*

The corrosion behaviour of carbon steel in soil simulating solution was investigated by the EIS method at 30 $\pm$ 1°C after immersion for 24 h. Impedance diagrams of steel/solution interface at various potentials imposed was obtained varying from the corrosion potential to the cathodic rest protection which simulates the pipes operating conditions. Figure 4 presents the evolution of Nyquist diagrams of steel pipeline obtained at the rest potential and protection potential in different pH range and immersion time of soil test solution. The impedance parameters derived from this investigation are given in Table 6. Nyquist plots displayed two impedance buckles, one capacitive buckle at the raised frequencies and diffusional loops to the low frequencies. Iron anodic dissolution and oxygen cathodic reduction phenomena are simultaneously made on surface electrode. Capacitive arc size of resistance transfer charge decreases to the slightly acidic pH. Impedance diagrams of

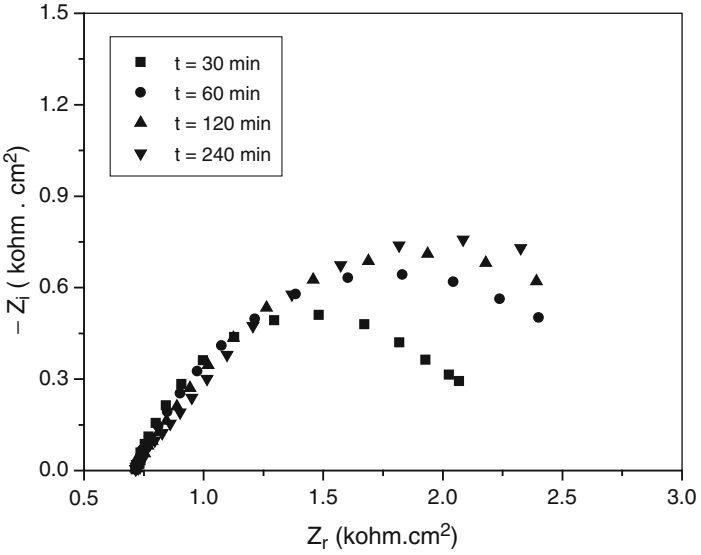


**Fig. 4** Nyquist slopes for low carbon steel in NS4 simulating solution of corrosive soil environment (pH ≈ 6.7) at different immersion times (t = 30°C)

**Table 6** Impedance parameters values of low carbon pipeline steel corrosion in soil simulating solution (t = 30°C)

| pH | $R_t$ (ohms.cm$^2$) | $E_{imp}$/SCE (mV) | $C_{dl}$ (μF.cm$^{-2}$) |
|---|---|---|---|
| 8.0 | 301.14 | −700 | 167.90 |
| 8.0 | 508.40 | −850 | 559.35 |
| 8.0 | 550.10 | −1,000 | 339.62 |
| 8.0 | 525.60 | −1,100 | 211.97 |

steel/solution interface at various potentials imposed varying from the corrosion potential to the cathodic over-protection shows that more the imposed potential is superior to ($E_{corr}$) values of ($R_{t)}$ charge transfer resistance decreases and more the imposed potential is inferior to ($E_{corr}$), charge transfer resistance values decreases also but remains always superior to ($R_{t)}$ value obtained with corrosion potential ($E_{corr}$ = −650 mV/SCE). Corrosion pipeline steel can be started according to operating conditions and soil environment. Immersion time influence where bare steel is in contact with the corrosive soil medium is a significant factor.

Nyquist diagrams of low carbon pipeline steel corrosion in simulating soil solution (pH ≈ 6.7) obtained at the abandonment potential according the immersion time influence and constant temperature are shown in Fig. 5. Impedance parameters values of charge transfer resistance ($R_t$) and capacitance $C_{dl}$ according the immersion time influence are given in Table 7. Results of time immersion influence shows that the charge transfer resistance ($R_t$) increases with increasing immersion duration in corrosive test solution. When the immersion time exceeds

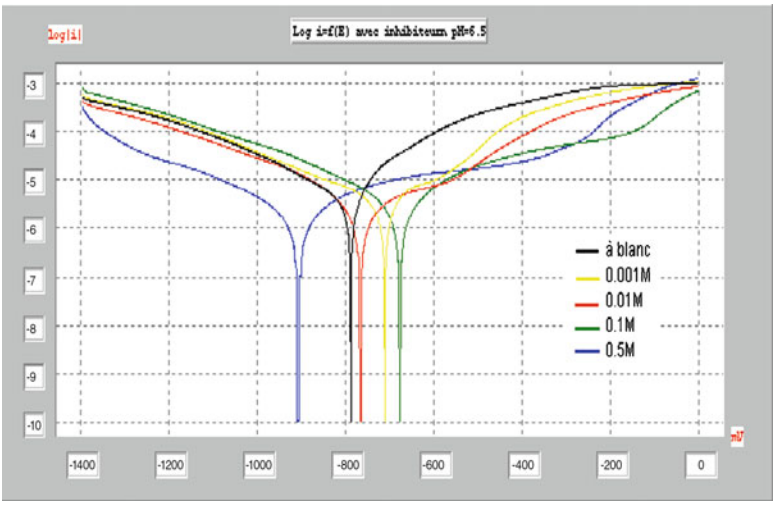


**Fig. 5** Potentiodynamic polarization curves of X60 carbon steel in NS4: simulating solution of corrosive soil environment at pH = 6.5 showed the polyphosphate inhibitor influence

**Table 7** Evolution of impedance parameters values ($R_t$) and ($C_{dl}$) according to immersion time of low carbon pipeline steel corrosion in soil test solution at constant temperature (t = 30°C) and pH ≈ 6.7

| Time immersion (min) | $R_t$ ($\Omega.cm^2$) | $C_{dl}$ ($\mu F.cm^{-2}$) |
|---|---|---|
| 30 | 0713.9 | 270.4 |
| 60 | 1,458.3 | 463.2 |
| 120 | 1,569.5 | 684.1 |
| 240 | 1,681.4 | 1,010.0 |

120 min steel corrosion resistance varies weakly. Capacitive arc size of resistance transfer charge increases to the time immersion increases (Fig. 4).

This result suggests the formation of protective film on steel surface whose protection increases with contact time.

## 4 Conclusions

Results of this investigation showed that some operating buried transmission pipeline systems will develop unforeseen pits and cracking surface corrosion problems. They are principal threats for the buried structure where the humid clay soil aggressiveness and bacterial activity appear. Steel surface must be protected by a full protective system defined by an active cathodic protection to maintain steel in potentials protection in addition to passive coatings protector aiming to avoid any corrosion interaction between steel surface and soil environment.

Future coating systems must answer the durability and reliability requirements in service in regard an economic aspect. Corrosion phenomenon is accentuated by the soils parameters influence such resistivity, pH, temperature, moisture content and chemical composition of electrolytes contained in soil. Potentiodynamic polarization curves showed that the steel corrosion increases at acidic pH environments. Corrosion current density and activation corrosion energy increases with temperature. EIS curves showed that the charge transfer resistance ($R_t$) increases with increasing immersion duration in corrosive test solution. Capacitive arc size of resistance transfer charge increases to the time immersion increases. This result suggests the protective film formation on steel surface. Soil resistivity decreases according to the increase in moisture content and temperature to support ionic exchange between buried steel surface and corrosive soil environment. Results showed low resistivity values in soil investigation particularly in montmorillonite clay soil characteristic of corrosive medium for buried pipeline structures. The electrochemical tests with inhibitor containing polyphosphates showed that the density of corrosion current values (I corr) decreased, for a pH of $NS_4$ solution equal to 5, in absence of inhibitor, the density is about 7.5 $\mu A/cm^2$ in the presence of inhibitor it is to 0.851 $\mu A/cm^2$ with inhibiting effectiveness of more than 88%. Damage problems raise questions as the remaining safe life of the tubes. Pitting or cracking are those most to be involved in remaining life of an existing structure, because of their greater propensity to cause a reduction in the utility duration. Some of the probabilistic approaches can be applied, or are being developed, to answer the corrosion related cracking and pitting phenomena. The research will provide data for risk assessment models to be used for maintenance and operation of the pipeline system.

## References

1. C.W. Petersen, K.T. Corbett, Presented at the International pipeline technology conference, Ostend, 9–13 May 2004, pp. 3–20
2. Sonatrach Gas Marketing & International Development, Yearly Gas newsmagazine published by Sonatrach - Marketing Activity, Alger, Dec 2004, http://www.mem-algeria.org/newsletter/141_en.htm
3. A. Benmoussat, M. Hadjel, Rapport d'expertise des tubes STT, Projet de recherche CNEPRU J 1301-03-05-98, FSI, Université de Tlemcen, Algérie, 1999
4. D.X. He, W. Chen, J.L. Luo, Corrosion **60**, 778 (2004)
5. Y.S. Choi, J.-G. Kim, Corrosion **61**, 293 (2005)
6. M.C. Li, Z. Han, H.C. Lin, C.N. Cao, Corrosion **57**, 913 (2001)
7. API specification 5L (SPEC 5L), *Specification for Line Pipe*, 14th edn. (Washington, 1992)
8. T. Jung, A. Pineau, *Résistance et ténacité des aciers pour gazoducs. Cas de l'arrêt des fissures en rupture par clivage* Revue de Métallurgie-CIT/Science et génie des matériaux, (Fev.1995), pp. 227–239, An International Journal of metallurgy Published by EDP Sciences
9. R.N. Parkins, W.K. Blanchard, B.S. Delanty, Corrosion **50**, 394 (1994)
10. F. Bentiss, M. Lagrenee, M. Traisnell, J.C. Hormez, Corrosion **55**, 968 (1999)
11. R.A. King, TRRL Supplementary Report 316, TTRL Crowthone, 1977

# Leak Detection: General Remarks and Examples

**Anita Calcatelli**

**Abstract** Structure defects may be detected by all the non-destructive analysis techniques from radiography, magnetic particles, liquid penetrating, to ultrasounds, to eddy currents, etc. Nevertheless, to evaluate the quantity of liquid or gas that may be lost in the surrounding ambient specific techniques related to leak detection should be considered. Frequently the maximum acceptable leaks must be evaluated to select the method suitable for the specified object and, finally, to compare the solutions on the basis of costs-benefit relationship. Various leak detection methods and related instrumentation are available (bubbles, ultrasound emission, radar, pressure/vacuum variation, thermal conductivity, halogens, radioisotopes, selective ion pumping, mass spectrometry). Before starting any type of leak testing, it is necessary to decide whether leaks have to be located or measured. Checking the tightness of an object or device implies the measurement of gas flow coming out from a defect or entering through it and reference devices should be provided by primary or accredited laboratories. After a short review of methods/instrumentation attention is given to the calibration of any kind of systems and methods to guarantee the validity of the whole test.

## 1 General Considerations on Leaks

It is not possible, to date, to have systems or components absolutely tight even if the technology had enormous developments (Fig. 1). Containers always have a leak, be it of gas or liquid from a high-pressure artefact whether entry of fluid in an object kept at low pressure (Fig. 2).

And then, some components for the operation of which a degree of tightness has to be guaranteed should be subjected to a control apt to show any leakage due to material defect, faulty workmanship, non hermetic assembly, material degradation

A. Calcatelli (✉)
I.N.RI.M. Scientific Consultant, Turin, Italy
e-mail: a.calcatelli@inrim.it

T. Boukharouba et al. (eds.), *Integrity of Pipelines Transporting Hydrocarbons*,
NATO Science for Peace and Security Series C: Environmental Security,
DOI 10.1007/978-94-007-0588-3_13, 

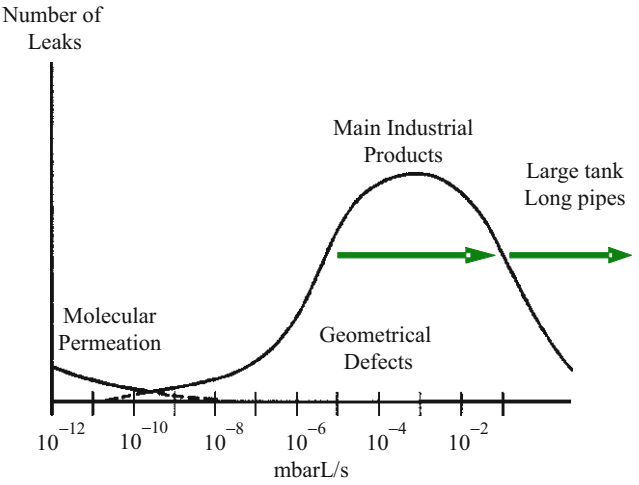


**Fig. 1** Typical occurrence of leaks in industrial products [1]

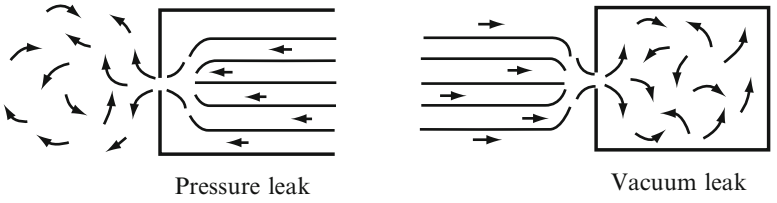


**Fig. 2** Pressure and vacuum leaks

during their operation, crack, pore. welding micro-gap or to non perfect coupling of gaskets in a wall of containment, etc.

The tightness test is a non-destructive test and may be defined as "a test performed to verify compliance of materials or components to specified requirements, using techniques that do not damage the characteristics or working performances".

Only in a very lucky situation, so very rarely, a leak is represented by a cylindrical channel, more often it is due to a tortuous small duct or may also occur through a permeation process.

The leak usually is not deformable, so it has a constant value unless strong mechanical or thermal stress occurs through the walls of a container located between two environments kept at different pressures (Fig. 3). A real leak causes a change of the pressure in the container and it is through a "hole" on a wall connecting the interior of the container with the atmosphere. Even a virtual leak causes a change in pressure inside the considered volume, but it is caused by the evolution of gas or vapour within the system itself, such as desorption of gas from the material of the container or diffusion within the wall followed by emission inside the chamber.

A tightness test implies, therefore, measuring the flow of gas (the amount of gas in time), that escapes from the defect or enters in. Over the years different

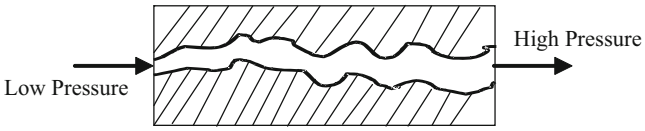


**Fig. 3** Example of geometrical leak

methodologies have been developed to perform qualitative or quantitative measurements. This entails an incentive to address the problem of measuring small gas flows so as to ensure proper traceability to SI (International System of units) for this derived quantity. The cost of the leakage test must be balanced by life time of the artefact under examination.

## 2 Gas Flow Definition

The rate of leak is therefore the amount of fluid entering or escaping from a given container in a time interval and it is commonly known as flow, q. From the ideal gas state equation the molar flow, $q_m$ [mol/s], i.e. the variation in the number of moles (n) of gas in the considered volume, V, is obtained:

$$q_m = \frac{dn}{dt} = \frac{1}{RT}\frac{d(pV)}{dt} = \frac{1}{RT}q = \frac{1}{RT}p\frac{dV}{dt} + \frac{1}{RT}V\frac{dp}{dt} - \frac{1}{RT^2}pV\left(\frac{dT}{dt}\right) \quad (1)$$

Where p is the pressure of the gas, R is the universal gas constant (8.3144 J/mol. K) and T is thermodynamic temperature of the gas. In practice very often the flow rate is given in $Pa.m^3/s$ or in mbar. L/s. 1/(RT) converts the molar flow qm into the throughput q. It is evident, when measuring q, that it is necessary to detect also the temperature. Flows q are referred to a standard temperature that generally, unless otherwise indicated, is 20°C (in some cases 15°C). Very often, and with high values, volumetric flow ($qV = dV/dt$ in $m^3/s$ or L/s) is given that is linked to the q through the pressure p. The capacity of a duct to let the gas flow is called conductance for the definition of which reference is made to the literature [2, 3].

## 3 Gas Flow Regimes

The factors affecting the gas flow through a leak are the molecular weight of gas (m), the viscosity of the gas (η, the pressure difference causing the flow, the absolute pressure in the system and the length and the section of the hole, the channel or leak in general. Depending on the level of considered pressures, there are various types of gas flows (Fig. 4 and Table 1). The dynamics of the flow is characterized by the Knudsen number ($K_n = \lambda/d$, λ = mean free path, d = pipe diameter) and the Reynolds number $Re = \rho v \tilde{d} \eta = [4/(\pi \eta d)] \times [\mu/(RT)] \times q$ where $\rho$ is the gas density, ν the velocity of the gas flow, d is the equivalent

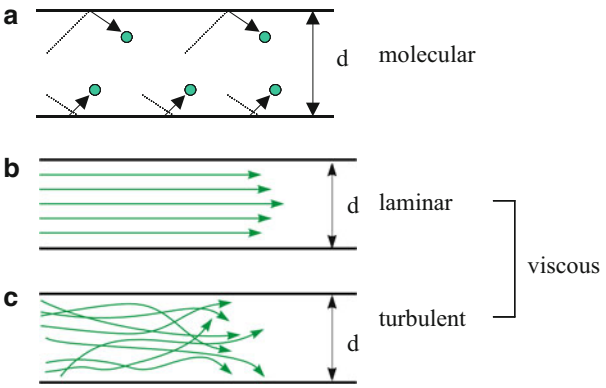


**Fig. 4** Visual representation of the regimes

**Table 1** Flow regimes in different pressure intervals

| Pressure range/Pa | Gas status | Flow regimes | Conditions |
|---|---|---|---|
| $10^5$ | Viscous | Turbulent | $\lambda/d < 10^{-2}$ |
| | | laminar | $1{,}200 < Re < 2{,}200$ |
| 133 | Intermediate | Transitory | $10^{-2}\lambda/d < 0.5$ |
| $10^{-1}$ | Rarefied | Molecular | $\lambda/d > 0.5$ |

diameter of channel and $\eta$ is the gas viscosity [2, 3]. The gas regimes are: molecular, viscous, transition.

The molecular flow occurs when the mean free path, $\lambda$, is greater than the section of the duct (large value of $K_n = \lambda/d > 0.5$) and when one side of the hole or the duct is at low pressure. This implies that the gas molecules pass through a small channel without colliding with each other; they just collide with the walls. The molecular flow is proportional to the difference of the pressure across the wall where the leakage is located. From equation (1), through a hole of area A with $p_1$ and $p_2$ the pressures upstream and downstream of leaking hole, q in [Pa $m^3$/s] is given by:

$$q = \sqrt{\frac{RT}{2\pi\mu}}(p_1 - p_2) \cdot A = \frac{1}{4}\sqrt{\frac{8kT}{\pi m}}(p_1 - p_2) \cdot A = \sqrt{\frac{kT}{2\pi m}}(p_1 - p_2) \cdot A \qquad (2)$$

For a duct of length $l$ and diameter $d$ Knudsen has found out the following expression:

$$q = \frac{1}{12 \cdot l}\pi \cdot (p_1 - p_2) \cdot d^3\sqrt{\frac{8RT}{\pi\mu}} \qquad (3a)$$

$$q = 3.342 \cdot \frac{r^3}{l} \cdot \sqrt{\frac{RT}{\mu}} \cdot (p_1 - p_2) \qquad (3b)$$

With m molecular mass and $\mu$ molar mass.

From (2) and (3) it is easy to evaluate gas flow rates for gas molar mass and temperature other than those measured during the leakage test without problems of measurement units.

Viscous regime occurs when the mean free path of the molecules is small compared with the characteristic dimensions of the hole or the duct, and collisions between molecules are more frequent than with the walls. Viscous flow is proportional to the difference of the squares of the pressures upstream and downstream of leak. In this case there are two different conditions of motion of the gases: laminar or turbulent corresponding to different range of $R_e$ values.

Laminar flow occurs when Reynolds number is 1,200; the gas moves along the duct in parallel paths following the container profile and even when the gas hits an obstacle such lines remain parallel. Laminar flow has the main characteristics of being:

1. proportional to the square of the difference in pressure through the leak;
2. inversely proportional to the viscosity of the gas passing through the leak as it is shown by the Poiseulle equation:

$$q = \frac{\pi}{128\eta} \cdot \frac{d^4}{l} \overline{p}(p_1 - p_2) = \frac{\pi d^4}{256} \left(p_1^2 - p_2^2\right) \tag{4}$$

with : $q_1 = \cos t\left(p_1^2 - p_2^2\right)$

Where $\overline{p}$ is the average pressure in the duct? Equation 4 is valid if the graph of flow rate is constant throughout the length of the channel, the velocity of gas flow on the walls is zero and has a parabolic profile; the molecules move in a non-turbulent way. When a gaseous flow is under laminar regime its value does not vary much with varying the gas because the viscosity varies at most by a factor of 2 while it is strongly dependent on pressure (Fig. 5). If, for leak testing, a mixture of two or more gases is used the viscosity of the mixture is assumed to be: $\eta_{\text{miscela}} = \eta_1 \cdot C_1 + \eta_1 \cdot C_1 + \ldots\ldots\ldots + \eta_1 \cdot C_1 = \sum_{i=1}^{i=n} \eta_i \cdot C_i$, here ci, and $\eta_i$ are viscosity and concentration of i-th gas in the mixture. From equation (4) it can be easily deduced that the flow of a given gas can be calculated for another gas simply by the ratio of the viscosity.

This is useful when a tracer gas is used and the flow must be calculated for a working gas. If the flow must be evaluated for a pressure, $p_3$, upstream of the leak different from the one involved in the leakage test from the same equation we have $q_2 = \frac{\left(p_3^2 - p_2^2\right)}{\left(p_1^2 - p_2^2\right)} q_1$.

In the turbulent regime the motion of gas is more disordered, it does not move along parallel paths and is influenced by any obstacles. This type of regime is encountered when a gas is travelling along pipelines at high and very high pressure. The viscous-turbulent flow occurs when $R_e$ is greater than 2,200. The chaotic and fluctuating nature of turbulent flow has made it impossible to find a theoretical

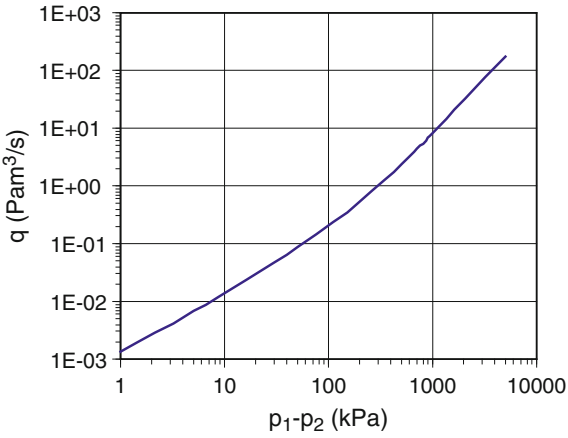


**Fig. 5** Evolution of flow values as a function of pressure difference across the channel

formula that completely represents it. All solutions to the problem of analytical representation led to semi-empirical equations including the best-known and widespread equation of Fanning:

$$q = \frac{\pi}{4}\sqrt{\frac{\left(p_1^2 - p_2^2\right)}{f \cdot \rho' \cdot l}} \quad \rightarrow$$
$$q = d\left(\frac{\pi^2 \cdot 20}{16 \cdot 3.2} \cdot \frac{d^3\left(p_1^2 - p_2^2\right)}{2l}\right) \cdot \left(\frac{R}{\mu}T_0\right)^{3/7}\left(\frac{4}{\pi\eta}\right)^{1/7} \tag{5}$$

Where $\rho'$ is the density per unit of pressure, f is the friction factor which depends on $R_e$, the diameter of the channel and the roughness of its inner surface. Lafferty [2] gives for a long and regular cylindrical duct and smooth surface $f = 0.316R_e - 0.25$.

Figure 6 shows the behaviour of the ratio, q/d, of the flow to the diameter of a duct as function of $d^3\left(p_2^2 - p_1^2\right)/2l$. This diagram can be useful when the gas flow in a duct of known diameter must be tentatively evaluated.

In the transition from molecular to viscous regime the mean free path, $\lambda$, of the molecules is roughly of the same magnitude order as the duct section. The characteristics of the laminar and molecular flow coexist ($1{,}200 < R_e < 2{,}200$): Both wall and intermolecular collisions influence the flow characteristics. The mathematical description of this regime is rather difficult. The flow may be represented with the following empirical relationship:

$$q = \frac{4}{3} \cdot \sqrt{\frac{2\pi RT}{\mu}} \cdot \frac{r^3}{l}\left[0.1472 \cdot \frac{r}{\lambda} + \frac{1 + 2.507 \cdot \frac{r}{\lambda}}{1 + 3.095 \cdot \frac{r}{\lambda}}\right] \cdot (p_1 - p_2) \tag{6}$$

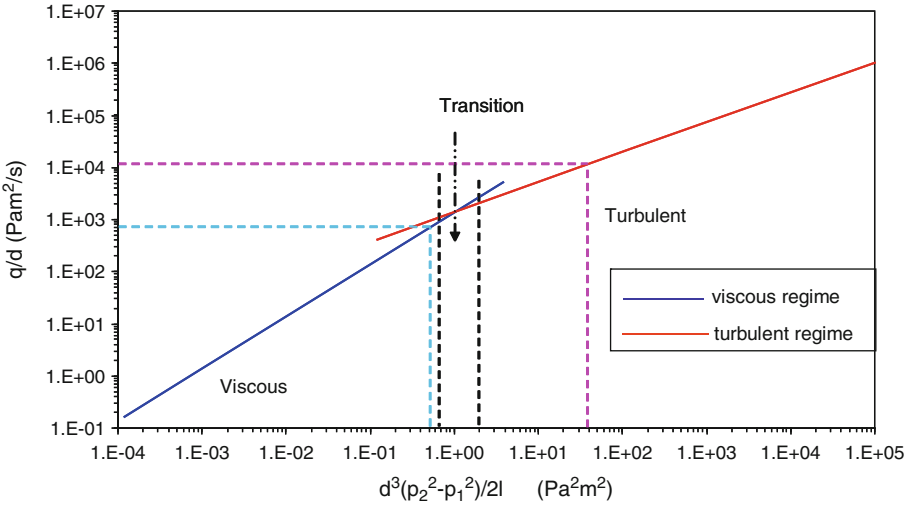


**Fig. 6** Behaviour of the *q*/*d* ratio values versus $d^3(p_1^2 - p_2^2)/2l$

This flow regime frequently occurs, such as with small cylinders as those used to calibrate the leak detectors, the so-called geometric leaks of wide industrial use as they are cheap, easy to be machined. If properly calibrated they may give acceptable reference gas flow rates.

## 4 Methods for Leak Detection

Regardless of the instrumentation used, the tests may be essentially of two main types: location and measurements or quantitative evaluation.

### *4.1 Location of Leaks*

These tests are always qualitative and their results are strongly linked to the ability of the investigator. Two routes may be followed:

(a) pressure tests,
(b) vacuum tests.

#### 4.1.1 Pressure Tests

The object under test is internally pressurized with tracer gas and then with a probe (a conductance named sniffer) it is carefully checked from the outside. The probe

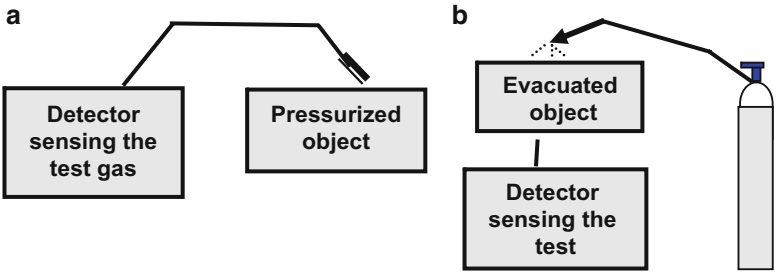


**Fig. 7** Localization of leaks

transfers part of the gas to the sensing element of the leak detector and so the leakage point can be identified (Fig. 7a).

#### 4.1.2 Vacuum Tests

The object in which the leak has to be located is emptied with a special pumping unit or with the same set of detector pumps. The tracer gas is sent to the object and if there is a micro-hole the gas passes through it inside the object to be tested and reaches the sensor of the detector (Fig. 7b).

### *4.2 Measurement and Quantitative Evaluation of a Leak*

To quantify a leak previously localized or not, there are two methods, depending on the object being tested, if pressurized or evacuated.

#### 4.2.1 Pressure or Vacuum-Pressure Tests

The object under test is filled with a tracer or test gas at a given pressure and the surrounding ambient closed or not is at lower pressure (Fig. 8a). If the test piece has a leak, the gas contained in it is released and reaches the detector whose output represents the total flow.

#### 4.2.2 Vacuum Tests

The object under test is connected to the detector, emptied and positioned inside a chamber in which a known quantity of tracer gas is let to enter (Fig. 8b). If there is a hole the gas enters though it and reaches the detector, giving an instantaneous measurement of the gas flow. To increase the sensitivity, the test gas can be cumulated

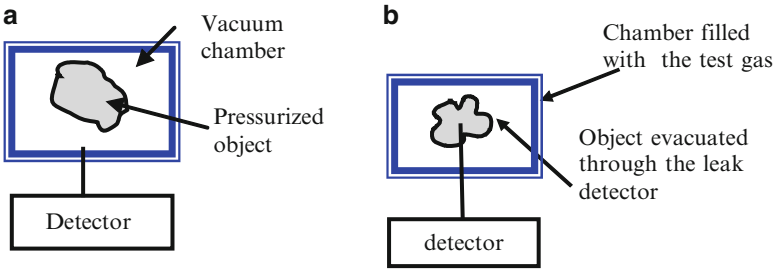


**Fig. 8** Leak measurement, (**a**) pressure-vacuum test and (**b**) vacuum test

for a defined time interval (bombing). One method or the other should be chosen carefully depending on the piece under consideration and the costs of the test.

## 5 Instrumentation for Leak Detection

The instruments dedicated to search of leaks, both for their location or for their quantification, are numerous [4] but we focus in little more details only on some of them. The most commons are: pressure variation, air bubbles in liquid, spark tester, vacuum sensors (Pirani, Thermocouple, Ion Gauge), radioactive elements, halogen leak detector, SF6 leak detector, chemical reactions, penetrating liquids, mass spectrometer, acoustic/ultrasounds devices (active and passive), microwave radar. Some instruments of more general use are modified and adapted for leak search, others are special for leak detection. It should be stressed here that any instrument that measures high or low (vacuum) pressure can be used, with certain precautions. Some methods are particularly useful for locating leaks and others for their quantification. Many systems used for the latter purpose serve, often but not always, even to locate leaks.

### *5.1 Location*

Some techniques/tools are used primarily to locate leaks (bubbles and ultrasound), even though sometimes a tentative value can be estimated.

#### 5.1.1 Bubble Test

This is a pressure test widespread on an industrial scale (typically for car tires) since it is simple and cheap. The object is pressurized and immersed (or sprayed) in a liquid having low surface tension so that it can not penetrate through the possible

defect. Under the leak formation of bubbles occurs that are emitted when the internal pressure exceeds the surface tension of the liquid outside, allowing a correct location of the point of leaking gas on the wall. The bubble size and their emission frequency are function of the type of gas flow, size of the leak, surface tension of the liquid. The bubbles can be seen directly by the operator or by remote viewing achieved by the use of a camera. This type of detection is suitable to highlight ($10^{-3}$ to $10^{-2}$) mba L/s flow. Very often the object being tested must be dried for later use and this is a major drawback.

### 5.1.2 Ultrasound

with ultrasounds the tests may be passive or active; with both techniques, the object must be pressurized [5]. With the passive one the ultrasounds are spontaneously emitted from large holes. If the object kept at high or very high pressure leaks the fluid escapes from the high-pressure zone and passes through the imperfection by creating a turbulent flow with frequencies from hearing (typical car tires) to over 20 kHz (ultrasound), there is a significant ultrasound component detectable with a special tool (Fig. 9). The ultrasound detectors are of active type when controls are carried out with the help of an ultrasonic generator. The instrumentation consist of two parts, together or separated: the generator and the detector, which receives, amplifies, filters and displays the signals returning to the probe after propagation. In this way it is possible to detect only the echoes reflected from any internal defects or the background echoes more or less attenuated depending on the flows. The element that generates and sends ultrasonic waves to the component to be tested is usually a piece of piezoelectric material.

Ultrasonic leak detection is extremely broadly used [6, 7]. Sensing ultrasounds generated by a leak, can be used to locate leaks in pressurized systems regardless of the type of gas used. This is especially beneficial in areas where there is a saturation of gases or where a wide variety of gases, pressurized vessels and vacuum processes exist. Time and convenience are also improved with ultrasonic detection since the equipment may be tested while on-line. This method can easily locate the position of a leak but only if the flow is within the range of $10^{-1}$ mbar L/s and a few tens of mbar L/s.

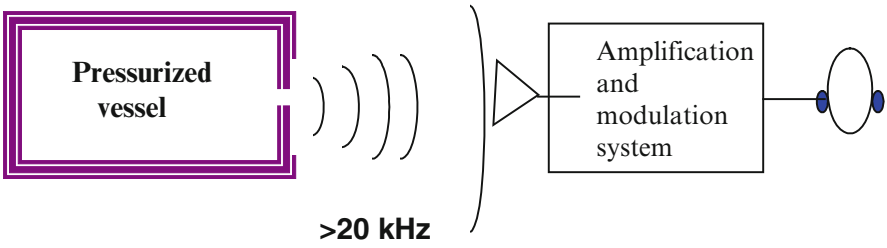


**Fig. 9** Ultrasound leak location on an artefact kept at high pressure

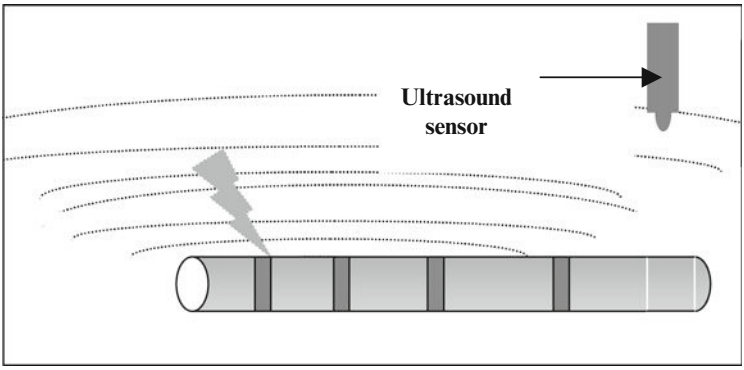


**Fig. 10** Location of leaks on long underground pipes at high pressure

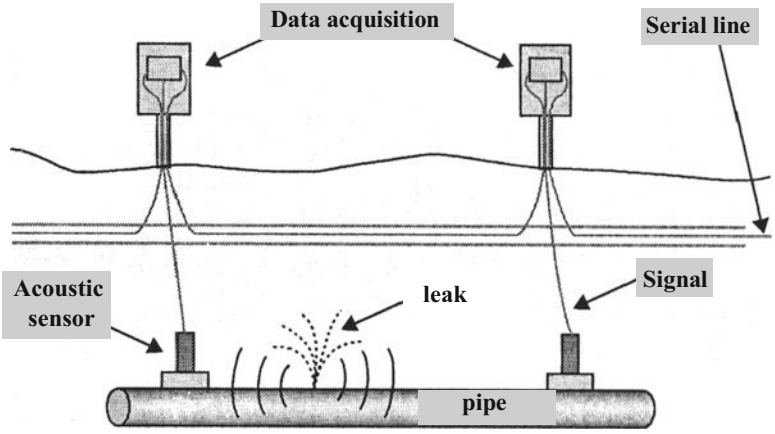


**Fig. 11** Location of leaks on underground pipes with acoustic sensors [10]

The main advantages of this method are related to the possibility of using the working gas under pressure and the absence of "memory" effects at the end of the test. This method is mostly useful whit high leaks, e.g. in pipelines or underground cables (Fig. 10), as in gas transmission lines. With ultrasounds it is possible to inspect the leaks on component in operation or partially loaded without the need of removing it. Microphone receivers are widely used also in the automotive industry for rapid diagnosis of brakes, tires, valves, cooling system, exhaust system of fuel gas and natural gas pipelines. Several probes are commercially available [8].

Even acoustic waves [9] can be used instead of ultrasounds as it is described by Foddis and Pedrielli [10]. The authors give a complete description of leak detection based on analysis of 3,000 Hz component of longitudinal acoustic waves transmitted along oil pipes (Fig. 11) and characteristic of vibrations starting in the pressurized fluid by its leakage from an hole or crack. By an appropriate positioning

of several piezoelectric sensors the exact position of a leak can be detected. This method has been checked by locating several sensors along oil pipes in Sicily and in underground water Scottish pipeline.

### 5.1.3 Microwave Radar

The detection of leaks is similar to radar weather prediction. It is based on the of refractive index variation. This method was used to locate underground oil or gas deposits of hydrocarbon gases [11]. The gas flow through a leak (hole in a pipe) depends on the difference between the pressure inside the pipe and the surrounding atmosphere and it is turbulent. When that method is used on natural gas pipeline, since the density of the methane is smaller than that of the air the leaking gas generates a force due to buoyancy; the gas flow is characterized by vortices whose size may range from 1 mm to 1 m. Ground penetrating radar (GPR) is commonly used to locate underground utilities and other buried systems and it used frequently to survey and prepare job sites for construction or repairs underground infrastructures (Fig. 12). GPR is one of the most accurate methods of mapping and marking what lies beneath the surface [12–14].


**Fig. 12** Microwave radar for leakage location from reference [12]

### 5.1.4 Thermal Conductivity Method

The leaks are detected by measuring the change in the thermal conductivity of air due to the presence of tracer gas that escapes from the leaks. The gas is sent to the sensitive element (thermistor), which, with another similar element cooled by the atmospheric air, makes a full bridge circuit. When the sensing element is affected by atmospheric air and tracer gas (helium) it changes its electrical resistance and therefore the bridge is unbalanced.

The instrument has, therefore, a control unit and a probe. The probe includes the sensor and the sniffer equipped with a small fan which conveys the gas escaping from the leak on the hot filament of the sensor kept in thermal equilibrium. The device under test can be pressurized with tracer gas or gas mixtures (typically mixtures of hydrogen with nitrogen at 5%). When leak gas reaches the sensor LEDs on the control unit will light up in numbers proportional to the leak. This system, which can detect leaks in the field of $10^{-4}$ mbarL/s, has the advantage of a low cost and it is easy to handle, but it has the disadvantage that the measure may be influenced by gases extraneous to the process. The commercially available instrument are known as "electronic sniffers"; they are widely used for total leakage tests on small objects but even to locate leaks in containers filled with tracer gas. Several sniffer may be used in detecting leakage in very large liquid or gas containers and even in the liquefied natural gas ships.

### 5.1.5 Mass Spectrometry

Any type of mass spectrometers based on magnetic sector or quadrupole analysers [15] can be used. The application of mass spectrometry with or without e tracer gas has a good sensitivity (even better than $10^{-6}$) and speed of response [1]. In the most commonly used mass spectrometers leak detectors (MSLD) helium is used as tracer gas because of its chemical and physical characteristics: it is not toxic, it does not pollute, does not disturb the environment, is chemically and physically inert and it is present in the atmosphere in small proportions (concentration of $5 \times 10^{-6}$). The MSLDs may be used both for locating or for measuring leaks with all the methods in pressure and vacuum. When a pressurized vessel is tested by the probe method (sniffer) much of the sensitivity is lost [1].

### 5.1.6 Selective Ion Pump Detector and Tracer Gas

It is based on the fact that permeability of quartz for helium is much greater than for other gases so that variation of helium concentration in the atmosphere can be read as a difference of potential in the ion pump. In the system shown on Fig. 13 a quartz capillary made is connected to an ion Pump working under ultra high vacuum conditions; the sensitivity of the commercially available leak detector is $5 \times 10^{-6}$ mbar L/s [16].

## 6 Measurements of Leaks

Several systems and procedures are available, but attention is concentrated on the most diffused or on those applicable to the oil/liquid gas transferring such as long underground pipes, ships, or storage thanks.

### *6.1 Method Based on Pressure Variation Δp*

It consists on pressurizing the test pieces and checking the pressure drop, or lowering the pressure in the piece (vacuum with a pump) and then checking the pressure rise. In large containers the pressure change is commonly measured. It is required to pressurise and isolate the container, then to adjust for temperature and water vapour; temperature and pressure must be recorded in time.

Measurements can be performed with absolute or differential pressure transducers (Δp measured between the work piece and a reference volume pressurized together and then separated). From the variation of pressure (Δp) measured in

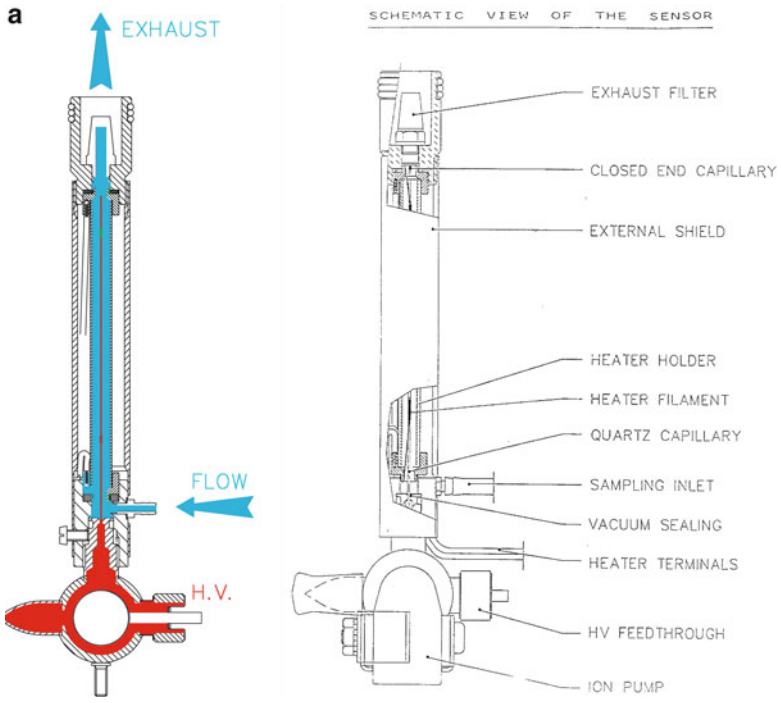


**Fig. 13** Selective ion pump leak detector [6]: (**a**) detection method and (**b**) application to detect leaks on underground telephone cables

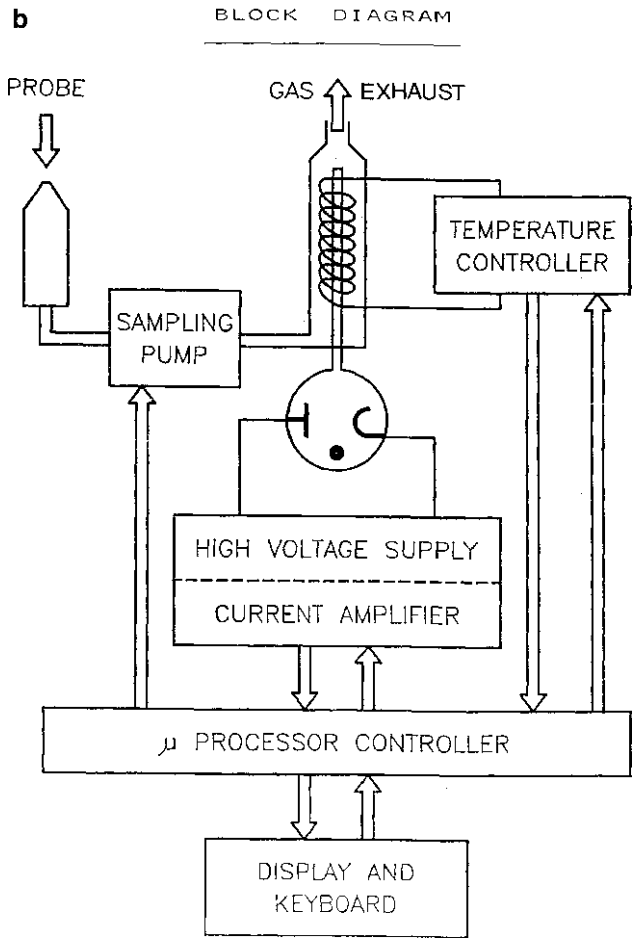


**Fig. 13** (continued)

the time interval ($\Delta t$) in a known volume (V) of the test artefact gas flow $q = (\Delta p \times V)/\Delta t$ is evaluated. It is clear that greater sensitivity of measurement will be obtained on small volumes and long intervals of time. If the test components is made of elastic material it is necessary to take into account that there will be variations in the volume of the product which then affect the calculation of the gas flow. When operating in vacuum (evacuated artefact) the effect due to desorption from the walls of the object must also be considered. The desorption results in an increase in pressure that is added to that due to the presence of leaks. Figure 14a shows the general behaviour of the pressure rise when there is a virtual leak that means that the pressure first increases and then stabilizes; the presence of both real and virtual leaks causes first a non-linear increase in pressure and then a continuous

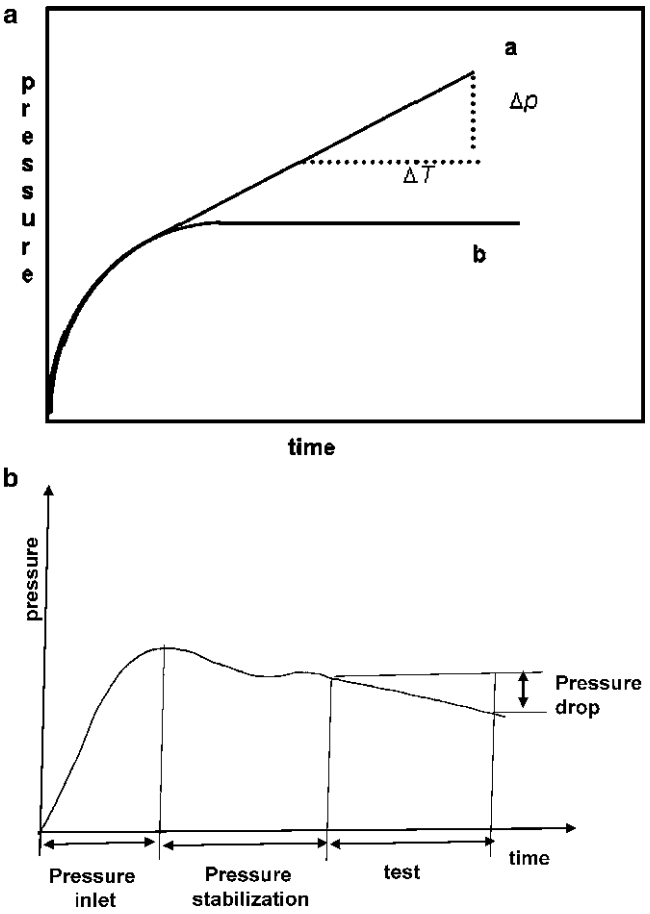


**Fig. 14** (**a**) Pressure versus time: in an evacuated volume (*1*) real leak, (*2*) virtual leak. (**b**) Pressure versus time: pressurized vessel (pressure drop)

linear increase. With the drop measurements the gas is let to enter in the volume under test and let to stabilize (Fig. 14b).

To evaluate the amount of the leak the linear part of the curve should be considered.

A typical industrial application of this method consists in verifying the rise of pressure in a bell enclosing the pressurized test object (pressure-vacuum method). The main advantage of this method lies in its cost; in fact relatively cheap pressure gauges may be used, compressed air and, there are no "memory" phenomena. The main disadvantage consists in the strong dependence on temperature whose changes during the tests may affect the measurement $p(T_1) = p(T_2)\,(T_2/T_1)$.

Finally, the measurement of small flows requires very long test times resulting in certainly larger variations in temperature not negligible. The pressure change is widely used in space modules when a quite fixed pressure must be guaranteed for a

defined time interval, mostly if there are persons on board. Leak tests are performed at ground and leak values are evaluated by using accurate differential pressure gauges such capacitance membrane gauges, traced to a metrological institution. Since the temperature variations may cause pressure changes it is mandatory to know the sensors temperature coefficient.

## 6.2 Pressure Waves

Another pressure method is based on the property of pressure waves generated in a transient pressure; the pressure waves travelling trough pressurized pipes interact with each irregularity they meet and are partly reflected back to their origin and partly transmitted. By the behaviour in time of the pressure in a measuring section it is possible to locate and to calculate the possible leaks with an appropriate mathematical tool (wavelet function) and calibration [17, 18].

## 6.3 Method with Mass Spectrometry and Gas Tracer

MSLD can be applied with the both methods (pressure-vacuum and vacuum) and the situations are similar to those shown in Fig. 8, but the detector consists of a mass spectrometer specially dedicated to this type of testing. A mass spectrometry can detect even very small leaks (down to 10–11 mbar L/s). As in the case of location and for the same reasons, the tracer gas is usually helium. Whether the device is a special spectrometer adapted to leak detecting equipped with its own pumping system or a common mass spectrometer, MSLD is one of the most used devices with any type of object to be tested. The leak detection may be used in classical configuration with direct flow or in the contra flow configuration [1, 19–21].

Many leak detectors are automated in order to reduce operator's influence; that has increased enormously the use of those devices in areas not previously considered in many industries, not only in research field.

Figure 15 shows an example of application of the MSLD [22], in which a commercial detector is used for approval tests of various components in cryogenic industry (compressors, heat exchangers) as well as in automotive industry (light alloy rims for automobiles or trucks, cylinder heads) for which the threshold value of the leaks must be defined to accept or to reject the considered components. The objects are tested by pressure-vacuum technique with helium as tracer gas. The leakage rate is rather high ($10^{-6}$ mbar L/s to $10^{-4}$ mbar L/s).

The module must have the shortest possible cycle time (not more than several tens of seconds) and high reliability; the measurement results must be as much as possible independent from the operator ability and attention. In addition its measurement uncertainty must be clearly defined.

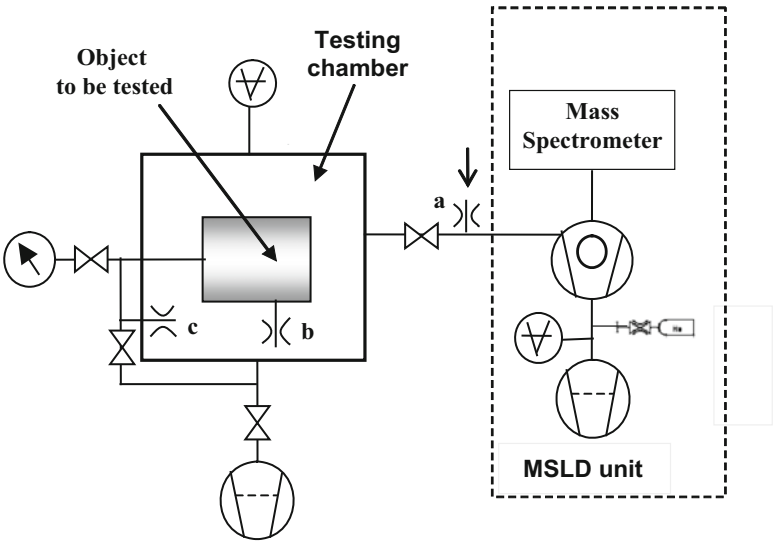


**Fig. 15** Schematic of a leak measurement apparatus [22]

### *6.4 Acoustic, Ultrasound and Radar*

Methods and instrumentation may be used to measure the quantity of the gas leaking provided they are appropriately calibrated by using calibration leaks (membranes with hole or capillaries [11–14].

## 7 Calibration of the Instruments Involved in the Leak Detection

Even for detection of leaks whatever method is chosen and whatever instrumentation is used, there is the need of calibration and of making reference calibrated leaks available. In the case of pressure measurements with both rise or drop of pressure the transducers used must be traced to National Metrology Institutes (NMIs) directly or through accredited laboratories. The NMIs, as I.N.RI.M. (www.inrim.it), provide primary measurements of all the base quantities and several of derived ones as e.g. pressures, flows, volumes, etc. in the most commonly requested working ranges. Figure 16 summarizes, for all the primary systems available at I.N.RI.M. [23], the uncertainty values related to the working ranges; the system are, of course, based on different methods of evaluating the pressure from vacuum standards to high pressure balances (also known as piston gauges) [24, 25]. If the leak detector provides the value of the flow-rate it will be necessary to trace the instrument to a primary flow-meter through calibrated leaks, which may be of

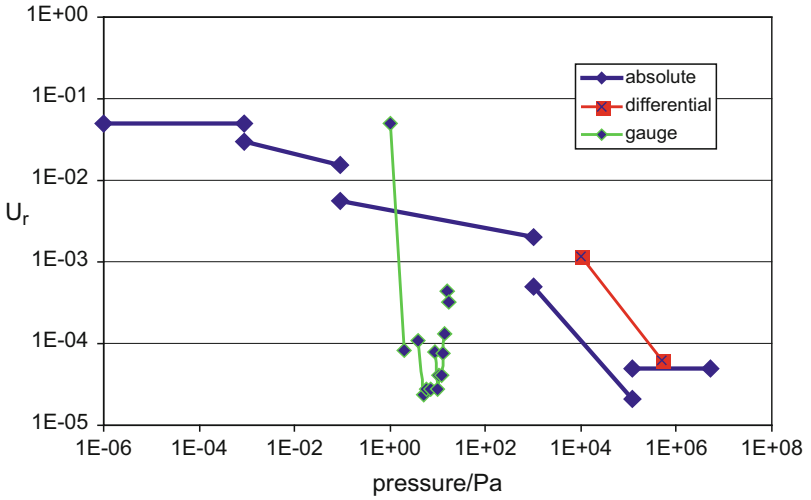


**Fig. 16** Primary pressure devices at I.N.RI.M. represented by the pressure ranges and the expanded uncertainty at 95% [23]

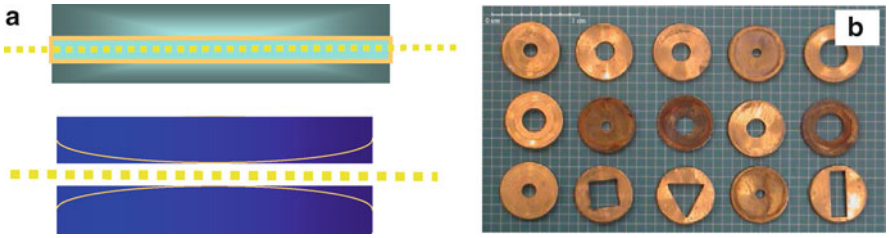


**Fig. 17** Geometrical leaks: (**a**) capillary type [13] and (**b**) holes in membranes [17]

the geometrical types, Fig. 17 (hole in a membrane, small capillary tube) or of the permeation type.

From equation (1) to generate and measure primarily a flow q can be done in three different ways depending on whether it may let to vary over time:

1. pressure and volume (most difficult),
2. volume while pressure is maintained constant,
3. pressure while volume is maintained constant.

The most diffused primary flow–meters are based on variable volume and constant pressure [25–27] where, in general, the pressure is kept constant by varying the volume by a movable piston whose displacement is measured or by an interferometric device or by a length transducer traced to length standard. Table 2 lists both mass or volume flow-meter available at I.N.RI.M. [22] and the expanded uncertainty values for the various ranges as listed in the BIPM database [23].

**Table 2** Primary gas flow rate and volume measurements at I.N.RI.M

| Notes | Mass flowrate | Ur | | | |
|---|---|---|---|---|---|
| | kg/s | % | | | |
| Gas-oil | 1.0E-03 | 0.2 | | | |
| Kerosene | 1 | 0.2 | | | |
| | 3.0E-04 | 0.1 | | | |
| | 0.1 | 0.1 | | | |
| | 1.0E-03 | 0.1 | | | |
| | 1 | 0.1 | | | |
| Liquid helium | 1.5E-02 | 0.5 | | | |
| | 0.3 | 0.5 | Notes | Volume | Ur |
| | g/s | | | l | |
| Inert gas | 2.0E-05 | 0.05 | Water | 1 | 0.2 |
| | 0.02 | 0.05 | | 50 | 0.2 |
| | 0.02 | 0.1 | | 0.01 | 0.05 |
| | 5 | 0.1 | | 0.1 | 0.05 |
| | Volume flowrate | | | 20 | 0.01 |
| | l/s | | | 200 | 0.01 |
| Inert gas | 20E-05 | 0.05 | Inert gas | 2.0E-04 | 0.2 |
| | 0.02 | 0.05 | | 45 | 0.2 |
| | 0.02 | 0.1 | | 50 | 0.1 |
| | 1 | 0.1 | | 120 | 0.1 |
| | 1 | 0.05 | | 120 | 0.05 |
| | 10 | 0.05 | | 800 | 0.05 |
| | 10 | 0.1 | | | |
| | 45 | 0.1 | | | |
| | 2.0E-04 | 0.2 | | | |
| | 45 | 0.2 | | | |

For very low pressure at I.N.RI.M. three home-built flow-meters are available: one is used for throughput measurements with outlet to vacuum and two for throughput measurements with outlet to atmospheric pressure (Figs. 18 and 19). They are essentially based on constant pressure-variable volume methods [26, 27] and cover the following gas flow-rate ranges:

- $2 \times 10^{-8}$ to $2 \times 10^{-7}$ mbar L/s, extended uncertainty 8% and $2 \times 10^{-7}$ to $10^{-3}$ mbar L/s, with extended uncertainty from 3% to 0.5%, with reference to vacuum,
- $2 \times 10^{-4}$ to $10^{-2}$ mbar L/s with reference to atmospheric pressure, extended uncertainty, 2%.

An example of calibration curve of a capillary leak is represented in Fig. 20 showing the behaviour of the scaled conductance in the full range from molecular to viscous though the transition regime depending on the pressure (mean free path) [22, 28–30].

With the radar leak detection in addition to install (on aircraft or car), test radar, data collection and signal processing several other steps are necessary as for

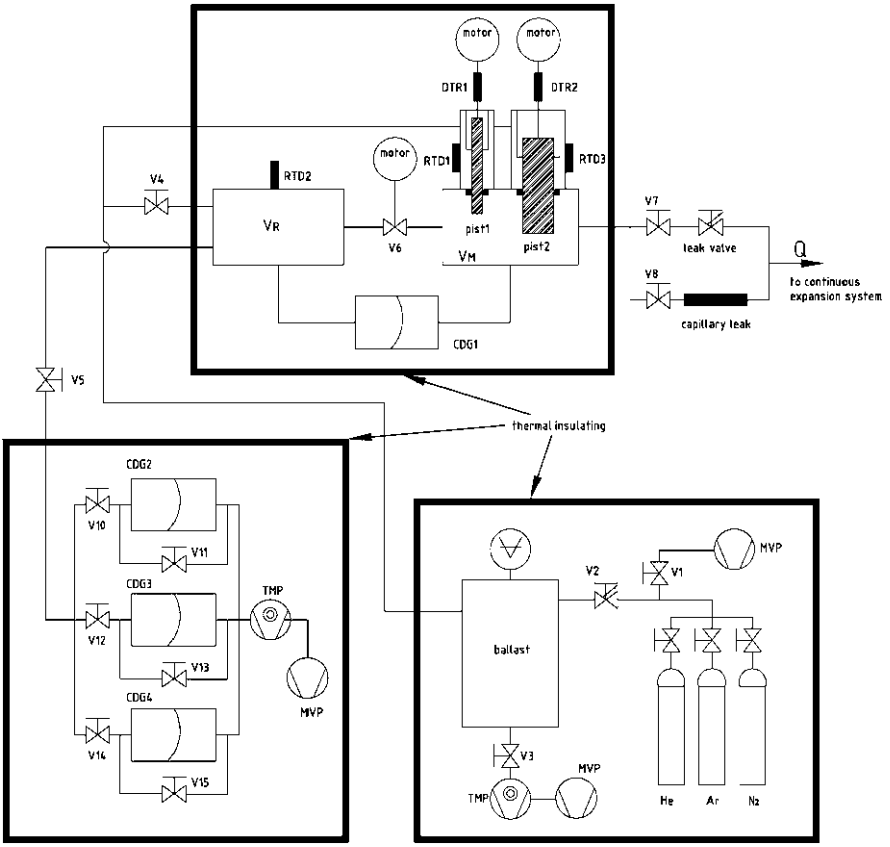


**Fig. 18** Schematic of one of the I.N.RI.M. flow-meters [25]

example [13]: modelling the leak plume and providing standard leaks to be able to measure the flow: some results are summarized in Fig. 21 and Tables 3 and 4 for methane pipeline from reference [13].

## 8 Mutual Recognition Agreement

The primary systems designed for measuring the pressures and gas flow [24, 26, 29] as well as all other fundamental or derived quantities of the SI must meet the requirements of Mutual Recognition Agreement (MRA). By this Agreement, the primary institutions that have signed it recognize the need to demonstrate their Calibration and Measurement Capabilities (CMC), and recognize the validity of calibration and measurement certificates issued by other NMIs (www.bipm.org).

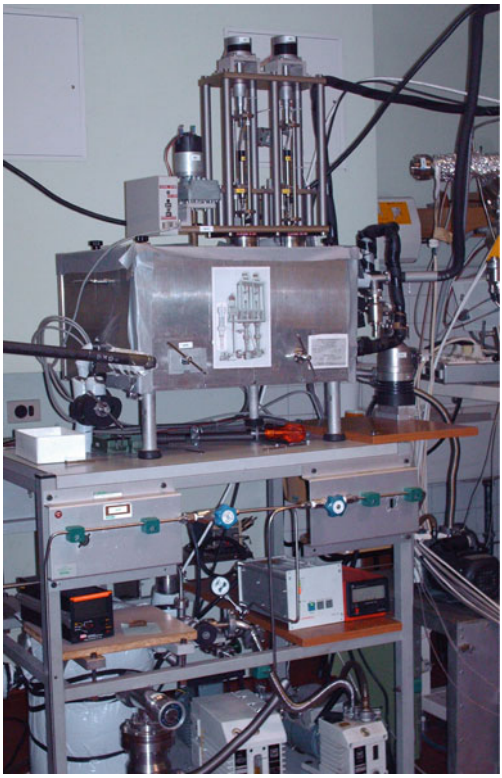

**Fig. 19** General view of one of the I.N.RI.M. flow-meters [25]

The practical realization of the MRA is based on the results of key comparisons or even additional regional or bilateral comparisons performed according to set of procedures, to determine the degree of equivalence of national measurement standards maintained by NMIs. Each laboratory that has signed the agreement must also ensure the quality of its measures through a system of quality to international standards [31]. On the basis of the results of all those actions, the degree of confidence that each laboratory may have on the calibration results and calibration certificates of the others is documented.

The results of various comparisons (key, supplementary and bilateral), after a process of evaluation and acceptance by participants are entered in a database maintained by the Bureau International des Poids et Mesures [32]. Even the CMCs (supported by the comparisons) are included in the BIPM database. Each line of the CMCs represents the calibration activity that the primary laboratory can perform for a given quantity and a particular type of instrument, in a defined range of measurement with a well definite uncertainty value [33].

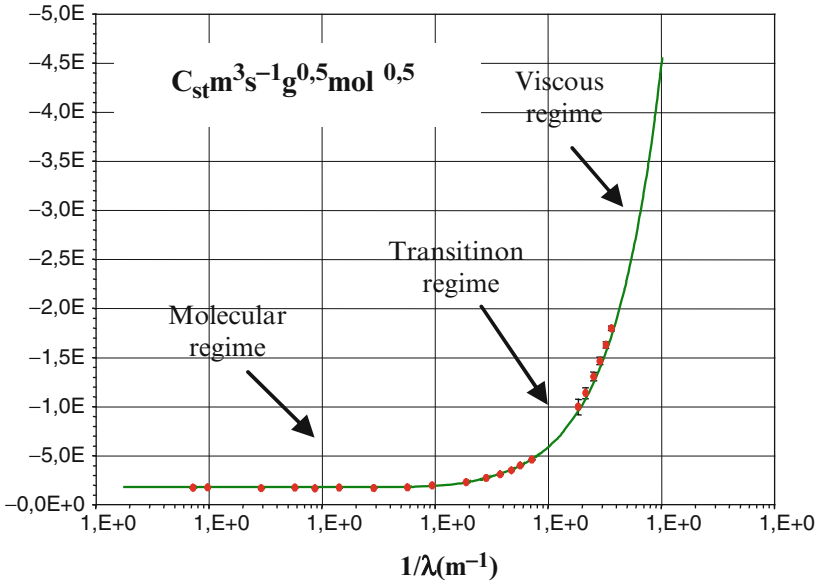


**Fig. 20** Calibration curve of a capillary leak, dots-measurement results, curve-Knudsen interpolation [22]

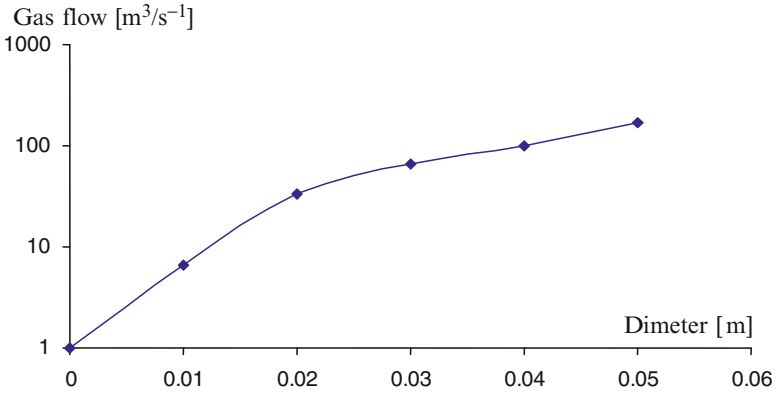


**Fig. 21** Gas leak: flow versus diameter [13]

**Table 3** Methane gas flow rate and hole diameter [13]

| Leak | Methane flow $m^3/s^{-1}$ | Hole diameter mm |
|---|---|---|
| Very small | $1.7 \times 10^{-2}$ | <5.4 |
| Small | $1.7 \times 10^{-2} \rightarrow 1.7 \times 10^{-1}$ | $5.4 \rightarrow 17$ |
| Medium | $1.7 \times 10^{-1} \rightarrow 1.7$ | $5.4 \rightarrow 54$ |
| Large | >1.7 | >54 |

**Table 4** European standards on leak detection: methods

| | | |
|---|---|---|
| EN 1330-8:1998 | May 1998 | Non-destructive testing-terminology-part 8: terms used in leak tightness testing |
| EN 1518:1998 | April 1998 | Non-destructive testing-leak testing-characterization of mass spectrometer leak detectors |
| EN 593:1999/ A1:2003 | Dec. 2003 | Non-destructive testing-leak testing-bubble emission techniques |
| EN 1779:1999/ A1:2003 | Dec. 2003 | Non-destructive testing-leak testing-pressure change method |
| EN 13184:2001/ A1:2003 | Dec. 2003 | Non-destructive testing-leak testing-pressure change method |
| EN 13185 :2001 | Dec. 2001 | Non-destructive testing-leak testing-tracer gas method |
| EN 13192:2001/ AC:2003 | Dec. 2003 | Non destructive testing-leak testing-calibration of reference leaks for gases |
| EN 13625:2001 | Dec. 2001 | Non-destructive testing-leak test-guide to the selection of instrumentation for the measurement of gas leakage |

**Table 5** Leaks permitted in most common artefacts

| Artefact/system | Leak mbar L/s | Notes |
|---|---|---|
| Large tanks for gases and liquids | $\geq 10^{-4}$ | Tested with tracer gas or pressure decay/depending on temperature stability in time (ex. dp/dt = $10^{-3}$ mbar/s for V = 15,000 $m^3$) |
| Long pipes | $\geq 10^{-4}$ | Natural gas transportation at high and very high pressure |
| Chemical process systems | $10-^{1}$ to 1 | High gas flow processes |
| Beverage cans | $10^{-7}$ to $10^{-6}$ | They must guarantee $CO_2$ tightness |
| Vacuum process systems | $10^{-7}$ to $10^{-5}$ | Dynamic systems with acceptable small leaks |
| Automobile airbags | $10^{-8}$ to $10^{-5}$ | They must be in operation for an established time interval |
| Packaging | $10^{-8}$ to $10^{-7}$ | Tightness against humidity or contaminants |
| Pace makers | $<10^{-9}$ | Once implanted long life must be guaranteed |

## 9 Standards

In addition to the various standards on NDT regarding all the techniques, specific standards on leak detection have been made available at European level (Table 4). In Europe, standards on leak detection are the task of the working group WG 6 "Leak testing" of the CEN/TC 138 (Non Destructive Testing); at international level ISO became active in the last years through the working group SC 6 "Leak detection methods" of the ISO/TC 135 (Non Destructive Testing).

Table 5 lists the European method standards to which the EN 473 must be added on qualification and certification of NDT personnel-general principles. It is important, besides desirable, that in the near future the whole standardization activity will

be the task of only one group working on the standards for all the available methods on leak detection, combining the various experiences on non destructive testing.

## 10 Conclusions

It is relatively easy to find out leaks while it is more complicated to quantify them; for the measurements of the leaks appropriate methods and techniques should be chosen in advance on the basis of needs and cost-benefit analysis. It is necessary to provide a traceability chain in which National Metrology Institutes have to be involved directly or through accredited laboratories The demands of leak measurements is increasing for quality and safety warranty. The following table shows some examples of acceptable leaks for the most common artefacts.

Mass spectrometry is widely used both for leaks identification/location and measurements; on large containers pressure rise or drop is frequently applied with careful attention to temperature stability or to the evaluation of its influence on the final result. Both method and related instrumentation need to be traced to reference standards for gas flow rate or pressure. Ultrasound and radar are widely employed to locate leaks, mostly for underground large tanks and gas pipes; several studies based on appropriate mathematical tools and calibration studies have been performed or are under way for quantification of leaks.

Frequently it necessary to combine several testing types (Table 5) to appropriately locate the leakage zone and to measure the corresponding flow. The choice of the measurement method and instruments depends on the type, geometry of the containers to be analyzed and, of course, on fluid and its pressure.

## References

1. *Introduction to Helium Mass Spectrometer Leak Detection*, Varian Associates Inc., Palo Alto, 1080
2. J.M. Lafferty (ed.), *Foundations of Vacuum Science and Technology* (Wiley, New York, 1997)
3. E.H. Kennard, *Kinetic Theory of Gases* (MacGraw-Hill, New York, 1938)
4. Leak testing of large containers, American Gas and Chemical Co. Ltd, Large.containers.mht
5. C. Moon, W.C. Brown, S. Mellen, E. Erenz, D.J. Pickering, Ultrasound techniques for leak detection, 2009-01-2159, SAE international, New York
6. Ultrasound leak detection, www.gasonic.com
7. S.D. Holland, R. Roberts, D.E. Chimenti, M. Shei, Leak detection in spacecraft using structure-born noise distributed sensors. Appl. Phys. Lett. **86**, 154105 (2005) (April 2005)
8. B. Reqiri, W. Scholl, S.P. Robinson, Measurement and testing of the acoustic properties of materials: review. Metrologia **47**, S156–S171 (2010)
9. W. Hertz, Advances of laser-acoustical leak testing for construction and operation of low temperature installations and superconducting experiments. J. Vac. Sci. Technol. **A20**(5), 1733–1737 (2002) (Sep/Oct 2002)

10. F. Foddis, F. Pedrielli, Sistema di rilevamento perdite in oleodotti, Manutenzione, Tecnica e management. 25–28 Sept 2003
11. N. Gopalsami, D.B. Kanareykin, V.D. Asanov, S. Bakthiari, A.C. Raptis, Microwave radar detection of gas pipeline leaks. Paper presented at the 29th Annual Review of Progress in Quantitative Nondestructive Evaluation, Bellingham, 14–19 July 2001
12. N. Gopalsami, A. Dron, T. Elmer, P. Raptis, A radar detection and monitoring gas pipelines leaks, in *Natural Gas Infrastructure Reliability Industry Forum*, Morgantown, 16–17 Sept 2002
13. N. Gopalsami, D.B. Kanareykin, V.D. Asanov, S Bakthiari, A.C. Raptis, Microwave radar detection of gas pipeline leaks, AIP Conf. Proc. **57**, 478–484 (27 March 2003)
14. N. Gopalsami, A. Dron, T. Elmer, A.C. Raptis, V.D. Asomov, S.V. Kakhatski, S.A. Nishim, The use of microwave radar for remote detection of gas pipeline leaks, www.netl.doc.gov
15. J. Robotz, *Introduction to Mass Spectrometry* (Interscience, New York, 1968)
16. A. Psacaropulo, Applicazionidi prove di tenuta in oggetti sotterranei, dai cavi telefonici ai serbatoi per liquidi Aipnd Annual Meeting, Milan, Sept 2007
17. B. Brunone, M. Ferrante, Detecting leaks in pressurized pipes by means of transients. J. Hydraul. Res., IAHR **39**, 539–547 (2001)
18. N. Ferrante, B. Brunone, Pipe system diagnosis and leak detection by un steady-state tests, 2. Wavelet analysis. Adv. Water Resour. **23**(5–7), 627–632 (1993)
19. W.G. Bley, Helium leak units. Vacuum **44**(5–7), 627–632 (1993)
20. G. Reich, Leak detection with tracer gases, sensitivity and relevant limiting factors. Vacuum **37**(8–9), 691–698 (1987)
21. L.J. Berquist, Y.T. Sasaki, Innovation in helium leak detector systems. J. Vac. Sci. Technol **A10**(4), 2650–2654 (1992) (July/Aug 1992)
22. A. Calcatelli, M. Bergoglio, D. Mari, Leak detection, calibrations and reference flows: practical examples. Vacuum **81**(11–12), 1538–1544 (2007) (Aug 2007)
23. Complete CMCs in Mass and related quantities for Italy (pdf file) on http://www.bipm.org/exalead_kcdb/exa_kcdb.jsp?_c=+16366751034942705708/_c=+18132149409823012435
24. A. Calcatelli, G. Molinar, Primary pressure scale in Italy from 10-6 Pa to 109 Pa, in *Basic Metrology*, Libreria Editrice Universitaria, Levrotto e Bella, Torino, 1984
25. M. Bergoglio, A. Calcatelli, The physical measurement of pressure. Vacuum **64**, 153–162 (2002)
26. A. Calcatelli, G. Raiteri, G. Rumiano, Gas flow measurements connected with the continuous expansion system, in *International Symposium on Pressure and Vacuum*, ed. by Acta Metrologica Sinica Press, Beijing, 22–24 Sept 2003, pp. 29–35
27. A. Calcatelli, G. Raiteri, G. Rumiano, The IMGC-CNR flow meter for automatic measurements of low-range gas flows. Measurement **34**(2), 121–132 (2003)
28. C.D. Ehrlich, J.A. Basford, Recommended practices for calibration and use of leaks. J. Vac. Sci. Technol. **A10**(1), 1–17 (1992) (Jan/Feb 1992)
29. M. Bergoglio, A. Calcatelli, G. Rumiano, Gas flowrate measurements for leak calibration. Vacuum **46**(8), 763–765 (1995)
30. M. Bergoglio, G. Brondimo, A. Calcatelli, G. Reiteri, G. Rumiano, Mathematical model applied to the experimental calibration results of a capillary standard leak. Flow Meas. Instrum. **17**, 129–138 (2006)
31. ISO/IEC 17025:2005, General requirements for the competence of testing and calibration laboratories, 2005
32. http://kcdb.bim.org/appenidxD, key comparisons
33. ISO ISBN 92-67-101889, Guide to the expression of the uncertainty in measurements, 1993 (revised with minor corrections in 2008)

# Corrosion Defect Assessment on Pipes Using Limit Analysis and Notch Fracture Mechanics

**Guy Pluvinage**

**Abstract** Two methods of corrosion defect assessment on pipes are described: Limit Analysis (LA) and Notch Modified Failure Assessment Diagramme (NMFAD). Limit pressure analysis are based on ASME B31G, modified ASME B31G, DNV RP-F101 codes and recent proposed formulations. The notch stress intensity factor concept and SINTAP structural integrity procedure are combined to assess pipelines integrity into a notch-based assessment diagram so-called 'NFAD'. Defect assessment is made by comparing safety factor to a prescribed value (deterministic approach) or failure probability at conventional level.

## 1 Introduction

Pipelines have been employed as one of the most practical and low price method for large oil and gas transport since 1950. The pipe line installations for oil and gas transmission are drastically increased in last three decades. Consequently, the pipeline failure problems have been increasingly occurred. The economical, environmental and human life considerations involve the current issue as structural integrity and safety affairs. The explosive characteristics of gas provide high wakefulness about the structural integrity. Therefore, the reliable structural integrity and safety of oil and gas pipelines under various service conditions including presence of defects should be warily evaluated. The external defects, e.g., corrosion defects, gouge, foreign object scratches, and pipeline erection activities are major failure reasons of gas pipelines. A typical example of a corrosion defect is given in Picture 1. According to numerous design codes, this kind of defects is considered as a semi elliptical crack–like surface defect of aspect ratio a/c. The aspect ratio

G. Pluvinage (✉)
Fiabilité Mécanique, Conseils, Silly sur Nied, France
e-mail: pluvinage@cegetel.net

T. Boukharouba et al. (eds.), *Integrity of Pipelines Transporting Hydrocarbons*,
NATO Science for Peace and Security Series C: Environmental Security,
DOI 10.1007/978-94-007-0588-3_14, 

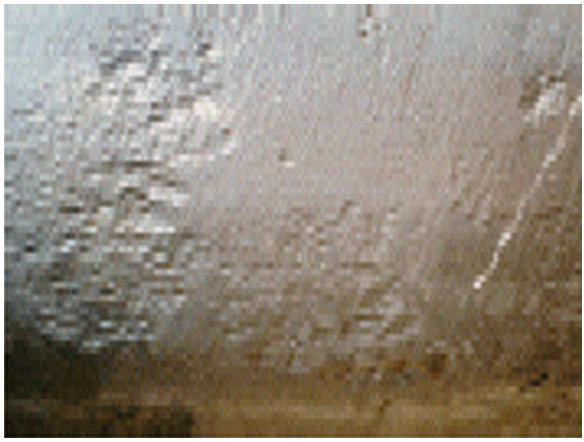

**Picture 1** Example of corrosion defect on pipe

varies in range [0.1–1] depending on corrosion rate anisotropy. Several types of pipes failures can be distinguished as longitudinal, circumferential or helicoidally failures. These types depend mainly on pipe diameter. For small diameter pipes, where bending stresses are predominant, circumferential failure occurs. For large diameters, hoop stresses are more important than bending stresses and longitudinal failure appears. When bending and hoop stresses are of the same importance, fracture path becomes spiraled.

Pipe steels have yield stress up to 700 MPa for the most recent quality in order to ensure enough ductility and weldability. Failures emanating from corrosion defect are elasto plastic fracture or plastic collapse. For these two situations, defect assessment is made generally by two tools: failure assessment diagram (FAD) and limit analysis (LA). In this paper the two major corrosion defect assessment tools for pipes are presented:

1. limit analysis,
2. a notch adapted failure assessment diagramme by modification of the SINTAP procedure using the Volumetric Method,

A comparison of methods is given as a conclusion.

## 2 Assessment of Corrosion Defect by Limit Analysis

The structural integrity of corrosion defects is substantially studied. In Fig. 1, A list of methods available for corrosion defect assessment is presented. They are grouped vertically by their type, codified methods or others, and horizontally by their applicability, pressure or combined loading, etc.

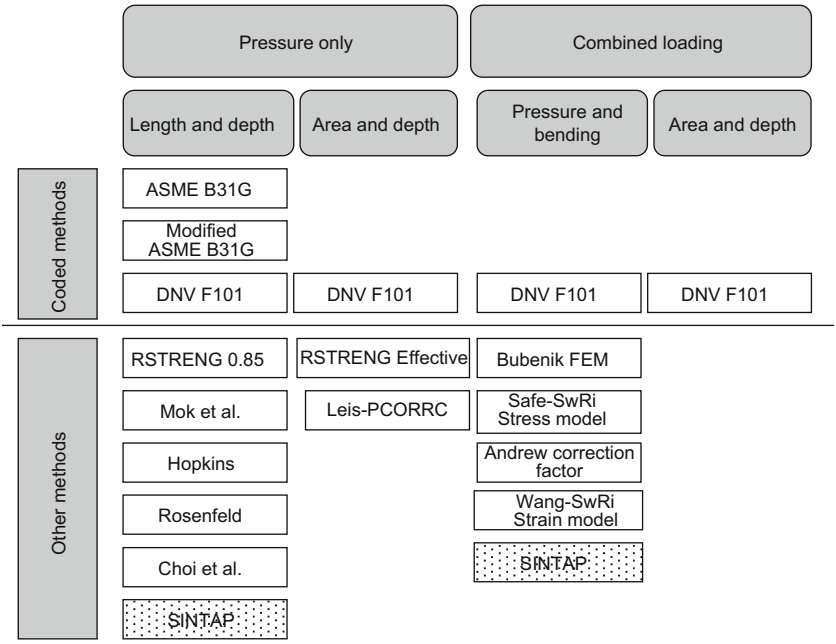


**Fig. 1** Methods for corrosion defect assessment based on limit analysis

## *2.1 ASME B31G and Modified ASME B31G*

ASME B31G [1] is a code for evaluating the remaining strength of corroded pipelines. It is a supplement to the ASME B31 code for pressure piping. The code was developed in the late sixties and early seventies at Battelle Memorial Institute and provides a semi-empirical procedure for the assessment of corroded pipes. Based on an extensive series of full-scale tests on corroded pipe sections, it was concluded that pipeline steels have adequate toughness and the toughness is not a significant factor. The failure of blunt corrosion flaws is controlled by their size and the flow stress or yield stress of the material. The input parameters include pipe outer diameter (D) and wall thickness (t), the specified minimum yield strength ($\sigma_Y$), the maximum allowable operating pressure (MAOP), longitudinal extent of corrosion ($L_c$) and defect depth (d).

According to the ASME B31G code, a failure equation for corroded pipelines was proposed by means of data of burst experiments and expressed with consideration of two conditions below:

First, the maximum hoop stress cannot exceed the yield strength of the material ($\sigma_{\theta\theta} \leqslant \sigma_Y$). Second, relatively short corrosion is projected on the shape of a parabola and long corrosion is projected on the shape of a rectangle. The failure pressure equation for the corroded pipeline is classified by parabola and rectangle as shown in Fig. 2.

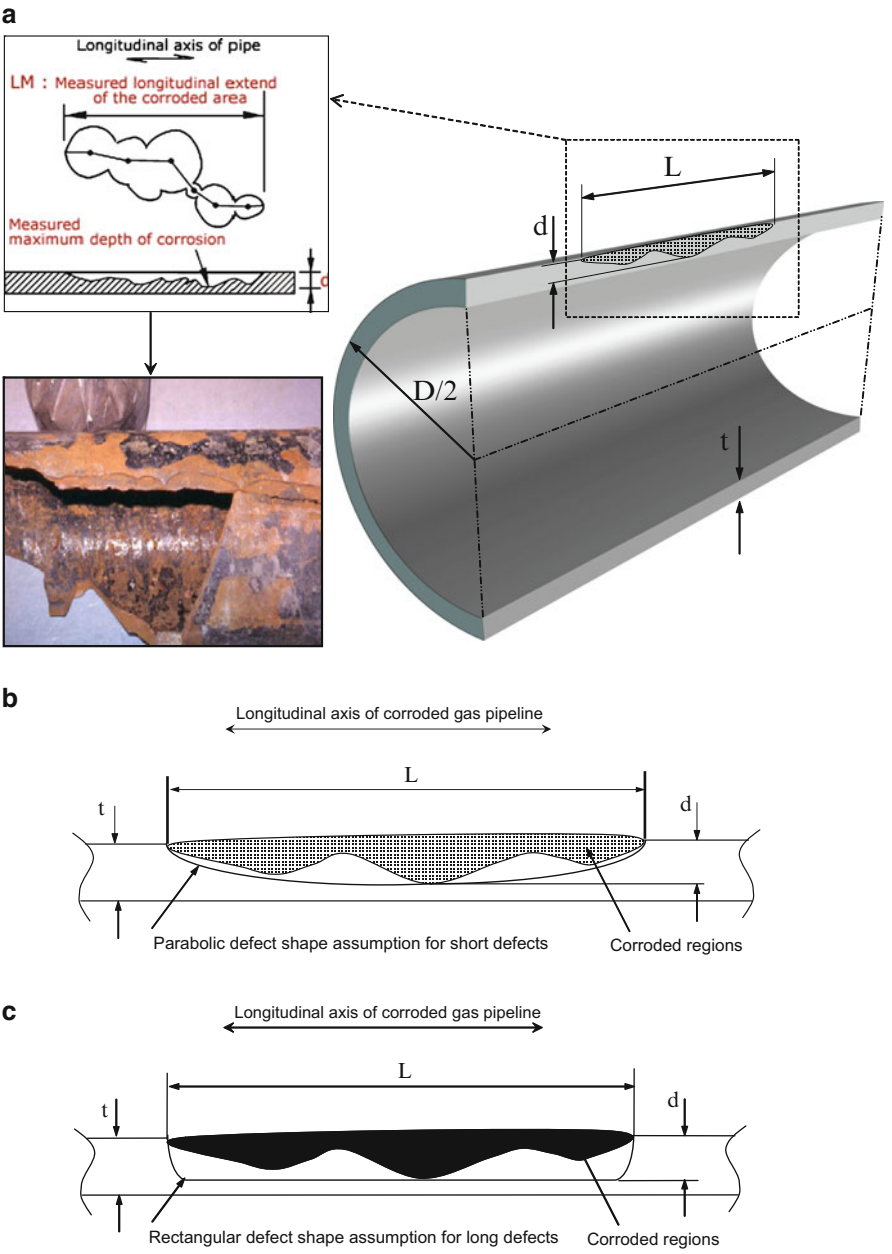


**Fig. 2** (**a**) Typical illustration of corrosion defects (longitudinal axis), (**b**) Short corrosion defect simplified as a parabolic curve (ASME B31G) and (**c**) Long corrosion defects simplified as a rectangular defect

Parabolic defects:

$$P_f = \frac{2(1.1\sigma_y)\cdot t}{D}\left[\frac{1-(2/3)\cdot(d/t)}{1-(2/3)\cdot(d/t)/M}\right] \tag{1}$$

where:

$$M = \sqrt{1+0.8\left(\frac{L}{D}\right)^2\left(\frac{D}{t}\right)}$$

for:

$$\sqrt{0.8\left(\frac{L}{D}\right)^2\left(\frac{D}{t}\right)} \le 4$$

Where, $P_f$, D, d, t, M, $\sigma_Y$ and L are the failure pressure, outer diameter, maximum corrosion depth, wall thickness, bulging factor, yield stress and longitudinal corrosion defect length, respectively. Due to some problems associated with the definition of flow stress, a new flow stress was proposed as:

$$\sigma_f = 1.1\sigma_Y + 69[\text{MPa}] \tag{2}$$

The modified ASME B31G including this new modified flow stress and bulging factor is a follows:

$$P_f = \frac{2(1.1\sigma_Y+69)\cdot t}{D}\left[\frac{1-0.85(d/t)}{1-0.85\dfrac{(d/t)}{M}}\right] \tag{3}$$

where:

$$M = \sqrt{1+0.6275\left(\frac{L}{D}\right)^2\left(\frac{D}{t}\right)-0.003375\left(\frac{L}{D}\right)^4\left(\frac{D}{t}\right)^2}$$

for:

$$\left(\frac{L}{D}\right)^2\left(\frac{D}{t}\right) \le 50$$

$$P_f = \frac{2(1.1\sigma_Y+69)\cdot t}{D}\left[\frac{1-0.85(d/t)}{1-0.85\dfrac{(d/t)}{M}}\right] \tag{4}$$

where:

$$M = 3.3 + 0.032\left(\frac{L}{D}\right)^2\left(\frac{D}{t}\right)$$

for:

$$\left(\frac{L}{D}\right)^2\left(\frac{D}{t}\right) > 50$$

It is necessary to recall that ASME B31G is limited to low stress concentration factors and internal pressure loading conditions. In the assessment procedure, one considers the maximum depth and longitudinal extent of the corroded area, but ignores the circumferential extent and the actual profile. If the corroded region is found to be unacceptable, B31G allows the use of more rigorous analysis or a hydrostatic pressure test in order to determine the pipe remaining strength. Alternatively, a lower maximum allowable operating pressure may be imposed.

## 2.2 DNV RP-F101

DNV RP-F101 [2] is the first comprehensive and extensive code for pipeline corrosion defect assessment. It provides guidance for internal pressure and combined loading. It covers all loading types e.g., pressure only and combined loading. Furthermore, it provides codified formulations for pressure, bending and area depth. DNV RP-101 proposes two methods to find the failure pressure. The first method is based on the partial safety factor and the second is classified as allowable stress design. Both methods entail information on the pipe outside diameter (D), wall thickness (t), ultimate tensile strength ($\sigma_U$), maximum allowable operating pressure (MAOP), longitudinal extent of corrosion ($L_c$) and defect depth (d). The allowable stress design method considering non-interacting defects is discussed here. The exact procedures for the partial safety factor method and interacting defects can be found within the DNV code.

To pursue the design procedure via DNV RP-101, it is required to determine the loading type (pressure only and combined loading) and consequently, the failure pressure can be obtained as:

$$P_f = \frac{2\sigma_U t}{D - t}\left[\frac{1 - (D/t)}{1 - \frac{(D/t)}{Q}}\right] \tag{5}$$

where:

$$Q = \sqrt{1 + 0.31\left(\frac{1}{\sqrt{Dt}}\right)^2}$$

Where $P_f$, D, d, t, Qand $\sigma_U$ are the failure pressure, outside diameter, corrosion depth, wall thickness, correction factor and ultimate tensile strength, respectively. According to DVN RP-101, the failure pressure should not exceed the maximum allowable stress design operating pressure (MAOP) otherwise, the corroded pipe will be repaired or replaced before returning to service.

## 2.3 Choi's Method

Based on limit load analysis assumptions and finite element analysis of corroded pipelines, Choi et al. [3] proposed a limit load solution as a function of $\frac{R}{t}$, $\frac{L}{\sqrt{Rt}}$ follows:

$$P_f = \begin{cases} 0.9\dfrac{2\sigma_U t}{D_i}\left[C_0 + C_1\left(\dfrac{L}{\sqrt{Rt}}\right) + C_2\left(\dfrac{L}{\sqrt{Rt}}\right)^2\right] & \text{for } \dfrac{L}{\sqrt{Rt}} < 6 \\ \dfrac{2\sigma_U t}{D_i}\left[C_3 + C_4\left(\dfrac{L}{\sqrt{Rt}}\right)\right] & \text{for } \dfrac{L}{\sqrt{Rt}} \geq 6 \end{cases} \tag{6}$$

$$\begin{cases} C_0 = 0.06\left(\dfrac{d}{t}\right)^2 - 0.1035\left(\dfrac{d}{t}\right) + 1 \\ C_1 = -0.6913\left(\dfrac{d}{t}\right)^2 + 0.4548\left(\dfrac{d}{t}\right) - 0.1447 \\ C_2 = 0.1163\left(\dfrac{d}{t}\right)^2 - 0.1053\left(\dfrac{d}{t}\right) + 0.0292 \\ C_3 = -0.9847\left(\dfrac{d}{t}\right) + 1.1101 \\ C_4 = 0.0071\left(\dfrac{d}{t}\right) - 0.0126 \end{cases}$$

where $P_f$, $\sigma_U$, $D_i$, d, t and R are the failure pressure or maximum pressure, ultimate tensile strength, inside diameter, defect depth, wall thickness and average pipe radius, respectively. In general, the corrosion pits are idealized into a semi-elliptical shape rather than rectangular and semi-spherical shapes.

## 2.4 Experimental Verification and Codes Comparison

An experimental verification has been made by burst tests. Specimens are rolled steel cylindrical pipes with .an external diameter of 219.1 mm and a thickness of 6.1 mm. A quasi-semi-ellipsoidal notch represents a corrosion external defect. The major axis of the ellipsoid is parallel to the axis of the tube and the length .of the notch is 30.5 mm. The depth of the notch is 3.05 mm and the width is also 3.05 mm. The radius of .the notch tip is 0.15 mm, as shown in Figs. 3 and 4. A schematic view of the notched tube is given in Fig. 3.

Some tubes containing a notch with the dimensions given here were loaded with a gas up to failure. Fracture occurs under a pressure of about 12 MPa. Only two results are available, but they give fracture pressures that are close together.

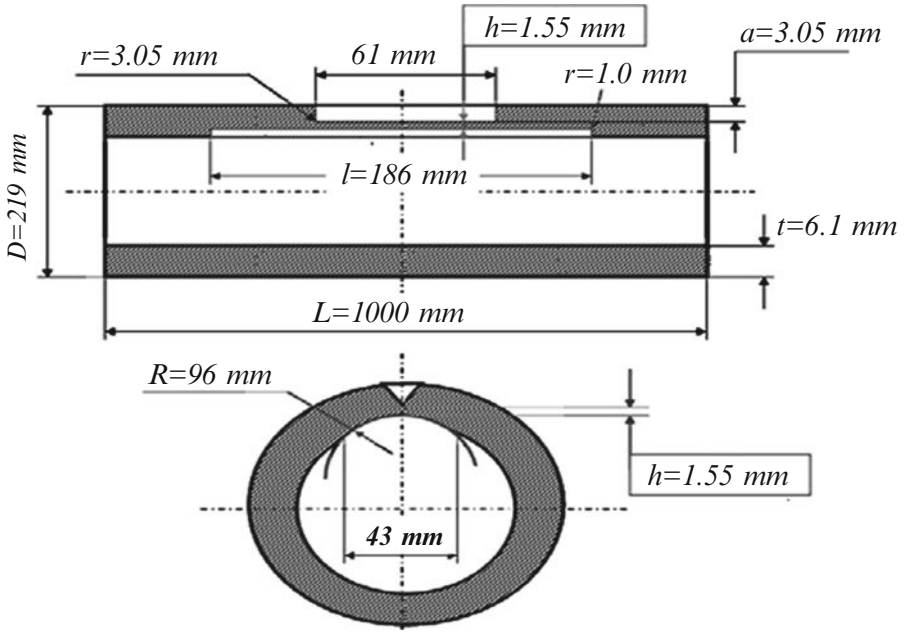


**Fig. 3** Geometry of the specimens used for burst test

**Fig. 4** Experimental device for burst test under gas pressure

Moreover, this type of burst test with gas is rare, as are papers on this subject. So it is very difficult to properly compare our results. If we consider the gross hoop stress, it appears that computation gives a maximum value that is less than the yield strength. The hoop stress acts along the circular direction of the tube, but the stress in a perpendicular direction acts in the longitudinal direction of the tube and the stresses in this direction are constrained by the great length of the tube. Consequently, a triaxiality effect is observed on the Von.Mises stress. This triaxiality effect induces an over stress to obtain the yield of the material. Here, the overstress factor is $\tau = \sigma_{VM}/\sigma_Y = 760$ MPa/528 MPa $= 1.44$. The .maximum stress value is about 760 MPa for an internal .pressure of 12 MPa (Fig. 5).

Predicted burst pressure was determined according to codes ASME-B31G and DVNRP-F101 and results are reported in Table 1. According to the experimental results, it seems that the ASME B31G code is the closest to experimental values. The DNVRP-F101 is the most conservative code.

**Fig. 5** Fracture of pipe specimen after burst test

**Table 1** Predicted burst pressures from codes

| | $P_L$ (MPa) | Error with experimental results (%) |
|---|---|---|
| ASME B31 G | 11.3 | 5.8 |
| Modified ASME B31 G | 10.8 | 10 |
| DNV RP-F101 | 6.6 | 45 |

## 3 Modified SINTAP Procedure for Fracture Emanating from Notches

The structural integrity of corroded pipes can assess using failure assessment diagramme. Classical failure assessment diagramme are established for crack-like defects and are not directly applicable to corrosion defect. However a notch-adapted procedure based on notch Fracture Mechanics and particularly Volumetric method can be used.

### *3.1 Volumetric Method*

The Volumetric method [4] is a local fracture criterion, which assumed that the fracture process requires a certain volume. This volume is assumed as a cylindrical volume with effective distance as its diameter. Physical meaning of this fracture process volume is "the high stressed region" where the necessary fracture energy release rate is stored. The difficulty is to find the limit of this "high stressed region". This limit is a priori not a material constant but depends on loading mode, structure geometry and load level. The size of the fracture process reduced to the effective distance according to the above mentioned assumptions is obtained by examination of the stress distribution.

The bi-logarithmic elastic–plastic stress distribution (Fig. 6) along the ligament exhibits three distinct zones which can be easily distinguished. The

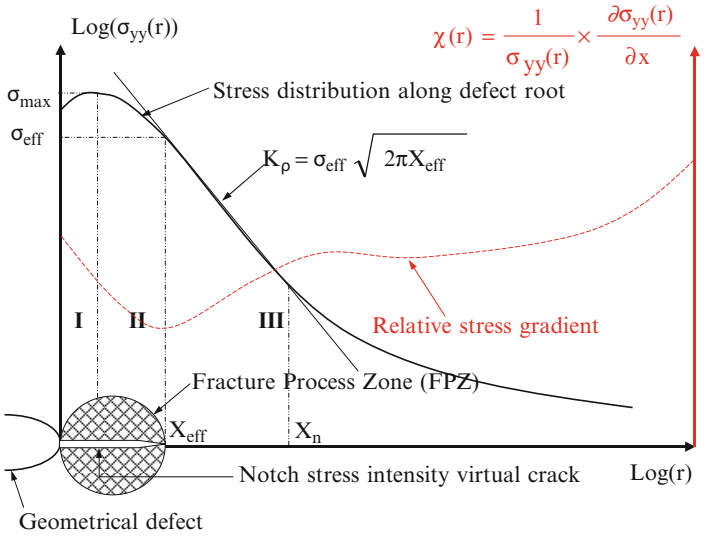


**Fig. 6** Schematic elastic–plastic stress distribution along notch ligament and notch stress intensity virtual crack concept

elastic–plastic stress primarily increases and it attains a peak value (zone I) then it gradually drops to the elastic plastic regime (zone II). Zone III represents linear behaviour in the bi-logarithmic diagram. It has been proof by examination of fracture initiation sites that the effective distance corresponds to the beginning of zone III which is in fact an inflexion point on this bi logarithmic stress distribution. A graphical method based on the relative stress gradient $\chi$ associates the effective distance to the minimum of $\chi$. The relative stress gradient is given by:

$$\chi(r) = \frac{1}{\sigma_{yy}(r)} \frac{\partial \sigma_{yy}(r)}{\partial r} \tag{7}$$

Where $\chi(\mathrm{r})$ and $\sigma_{\mathrm{yy}}(\mathrm{r})$ are the relative stress gradient and maximum principal stress or crack opening stress, respectively.

The effective stress for fracture is then considered as the average volume of the stress distribution over the effective distance. However stresses are multiply by a weight function in order to take into account stress gradient due to geometry and loading mode. The stress distribution is given by:

$$\sigma_{\mathrm{eff}} = \frac{1}{\mathrm{X_{eff}}} \cdot \int_0^{\mathrm{X_{eff}}} \sigma_{\mathrm{yy}}(\mathrm{r}) \cdot (1 - \mathrm{r} \cdot \chi(\mathrm{r}))\ \mathrm{dr} \tag{8}$$

Therefore, the notch stress intensity factor is defined as a function of effective distance and effective stress:

$$\mathrm{K}_{\rho} = \sigma_{\mathrm{eff}} \sqrt{2\pi \cdot \mathrm{X_{eff}}} \tag{9}$$

Where $\mathrm{K}_{\rho}$, $\sigma_{\mathrm{eff}}$ and $\mathrm{X_{eff}}$ are notch stress intensity factor, effective stress and effective distance, respectively. Description of this kind of stress distribution at notch tip and the procedure with the help of the relative stress gradient is given in Fig. 6.

## 3.2 Notch Adapted Failure Assessment Diagramme (NFAD)

An example of Notch Adapted Failure Assessment Diagramme is given by Matvienko [5]. The parameter $\mathrm{k_r}$ is defined as the ratio of the applied notch stress intensity factor and fracture toughness $\mathrm{K_{IC}}$.

$$\mathrm{k_r} = \frac{\mathrm{K}_{\rho}}{\mathrm{K_{IC}}} = \frac{\sqrt{1 - \left(\frac{\sigma_{\mathrm{g}}}{\sigma_{\mathrm{coh}}}\right)^2}}{\sqrt{1 - \left(\frac{\sigma_{\mathrm{g}}}{\sigma_{\mathrm{coh}}}\right)^2 \cdot \frac{1}{\mathrm{k_t^2}}}} \tag{10}$$

The failure assessment curve is taken from the cohesive zone model and the criterion of average stress in the cohesive zone head of the notch tip as indicates in [5]. However the critical stress intensity factor is shown as to be a decreasing function of the elastic stress concentration factor and consequently failure assessment curve is notch radius dependant. In order to get a NFAD interpolation curve independent of the notch radius, the parameter $k_r$ is defined as follows:

$$k_r = \frac{K_{\rho,app}}{K_{\rho,c}(\rho)} \tag{11}$$

Where the fracture toughness $K_{\rho,c}$ is a function of notch radius. $L_r$ parameter keeps the same definition. By assumption, the interpolation curve is independent of notch radius and is the same that the crack's one. Consequently, the SINTAP interpolation curves [6] were used in the NFAD.

### 3.3 *Failure Assessment Curve*

Two SINTAP levels are used (Level 0 and Level 1). Characteristics of these two levels are given in Table 2. The mathematical expression of the interpolation curve f(Lr) are given in formulae (22) and (23).

**Level 0**

$$f(L_r) = \left[1 + \frac{L_r^2}{}\right]^{\frac{-1}{2}} \left[0.3 + 0.7e^{\left(-0.6L_r^6\right)}\right] \tag{12}$$

for:

$$0 \le L_r \le 1$$

where:

$$L_r^{max} = 1 + \left(\frac{150}{\sigma_Y}\right)^{2.5}$$

**Table 2** SINTAP levels 0 and 1 description

| Level | Data needed | When to use |
|---|---|---|
| Default level | | |
| Level 0 | Yield or proof strength | When no other tensile data available |
| Standard level | | |
| 1. Basic | Yield or proof strength: ultimate tensile strength | For quickest result. Mismatch in properties less than 10% |

**Level 1**

$$f(L_r) = \begin{cases} \left[1 + \frac{L_r^2}{2}\right]^{\frac{-1}{2}} \left[0/3 + 0.7e^{\left(-\mu L_r^6\right)}\right], 0 \le L_r \le L_r^{max} \\ \left[1 + \frac{1}{2}\right]^{\frac{-1}{2}} \left[0/3 + 0.7e^{(-\mu)}\right] \cdot L_r^{\frac{N-1}{2N}}, 1 \le L_r \le L_r^{max} \end{cases} \quad (13)$$

where:

$$\mu = \min\left[0.001\frac{E}{\sigma_Y}, 0.6\right], L_r^{max} = \frac{1}{2}\left(\frac{\sigma_Y + \sigma_U}{\sigma_U}\right) \text{ and } N = 0.3\left(1 - \frac{\sigma_Y}{\sigma_U}\right)$$

## *3.4 Safety Factor Obtained from Different Defect Geometry*

In the failure assessment diagramme, service conditions of a structure exhibiting a corrosion defect is represented by the assessment point A of coordinates [$l^*_r$, $k^*_r$] in the NFAD plane ($l_r$, $k_r$). Due to the definition, $l_r$ and $k_r$ parameters are proportional to pressure and the loading path is linear passing through A and intercepting the failure assessment curve at point C. The safety factor is then defined as:

$$f_s = OC/OA \quad (14)$$

Safety factor on corrosion defect have been determined for pressure service conditions of 70 bars for a gas pipe made in X52 steel (yield stress 410 MPa). Three kinds of surface defects are examined semi spherical, semi elliptical and long semi elliptical defects (Fig. 7).

In Figs. 8a, b and c, the geometrical configuration of these defects is presented. The defect depth for all models is equal to one-half of pipe wall thickness and the defect length over defect depth ratio is considered as 10 (L/d = 10).

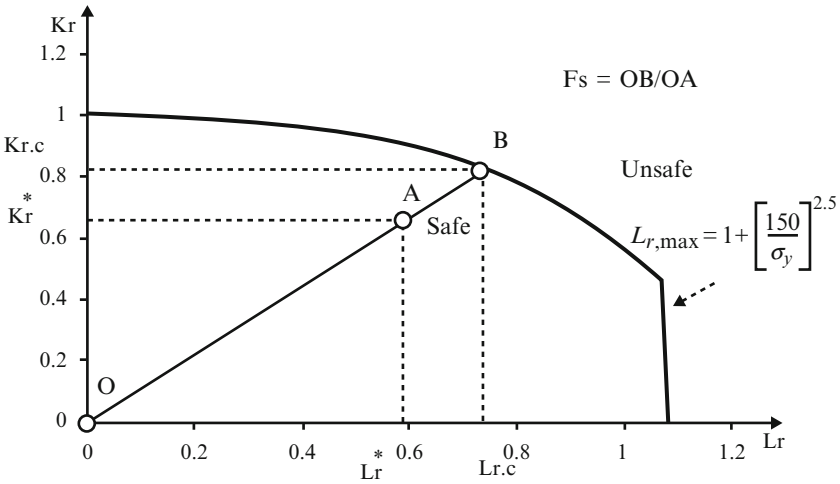


**Fig. 7** Failure assessment diagramme and definition of safety factor Fs

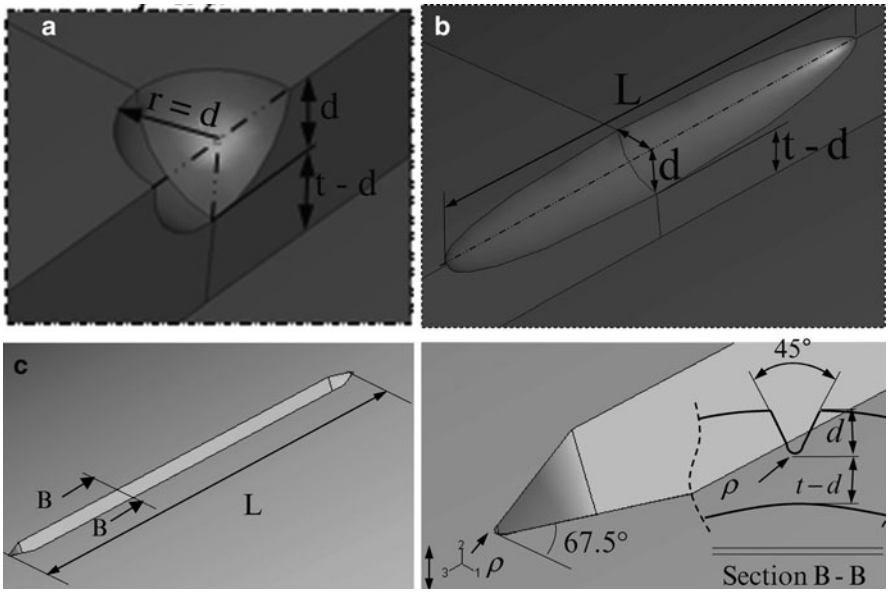


**Fig. 8** (**a**) Central semi-spherical defect (t = 6.1 mm, d = t/2), (**b**) Central semi-elliptical defect (t = 6.1 mm, d = t/2, d/L = 0.1), (**c**) Central longitudinal semi-elliptical defect (t = 6.1 mm, d = t/2, d/L = 0.1, $\rho$ = 0.15 mm)

**Table 3** Effective stress, effective distance and notch intensity factors along radial and longitudinal direction using 70 bars as applied internal pressure

| Defect type | Effective distance (mm) | Effective stress (MPa) | $K_\rho$ (MPa.m$^{0.5}$) |
|---|---|---|---|
| *Radial direction* | | | |
| Semi-spherical | 0.42 | 202.7 | 10.4 |
| Semi-elliptical | 0.67 | 343.4 | 22.3 |
| Long | 0.38 | 539.6 | 26.3 |
| *Longitudinal direction* | | | |
| Semi-spherical | 0.72 | 184.4 | 12.4 |
| Semi-elliptical | 0.53 | 252.1 | 14.5 |
| Long Blunt notch | 0.63 | 311.4 | 19.7 |

The obtained notch stress intensity factors and applied internal pressure are utilized to define the required assessment points which are used in the failure assessment prediction (Table 3).

The safety factor has been determined on the Failure Assessment diagram according to the procedure described in Fig. 6. In Table 4, different safety factors according to the SINTAP procedure are presented.

We note that all values of the safety factor are above the conventional value of 2 and consequently all the defect sizes are acceptable.

**Table 4** Safety factors according to the SINTAP procedure

| Type | SINTAP 0B | SINTAP 1B |
|---|---|---|
| Semi-spherical | 4.095 | 4.106 |
| Semi-elliptical | 3.407 | 3.750 |
| Blunt notch | 3.186 | 3.583 |

**Table 5** Calculated safety factors using mentioned coded and other methods

| Type | SINTAP 0B | SINTAP 1B | ASME B31G |
|---|---|---|---|
| Semi-spherical | 4.0 | 4.1 | 3.5 |
| Semi-elliptical | 3.4 | 3.7 | 3.4 |
| Blunt notch | 3.1 | 3.5 | N/A |
| Type | mASME B31G | DNV RP F-101 | Choi et al. |
| Semi-spherical | 4.0 | 4.2 | 3.3 |
| Semi-elliptical | 3.9 | 4.2 | 2.8 |
| Blunt notch | N/A | N/A | N/A |

The failure pressure is extracted by means of the maximum failure pressure according to the above-mentioned codes (ASME B31G, Modified ASME B31G, DNV RP-101 and Choi's method). The safety factor is determined by means of the applied pressure $P_{app}$ over failure pressure $P_f$ as:

$$F_s = \frac{P_{app}}{P_f} \tag{15}$$

In Table 5, different safety factors according to the SINTAP procedure and limit load analysis methods are computed using implemented MATLAB code.

As expected earlier, the SINTAP 0B is more conservative than SINTAP 1B. Nevertheless, ASME B31G, modified ASME B31G, DNV RP F-101 and Choi's method do not offer any structural integrity formulae for blunt notch defects and DNV RP F-101 does not exhibit any variation in safety factor for the chosen semi-spherical and semi-elliptical defects. The comparison of computed safety factors emphasizes that DNV RP F-101 and Choi's method provide the upper bound and lower bound margins.

## *3.5 Probabilistic Safety Factor*

On the probabilistic point of view, the Failure Assessment Diagramme can divide into zone of ISO failure probabilities. The material failure curve is a particular case for which the failure probability is equal to 1 because failure is then a certainty. Any assessment point of coordinates $[L_r^* - k_r^*]$ is situated on an equi probability curve $P_r^*$. The following conventional failure probability are often used $Pr = 10^{-4}$

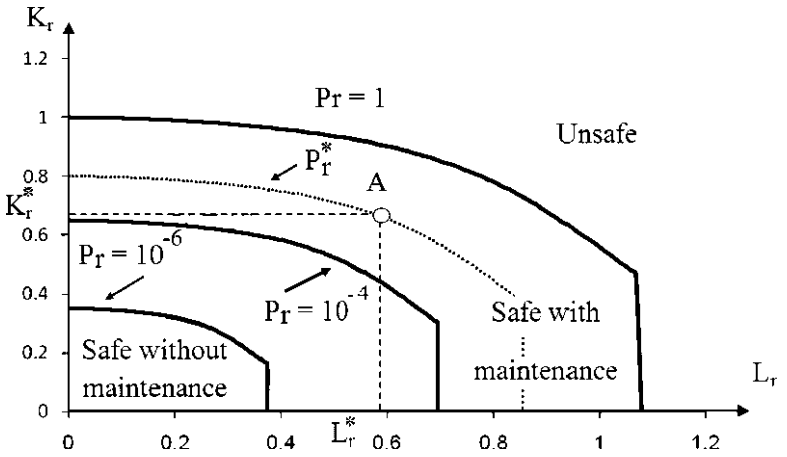


**Fig. 9** Probabilistic Notch Failure Assessment Diagramme (PNFAD) with definitions of material failure curve, assessment point, save and unsafe zones and safety factor

if there is no human life risk and Pr $= 10^{-6}$; if there is. These conventional iso failure probabilities divided the Failure Assessment Diagramme into three zones: the unsafe zone with $P_r = 1$; the safe zone with maintenance $P^*_r > 10^{-4}$ or $10^{-6}$ and the safe zone without maintenance $P^*_r < 10^{-4}$ or $10.^{-6}$ This type of failure assessment diagramme is called probabilistic N FAD (Fig. 9).

The pipes located in a water network which consists of a pump, a reservoir and 5 pipe sections are submitted to a stochastic water hammer. Fracture toughness, yield stress and corrosion depth are assumed to be randomly distributed to allow determination of safety factor by Monte-Carlo and Form/Sorm methods.

Within the chosen procedure, the following parameters are treated as random parameters and introduce into the Notch Failure Assessment Diagramme:

- notch fracture toughness $K_{\rho,c}$,
- yield strength Re,
- ultimate tensile strength $\sigma_{ult}$,
- defect depth a,
- maximum pressure $p_{max}$.

These random parameters are treated as not being correlated with one another. Fracture toughness is assumed as Weibull's distribution. Yield strength ultimate, tensile strength and internal pressure can be mainly assumed as following a normal distribution. For defect, depth (a) is assumed to follow an exponential distribution.

The exponential distribution generally governs for defect size analysis. Consequently, the probability density function has the following form:

$$F(X) = \lambda \exp(-\lambda a) \tag{16}$$

where $\lambda$ is the exponential distribution parameter.

**Table 6** Mechanical properties of pipe steel and used distribution

| Mechanical properties | Yield strength Re | Ultimate strength | circumferential stress | Fracture toughness | Defect |
|---|---|---|---|---|---|
| Mean | 410 MPa | 528 MPa | 41.8 MPa | 116 MPa.m$^{0.5}$ | 2 mm |
| CV | 0.1 | 0.1 | 0.4 | 0.1 | |
| σ | 41 MPa | 52.8 MPa | 18.44 MPa | 11.6 MPa.m$^{0.5}$ | |
| Distribution | Normal | Normal | Normal | Weibull | Exponential |

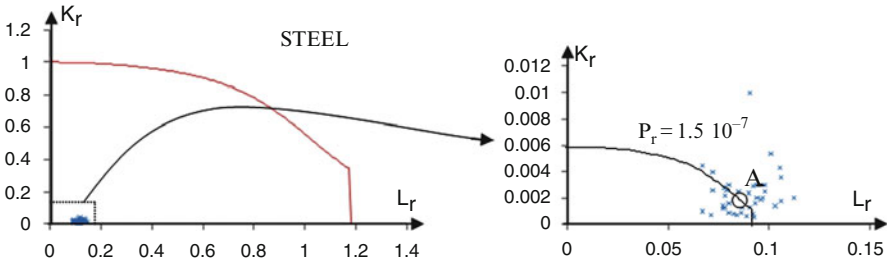


**Fig. 10** Example of probabilistic Notch Failure assessment diagramme for steel

The mechanical properties of the studied steel materials are presented in Table 6.

We have chosen the lower bound for variation coefficient CV = 0.1. Using Monte Carlo method, several assessment points (40–50) were generated using the characteristic parameters of the distribution. The obtained NFAD are presented in Fig. 10.

The NFAD can be presented into polar coordinates (r, θ). Two particulars value are noted in this polar diagramme $\theta_1$ and $\theta_2$. The first polar angle $\theta_1$ corresponds to the angle of the intercept of the failure curve at abscissa $L_r = 0.62$. This corresponds to a conventional value of gross failure stress of 62% of the yield stress. The second polar angle $\theta_2$ corresponds to the intercept of the vertical line of $L_{r,max}$ abscissa. These two angles determine three domains in the NFAD diagramme (Fig. 11).

If $\theta < \theta_1$ brittle fracture.
If $\theta_1 < \theta < \theta_2$ elasto plastic fracture.
If $\theta > \theta_2$ plastic collapse.

These three different failure zones are presented in Fig. 8. For any assessment point A we can define the safety factor according to Eq. 23.

$$f_s = \frac{OA}{OB} \tag{17}$$

However, and mainly for steel and cast iron, the assessment points lay in the plastic collapse zone. Another way to define safety, is to consider that we have plastic collapse only for $\theta = 0$. In this case the safety factor is defined as:

$$f_s^* = \frac{OA^*}{OB^*} \tag{18}$$

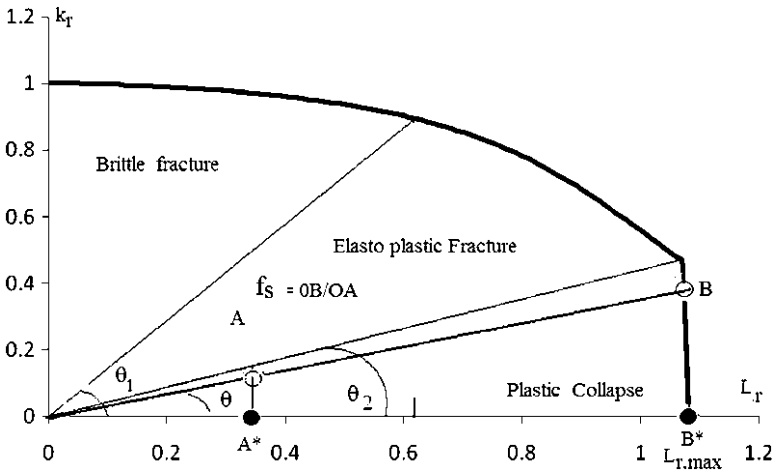


**Fig. 11** Definition of zones of brittle fracture, elasto plastic failure and plastic collapse in NFAD and definition of theta angle

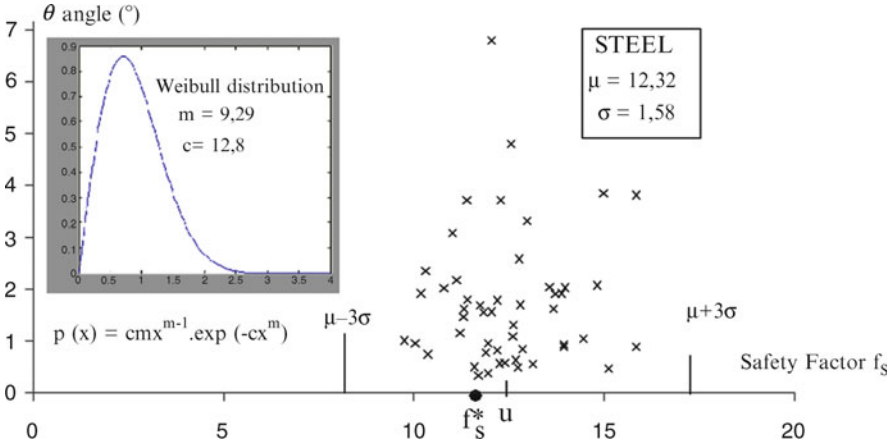


**Fig. 12** Distribution of the safety factor with q angle for pipe steel

Values of $\theta_1$ and $\theta_2$ are respectively $\theta_1 = 55$ and $\theta_2 = 22$. Muhammed and al. [7] have shown that the general trend that emerges is that on average the margin of safety on the FAD is minimum in the middle (elastic–plastic) region, slightly higher in the 'plastic collapse' region and maximum in the 'brittle fracture' region. However, this overall trend is complicated by varying degree of scatter in the different regions. For this reason, we have examined the evolution of the safety factor with θ angle. It has been shown that the θ angle is in range [0–7°] for steel, [0–15°] for cast iron and [0–4°] for polyethylene. All data are in a narrow scatter band of range [μ − 3σ; μ + 3σ] and in the region of plastic collapse. For this reason the safety factor $f^*_s$ computed from the ultimate pressure done by code

**Table 7** Mean values and standard deviation for the safety factor of the material

| Material | Steel |
|---|---|
| Mean μ | 12.32 |
| $f^*_s$ | 11.63 |
| Standard deviation σ | 1.26 |
| Variational coefficient CV | 0.12 |

ASME B31G is also reported (Fig. 12). Mean values and standard deviation for the safety factor of the three material are reported in Table 7.

The safety factor computed for fully plastic collapse is less than the mean value of $f_s$.

The safety factor distribution is represented with a Weibull distribution. Kolmogorov-Smirnov test results indicate that the Weibull distribution is significant at 57%.

## 4 Conclusions

The structural integrity of corroded pipelines subjected to internal pressure is studied in this paper. The semi-spherical, semi-elliptical and blunt notch defects are examined under this loading and safety factors are evaluated by means of the SINTAP procedure which is modified using a Notch-based Failure Assessment Diagram or so called "NFAD". The ASME B31G, Modified ASME B31G, DNV RP F-101 and Choi's method have been also utilized.

The values of deterministic safety factor are codified in codes such as EUROCODE 3[8] However, the actual trend is to adopt partial safety factor according to the degree of uncertainties of the material properties in order to avoid over conservatism. The design material properties are then defined as some percentile of the material resistance distribution (The mean values is generally used for metals and alloy but for wood, the admissible stress is defined as the fifth percentile of the distribution). The use of probabilistic Notch Failure Assessment Diagramme allows getting global safety factor without introducing a series of partial safety factors on material properties, defect size and applied loading. In addition, the probabilistic safety factor is associated to a failure probability. Then, with a conventional allowed failure probability, it is possible to have a maintenance policy and to compute the economic cost of the risk of structure failure. Under stochastic service pressure, the safety factor is distributed randomly according to Weibull distribution. It has been seen that the Weibull modulus of the distribution is about ten and the confidence interval of the safety factor has a satisfactory value.

## References

1. American National Standard Institute (ANSI)/American Society of Mechanical Engineers (ASME), Manual for determining strength of corroded pipelines, ASME B31G, 1984
2. DNV RP-F101: Corroded pipelines, Det Norske Veritas, 1999

3. J.B. Choi, B.K. Goo, J.C. Kim, Y.J. Kim, W.S. Kim, Development of limit load solutions for corroded gas pipelines. Int. J. Press. Vessel Piping **80**(2), 121–128 (2003)
4. G. Pluvinage, *Fracture and Fatigue emanating from stress concentrators* (Kluwer, Rueil-Malmaison, 2003)
5. Yu Matvienko, Local fracture criterion to describe failure assessment diagrams for a body with crack/notch. Int. J. Fract. **124**, 107–112 (2003)
6. SINTAP, Structural integrity assessment procedure, final report EU project BE95-1462 (Brite Euram Programme, Brussels, 1999)
7. A. Muhammed, H.G. Pisarski, R.M. Sanderson, Calibration of probability of failure estimates made from probabilistic fracture mechanics analysis, Offshore technology report, 2000/021, TWI Ltd, 2000
8. Eurocode 3, Design of steel structures. General rules and rules for buildings, Division 1, Class 1, 2005

# A Damage Evolution Approach in Fracture Mechanics of Pipelines

**Yu.G. Matvienko**

**Abstract** The paper concentrates on perspectives of the damage evolution approach in fracture mechanics of oil and gas pipelines. This approach is based on the generalised concept of damage. It is postulated that deformation and fracture processes in solids are determined by some general functional law related to the accumulation of damage. Fracture mechanics parameters are accepted as the controlling parameters for the failure processes. The approach leads to a description of fatigue crack growth, stress corrosion cracking, a correlation between hydrogen redistribution in the vicinity of a crack tip and the stress intensity factor during crack propagation under cyclic loads. The damage evolution approach has been also employed to quantify the shift of the ductile-to-brittle transition temperature of gas pipelines due to physical-mechanical damage of the steel during long-term operation of pipelines. The ductile–brittle transition curve of the steel pipeline shifts to higher temperature which decreases operation margins in both the temperature and pressure. The methodology of the above-mentioned approach and the failure assessment diagram has been employed for the structural integrity analysis including assessment of the ductile-to-brittle transition temperature and allowable sizes of surface longitudinal crack-like defects in gas pipelines.

## Nomenclature

| | |
|---|---|
| a | crack size |
| A | constant in the damage evolution law |
| $C_H$ | hydrogen concentration |
| E | Young's modulus |
| J | *J*-integral |

Yu.G. Matvienko (✉)
Mechanical Engineering Research Institute of the Russian Academy of Sciences,
4 M. Kharitonievsky Per., 101990 Moscow, Russia
e-mail: matvienko7@yahoo.com

T. Boukharouba et al. (eds.), *Integrity of Pipelines Transporting Hydrocarbons*,
NATO Science for Peace and Security Series C: Environmental Security,
DOI 10.1007/978-94-007-0588-3_15, 

| | |
|---|---|
| K | stress intensity factor |
| $K_{mat}$ | fracture toughness |
| m | strain hardening exponent |
| n | power exponent in the damage evolution law |
| N | number of fatigue loading cycles |
| $N^*$, $\tau^*$ | fixed (or a unit) number of cycles and time, respectively |
| $SF_K$ | safety factor against fracture |
| $T_0$ | ductile-to-brittle transition temperature |
| $V^*$,$V_0$ | coefficients in the Paris and the corrosion crack growth laws, respectively |
| $\Delta a_j$ | crack increment length |
| $\sigma$ | nominal applied stress |
| $\sigma_Y$ | yield strength |
| $\sigma_0$ | local strength |
| $\beta$ | local biaxiality ratio |
| $\tau$ | time |
| $\xi$ | controlling parameter |
| $\Psi$ | continuum parameter |

## Subscripts

| | |
|---|---|
| i | initiation |
| max | maximum |
| scc | stress corrosion cracking |

# 1 Introduction

It is well-known that failure of gas and oil pipelines can be associated with initiation or crack propagation as a result of various physical-mechanical damage processes of the steel, namely, corrosion, fatigue, hydrogen embrittlement, the ductile-to-brittle transition temperature shift during long-term operation of pipelines. It should be noted that the risk of fracture increases at low climatic temperatures, degradation and strain aging of steel which cause in plasticity drop (Fig. 1). There are different concepts for describing crack initiation and propagation in the case of various mechanisms of pipeline failure including a damage evolution approach.

A concept of damage evolution in solids has been suggested by Kachanov [1] and Rabotnov [2] for the analysis of damage under creep loading. It was essentially a mathematical treatment to quantify damage and as such had no physical interpretation. When both mechanisms and processes of failure events became better

**Fig. 1** Fracture of the gas-main pipeline in Yakutia at low climatic temperature

understood, the damage evolution approach was itself seen to be insufficient – particularly when the mechanisms and the processes of failure changed during the lifetime. For this case, the damage evolution approach needs to be accompanied by fundamental principles and laws of thermodynamic, mechanics and physics of solids, materials science.

The concept of damage evolution has been used in different later versions (e.g. [3–5]) for the analysis of various processes of damage accumulation. The accumulation of damage can be associated with a change of continuity $\psi$. The continuum parameter $\psi$ (or damage parameter $D = 1 - \psi$) has not a physical interpretation. A change of the parameter $\psi$ means the appearance and growth of cracks and/or voids, and a change in the mechanical and physical properties of a solid. Consequently, the value of $\psi$ reflects damage evolution (the state) of solids under an external influence. The description of the evolution phenomena in various branches of knowledge can be based on an interdisciplinary or a synergetic branch of science. A typical non-linear evolution equation of the state of autonomous systems can be expressed in the form [6].

$$q = F[\ \xi, q(\tau)] \tag{1}$$

For practical applications of the evolution approach it is important to choose the vector of state parameters q of the system and the controlling parameters $\zeta$. A specific form of the function given by Eq. 1 can be obtained from data of basic experiments and an analysis of the system behaviour under the influence of various external factors during time $\tau$.

This paper presents a concept of damage evolution to some problems of fracture mechanics when the mechanisms and the processes of failure do not change in the

time period being considered. Moreover, this concept has been employed to estimate the transition temperature shift of the pipeline steel and incorporated into structural integrity assessment of a gas main pipeline.

## 2 Damage Evolution in Solids

The evolution approach has been extended to deformation and fracture processes of a mechanical loaded system, i.e. "solid – damage". It is assumed that the accumulation of damage (the system state) is determined by the scalar $0 \leqslant \psi \leqslant 1$ which is the single state variable $q = \psi$. The controlling parameters $\xi$ for deformation and failure processes of solids could be stress and strain, the stress intensity factor, temperature and other parameters, which are essential in the consideration of the damage accumulation process.

It is postulated that deformation and fracture processes are governed by some general functional law of damage accumulation [7]. For a simple case the damage evolution law can be formulated as:

$$\frac{d\psi}{d\tau} = -A\left(\frac{\zeta}{\psi}\right)^n \tag{2}$$

Where $A>0$ and $n \geq 0$are material (the "solid – damage" system) constants for the fracture process under study. The evolution law (2) can be made more precise when the physical and mechanical aspects of a failure process are more clearly understood by examining the fracture mechanisms of the solid and the type of loading under study. The value of $\psi$ decreases with an increase in time $\tau$ during the process of the accumulation of damage in a solid. The value $\psi = 1$ corresponds to the non-damaged state of a solid when $\tau = 0$, and the value $\psi = \psi_c$ corresponds to the critical state when $\tau = \tau_c$, where $\tau_c$ is the critical time. So, failure occurs in a solid if the damage reaches the critical value $\psi = \psi_c$ at $\tau = \tau_c$. The following relationship can be written as follows by integrating Eq. 2 from $\psi = 1$ to $\psi = \psi_c$:

$$\psi_c^{1+n} = 1 - A(1+n)\int_0^{\tau_c} \zeta^n d\tau \tag{3}$$

Equation 3 is transformed into the following equation for the determination of the critical time $\tau_c$:

$$\tau_c = \frac{1 - \Psi_c^{1+n}}{A(1+n)\xi^n} \tag{4}$$

if the controlling parameter $\xi$ is constant.

Taking into account Eqs. 2 and 4, the cumulative damage law is expressed in the integral form:

$$\int_0^{\tau_c} \frac{d\tau}{\tau_c} = 1 \tag{5}$$

The cumulative damage law given by Eq. 5 may be rewritten using number of cycles N or other similar parameters, which are dependent on time of loading, instead of time. This conclusion follows from the following argument, for example, considering the application of a number of cycles. The left hand-side of Eq. 2 may be represented by the expression $d\Psi/d\tau = (d\Psi/dN) \cdot (dN/d\tau)$. The form of the damage evolution law, Eq. 2, will be conserved if the constant $A$ contains the value $dN/d\tau = \text{const}$. As a result, the cumulative damage law can be given as:

$$\int_0^{N_c} \frac{dN}{N_c} = 1 \tag{6}$$

Where: $N_c$ is the critical number of cycles.

The influence of the controlling parameter $\xi$ on the critical time may now be analysed for damage evolution in solids. First of all, it is assumed that the critical value $\Psi_c$ is constant for the deformation and failure process under study, and the critical state of a damaged solid can be reached for various combinations of the controlling parameter and time $\tau$. Therefore, it has been suggested that the critical value $\Psi_c$ (Eq. 3) is also reached when the controlling parameter $\xi$ is equal to the critical value $\xi_c$ at some fixed time (or a unit of time) $\tau = \tau^* < \tau_c$, that is

$$\Psi_c^{1+n} = 1 - A(1+n)\ \xi_c^n \tau^* \tag{7}$$

The evolution equation at $\Psi_c = const$ is derived from Eqs. 3 and 7 namely:

$$\int_0^{\tau_c} \xi^n d\tau = \xi_c^n \tau^* \tag{8}$$

This equation may be rewritten at $\xi = \text{const}$ as:

$$\tau_c = \tau^* \left(\frac{\xi_c}{\xi}\right)^n \tag{9}$$

The damage evolution equation allows estimating the critical time for a solid to reach its critical state under the given controlling parameter for deformation and fracture processes being studied. A monotonic increase of the critical time $\tau_c$ is

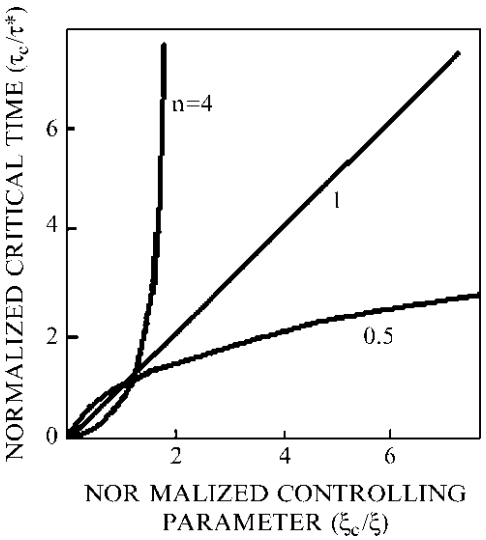


**Fig. 2** The influence of the controlling parameter on the critical time to cause failure

observed for an increase of the critical controlling parameter (at $\xi = \text{const}$) or for a decrease of the controlling parameter (at $\xi_c = \text{const}$) (Fig. 2). The relationship $\tau_c/\tau^*$ is more rapidly increased with larger a value of index $n$ in the damage evolution law. Examples of the application of the damage evolution equation will be now discussed for various processes of deformation and failure.

## 3 Application of the Damage Evolution Approach for the Crack Growth Analysis

### *3.1 Fatigue Crack Propagation*

Fatigue crack growth may be described by an equation of the type of Eq. 2. In this case, the stress intensity factor $K$ can be used as the controlling parameter to describe fatigue failure when linear fracture mechanics is valid. Furthermore, it is assumed that the mechanism and the process of fatigue failure remain uninterrupted. Therefore, the maximum (or the range) of the stress intensity factor $K_{max}$ is chosen as the controlling parameter $\xi$ for fatigue crack growth.

Taking into account the functional relation of the value $\Psi$ and the fatigue crack size a and replacing $\tau$ with the number of fatigue loading cycles $N$, Eq. 2 can be expressed as:

$$\left(\frac{d\Psi}{da}\right)\frac{da}{dN} = -A\left(\frac{K_{max}}{\Psi}\right)^n \tag{10}$$

Where the value $A$ includes the parameter $dN/d\tau$,

It has been suggested that a crack increment ( $\Delta a_j = a_j - a_{j-1}$) occurs when damage accumulation reaches a critical value in the vicinity of the fatigue crack tip, that is $\Psi = \Psi_c$. Dividing variables in Eq. 10 and taking into account the boundary conditions, the following equation is deduced:

$$\Psi_c^{1+n} = 1 - A(1+n)\int_{a_j-1}^{a_j}\left(\frac{K_{max}^n}{da/dN}\right)da \tag{11}$$

It is understood that the fatigue crack growth rate $da/dN$ is some average value of the rate during crack incremental growth. Therefore the crack growth rate, as well as the maximum stress intensity factor, can be accepted as constant values in the limits of integration from $a_{j-1}$ to $a_j$. From Eq. 11 the useful relation is obtained:

$$\Psi_c^{1+n} = 1 - A(1+n)\frac{K_{max}^n \Delta a_j}{da/dN} \tag{12}$$

The critical value $\Psi_c$ can also be reached after the application of the number of cycles $N^*$ under the controlling parameter $\xi = \xi_c$. From Eqs. 12 and 7 at $\tau^* \to N^*$ the equation for the fatigue crack growth rate can be given as:

$$\frac{da}{dN} = V^*\left(\frac{K_{max}}{\xi_c}\right)^n,\ V^* = \Delta a_j/N^*. \tag{13}$$

Considering the value:

$$C = \frac{V^*}{\xi_c^n} \tag{14}$$

The well-know empirical Paris type law $da/dN = CK_{max}^n$ follows.

It can be seen that the parameters $\xi_c$ and $V^*$ are interdependent for a given interpretation [Eqs. 13 and 14], namely, various rates $V^*$ correspond to various critical parameters $\xi_c$ for the fatigue crack growth diagram ($C = const$). Using Eq. 13, there is a possibility of physically modelling the fatigue crack growth processes when various crack growth mechanisms have been realised. Such parameters as $\Delta a_j, N^*$ and $\xi_c$ will have a defined physical meaning. From this point of view the middle section of the fatigue crack growth diagram can be analysed. Here, the failure mechanisms are identified on the basis of the microrelief of the fracture surface. Fatigue crack growth can be accompanied by striation formation on the fatigue fracture surface [8, 9]. If the striation spacing coincides with the substructural grain size arising in the plastic zone ahead of the crack tip, the value $V^*$ is approximate equal to $10^{-7}$m/cycle. The critical parameter $\xi_c$ corresponds to the stress intensity factor, i.e. $\xi_c = K^* = K_{max}$, and the crack increment length $\Delta a_j$ is equal to the striation spacing and $N^* = 1$. The stress intensity factor

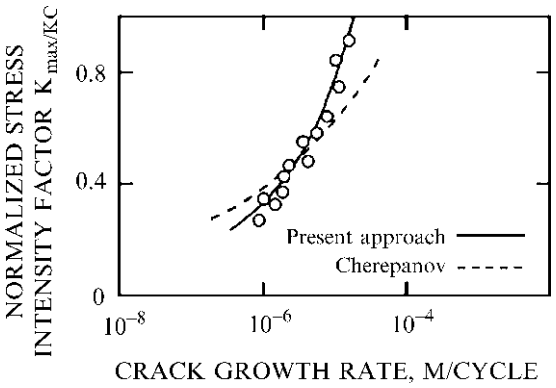


**Fig. 3** Fatigue crack propagation rates for 300 steel: The experimental results are denoted by dots

$K^*$ is calculated using Young's modulus, the Burgers vector, and the size of the plastic zone ahead of the fatigue crack tip and the grain size of the metal [8].

A theoretical approximation (see Eq. 13) of fatigue crack growth describes experimental results [10] very well (Fig. 3). Prediction of crack behaviour in a 300 steel was carried out at: $n = 2.5$, $\xi_c = K_{mat}$, $V^* = 4.38 \cdot 10^{-6}$ m/cycle. As a special case for $n = 4$, $\xi_c = K_{mat}$, $V^* = \alpha/2$ and $K_{min} = 0$ the unified crack growth expression given by Eq. 13 can be transformed into the equation given by Cherepanov [10]. Here the parameter $\alpha$ (according to Cherepanov) characterises the increase in fatigue crack length.

Apparently, the evolution approach will be useful for fractographic analysis of fatigue crack propagation, because the crack growth equation includes the parameter $\Delta a_j$, which characterises the crack growth by discrete jumps.

## *3.2 Fatigue Life of Notched Components*

There are two basic scientific approaches to analyse fatigue life of notched specimens. Firstly, if the fatigue initiation phase is considered to be negligible, crack growth is quantified in terms of microstructural fracture mechanics [11, 12]. In this case the period of time for the macrocrack initiation phase is equated to the period of time for the microcrack propagation phase. Secondly, an approximate analysis of fatigue macrocrack initiation life can be based on a phenomenological consideration of deformation and the failure process ahead of the notch tip without reference to a microstructural crack propagation theory [13–15]. The fatigue crack initiation life is defined as the number of cycles to initiate a main macrocrack. For example, experimental values of the crack initiation life, defined as a crack length of 50 μm on the specimen surface, were well fitted for the two alloys, AC8A-T6 and AC4C-T6, by the value $K_{max}$, which is dependent on the kind and sizes of initial defect and applied stress amplitude [16].

In present section fatigue of notched specimens and macrocrack initiation at notches has been discussed from the point of view of the damage evolution approach presented in terms of continuum non-linear fracture mechanics parameter, namely, the counter J-integral. It should be noted that, strictly, the concept of the J-integral loses theoretical ground when local unloading in the vicinity of the notch/crack tip occurs and the monotonic loading conditions assumed by deformation theory of plasticity are destroyed. However, it is expected that the non-linear solutions to J-integral give a reasonable approximation as demonstrated in the literature [17–20]. These results indicate that the crack growth rate and fatigue life can be characterised by the J-integral under general yielding conditions when the use of linear elastic fracture mechanics to model fatigue processes becomes questionable.

If it is assumed that a material ahead of the notch tip is under strain control loading, fatigue life can be calculated [7] for macrocrack initiation

$$N_i = 0.25\left(\frac{J_c}{J_{max}}\right)^k \tag{15}$$

Where $J_{max}$ is the maximum value of the J-integral for a solid with a notch and k is the power index in the fatigue crack growth equation $da/dN \sim J_{max}^k$. The critical value $J_c$ is the J-integral calculated for the nominal (applied) stress $\sigma = \sigma_u$, where $\sigma_u$ is the ultimate strength.

If conditions of plastic deformation in the vicinity of the notch tip correspond to stress control loading, the equation for the prediction of fatigue life to macrocrack initiation is given by [7]:

$$N_i = N_s^*\left(\frac{J_c}{J_{max}}\right)^{12.5m(1+m)} \tag{16}$$

Here $N_s^*$ is the number of cycles required to initiate a crack at the stress $\sigma = \sigma_u$ (that is $J = J_c$) and m is the strain hardening exponent in the relation between stress and plastic strain as given by the expression $\sigma = \sigma_* \varepsilon^m$, where $\sigma_*$ is the constant of the material.

In general case, the character of deformation in the vicinity of the stress concentration corresponds to the loading conditions, which are intermediate between strain and stress control loading. In this case the fatigue equation may be written [from Eq. 9 by setting $\tau \to N$] in a more general form choosing the J-integral as the controlling parameter:

$$N_i = N_i^*\left(\frac{J_c}{J_{max}}\right)^n \tag{17}$$

To calculate the J-integral in the case of non-linear deformation of notched solids, approximate formulae can be used [21].

Although this approach concentrates on the J-integral, the methodology is equally applicable to other parameters of fracture mechanics, for example, the stress or strain intensity factor, and the opening displacement at the notch tip.

### 3.3 Stress Corrosion Cracking

It has been suggested that the process of stress corrosion cracking (SCC) is initiated at some initial (applied) stress intensity factor $K_i$. Therefore, the value $K_i$ is chosen as the controlling parameter. Then Eq. 9 should be rewritten in the following form:

$$K_i^n \tau_c = (K_{ic})^n \ \tau^* = \text{const} \tag{18}$$

Here, $\tau_c$ is the time required to initiate the SCC process at the stress intensity factor $K_i$ and $\tau^*$ is some standard time (or a unit of time) required to initiate the SCC process at some stress intensity factor $K = K_{ic}$, and n is the constant for a given "solid – environment" system. The critical time $\tau_c$ is increased for a reduction of the initial stress intensity factor. From Eq. 18 the following conclusion can be drawn, namely, there is no physical threshold $K_{1scc}$. Apparently, the experimental value of the threshold stress intensity factor is the value $K_{1scc}$ at some defined time $\tau_{scc}$ of testing. A similar situation can be observed in fatigue for the threshold stress intensity factor$K_{th}$, defined as the value of $K_{max}$ below which the crack does not grow. The fatigue crack growth threshold is determined as the value of $K_{max}$ that corresponds to a certain fatigue crack growth rate$V_{th}$, which is conventionally assumed to be equal, for example, to $10^{-10}$ m/cycle.

Corrosion crack propagation (the kinetic diagram of SCC) can be expressed by the function [7]:

$$\frac{da}{d\,\tau} = V_0 \left(\frac{K}{K_i}\right)^n, \ K \geq K_i \tag{19}$$

Here,$V_0 = \Delta a_j/\tau_c$, where $\Delta a_j$ is the incremental length extension of a corrosion crack and K is the current stress intensity factor. Equation 19 describes the experimental results on stable crack propagation in the steel under the influence of distilled water (Fig. 4). The following important considerations need to be noted.

The SCC kinetic diagram depends on the initial stress intensity factor, namely, the fastest corrosion crack growth rates correspond to higher $K_i$ levels [22]. A clear explanation of this phenomenon is found out in a SCC model based on Eq. 19. If the value $K_i$ is increased, then the critical SCC time is reduced due to the expression $K_i^n \tau_c = \text{const}$ that leads to the increase of the value$V_0$. It is possible that the length of the crack growth increment is also increased. As a result, corrosion crack growth occurs at higher rates in terms of $da/d\tau$.

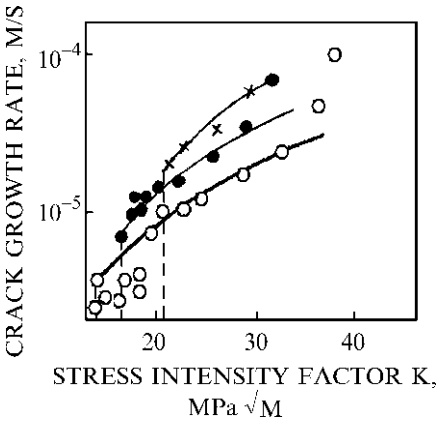


**Fig. 4** Stress corrosion cracking rates in 50X steel under the influence of distilled water: Predicted crack growth behaviour [Eq. 19] and experimental data [22]

## *3.4 Crack Tip Hydrogen Distribution Under Fatigue Loading*

Until recently only a few papers [7, 23–25] have reported on the hydrogen distribution ahead of a crack tip. Hydrogen distribution in the vicinity of the fatigue crack tip is related to the stress-strain fields surrounding the crack tip. Under monotonic mixed (I/II) mode loading there are two hydrogen accumulation peaks ahead of the crack tip, which correspond to the maximum hydrostatic stress and the maximum equivalent plastic strain, respectively.

At a low stress level and hydrogen, a negligible crack tip plastic zone is created which implies that a linear elastic fracture mechanics methodology can be used to quantify fatigue crack growth behaviour. It follows that the maximum stress intensity factor must have an influence on fatigue damage evolution and the hydrogen distribution in the vicinity of the crack tip and, as a result, the physical growth of the fatigue crack. Using the maximum stress intensity factor instead of the controlling parameter $\xi$ and replacing $\tau_c$ with the critical hydrogen accumulation peak (maximum local hydrogen concentration) $C_{Hmax}$ ahead of the crack tip, an evolution relationship (see Eq. 9 as an example) can be rewritten as

$$C_{Hmax} K_{max}^{n} = \text{const} \tag{20}$$

Where it is assumed that the shape of the loading cycle is not changed.

Equation 20 gives the physical criterion for local failure in the fracture process zone, i.e. in the vicinity of the fatigue crack tip, and reflects changes in the hydrogen peak which resulted from hydrogen redistribution due to the increase of the maximum stress intensity factor as the crack length increases under fatigue loading.

Experimental analysis of the distribution of hydrogen ahead of the crack tip under hydrogen induced cracking and fatigue I mode loading conditions has been studied on a secondary ion mass spectroscope. Details of the experimental

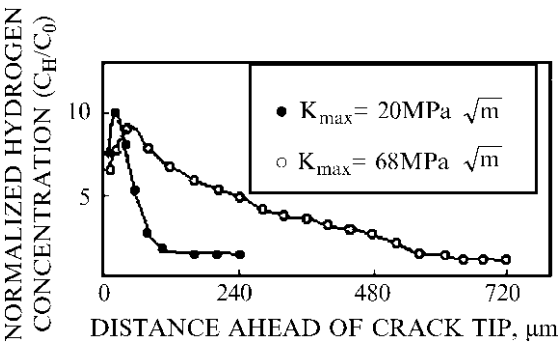


**Fig. 5** Hydrogen distribution in front of the fatigue crack tip

procedure, the tensile properties of the high strength steel and the fatigue crack growth diagram have been reported in [7].

Experimental results on hydrogen distribution for various periods during fatigue crack growth (or the maximum stress intensity factor) are plotted in Fig. 5, where $C_H$ is the local hydrogen concentration and $C_0$ is the concentration of hydrogen far away from the crack tip. There is a hydrogen accumulation peak ahead of the crack tip, which is located some distance ahead of the crack tip. Changes in hydrogen concentration were observed in the vicinity of the propagating crack tip and at a remote site. The hydrogen peak $C_H$ is reduced and the hydrogen concentration $C_0$ is increased by increasing the value of $K_{max}$. So, the levels and sites of hydrogen accumulation under fatigue loading are dependent on the magnitude of the maximum stress intensity factor. This coincides with the hydrogen redistribution given by Eq. 20. Thus, Eq. 20 can be employed for the analysis and prediction of hydrogen redistribution under conditions of fatigue crack propagation.

## 4 Structural Integrity Assessment of the Pipelines with a Crack-like Defect

### *4.1 The Ductile-To-Brittle Transition Temperature Shift*

The ductile-to brittle transition temperature $T_0$ can be considered as a very important mechanical characteristic which reflects liability of the pipe steel to brittle fracture. Corrosion damage of the steel pipeline including hydrogen embrittlement, surface irregularity and crack nucleation causes in the transition temperature shift to higher temperature which decreases operation margins in both the temperature and pressure. The damage evolution approach can be employed to quantify the shift ($\Delta T_c$) of the ductile-to-brittle transition temperature ($T_0$) of gas pipelines due to corrosion damage as follows from Eq. 8:

$$\Delta T_c = \Delta T_{ko}\left(\tau/\tau^*\right)^{1/n} \tag{21}$$

Where $\Delta T_{ko}$is the transition temperature shift during time $\tau^* = 1$ month, $\tau$ is operating time. The power exponent n is assumed to be two. Moreover, stored elastic energy of gas ( $\Delta T_e$), oversize of pipe thickness in comparison with thickness of the Charpy specimen ( $\Delta T_t$), degradation and strain aging ( $\Delta T_d$) of steel, which cause in changes of plasticity during long-term operation of pipelines, shift the transition temperature to higher temperature. Finally, the ductile-to-brittle transition temperature of the gas pipeline after long-term operation can be estimated by the following equation:

$$T_{ko} = T_o + \Delta T_{ko}(\tau/\tau^*)^{1/n} + \Delta T_e + \Delta T_t + \Delta T_d. \tag{22}$$

Thus, the value of $T_{ko}$ can be considered as the shift-corrected transition temperature.

## 4.2 Failure Assessment Diagram and Allowable Surface Defects

The failure assessment diagram in the form reported in Refs. [26, 27] has been adopted for a pipeline with a crack-like defect. To determine an allowable (safe) defect, safety factors [28] were introduced in the failure criterion. The following condition should be fulfilled if detected or assumed crack-like defect of a certain size should be assessed as acceptable

$$K_I \le \frac{K_{mat}}{SF_K}\sqrt{1-\left(\frac{\sigma_c}{\sigma_0}\right)^2} \tag{23}$$

Where $SF_K$ is safety factor against fracture, $K_I$ is the applied stress intensity factor, $K_{mat}$ is the fracture toughness. Thus, the right-hand side of Eq. 23 defines the allowable region in the failure assessment diagram. If the assessment point falls within this region, the component with a crack-like defect is acceptable, i.e. it fulfils the required safety demands.

The local strength (called the cohesive strength in previous papers [26–28]) ahead of the crack tip is determined by von Mises yielding criterion within the fracture process zone. For the evaluation of critical conditions for the acceptable stress $\sigma_c$, the safety factor $SF_K$ in Eq. 23 is set to unity. The acceptable applied stress is suggested to be not more than $\sigma_Y/SF_Y$, i.e. $\sigma_c \le \sigma_Y/SF_Y$. Here, $SF_Y$ is safety factor against plastic collapse. The local strength can be defined for plane stress as follows [28]:

$$\frac{\sigma_0}{\sigma_Y} = -\frac{\beta}{2SF_Y} + \sqrt{1-\frac{3}{4}\left(\frac{\beta}{SF_Y}\right)^2} \tag{24}$$

Where $\beta$ is a dimensionless parameter (so-called local biaxiality ratio) which depends on geometry and loading mode? Values of $\beta$ can be considered as a normalized measure of the crack tip constraint and have been tabulated for various geometries in Refs. [29–31].

The safety factor $SF_K$ can be calculated by making an assumption that the applied acceptable stress should be not less than the yield stress of material for an engineering component with a crack-like defect of the allowable size [28]. The safety factor against fracture of cracked component can be written as:

$$SF_K = SF_Y \frac{\sqrt{1 - \left(\frac{\sigma_Y / SF_Y}{\sigma_0}\right)^2}}{\sqrt{1 - \left(\frac{\sigma_Y}{\sigma_0}\right)^2}} \tag{25}$$

It can be seen from Eq. 25 that the safety factor against fracture is a function of the yield stress and the local strength as well as the safety factor against plastic collapse.

Thus, the right-hand side of Eq. 23 defines the acceptable region in the failure assessment diagram. If the assessment point falls within this region, the component with a crack-like defect is allowable, i.e. it fulfils the required safety demands.

## 4.3 The Allowable Surface Longitudinal Crack-like Defects

An assessment of the allowable surface longitudinal crack-like defects in a gas pipeline is based on the failure assessment diagram according to Eq. 23. The pipeline/defect geometry is described by the wall thickness, $t = 18$ mm, outer diameter, $D = 1{,}420$ mm and defect depth, $a$. The crack-like defect length is assumed to be an infinite value, i.e. $a/t \leq 0.04$. In this case, the applied stress intensity factor can be written as follows [7]:

$$K_I = 1.1\sigma_C \sqrt{\pi a} \cdot f_C \tag{26}$$

Here, $\sigma_c = 270$MPa is the applied circumferential stress corresponding to the internal pressure 7 MPa, $f_C$is the correction factor given by:

$$f_C = \left[\frac{R_0^2 + R^2}{R_0^2 - R^2} + 1 - 0.5\sqrt{\frac{a}{t}}\right]\frac{t}{R} \tag{27}$$

Where $R_0$ and R are outer and inner radius, respectively.

The transition temperature determined on the level of 50% shear fracture for the Charpy tests has been established. The transition temperature of the low-alloy pipe steel is equal to $-30°C$. The mechanical properties of the steel are given in Figs. 6 and 7.

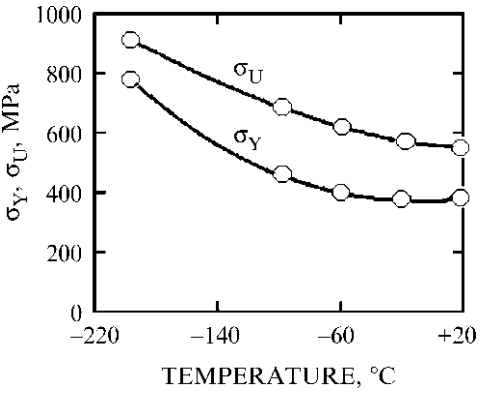


**Fig. 6** Temperature dependence of the yield stress and the ultimate strength

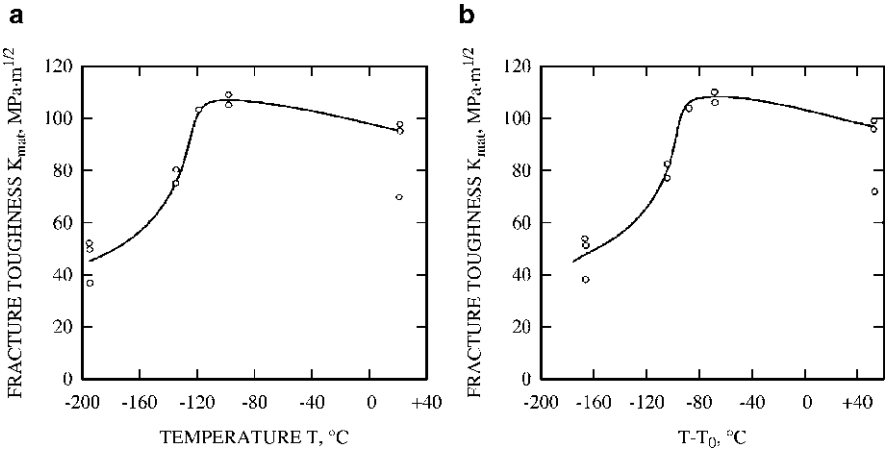


**Fig. 7** The fracture toughness against temperature (**a**) and effective temperature (**b**)

It should be noted that the temperature dependence of the fracture toughness was converted into the $K_{mat} - (T - T_o)$ diagram which takes into account the operation temperature T as well as the transition temperature $T_0$. The safety factor against plastic collapse is assumed to be $SF_Y = 1.5$.

For structural integrity assessment of the aging pipeline, the fracture toughness $K_{mat}$ of the gas pipeline for the effective temperature $(T - T_{ko})$ (see Eq. 22) should be estimated from Fig. 7b and incorporated into the fracture criterion (23) to define the allowable crack size for operation conditions. The local biaxiality ratio $\beta$ is assumed to be $-0.5$. Calculation of the safety factor against fracture gives from Eqs. 25 and 24 $SF_K = 1.6$ for the operation temperature $T = 0°C$. It is can be seen that the allowable size $[a/t]$ of a crack-like defect decreases with gas pipeline ageing. Such tendency is caused in changes of the transition temperature due to physical-mechanical damage of the steel during long-term operation of pipelines (Fig. 8).

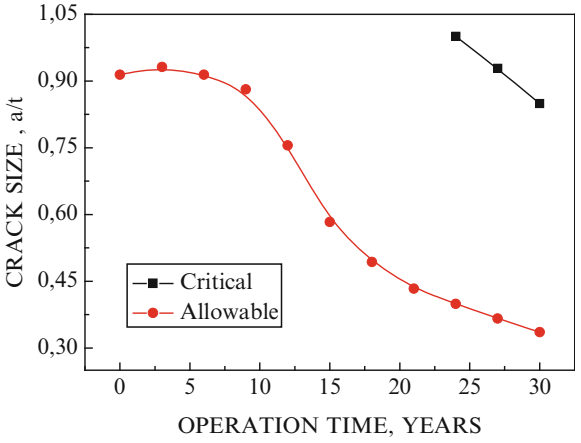


**Fig. 8** Critical and allowable surface longitudinal crack-like defects in a gas-main pipeline at operation temperature T = 0°C

## 5 Concluding Remarks

A damage evolution approach has been employed to describe various failure processes. This approach is based on the concept of damage and synergetic principles. The damage evolution approach can be seen to be synonymous with the present day laws to analyse (i) fatigue crack growth; (ii) low cycle fatigue life of notched structural components; (iii) stress corrosion cracking and (iv) the correlation between hydrogen redistribution in the vicinity of a crack tip and the stress intensity factor during crack propagation under fatigue loading.

The methodology of the above-mentioned approach and the failure assessment diagram has been employed for the structural integrity analysis including assessment of the ductile-to-brittle transition temperature shift due to stored elastic energy of gas, oversize of pipe thickness in comparison with thickness of the Charpy specimen, degradation and strain aging of steel, which cause in changes of plasticity during long-term operation of pipelines. Allowable sizes of surface longitudinal crack-like defects in gas-main pipelines have been estimated for long-term operation of pipelines up to 30 years.

**Acknowledgements** This work is part of the project No. 10-08-00393-a supported by the Russian Foundation of Basic Research.

## References

1. L.M. Kachanov, *Fundamentals of the Fracture Mechanics* (Nauka, Moscow, 1974) (in Russian)
2. Yu.N. Rabotnov, *Creep Problems in Structural Members* (North-Holland Publishing Company, Amsterdam, 1969)

3. S. Murakami, Mechanical modelling of material damage. Trans. ASME J. Appl. Mech. **55**, 280–286 (1988)
4. H. Altenbach, A. Zolochevsky, A generalised fatigue limit criterion and a unified theory of low-cycle fatigue damage. Fatigue Fract. Eng. Mater. Struct. **19**, 1207–1219 (1996)
5. B. Bhattacharya, B. Ellingwood, Continuum damage mechanics analysis of fatigue crack initiation. Int. J. Fatigue **20**, 631–639 (1998)
6. H. Haken, *Advanced Synergetic: Instability Hierarchies of Self-Organizing Systems and Devices* (Springer, Berlin/Heidelberg/New York/Tokyo, 1983)
7. Yu.G. Matvienko, *Models and Criteria of Fracture Mechanics* (Nauka, Moscow, 2006) (in Russian)
8. N.M. Grinberg, V.A. Serdyuk, T.I. Malinkina, *Structure and Fatigue Strength of Magnesium Alloys* (Metallurgia, Chelabinsk, 1991) (in Russian)
9. L.R. Botvina, *Failure Kinetic of Structural Materials* (Nauka, Moscow, 1989) (in Russian)
10. G.P. Cherepanov, *Mechanics of Brittle Fracture* (McGraw-Hill, New York, 1979)
11. K.J. Miller, Materials science perspective of metal fatigue resistance. Mater. Sci. Technol. **9**, 453–462 (1993)
12. Yu.G. Matvienko, M.W. Brown, K.J. Miller, Modelling threshold conditions for cracks under tension/torsion loading, in *Mutiaxial Fatigue and Fracture*, ed. by E. Macha, W. Bedkowski, T. Lagoda (Elsevier, Oxford, 1999), pp. 3–12
13. M.N. James, C. Dimitrion, H.D. Chandler, Low cycle fatigue lives of notched components. Fatigue Fract. Eng. Mater. Struct. **12**, 213–225 (1989)
14. C. Ling, X. Zheng, Effects of cold expansion of a hole on fatigue crack initiation location and life of an LY12CZ alloy. Fatigue Fract. Eng. Mater. Struct. **15**, 241–247 (1992)
15. G. Shatil, E.G. Ellison, D.J. Smith, Elastic-plastic behaviour and uniaxial low cycle fatigue life of notched specimens. Fatigue Fract. Eng. Mater. Struct. **18**, 235–245 (1995)
16. K. Shiozawa, Y. Tohda, S.-M. Sun, Crack initiation and small fatigue crack growth behaviour of squeeze-cast Al-Si aluminium alloys. Fatigue Fract. Eng. Mater. Struct. **20**, 237–247 (1997)
17. N.E. Dowling, J.A. Begley, Fatigue crack growth during gross plasticity and the J-integral, in *Mechanics of Crack Growth* (ASTM STP 590, 1976), pp. 82–103
18. M. Zheng, H.W. Liu, Fatigue crack growth under general-yielding cyclic loading. J. Eng. Mater. Technol. **108**, 201–205 (1986)
19. U. Lindstedt, B. Karlsson, M. Nystrom, Small fatigue cracks in an austenitic stainless steel. Fatigue Fract. Eng. Mater. Struct. **21**, 201–213 (1998)
20. Y. Wang, J. Pan, A plastic fracture mechanics model for characterisation of multiaxial low-fatigue. Int. J. Fatigue **20**, 775–784 (1998)
21. F. Berto, P. Lazzarin, Yu.G. Matvienko, J-integral evaluation for U- and V-blunt notches under Mode I loading and materials obeying a power hardening law. Int. J. Fract. **146**, 33–51 (2007)
22. O.N. Romaniv, G.N. Nikiforchin, *Corrosion Fracture Mechanics of Structural Alloys* (Metallurgia, Moscow, 1986) (in Russian)
23. S. Wu, L. Chen, M. Liu, Distribution of hydrogen concentration near notch tip under mode I loading. Acta Metall. Sin. **26**, A86–A90 (1990)
24. Yu.G. Matvienko et al., Hydrogen distribution in the fatigue crack zone and crack kinetic in electrolytic hydrogenated 07X16H6. Physicochem. Mech. Mater. **26**(3), 9–14 (1990) (in Russian)
25. H. Gao et al., Analysis of crack tip hydrogen distribution under I/II mixed model loads. Fatigue Fract. Eng. Mater. Struct. **17**, 1213–1220 (1994)
26. Yu.G. Matvienko, Local fracture criterion to describe failure assessment diagrams for a body with a crack/notch. Int. J. Fract. **124**, 107–112 (2003)
27. Yu.G. Matvienko, Erratum: local fracture criterion to describe failure assessment diagrams for a body with a crack/notch. Int. J. Fract. **131**, 309 (2005)
28. Yu.G. Matvienko, Failure assessment diagrams in structural integrity analysis, in *Damage and Fracture Mechanics. Failure Analysis of Engineering Materials and Structures,* ed. by T. Boukharouba, G. Pluvinage, M. Elboujdaini (Springer, New York, 2009), pp. 173–182

29. T.-L. Sham, The determination of the elastic *T*-term using higher order weight functions. Int. J. Fract. **48**, 81–102 (1991)
30. P.S. Leevers, J.C. Radon, Inherent stress biaxiality in various fracture specimen. Int. J. Fract. **19**, 311–325 (1982)
31. A.H. Sherry, C.C. France, M.R. Goldthorpe, Compendium of *T*-stress solution for two and three dimensional cracked geometries. Fatigue Fract. Eng. Mater. Struct. **18**, 141–155 (1995)

# Two Parameter Engineering Fracture Mechanics: Calculation of the Relevant Parameters and Investigation of Their Influence on the Surface Notch

**Mohamed Hadj Meliani, Zitouni Azari, Guy Pluvinage, and Yu.G. Matvienko**

**Abstract** In the present research, T-stress solutions are provided for a U-shaped notch in the case of four specimens: CT, DCB, SENT and Romain Tile (RT). The U-shaped notch is analyzed using the finite element method to determine the stress distribution ahead of the notch tip. In contrast to a crack, it was found that the T-stress is not constant and depends on distance from the notch-tip. To estimate the T-stress in the case of a notch, a novel method, namely, method of line, inspired from the volumetric method approach proposed by Pluvinage has been developed. Thus, the two-parameter approach was adopted for the notch two-parameter fracture mechanics in terms of the notch stress intensity factor $K\rho c$ and the effective (average) T-stress, *Tef*. Fracture toughness transferability curve ($K\rho c$ *-Tef)* of X52 pipe steels has been established.

## 1 Introduction

Classical fracture mechanics is based on a one-parameter estimation of the limit state of a cracked body. Accordingly, constraint effect must be considered when it is applied to an in service structure. This limitation has motivated the developments

Mohamed Hadj Meliani (✉)
Laboratoire de Physique Théorique et Physique des Matériaux (LPTPM), FSSI, Université Hassiba Benbouali, Chlef 02000, Algeria
e-mail: hadjmeliani@yahoo.fr

Zitouni Azari and Guy Pluvinage,
Laboratoire de Mécanique, Biomécanique, Polymères et structures, LaBPS-ENIM, île de saulcy, Université Paul Verlaine de Metz, Metz 57045, France
e-mail: azari@univ-metz.fr; pluvina@univ-metz.fr

Yu.G. Matvienko
Laboratory of Modelling Damage and Fracture, Mechanical Engineering Research Institute of the Russian Academy of Sciences,
4 M. Kharitonievsky Per, Moscow 101990, Russia
e-mail: matvienko7@yahoo.com

T. Boukharouba et al. (eds.), *Integrity of Pipelines Transporting Hydrocarbons*, NATO Science for Peace and Security Series C: Environmental Security,
DOI 10.1007/978-94-007-0588-3_16, 

of theories which extend significantly the range of deformation over which fracture can be applied accurately to predict the load capability of a given structure. In this way, recent numerical and experimental studies have attempted to describe fracture in terms of two or three fracture parameters [1]. One of candidate parameters is the elastic *T*-term stress [2]. The T-stress is not singular as $r \rightarrow 0$, but is can alter the elastic crack-tip stress state described by the stress intensity factor $K_I$. The *T*-stress is a function of geometry, loading conditions, and is proportional to the nominal applied stress [3, 4]. Sufficient information about the stress state is available, if the Stress Intensity Factor, SIF and the constant stress term, the *T*-stress, are know. While SIF solutions are reported in handbooks for many crack geometries and loading cases, *T*-stress solutions are available only for a small number of test specimens and simple loading cases for instance pure tension and bending.

Recent studies [5–10] have shown that fracture toughness can be strongly affected by specimen size, crack depth and loading configuration. This dependency is often referred to the effect of crack-tip constraint. However, the fracture toughness estimated from the standard test specimens may lead to unduly conservative results. It is commonly accepted that the standard specimens in laboratory testing are typically of high constraint while non-standard specimen and actual cracked structures may be low constraint configurations. The ASTM E-399 [11] testing procedure recommends certain types of specimen geometries and $K_{Ic}$ can be considered as the plane-strain fracture toughness. All specimen geometries recommended by ASTM E-399 are high constraint. Using the recommendation specimen geometry for testing creates an "ASTM Window" since their corresponding *T* values are within a certain range. A $K_{IC}$ value is believed to represent a lower limiting value of fracture toughness and the ASTM E-399 may not be generally valid. Increasing the size of a specimen shifts the stress distribution closer to the K-stress. Consequently, larger specimens tend to possess better K-dominance. This may explain why a large specimen is better suited for ASTM fracture toughness $K_{Ic}$ testing in addition to the reason for the plastic zone size. This phenomenon limiting the recommendation of ASTM and can be explained using the analytical *K-T* relation for common the effects of specimen geometries. Real cracks exist in three dimensions. However, the two-dimensional approximation itself is only valid asymptotically. Three-dimensional analysis is needed, and almost has yet been performed [12]. We proposed an elastic solution for two dimensional geometries, including stress intensity factor and constraint parameter under various loading conditions. It's very important, in practical structural pipe integrity assessment with gouges, to estimate these parameters with a longitudinal surface notch under internal pressure. For the discussion above, it is now well-known in fracture-mechanics community that single fracture parameter alone may not be adequate to describe crack-tip condition. To address this problem, there has been a recent surge of interest in crack-growth behaviour under conditions of low crack-tip stress triaxiality. This paper exploited the *K-T* crack approach which was derived from a rigorous asymptotic solution and has been developed for a two-parameter fracture. With K as the driving force and *T* a constraint parameter, this approach has been successfully used to quantify the constraints of notch-tip fields for various proposed geometry and loading configurations. Finally, we suggest extending the *K-T* to the higher terms of Williams's equation.

In engineering practice two completely different approaches are applied for cracked and notched components. In the first approach, several works have carried out to estimate the Stress Intensity Factor with the presence of the higher stresses terms; they have exclusively focused estimate the fracture toughness in different constraint conditions. In the second, we proposed the notch fracture mechanics and particularly the Volumetric Method approach in the aim to study stress distribution at the tip of notch in pipes submitted to internal pressure.

## 2 Extend of the Single Parameter Fracture Mechanics (SPFM)

### *2.1 Classical Theoretical Background and Motivation*

Many researchers have long advocated more pragmatic, engineering approach to assess the fracture integrity of cracked structures [13]. This approach requires that constraint in the test specimen approximate that of the structure to provide an "effective" toughness for use in a structural integrity assessment. The appropriate constraint is achieved by matching thickness and crack depth between specimen and structure. Experimental studies by Sumpter [14] and by Kirk and Dodds [15] demonstrate the validity of this approach. Many of the research efforts discussed in the second ASTM/ESIS symposium on constraint [16]. The concept of relating the stress intensity factor to the crack-extension resistance is based on the assumption that *K*-dominance exists at a crack-tip; that is, in a region surrounding the crack-tip; the stress fields can be characterized by the mathematical solution:

$$\mathrm{K} = \sigma_{\mathrm{ij}}\sqrt{2\pi \mathrm{r}} \cdot \mathrm{f}_{\mathrm{ij}}(\theta) \qquad \text{as } \mathrm{r} \rightarrow 0 \tag{1}$$

Where $K$ is the stress intensity factor $f_{ij}(\theta)$ defines the angular function. A polar coordinate system $(r, \theta)$ with origin at the crack tip is used. Note that Eq. 1 is derived from a linear elastic assumption and predicts infinite stress at the crack-tip.

### *2.2 The K-T Approach for Crack*

In this discussion, our primary emphasis is Mode I fracture. It is noted above that there is a region or volume around the crack tip where plastic deformation occur. In order to correlate the higher term effects to an appropriate physical parameter, some works [17–20] simplified the higher terms and define the $T$-stress. $T_{xx}$, or simply the $T$ in the direction $xx$ is defined as constant stress acting parallel to the crack and its magnitude is proportional to the nominal stress in the vicinity of the crack.

$$\mathrm{K} \approx \sigma_{\mathrm{ij}}\sqrt{2\pi \mathrm{r}} \cdot \mathrm{f}_{\mathrm{ij}}(\theta) - \mathrm{T}\sqrt{2\pi \mathrm{r}} \cdot \delta_{1\mathrm{i}}\delta_{1\mathrm{j}} \qquad \text{as } \mathrm{r} \rightarrow \infty \tag{2}$$

The non-singular term $T$ represents a tension (or compression) stress. Positive $T$-stress strengthens the level of crack tip stress triaxiality and leads to high

crack-tip constraint; while negative $T$-stress reduces the level of crack-tip stress triaxiality and leads to the loss of the crack tip constraint. Various studies have shown that $T$-stress has significant influence on crack growth direction, crack growth stability, crack tip constraint and fracture toughness. In addition, crack path direction has received attention in two early studies presented by Cotterell [21, 22]. In the first study, Cotterell [21] shows analytically that the sign of the T-stress determines crack path stability; for a positive T-stress the crack will deviate form its original path; whereas if it is negative, the crack will continue along a straight path. In the second study, Cotterell [22] observes that this criterion does not correctly predict path stability. However, a counterexample by Melin [23] showed that the sign of the T-stress is not applicable in a general criterion for directional stability of cracks. For $T > 0$, yet experience shows the path to be stable. Furthermore, Marder [24] made the assumption that the transition from the straight to the oscillatory crack path occurs at the point where $T = 0$; in order to be consistent with the experimental results of Yuse and Sano [25], Marder found that the fracture energy should be a function of the crack growth rate. This, however, cannot be justified on physical grounds over the range of crack speeds observed in experiments. Cottell and Rice [26] showed that a curved or kink crack will continue to diverge from the main crack direction when $T > 0$, the divergent angle increases further as $(K_1/T)$ increases; for $T < 0$, the kink trends toward the main crack direction. Selvarathinam and Goree [27] extended the Cotterell and Rice [26] model and calculated the T-stress at a small branch of the main crack in various directions in an isotropic material. They define a $T_{crit}$ value as material parameter which they obtain from fracture tests. If $T < \mathrm{T_{crit}}$ the crack path is stable. If it is greater than $T_{crit}$, it is unstable. Experiments, Ramulu and Kobayashi [28] and Ravi-Chandar [29] and Knauss [30] have show that the Cotterell criterion is not valid for a propagating crack. Fleck et al., [31] have developed a criterion for crack path direction of a crack in a joint accordingly, a stable path can exist only if a pure mode I crack path exists and if $T < 0$. The crack seeks the direction of $K_{II} = 0$. Thus, it is possible to consider the sign of the derivative of $K_{II}$ with respect to its position wither layer to determine crack path [32]. Larsson and Carlsson [3] and Rice [2] showed that the sign and magnitude of the T-stress substantially change the size and shape of the plane strain crack tip plastic zone. Kirk et al., [33] and Sorem et al., [34] in their experimental studies have also shows that the fracture toughness of a given material can be considerably dependent on the size and geometry of the crack body. Analytical and experimental studies have show that T can be used as a measure of constraint for contained yielding; see for example Handcok at al., [35] and Sumpter [36]. Recently, Ganti and Parks [37] and Zhang et al., [38] investigated the effect of the $T$-stress on the constraint of elastic- plastic interface crack. Very recently, Li and Xu [39] extensively discussed the $T$-stresses across static crack kinking. Analytical results on the $T$-stress change across dynamic crack kinking are still not available. Some researchers also show the sign of the $T$-stress was not enough to judge the crack stability and other parameters should be introduced. Melin [40] showed that when $T > 0$, the crack path was still stable. Richardson and Goree [41] also observed that in PMMA specimens of different

dimensions, the crack did not kink immediately if the $T$- stress become positive. Richardson [41], with experimental tests, has also shown that the crack path direction stability criterion suggested by Cotterell may not be accurate in all cases. Near the tip of the crack, where the higher order terms of the series expansion are negligible, stresses for mode I are written as:

$$\sigma_{xx} = \frac{K_I}{\sqrt{\pi r}} \cos\frac{\theta}{2}\left(1 - \sin\frac{\theta}{2}\sin\frac{3\theta}{2}\right) + T \tag{3a}$$

$$\sigma_{yy} = \frac{K_I}{\sqrt{\pi r}} \cos\frac{\theta}{2}\left(1 + \sin\frac{\theta}{2}\sin\frac{3\theta}{2}\right) \tag{3b}$$

$$\sigma_{zz} = \frac{K_I}{\sqrt{\pi r}} 2\upsilon\cos\frac{\theta}{2} + E\,\varepsilon_{zz} + \upsilon T \tag{3c}$$

$$\sigma_{xy} = \frac{K_I}{\sqrt{\pi r}} \sin\frac{\theta}{2}\cos\frac{\theta}{2}\cos\frac{3\theta}{2} \tag{3d}$$

In this paper, the $T$-stress was evaluated by the difference method proposed by Yang et al., [42] using directly a single finite element (FE) analysis. This method, namely the stress difference method (SDM), for computing the elastic $T$-stress efficiently and accurately by evaluating $(\sigma_{xx} - \sigma_{yy})$ at a point ahead of a crack tip. The underlying idea is that the errors in the numerically obtained values of $\sigma_{xx}$ and $\sigma_{yy}$ near a crack tip evolve with distance from the crack tip and their difference must eliminate the errors effectively. For homogeneous material, they calculated the T-stress using the difference of the normal stresses along $\theta = 0$, i.e. $(\sigma_{xx} - \sigma_{yy})$, which is a method that can lead to significant numerical errors due to the recovery of stresses very close to the crack tip. In mode I loading, Eq. 3 shows that $\sigma_{xx}$ includes the singular term and $T$. This implies that $T$ can be determined along any direction where the singular term of $\sigma_{xx}$ vanishes or can be set to zero by superposing with a fraction of $\sigma_{yy}$. This corresponds to mode I positions around the crack tip.

$$T = \left(\sigma_{xx} - \sigma_{yy}\right)_{r=0,\theta=0} \tag{4}$$

## 3 Volumetric Method Mesofracture to Extend SPFM to Notch

Although many works have carried out estimation for the stress intensity factor with the presence of T-stress of pipeline, they have exclusively focused on classical fracture mechanics with crack to estimate the toughness. For a sharp V-notch, Kuang and Xu [43] derived a series singular solution for the first order of the stress and strain fields at the tip of a V-notch with different corner angles in a power hardening material. Yang and Yu [44] presented an asymptotic analysis up to the

second order at the tip of a V-notch. The asymptotic stress, strain in a displacement fields at the tip of a U-notch for both plane stress and plane strain conditions in an elastic–plastic material were studied by Yang and Chao [45]. In this paper, we present notch fracture mechanics (NFM) principles applied to study stress distribution at the notch tip of pipes submitted to internal pressure. Volumetric Method, presented by Pluvinage [46] is a meso-mechanical method belonging to this NFM. The notch root, plotted in bi-logarithmic axes; the relative stress gradient (see Eq. 5), plotted on the same graph, allows obtaining an effective distance precise value.

$$\chi(\mathrm{r}) = \frac{1}{\sigma_{\mathrm{yy}}(\mathrm{r})} \cdot \frac{\partial \sigma_{\mathrm{yy}}(\mathrm{r})}{\partial \mathrm{r}} \tag{5}$$

Where $\chi(\mathrm{r})$ and $\sigma_{\mathrm{yy}}(\mathrm{r})$ are the relative stress gradient and maximum principal stress or crack opening stress, respectively. The relative stress gradient depicts the severity of the stress concentration around the notch and crack tips. However, the stress distribution effect is not solely a major parameter for the fracture process zone. The minimum point of the relative stress gradient in the bi-logarithmic diagram is conventionally taken into account as the relevant effective distance and signifies the virtual crack length. The effective stress is defined as the average of the weighted stress inside the fracture process zone:

$$\sigma_{\mathrm{ef}} = \frac{1}{\mathrm{X}_{\mathrm{ef}}} \int_0^{\mathrm{X}_{\mathrm{ef}}} \sigma_{\mathrm{yy}}(\mathrm{r}) \cdot \Phi(\mathrm{r})\ \mathrm{dr} \tag{6}$$

Where $\sigma_{\mathrm{eff}}$, $\mathrm{X}_{\mathrm{ef}}$, $\sigma_{\mathrm{yy}}(\mathrm{r})$ and $\Phi(\mathrm{r})$ are effective stress, effective distance, maximum principal stress and weight function, respectively. The unit weight function and Peterson's weight function are the simplest definitions of weight function the effective distance. The unit weight function deals with the average stress and Peterson's weight functions gives the stress value at a specific distance and it is not required to compute numerical integration. Therefore, the, noted, Notch Stress Intensity Factor, NSIF, is described and defines as a function of effective distance and effective stress given by relationship:

$$\mathrm{K}_{\rho} = \sigma_{\mathrm{ef}} \sqrt{2\ \pi \mathrm{X}_{\mathrm{ef}}} \tag{7}$$

The NSIF is considered as a value of facture toughness with units MPa$\sqrt{\mathrm{m}}$, and the minimum effective distance corresponds to the abscissa of the upper limit of zone II and its distance from notch rot was suggested to be the effective distance $X_{ef}$.

## 4 Proposed Method

The T-stress is according to the geometry, the loading conditions and it proportional to the nominal applied stress. The Stress Difference Method (SDM), used to determine the T parameter, does not produce constant values, except for the short

notches [47, 48]. What implies, that the application of this method, to determine T in structures under pressure, remains conservative in the presence of notches. Let us note that this method was criticized by several authors in the literature [37, 49–51] regarding the constant values at a certain distance of the crack. Moreover, for a crack, the Stress Intensity Factor is calculated at the tip by taking into account the depth. On the other hand when on corrects this factor by the T parameter, we take it starting from a certain distance, noted stabilization distance '', which remains to be discussed. Basing itself on these observations, the sensitivity to the change of the plastic zone size and the amplitude of the T-stress, we propose a modification of the Williams formula by taking into account the effects of several parameters observed on the evolution of the constraint T along the ligament.

## 4.1 Presentation of the New Method

The volumetric method results are very useful, and the new formula of fields stress proposed, at the notch-tip, follows the same principles. We point out that the volumetric method consists in giving a average value of the opening stress, noted effective stress $\sigma_{ef}$, determined by an approach of the stress distribution by a polynomial of $n$ degrees. The degree of polynomial is given for a strong coefficient of correlation. A minimum of the opening stress gradient give an effective distance, $X_{ef}$. The projection of the latter on the curve of stress opening distribution enables us to obtain an effective stress $\sigma_{ef}$, Fig. 1a. In the same Fig. 1b, we trace the evolution of the T-stress along the ligament. The first remarks show that the error made, on the stresses difference $(\sigma_{xx} - \sigma_{yy})$, follow the same pattern as the opening stress in a bilogaritmic diagram.

From these remarks, we committed ourselves calculating an effective stress, or rather an average T-stress for notches, instead of taking the stabilization value illustrated in the cracks. We noticed, previously, that this distribution of the T-stress does not give constant values to a certain distance from the point of the notch [48, 52]. The Stress Difference Method for cracks remains very conservative. We propose methods of calculating of the T-stress; named 'point method'.

## 4.2 Determination of the Effective T-Stress

The proposed method is inspired from the volumetric method, suggested by Pluvinage et al., [46]. It consists in using, in a bilogarithmic diagram, the minimal distance from the gradient of the opening stress on determine the effective T-stress. The smoothing the curve of the opening stress distribution is described by the following equation:

$$\sigma_{yy}(x) = \sum_{i=0}^{n} a_i x^i \tag{8}$$

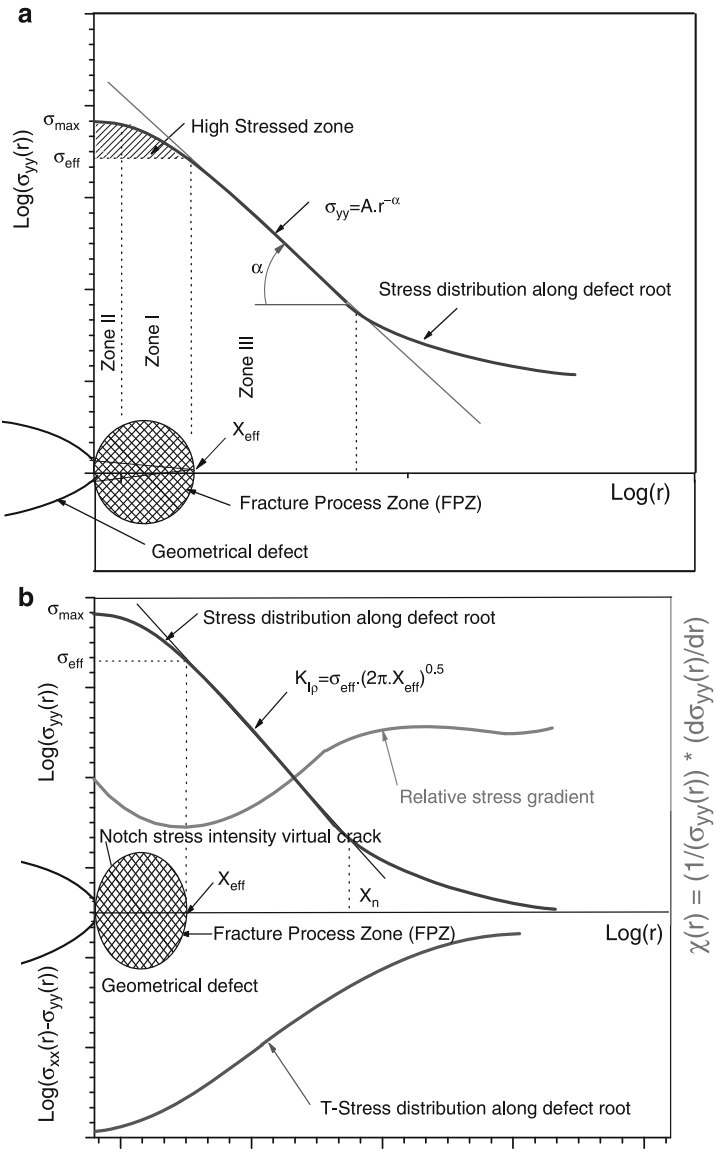


**Fig. 1** (**a**) Schematic representation of the opening stress evolution in a bilogaritmic scale and (**b**) procedures to determine the effective stress and the effective distance by the volumetric method

The gradient of the opening stress leads to equation:

$$\chi(x) = \frac{1}{\sigma_{yy}(x)} \cdot \frac{d\sigma_{yy}(x)}{dx} \cdot \frac{\sum_{i=0}^{n} i a_i x^{i-1}}{\sum_{i=0}^{n} a_i x^i} \tag{9}$$

The weight function can be written as follows:

$$\phi(x) = 1 - \frac{x\sum_{i=0}^{n} i a_i x^{i-1}}{\sum_{i=0}^{n} a_i x^i} \tag{10}$$

The effective distance in the vicinity of the notch tip can be obtained by the Taylor approach. It corresponds to the minimum point in the opening stress gradient:

$$\frac{d\chi(x)}{dx} = 0 \tag{11}$$

Substituting Eq. 10 in Eq. 11 gives the following relation to calculate the effective distance:

$$\frac{d\chi}{dx} = \frac{\sum_{i=0}^{n}\left(a_i i^2 x^{i-2} - a_i i x^{i-2}\right)}{\sum_{i=0}^{n} a_i x^i} - \frac{\left(\sum_{i=0}^{n} a_i i x^{i-1}\right)}{\left(\sum_{i=0}^{n} a_i x^i\right)} = 0 \tag{12}$$

Averaging the T-stress inside the effective distance, the effective T-stress ($T_{ef}$) can be defined by the interaction between the effective distance, noted $X_{ef}$ and the opening stress distribution along the ligament.

$$T_{ef} = \frac{1}{X_{ef}} \int_0^{X_{ef}} \left[\sigma_{yy}(x) \times \Phi(x)\right] dx \tag{13}$$

Here, $\sigma_{yy}(x)$ is the opening stress distribution along of the ligament in the $xx$ direction and $\Phi(r)$ is the weight function. Figure 2 shows a graphic representation of the T-stress along the ligament, the gradient of the opening stress distribution and the technique to calculate the effective distance $X_{ef}$ and the effective $T$-stress, $T_{ef}$.

We note that the distribution of the T-stress is determined by the difference of the principal stresses $\sigma_{xx}$ and $\sigma_{yy}$ and along of the ligament in the principal direction.

$$T = T_{xx} = \left(\sigma_{xx} - \sigma_{yy}\right)_{\theta=0} \tag{14}$$

The Notch Stress Intensity Factor can be determinate by:

$$K_\rho = \sigma_{ef}\sqrt{2\,\pi X_{ef}} \quad \text{for } x \to X_{ef} \tag{15}$$

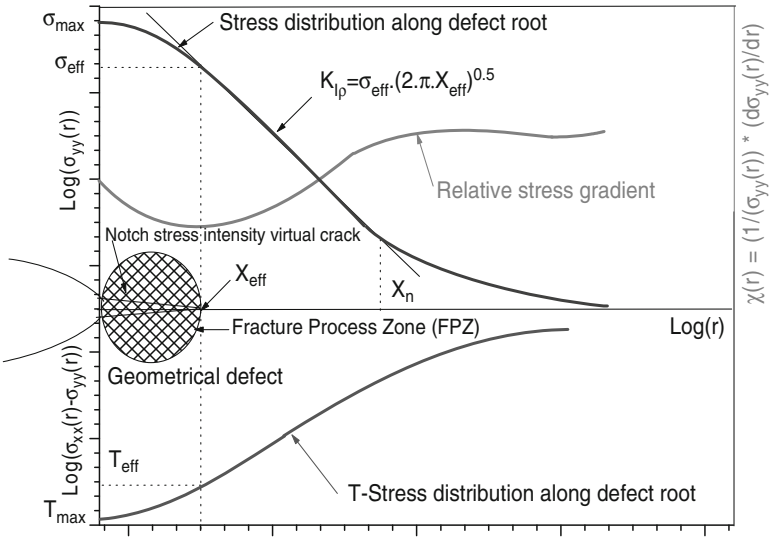


**Fig. 2** Schematic bilogarithmic diagram of the determination of the effective T-stress by averaging the opening stress inside the effective distance

## *4.3 Finite Element Analysis*

The Finite Element method was used to determine the notch-tip parameters for the API-5 L X52 pipe specimens with a V-notch. The considered surface defects, in this study, are chosen as notches as the main important pipe defect type. They are of complex geometries and mostly assumed as semi-elliptical or rectangular shape in some well-know codes (Fig. 3). According to numerous design codes, this kind of defects is considered as a semi-elliptical or rectangular notch-like surface defect of aspect ratio a/c.

The real notches exist in three dimensions, however, and the two-dimensional approximation used itself is for large radius of curvature of the notch edge, e.g., $a << c$. The specimen was modelled by CASTEM 2000 code in two dimensions under plane strain conditions using free meshed isoperimetric triangulateral elements only on half of the specimen. Support and symmetric boundary condition are used in this model. A detailed stress analysis was carried out in the vicinity of the notch front to emphasize the characteristics of the two dimensional stress fields. The coefficients of the higher order stress terms represent one part of a larger database which will also include information on various constraint parameters. For more detail see [48, 52] (Fig. 4).

A detailed example on the different steps of the point method is illustrated in Figs. 5–7. The opening stress is presented, in a bilogarithmic diagram, for a pipe under a pressure from 20 to 50 bars, for a ratio of $R/t = 20$ and one longitudinal surface defect of depth $a/t = 0.5$. The Fig. 5a reported the distribution of the

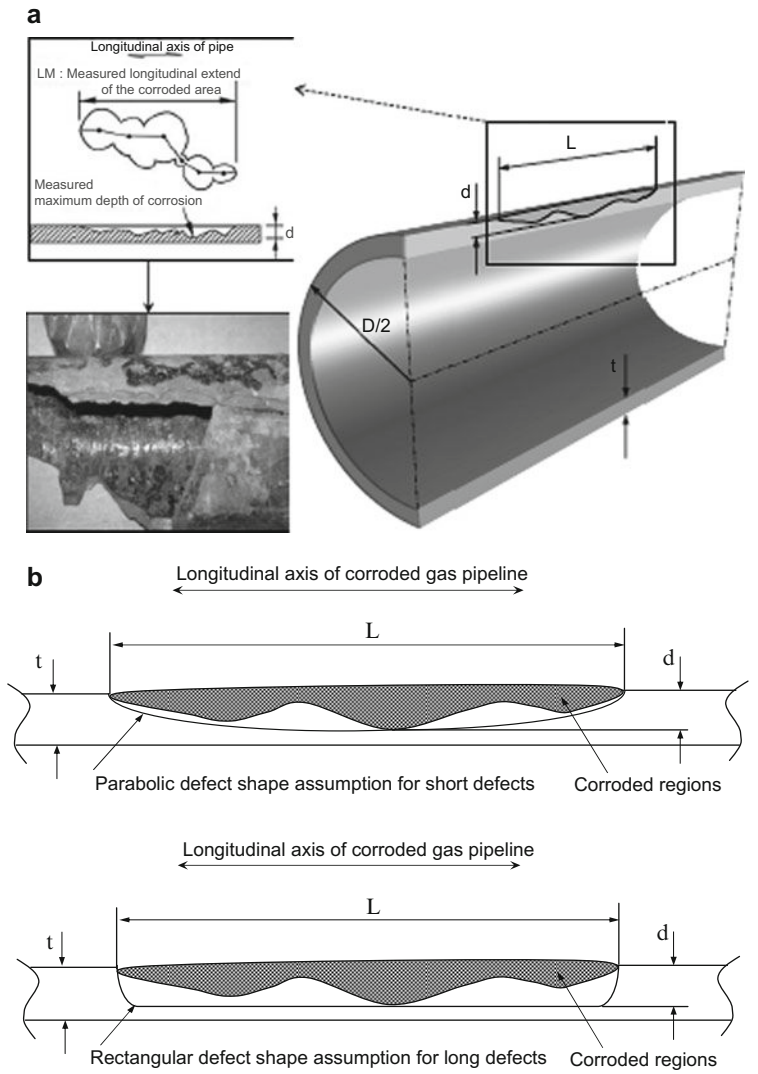


**Fig. 3** Typical illustration of foreign object scratches defects in longitudinal axe of pipe modelled by (**a**) semi-elliptical and (**b**) rectangular shapes

opening stress and the various zones along the ligament. A detail of the zone (I), Fig. 5a, is presented in the Fig. 5b. The polynomial approximation distribution of the T-stress is given in Figs. 6 and 7 illustrated the gradient of this distribution.

Table 1 collect the results obtained by Finite Elements Analysis for the suggested method, compared with those of our results, presented in [53, 54]. We calculated the various parameters: the effective T-stress, $T_{ef}$, the effective distance, $X_{ef}$ and the Notch Stress Intensity Factor, $K_{\rho}$. For the determination of the effective

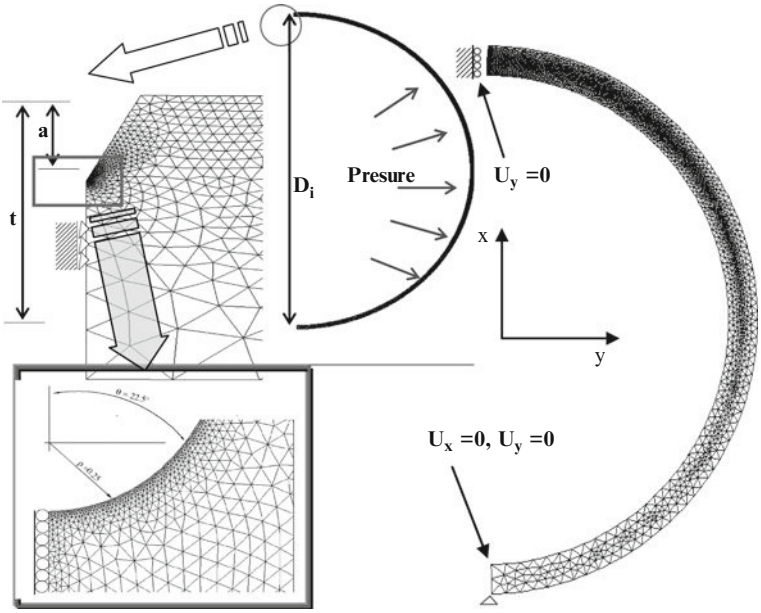


**Fig. 4** Typical 2D finite element mesh and boundary conditions used in the model of the cracked pipeline

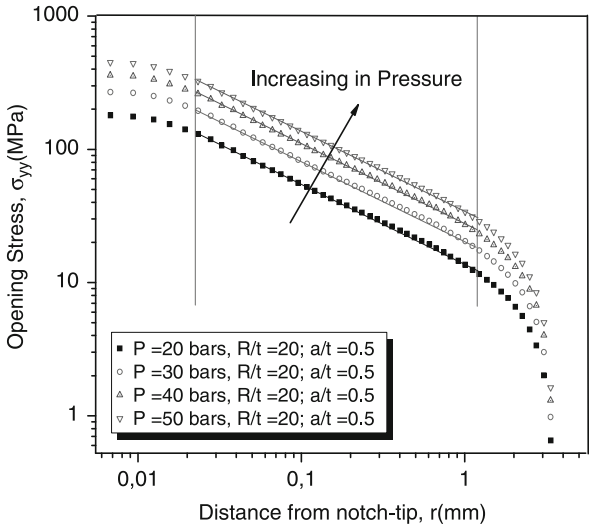


**Fig. 5** The opening stress distribution along ligament of the pipe under pressure (P = 20, 30, 40 and 50 bars, R/t =20 et a/t = 0.5)

**Fig. 5** (continued)

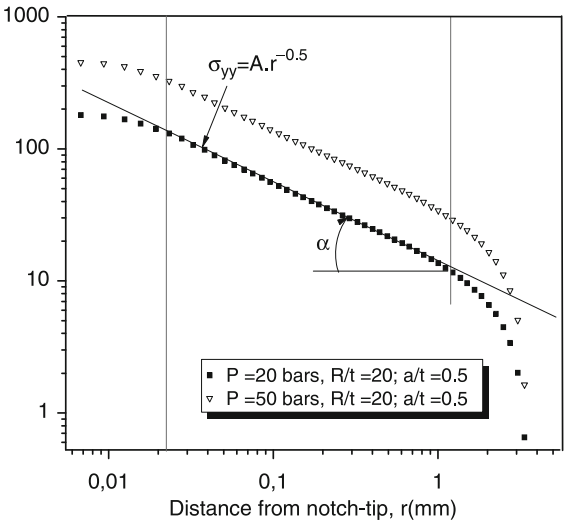


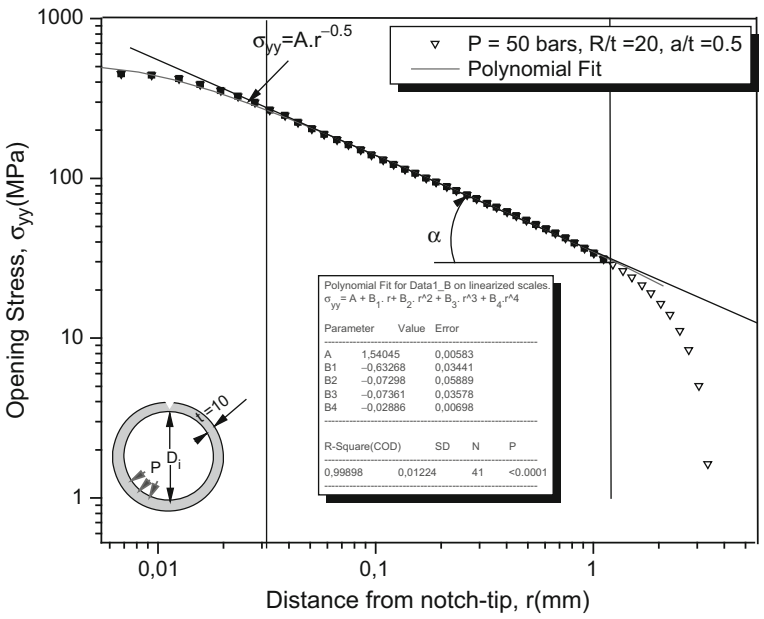


**Fig. 6** Approximation of the T-stress distribution

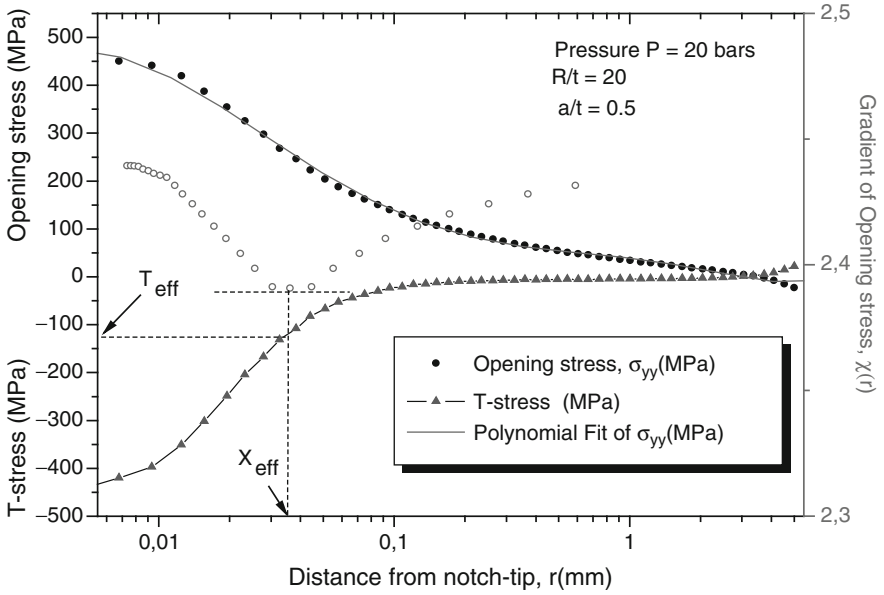


**Fig. 7** Gradient of the opening stress distribution according to Eq. 13 (P = 50 bars, R/t = 20 and a/t = 0.5)

T-stress, the Table 1 shows that the results are very close. For the short notches, the standard deviation is about 3.74% and for the long notches, we assume a standard deviation of 5.45%.

## 5 Study of the Relevant Parameters

### *5.1 Effect of Pressure*

Figure 8a–d show, the variations of the effective *T*-stress and Notch Stress Intensity Factor, $K_\rho$ value at the deepest points of external surface notches in the cylinders for different relative crack depths a/t (notch depth/cylinder thickness). It can be seen that the $T_{\text{eff}}$ and the $K_\rho$ value increases with an increase of the relative crack size, a/t. For the same a/t; when a/t tends towards 0,1, $K_\rho$ and $T_{\text{eff}}$ values for both notch types become similar, with both $K_\rho$ and $T_{\text{eff}}$ value reaching their largest values at a/t = 1. In such a crack size range, the deeper the notch, the larger the dangerous influence of external surface notch on pipes. Note that the numerical solutions are for a range of a/t = 0.1 to 0.75 and for pressure from 20 to 50 bars. It can be seen that absolute values of both *NSIF* and effective *T*-stress solutions are significantly lower for smaller notches and diameter case than for long notches for a given pressure, as to be expected. Of significance to note too is that for all cases

**Table 1** Results of the proposed method to determine the effective T-stress, compared to the results of [48]

| | | Proposed method | Results of [48] | Ecart type | | | | | |
|---|---|---|---|---|---|---|---|---|---|
| Pressure (bars) | R/t | a/t | $X_{ef}$ (mm) | $T_{ef}$ (MPa) | $K_\rho$ (MPa.m$^{0.5}$) | $X_{ef}$ (mm) | $T_{ef}$ (MPa) | $K_\rho$ (MPa.m$^{0.5}$) | E(%)$T_{ef}$ | E(%)$K_\rho$ |
| 20 | 5 | 0.1 | 0.03126 | −3.4545 | 0.06405 | 0.03772 | −3.4467 | 0.06645 | 0.22579 | 3.74707 |
| | | 0.3 | 0.02381 | −8.5409 | 0.16908 | 0.02810 | −8.4798 | 0.16869 | 0.71538 | 0.23066 |
| | | 0.5 | 0.01945 | −7.4988 | 0.32785 | 0.02327 | −7.1350 | 0.32943 | 4.85144 | 0.48193 |
| | | 0.75 | 0.01713 | −10.098 | 0.70112 | 0.02240 | −9.5470 | 0.70285 | 5.45653 | 0.24675 |
| | 10 | 0.1 | 0.03125 | −7.2266 | 0.13376 | 0.03772 | −7.2001 | 0.13897 | 0.36670 | 3.89504 |
| | | 0.3 | 0.01951 | −21.2456 | 0.34835 | 0.02381 | −21.202 | 0.35914 | 0.20334 | 3.09746 |
| | | 0.5 | 0.01945 | −38.554 | 0.73181 | 0.02327 | −38.213 | 0.73630 | 0.88447 | 0.61355 |
| | | 0.75 | 0.02240 | −71.098 | 1.83964 | 0.03023 | −67.599 | 1.84849 | 4.92138 | 0.48107 |
| | 20 | 0.1 | 0.03125 | −14.6845 | 0.27361 | 0.03772 | −14.644 | 0.28302 | 0.27716 | 3.43920 |
| | | 0.3 | 0.01951 | −44.234 | 0.72104 | 0.02380 | −43.939 | 0.74363 | 0.66691 | 3.13297 |
| | | 0.5 | 0.01945 | −82.574 | 1.56681 | 0.02327 | −81.588 | 1.57496 | 1.19408 | 0.52017 |
| | | 0.75 | 0.02240 | −73.342 | 4.48748 | 0.03023 | −71.820 | 4.61226 | 2.07521 | 2.78063 |
| | 40 | 0.1 | 0.02546 | −32.9345 | 0.52905 | 0.03125 | −32.884 | 0.55350 | 0.15425 | 4.62149 |
| | | 0.3 | 0.01951 | −90.3205 | 1.46720 | 0.02380 | −89.523 | 1.51465 | 0.88297 | 3.23405 |
| | | 0.5 | 0.01945 | −172.341 | 3.26049 | 0.02327 | −169.51 | 3.27251 | 1.64267 | 0.36866 |
| | | 0.75 | 0.02240 | −385.4983 | 10.40314 | 0.03023 | −377.83 | 10.43824 | 1.98919 | 0.33740 |

study, the $T_{eff}$ values are negative, suggesting low stress triaxiality conditions at the notch-tip for this geometry. Physically, the magnitude of high term series solution of Williams directly determines difference between stress distribution and HRR field [4] (Hutchinson, 1968; Rice and Rosengren, 1968). Note that the HRR solution is valid as $r \to 0$. The absolute value of effective $T$-stress must increase in order that the higher order terms continue to represent the deviation from the HRR field. For pipe having $T_{eff=}0$, the critical stress is uniquely characterized by the HRR

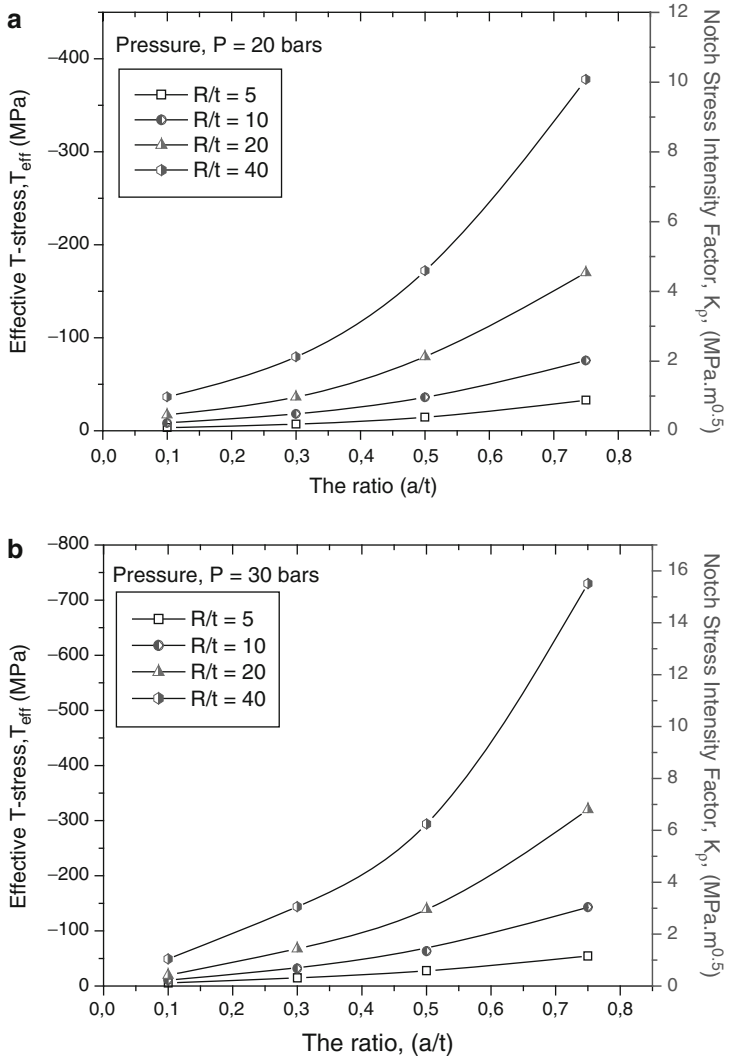


**Fig. 8** Development of notch tip constraint represented by the effective $T$-stress for various situations of pressure and diameters of Pipeline with the presence of $K_\rho$

stress. All the case study provides a quantitative measure of the level of constraint. Noted as, geometries with positive or near zero effective $T$-stress are found to give lower bound effective Stress Intensity Factor $K_{eff}$ values; however, geometries with significantly negative effective $T$-stress are found to give elevated $K_{eff}$ values. From the Fig. 9a, it can be seen that the effective T-stress and the Notch Stress Intensity Factor for the four pipe diameter are proportional to the internal pressure; P. They can be very well expressed as the following linear functions of internal pressure, P:

$$T_{eff} = \alpha_i P \quad i = 1, 4 \tag{16a}$$

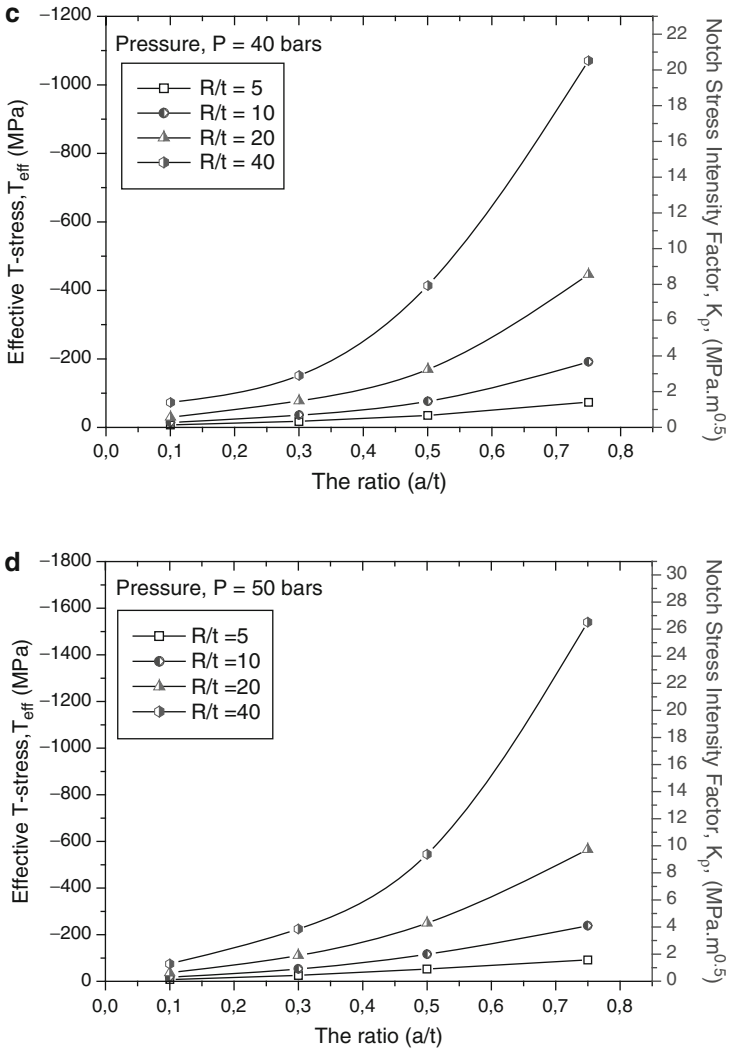


**Fig. 8** (continued)

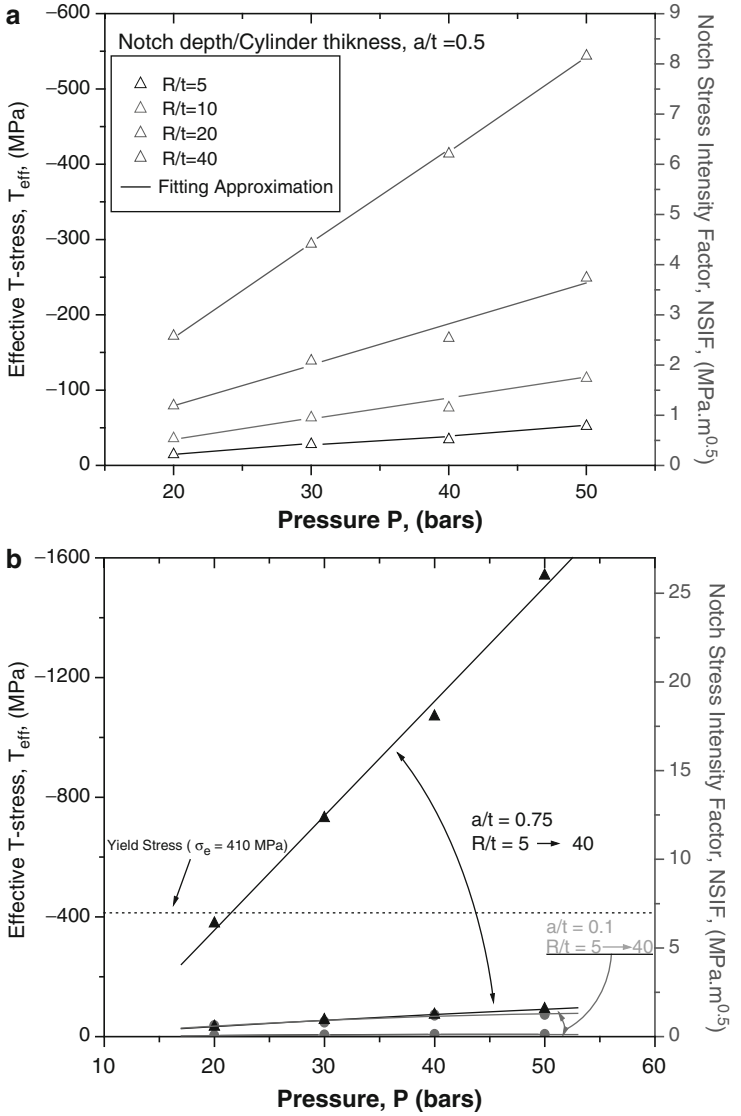


**Fig. 9** (**a**) Evolution of the effective T-stress and the Notch Stress Intensity Factor with internal pressure, P for a/t = 0.5 and (**b**) transition of $T_{eff}$ and NSIF for a/t = 0.1 to 0.75 for the diameter pipe R/t = 5 to 40

and:

$$K_{\rho} = \omega_i P \quad i = 1, 4 \tag{16b}$$

Where $\alpha_i$ and $\omega_i$ represents the slope for the four different pipe diameter. The Fig. 9b shows a comparison between a short and along notches according to the

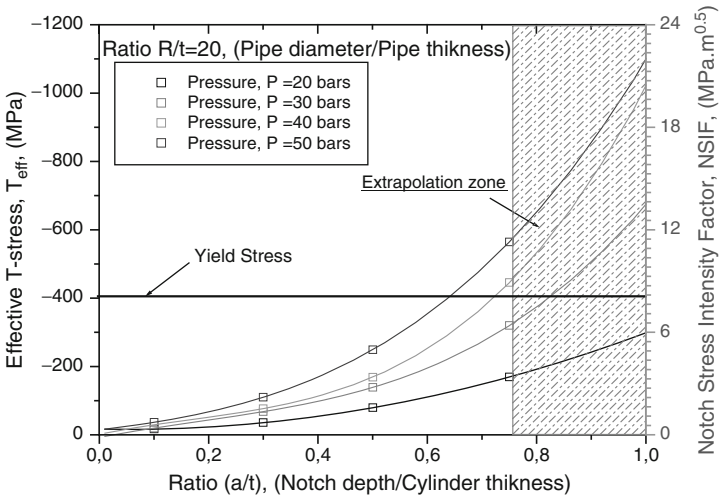


**Fig. 10** Extrapolation of the variation of the effective T-stress and the Notch Stress Intensity Factor with internal pressure $P$ for $R/t = 20$

pressure for a pipe diameter ($R/t$) which varies in the range of 5–40. For the notches, the increase of a diameter of 5–40 facts varies the Notch Stress Intensity Factor and effective T-stress of 2%. On the other hand, for the long notches, the NSIF and $T_{eff}$ pass from 7% to the 45%.

From the Fig. 10, it can be seen that the effective $T$-stress and the Notch Stress Intensity Factor value increases with an increase of the relative notch size, a/t. when a/t tends toward 0.1, the $T_{eff}$ and $NSIF$ values for both notch types become similar, with both the $T_{eff}$ and $NSIF$ value reaching their largest value at a/t = 1. The above analyses also show that through = wall axial surface notch ($a/t \rightarrow 1$) is a special state, which has a strong dangerous influence on the pipe, compared with those of other axial surface notches ($a/t < 1$). This special state will end if the state of the pipe with the through = wall notch ($a/t = 1$) has an axial surface notch that extends continuously because the internal pressure, P, increases at the pipe is continuously being loaded.

Therefore, it is necessary to carry out some research about the gas pipe with though-wall notches. A example about the influence of the internal pressure, $P$, on the effective $T$-stress and the Notch Stress Intensity Factor value for the deepest point ($a/t = 0.1 - 0.75$) of the pipe with longitudinal surface notches and pipe with though-wall notches have been carried out and the results are shown in Fig. 10. The influence of the internal pressure, $P$, on the effective $T$-stress and the Notch Stress Intensity Factor value of the thought-wall notch is the largest. At the same internal pressure, the $T_{eff}$ and $NSIF$ value increases with increasing in the ratio ($a/t$). This means that the thought-wall notch has a more dangerous effect on the high diameter pipe than either the small diameter pipe, if the notch length and internal pressure, $P$, are the same for all cases. The direction of propagation depends noticeably on the effective $T$-stress. A negative $T_{eff}$ decreases significantly the tangential stress

whereas the effect of positive $T_{eff}$ on the tangential stress is negligible. A reduction in the tangential stress increases fracture toughness for specimens failing by brittle fracture. The results are compatible with, Ozmat et al., [55], through experiences on various cracks geometries having different constraints. Nguyen et al., [56] showed through their study that for a value of $T_{eff} = -2$, lasted life corresponding to an analysis with fields HRR is increased by 40% in the case of ductile fracture and by 18% for the brittle fracture.

## 5.2 *Evolution of the Effective Biaxiality Factor*

The effective notch-tip constraint is given by the biaxiality factor $\beta_{eff}$ related the effective *T*-stress to the Notch Stress Intensity Factor and defined as

$$\beta_{eff} = \frac{T_{eff}\sqrt{2\pi X_{eff}}}{K_{\rho}} \tag{17}$$

Figure 11a shows the variation of $\beta_{eff}$ with the ratio a/t and pipe diameter under different internal pressures. For 50 bars pressure, for example, it is approximately in the range of [−0.21 to 0.29] for the range of a/t from [0.1, 0.75], however, the biaxiality is note sensitive to the pipe diameter size. It should be mentioned that this parameter is always negative and for shortly notched specimens the predicted results is larger compared to deep notch geometries.

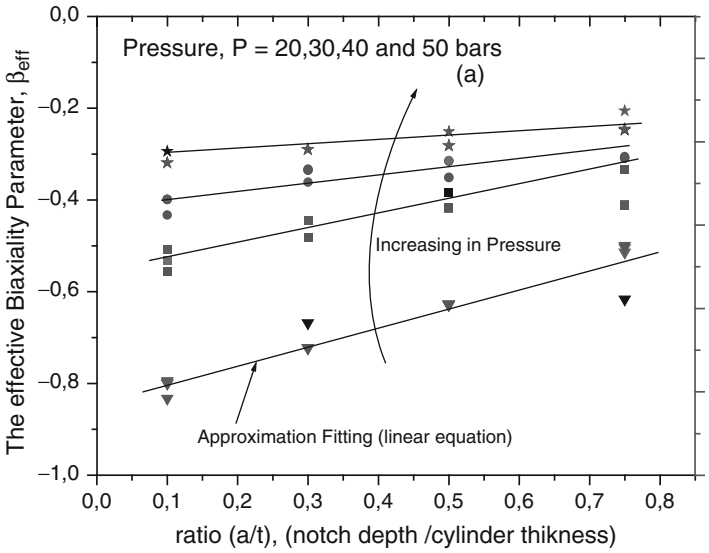


**Fig. 11** Representation of the Biaxiality parameter versus the ratio a/t for various pressures at the notch (P = 20,30,40 and 50 bars and R/t = 20)

The magnitude for the range of pipe diameter is essentially represents a linear relationship. The biaxiality parameter along of ligament is given by $\beta_{\text{eff}} = \beta_0 + \text{D}(\text{a/t})$, were D is the slope. By plotting $\beta_{\text{eff}}$ as a function of (a/t), we obtain an extrapolated value of $\beta_{\text{eff}}$ at a/t = 0 as $\beta_0$.The illustrated Fig. 11a depicts that the effective biaxiality parameter is sensitive to changes in loading and notch length. The values of $\beta_{\text{eff}}$ with a pressure of 50 bars remain constant at approximately in range [−0.21 to 0.29] while the effective value T-stress for 20 bars pressure decreases with crack length in the range [−0.8, −0.5]. The discussions above presented in detail the mathematical derivation of the biaxiality, and qualitatively the uses of the biaxiality. The decreasing effective biaxiality values for differed deep notches and pressures can be explained by the degree of constraint. Increasing the pressure decrease the effective biaxiality parameter. For R/t = 5 specimen, has the lowest constraint because this loading provides pure tension on the ligament. Pluvinage [46] explain this observation, for small diameter pipes, where bending stresses are predominant, circumferential failure occurs. For large diameter, hoop stresses are more important than bending stresses and longitudinal failure appears. When bending and hoop stresses are of the same importance, fracture path becomes helicoidally.

## 5.3 *Influence of the Constraint in the Plastic Zones*

To include the constraint level in the notch tip analytical solutions, the asymptotic including higher order terms may be used. Using Williams' series solution and keeping only two terms, the opening strain in front of a crack tip can be written as:

$$\varepsilon_{\text{yy}}|_{\theta=0} = \frac{(1+v)}{\text{E}} \cdot \frac{\text{K}_\text{I}}{\sqrt{2\pi r}} - \frac{v}{\text{E}} \cdot \text{T} \quad \text{(plane stress)} \tag{18}$$

Where $\varepsilon_{\text{yy}}|_{\theta=0}$ is the opening strain along. Equation 1 show that the opening strain can be either or lower than the HRR strain, i.e. the first term, depending upon the signs of the second terms. In order to examine the effect of the second terms of Williams' solutions, i.e. effective *T*-stress, on the shape and size of the plastic zone, notch tip plastic zones for different diameter of pipeline are displayed in Fig. 12a–c. These figures pertain to a fixed value of pressure, $P = 20$ bars and the depth of a/t = 0.5. It can be seen that with increase in diameter, i.e., increase in negative $T_{eff}$, the plastic zone rotates considerably clockwise and increases significantly in size [14]. Figure 13 show the schematically representation of development size notch-tip plastic zones.

The crack tip plastic zones obtained from the static analyses corresponding to different values of pressure are displayed in Fig. 14. It is recalled in the Section 1 that the shape and size of the plastic zone are affected by the presence of the effective *T*-stress. However, it was found that with increase in negative $T_{eff}$ the plastic enhances significantly in size. Comparison of Fig. 14a with b shows that with increase in depth of crack and the diameter, the maximum extent of the plastic zone slightly reduces and it is less elongated in shape (Fig. 15).

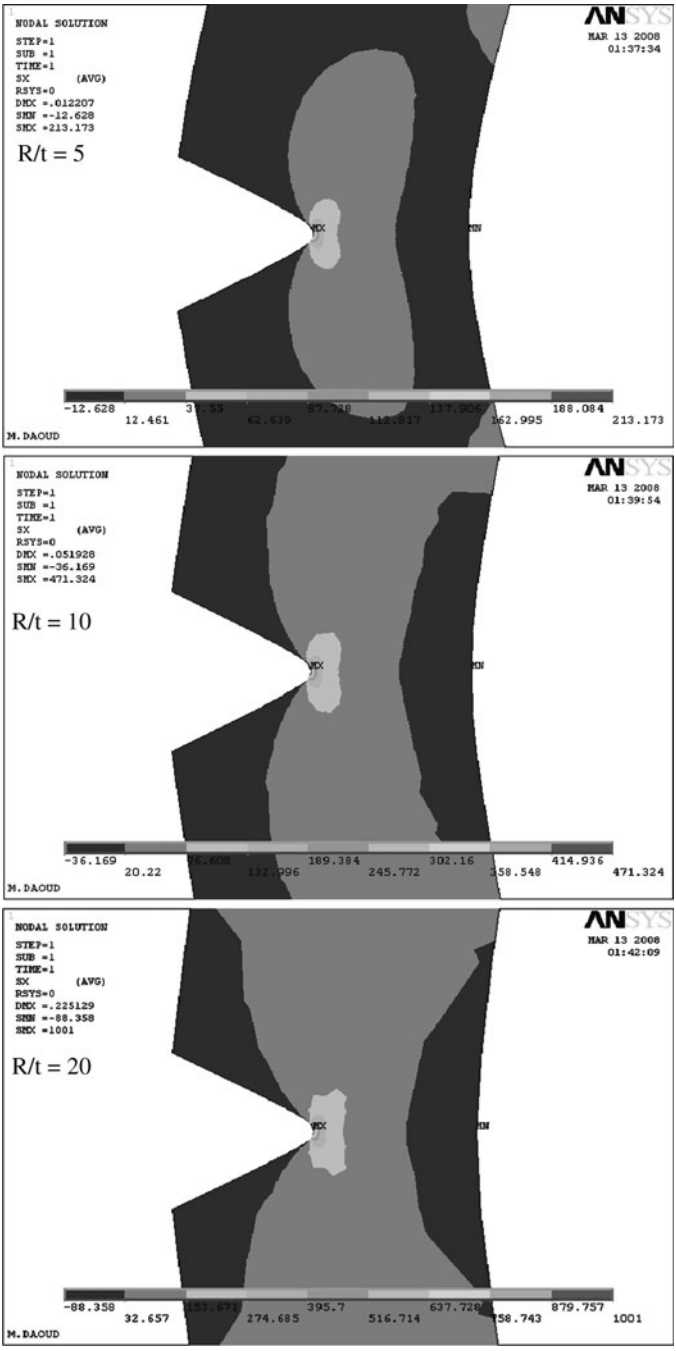


**Fig. 12** Notch-tip plastic zones obtained for different diameter of P = 20 bars and a/t = 0.5

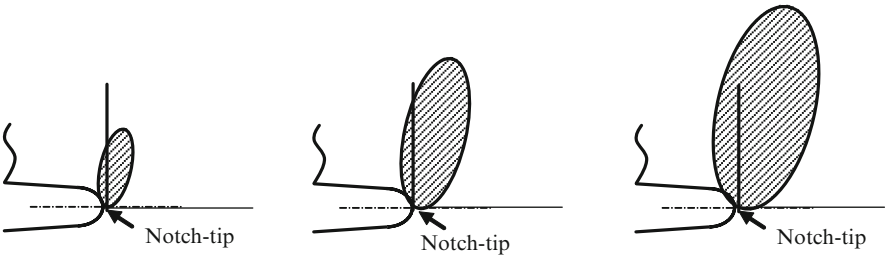


**Fig. 13** Schematic representation of development size notch-tip plastic zones

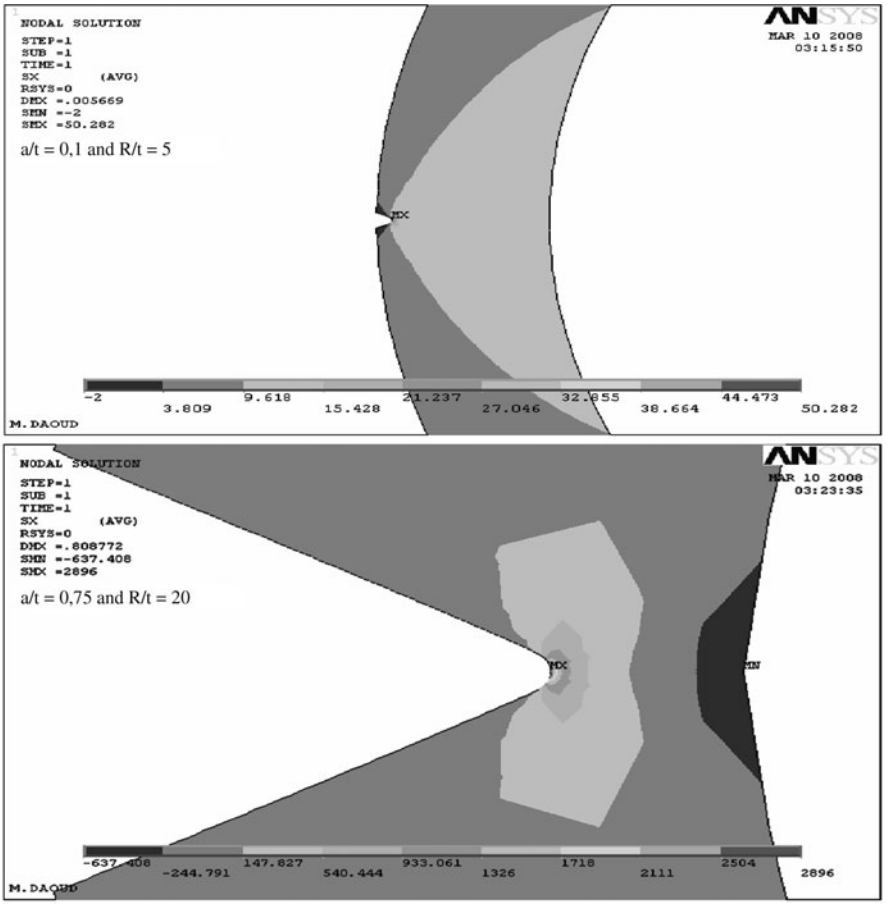


**Fig. 14** The shape of plastic zone for different situation

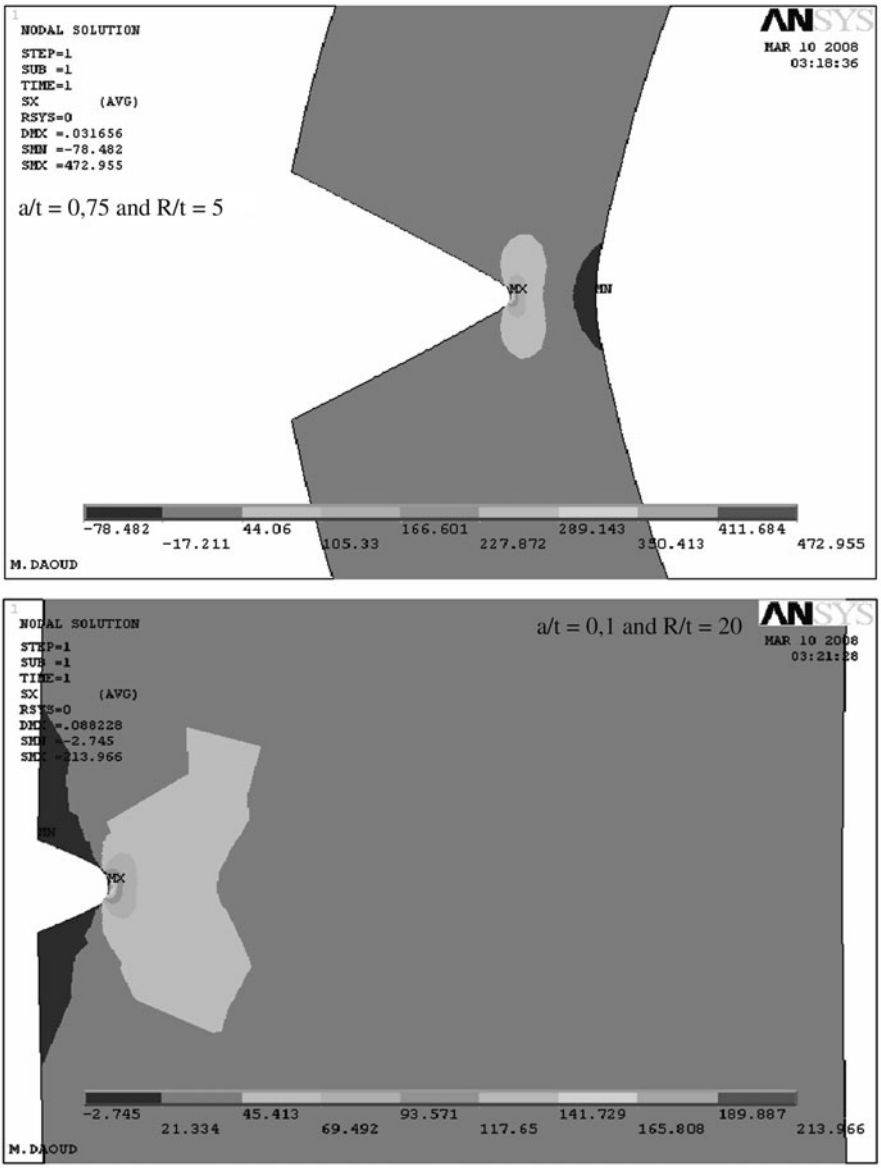


**Fig. 14** (continued)

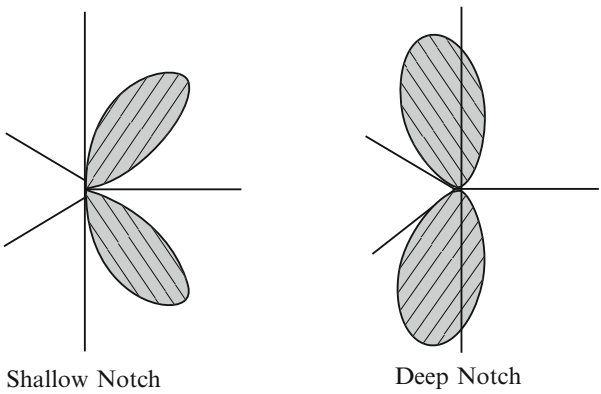


**Fig. 15** Schematic representation of development crack tip plastic zones

## 6 The Fracture Driving Force Line for a Pipe with a Surface Notch

The applied notch stress intensity factor $K_{\rho,app}$ of a component with a notch versus the applied $T_{ef,app}$-stress can be used to establish a fracture driving force line of this component. These two parameters are calculated using loading conditions, component and notch sizes. The intersection of the failure material curve with the fracture driving force line provides fracture conditions. Experience shows that the majority of pipeline failure initiates from defects or cracks which are either inherent in the material introduced during manufacturing or damage during service. The surface defects in a pipe under internal pressure are simulated by a very long semi elliptical notch with parallel sides, a notch radius $\rho = 0.25$ mm and the notch depth $a$. This notch is oriented along the longitudinal direction. The pipe has an internal radius R and a wall thickness $t = 10$ mm. To cover practical and interesting ranges of these three variables, four different values of $R/t = 5$, 10, 20 and 40 were analyzed. In addition, four different notch depth $a/t$ ranging from 0.1 to 0.75 and different internal pressure $P = 20$, 30, 40 and 50 bars were introduced in the consideration. Stress distributions at the notch tip are computed by finite element method. The applied notch stress intensity factor was calculated using the volumetric method. The applied $T_{ef,app}$-stress was determined by numerical line method described in [52, 54]. Evolution of the T-stress along ligament is presented in Fig. 16.

For any pressure values and pipe diameter, the $T$-stress values are negative along the ligament where the crack length ratio is less than $a/t < 0.5$. The ligament is submitted to compression. On the other hand, when the ratios $a/t$ exceeds 0.5, the $T$-stress values become positives (tension case). Eventually, near the notch tip, it is shown that the effect of $R/t$, $a/t$ and $P$ on the distribution of the T-stress is significant. The change of the $T$-stress sign for negative to positive values may be due to the fact that the magnitude of local moment closing the crack increases with increase in crack depth. The negative values for the pipe specimens indicate low crack front constraint and extended plastic deformation around the crack front.

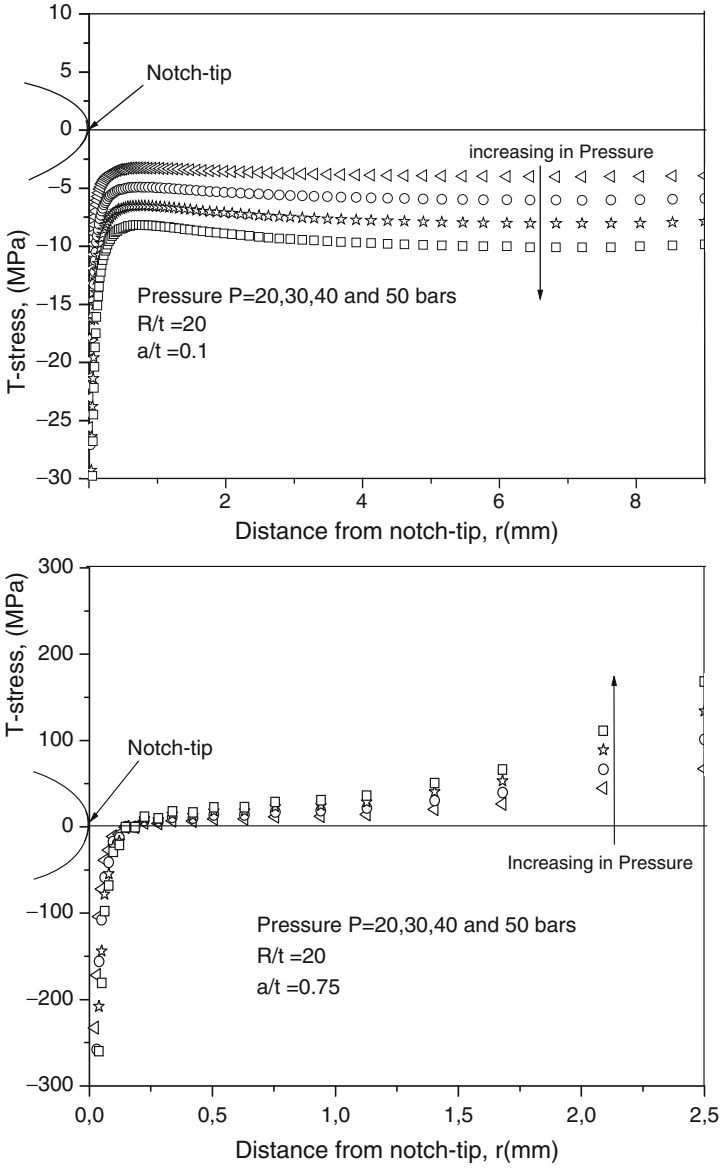


**Fig. 16** Evolution of the T-stress along ligament in a pipe with a longitudinal surface notch under different internal pressure

A constraint parameter seems to be immediately plausible and the elastic *T*-stress seems to be convenient for constraint analysis. The predicted fracture driving force lines $K_{\rho,app} = f(T_{ef,app})$ are constructed for a pipe with a longitudinal surface notch under increasing pressure and compared with the material failure curve of the X52 pipe steel. The fracture driving force line $K_{\rho,app} = f(T_{ef,app})$ is a parabolic function

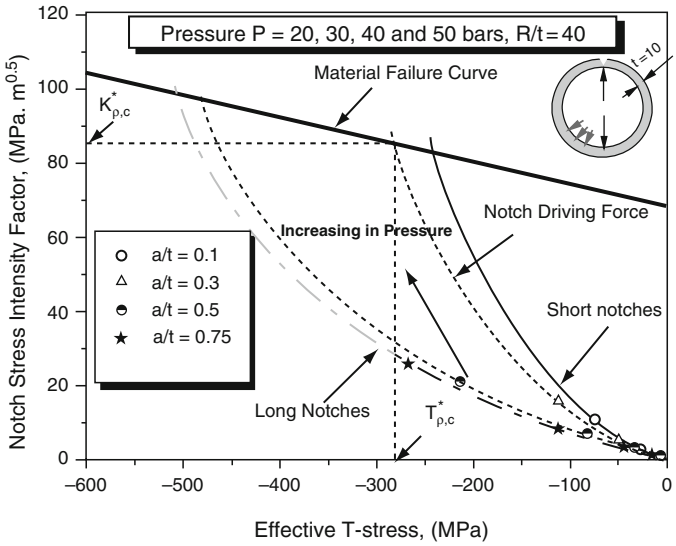


**Fig. 17** Notch driving force lines and material failure curve for a pipe with a longitudinal surface notch: a/t = 0.1; 0.3; 0.5; 0.75 and R/t = 40

for low value of the applied notch stress intensity factor and becomes practically linear when the value of $K_{\rho,app}$ increases. The notch driving force line is shifted to higher values of $(-T_{ef,app})$ when the constraint decreases, i.e. the notch aspect ratio $a/t$ increases (Fig. 17). Intersection of the material failure curve with the notch driving force line leads to fracture and can be written in the form

$$K_{\rho,app}\left(T_{ef,app}\right) = K_{\rho,c}f\left(T_{ef,c}\right) \tag{19}$$

## 7 Conclusions

The concept of the T-stress in the case of the crack stress distribution has been extended to the notch stress distribution. It should be noted that the present results of the effective T-stress estimation is consistent with the results obtained by the method proposed by Hadj Meliani et al., [48]. We have adopted the first nonvanishing term from the series solutions of Williams'. Its applicability for every crack length is studied. The effects of the next nonvanishing term on the stress level are studied for extreme cases such as very shallow or very deep notches. We found that the next term may not be negligible for notch length. Using the principle of superposition, by varying the applied load parallel to the notch line, different constraint levels can be obtained for single Pipeline geometry. The Biaxiality parameter concept also has the potential to predict crack branching. Because the $B$ can account for differences in fracture behaviour, summarized by several authors, that the T-stress plays a significant role in fracture. The magnitude of compression

T-stress (on the average) and the biaxiality are greater than those of large diameters of Pipelines. The failure mechanisms caused by less constraint in the thickness direction alleviate the stress intensification near the crack tip and result in elevated apparent $K$. The $K$-$T$ methodology is used and T-stress is identified to quantify the constraint at the notch tip. Procedures to shift the mechanical properties curve between Pipelines of different in plane constraint levels are developed which enables the determination of the transition curve of non-standard flawed structures from the experimental results of standard specimens.

## References

1. M.L. Williams, On the stress distribution at the base of stationary crack. ASME J. Appl. Mech. **24**, 109–14 (1957)
2. J.R. Rice, Limitations to the-scale yielding approximation for crack-tip plasticity. J. Mech. Solids **22**, 17–26 (1974)
3. S.G. Larsson, A.J. Carlsson, Influence of non-singular stress terms and specimen geometry on small-scale yielding at crack tips in elastic-plastic materials. J. Mech. Phys. Solids **21**, 263–278 (1973)
4. P.S. Leevers, J.C. Radon, Inherent stress biaxiality in various fracture specimen geometries. Int. J. Fract. **19**, 11–25 (1982)
5. D.E. Richardson, A new biaxial stress fracture criterion, Ph.D. dissertation, Clemson University, 1991
6. Y.J. Chao, X. Zhang, Constraint effect in brittle fracture. 27th National Symposium on Fatigue and fracture, ASTM STP 1296, ed. by R.S. Piascik, J.C. Newman, Jr., D.E. Dowling, American Society for Testing and Materials, Philadelphia, 1997, pp. 41–60
7. Y.J. Chao, S. Liu, B.J. Broviak, Variation of fracture toughness with constraint of PMMA specimens. Proc. ASME-PVP Conf. **393**, 113–120 (1999)
8. Y.J. Chao, S. Liu, B.J. Broviak, Brittle fracture: variation of fracture toughness with constraint and crack curving under mode I conditions. Exp. Mech. **41**(3), 232–241 (2001)
9. D.J. Smith, M.R. Ayatollahi, M.J. Pavier, The role of T-stress in brittle fracture for linear elastic materials under mixed mode loading. Fatigue Eng. Mater. Struct. **24**(2), 137–150 (2001)
10. M.R. Ayatollahi, M.J. Pavier, D.J. Smith, Mode I cracks subjected to large T-stresses. Int. J. Fracture **117**(2), 159–174 (2002)
11. ASTM E399, Standard test methods for plane-strain fracture toughness of metallic materials, Annual Book of ASTM Standards, (1997) Vol. 03.01.
12. J.R. Willis, Asymptotic analysis in fracture: an update. Int. J. Fracture **100**, 85–103 (1999)
13. M.G. Dawes, H.G. Pisarski, O.L. Towers, S. Williams, Fracture mechanics measurements of toughness in welded joints, in *Fracture Toughness Testing: Methods, Interpretation, and Application* (The Welding Institute, Cambridge, 1982), pp. 165–178
14. J.D.S. Sumpter, An experimental investigation of the T stress approach, in *Constraint effects Fracture, ASTM STP 1171*, ed. by E.M. Hackett, K.-H. Schwalbe, R.H. Dodds (American Society for Testing and Materials, Philadelphia, 1993), pp. 492–502
15. M.T. Kirk, R.H. Dodds, J and CTOD estimation equations for shallow cracks in single edge notch bend specimens. Shallow crack fracture mechanics, toughness tests and applications. TWI (1992).
16. M.T. Kirk, The second ASTM/ESIS symposium on constraint effects in fracture; an overview. Int. J. Pres. Vessels Piping **64**, 259–275 (1995)
17. T. Nakamura, D.M. Parks, Determination of elastic T-stress along three-dimensional crack fronts using an interaction integral. Int. J. Solids Struct. **29**, 1597–1611 (1991)
18. B.A. Bilby, G.E. Cardew, M.R. Goldthorpe, I.C.A. Howard, Finite element investigation of the effect of specimen geometry on the fields of stress and strain at the tips of stationary

cracks, in *Size Effects in Fracture* (Mechanical Engineering Publications Limited, London, 1986), pp. 37–46
19. C. Betegon, J.W. Hancock, Two-parameter characterization of elastic plastic crack tip fields. ASME J. Appl. Mech. **58**, 104–110 (1991)
20. Z.Z. Du, J.W. Hancock, The effect of non-singular stresses on crack tip constraint. J. Mech. Phys. Solids **39**, 555–67 (1991)
21. B. Cotterell, Notes on the paths and stability of cracks. Int. J. Fracture Mech. **2**, 526–533 (1966)
22. B. Cotterell, On fracture path stability in the compact tension test. Int. J. Fracture Mech. **6**, 189–192 (1970)
23. S. Melin, Why do cracks avoid each other? Int. J. Fracture **23**, 37–45 (1983)
24. M. Marder, Instability of crack in a heatep strip. Phys. Rev. E. **49**(1), 49–53 (1994)
25. A. Yuse, M. Sano, Transition between crack patterns in quenched glass plates. Nature **362**, 329 (1993). London
26. B. Cotterell, J.R. Rice, Slightly curved or kinked cracks. Int. J. Fracture **16**, 155–169 (1980)
27. A.S. Selvarathinam, J.G. Goree, T-stress based fracture model for cracks in isotropic materials. Eng. Fract. Mech. **60**, 543–561 (1998)
28. M. Ramulu, A.S. Kobayashi, Dynamic crack curving: a photoelastic evaluation. Exp. Mech. **23**, 1–9 (1983)
29. K. Ravi-Chandar, W.G. Knauss, An experimental Investigation into Dynamic Fracture: III. On Stready-state Crack Propagation and Crack Branching. Int. J. Fracture. **26**, 141–154; 198–200 (1984)
30. W.G. Knauss, K. Ravi-Chandar, Some basic problems in stress wave dominated fracture. Int. J. Fracture **27**, 127 (1985)
31. N.A. Fleck, J.W. Hutchinson, Z. Suo, Crack path selection in a brittle adhesive layer. Int. J. Solids Struct. **27**, 1683–1703 (1991)
32. L. Banks-sills, J. Schwartz, Fracture testing of Brazilian disk sandwich specimens. Int. J. Fracture **118**, 191–209 (2002)
33. M.T. Kirk, K.C. Koppenhoefer, C.F. Shih, Effect of constraint on specimen dimensions needed to obtain structurally relevant toughness measures, in *Constraint in Fracture, ASTM STP 1171*, ed. by E.M. Hachett, K.-H. Schwalbe, R.H. Dodds (American Society for testing and Materials, Philadelphia, 1993), pp. 79–103
34. W.A. Sorem, R.H. Dodds, S.T. Rolfe, Effects of crack depth on elastic plastic fracture toughness. Int. J. Fracture **47**, 105–126 (1991)
35. J.W. Hancock, W.G. Reuter, D.M. Parks, Constraint and toughness parameterized by T, in *Constraint effects in Fracture, ASTM STP 1171*, ed. by E.M. Hackett, K.-H. Schwalbe, R.H. Dodds (American Society for Testing and Materials, Philadelphia, 1993), pp. 21–40
36. J.D.S. Sumpter, An experimental investigation of the T stresses approach, in *Constraint effects in Fracture, ASTM STP 1171*, ed. by E.M. Hackett, K.-H. Schwalbe, R.H. Dodds (American Society for Testing and Materials, Philadelphia, 1993), pp. 492–502
37. S. Ganti, D.M. Parks, Elastic plastic fracture mechanics of strength-mismatch interface cracks, in *Recent Advances in Fracture*, ed. by R.K. Mahudhara, et al. (The Minerals, Metals and Material Society, London, 1997), pp.13–25
38. Z.L. Zhang, M. Hauge, C. Taulow, The effect of T -stress on the near tip stress field of an elastic-plastic interface crack, in *Proceedings of the Ninth International Conference on Fracture*, ed. by B.L. Karihaloo, et al., vol 4 (Pergamon, Amsterdam, 1997), pp. 2643–2650
39. X.F. Li, L.R. Xu, T-stresses across static crack kinking. J. Appl. Mech. **74**, N2, 181–190 (2007)
40. S. Melin, The influence of the T-Stress on the directional stability of cracks. Int. J. Fracture **114**, 259–65 (2002)
41. D.E. Richardson, J.G. Goree, Experimental verification of a new two parameter fracture model, in *Fracture Mechanics: Twenty-Third Symposiums.* ASTM STP 1189, 1993, pp. 738–750
42. B. Yang, K. Ravi-Chandar, Evaluation of elastic T-stress by the stress difference method. Eng. Fract. Mech. **64**, 589–605 (1999)

43. Z.B. Kuang, X.P. Xu, Stress and strain fields at the tip of a sharp V-notch in a power-hardening material. Int. J. Fracture **35**, 39–50 (1987)
44. M. Yang, S.W. Yu, in: V.V.Panasijuket. al. ed., Advances in fracture resistance in materials, in *Proceedings of the International Conference Fracture (ICF9)*, Turin, 1993, pp. 301–308
45. S. Yang, Y.J. Chao, Asymptotic deformation and stress fields at the tip of a sharp notch in an elastic-plastic material. Int. J. Fracture **54**, 211–224 (1992)
46. G. Pluvinage, *Fracture and Fatigue Emanating from Stress Concentrators* (Kluwer, Dordrecht, 2003)
47. M.H. Meliani, M. Benarous, A. Ghoul, Z. Azari, Volumetric method to understand the effect of T-stress and stress intensity factor in arc of pipe. African Phys. Rev. 1 Special Issue (Microfluidics):0006 12 (2007)
48. M. Hadj Meliani, Z. Azari, G. Pluvinge, Constraint Parameter for a Longitudinal Surface Notch in a Pipe Submitted to Internal Pressure. Key Eng. Mater. **399**(Advances in Strength of Materials), 3–11 (2009)
49. P. Hutar, S. Seitl, Z. Knésl, Quantification of the effect of specimen geometry on the fatigue crack growth response by two-parameter fracture mechanics. Mater. Sci. Eng. A **387–389**, 491–494 (2004)
50. S. Stanislav, Z. Knésl, Two parameter fracture mechanics: fatigue crack behavior under mixed mode conditions. Eng. Fract. Mech. **75**, 857–865 (2008)
51. M. Creager, P.C. Paris, Elastic Celd equations for blunt cracks with reference to stress corrosion cracking. Int. J. Fracture **3**, 247–251 (1967)
52. M.H. Meliani, Z. Azari, G. Pluvinge, Y. Matvienko, New approach for the T-stress estimation for specimens with a U-notch. New Trends in Fatigue and Fracture, 9th Meeting – NT2F9 –, Failures of materials and structures by fatigue and fracture, Belgrade, 12–14 Oct 2009
53. M.H. Meliani, G. Pluvinage, J. Capelle, Gouge assessment for pipes and associated transferability problems. Eng. Fail. Anal. **17**(2010), 1117–1126 (2009)
54. M.H. Meliani, Z. Azari, G. Pluvinge, YuG Matvienko, The effective T-stress estimation and crack paths emanating from U-notches. Eng. Fract. Mech. **77**, 1682–1692 (2010)
55. B. Ozmat, A.S. Argon, D.M. Parks, Growth modes of cracks in creeping type 304 stainless steel. Mech. Mater. **11**, 1–17 (1999)
56. B. Nguyen, P. Onck, E. Van der Giessen, Crack-tip constraint effects on creep fracture. Eng. Fract. Mech. **65**, 467–490 (2000)

# Crude-Oil Flow Modelling in Pipeline Conditions

**Madjid Meriem Benziane and Abdelkrim Liazid**

**Abstract** This paper deals with the relation between rheological properties and crude oil structure for describing its flow characteristics during transport by pipeline mode. The aim is focused on testing the Phan-Thien and Tanner model resulting from polymers rheology. Algerian crude-oil is considered for application. The axisymmetric flow problem with isothermal conditions is considered in this work. The stresses computation using this model is an important step allowing a subsequently study of some important phenomena like pipe corrosion or pressure drop which is controlled by the friction factor under turbulent flow conditions. The obtained results are presented and discussed. The tested model seems to be an interesting predictive tool to capture the crude-oil characteristics.

## 1 Introduction

The Crude oil flow generates normal and tangential stresses when pipeline transport mode is used. In order to capture the fluid-wall interaction of the technical installations, it is necessary to determine these stresses. As measurements in vivo are difficult, it is interesting to use modelling technique with realistic considerations to evaluate crude oil flow properties. The crude oil flow is very particular and cannot be represented by the traditional models based on the homogeneous fluid assumption which considers only the viscosity variation according to the shearing rate. The theory of the diluted suspensions constitutes the first step towards consideration of the micro-structural characteristic of crude oil which is considered as a solution of rigid particles. A dynamical model with a non-linear differential structure makes

M.M. Benziane
University Hassiba Benbouali Chlef, B.P. 151, Chlef 02000, Algeria
e-mail: mbmadid2001@yahoo.fr

A. Liazid (✉)
Laboratory LTE ENSET-Oran, B.P. 1523, El Mnaouer, Oran 31000, Algeria
e-mail: ab_liazid@hotmail.com

T. Boukharouba et al. (eds.), *Integrity of Pipelines Transporting Hydrocarbons*,
NATO Science for Peace and Security Series C: Environmental Security,
DOI 10.1007/978-94-007-0588-3_17, 

possible to consider the flow unstable character. Lastly, a very significant branch of rheology is interested with polymer solutions. So, there are many analogies in flow behaviour between these polymer solutions and crude oils. There are two theories, rising from this branch, allowing a micro-structural analysis: The Dumbbell theory and the network analysis. The model of Phan-Thien and Tanner [1], resulting from the network analysis, is considered in this work. This model is proposed to avoid the deficient of the traditional modelling approach.

## 2 Crude Oil Description

Crude oil is a complex fluid in perpetual renewal, ensuring multiple functions essential to the industrial activities. Deformability is, with the capacity of stacking, a significant characteristic in the dynamics of the crude oil flow. The methodology for measuring the rheological properties is now well established. To understand the complex behaviour of crude oils, a more fundamental knowledge of the relationship between microstructure and rheology is, however, necessary. In addition, the influence of the molecular composition on the mechanisms of crystallisation should help to explain the differences between crude oils from various sources. This investigation was based on the following guide lines:

- In static conditions of cooling, an accurate determination of the storage and loss moduli, measured under small deformations can be undertaken. The storage moduli of the gelled oils are in general very high, (106 Pa) in the range of temperatures between 8°C and ambient temperature. One can establish experimentally the relation between the amount of crystals and the shear moduli for oils with different molecular compositions.
- The morphology of the crystals is an important aspect which is in direct relation with the rheology of crude oils and which is determined by the crystallisation process. The rheological behaviour of the studied crude oil is shown in the Fig. 1.

## 3 Flow Regime

When pipeline transport mode is used for crude oil, flow conditions depend on the rheological characteristics of the hydrocarbon phase. Laminar or turbulent flow regime can be found depending on the apparent shear viscosity. Typically, liquid velocity is between 1 and 5 m/s. At 1 m/s, a viscosity of 100 cP (0.1 Pa·s) leads to a Reynolds number magnitude of the order of 1,000 [2] and flow can be considered laminar. But when viscosity is around 10 cP (0.01 Pa·s), Reynolds number increases to 10,000. So, for light crude oil and condensate, flow regime is mainly turbulent. In this work, a cylindrical pipe with radius R and cylindrical coordinates $(r, \theta, z)$ are considered, Fig. 2:

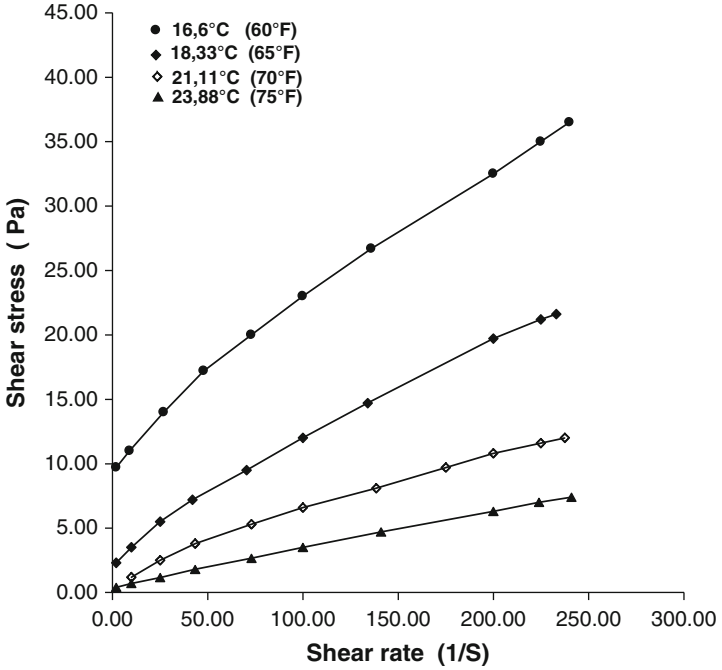


**Fig. 1** Rheological behaviour of Algerian crude oil

**Fig. 2** Velocity profile

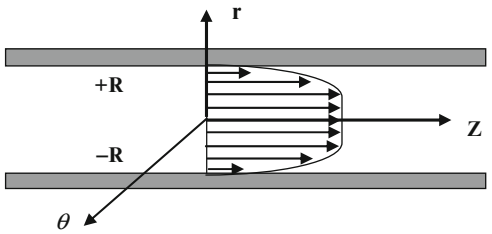


With considering the flow symmetry, the Navier Stokes equation can be written as:

$$\frac{dP}{dz} = \frac{1}{r}\frac{d}{dr}\left[r\,\eta\frac{dV}{dr}\right] \tag{1}$$

Where $\eta$ represents the apparent viscosity, setting:

$$-a\,r = \frac{d}{dr}\left[r\,\eta\,\frac{dV}{dr}\right] \text{ with } a \rangle 0 \tag{2}$$

The equation (2) can be written as:

$$-\,\mathrm{a\ r} = \frac{\mathrm{d}}{\mathrm{dr}}[\mathrm{r}\ \ \tau_{\mathrm{rz}}] \tag{3}$$

After testing various models for describing the apparent viscosity (Cross, Quemada,...), the Krieger and Dougherty law defined by the Eq. 4 seems to be the more adapted.

$$\eta = \eta_{\infty} + \frac{\eta_0 - \eta_{\infty}}{1 + \left[\dfrac{\tau}{\tau_{\mathrm{c}}}\right]^{\mathrm{m}}} \tag{4}$$

We have:

$$\tau = \left(\frac{\eta_0 - \eta}{\eta - \eta_{\infty}}\right)^{\frac{1}{\mathrm{m}}} \cdot\ \tau_{\mathrm{c}} \tag{5}$$

After integration, the Eq. 3 becomes:

$$-\frac{\mathrm{ar}}{2} = \left(\frac{\eta_0 - \eta}{\eta - \eta_{\infty}}\right)^{\frac{1}{\mathrm{m}}} \cdot\ \tau_{\mathrm{c}} \tag{6}$$

As $\tau_c$ is negative we can write:

$$\frac{\mathrm{ar}}{2} = \left(\frac{\eta_0 - \eta}{\eta - \eta_{\infty}}\right)^{\frac{1}{m}} \cdot |\tau_c| \tag{7}$$

$$\eta = \frac{(\tau_{\mathrm{c}})^{\mathrm{m}} \cdot \eta_0 + \eta_{\infty}\left(\frac{\mathrm{ar}}{2}\right)^{\mathrm{m}}}{\left(\frac{\mathrm{ar}}{2}\right)^{\mathrm{m}} + (\ \tau_{\mathrm{c}})^{\mathrm{m}}} \tag{8}$$

and:

$$\dot{\gamma} = \frac{|\tau|}{\eta} = \frac{-\frac{\mathrm{ar}}{2}\left[\left(\frac{\mathrm{ar}}{2}\right)^{\mathrm{m}} + (\tau_{\mathrm{c}})^{\mathrm{m}}\right]}{\left[(\ \tau_{\mathrm{c}})^{\mathrm{m}} \cdot \eta_0 + \eta_{\infty}\left(\frac{\mathrm{ar}}{2}\right)^{\mathrm{m}}\right]} \tag{9}$$

Thus the velocity profile can be obtained from Eq. 10:

$$\frac{\mathrm{dU}}{\mathrm{dr}} = \frac{-\frac{\mathrm{ar}}{2}\left[\left(\frac{\mathrm{ar}}{2}\right)^{\mathrm{m}} + (\tau_{\mathrm{c}})^{\mathrm{m}}\right]}{\left[(\ \tau_{\mathrm{c}})^{\mathrm{m}} \cdot \eta_0 + \eta_{\infty}\left(\frac{\mathrm{ar}}{2}\right)^{\mathrm{m}}\right]} \tag{10}$$

For m =1, we get:

$$\frac{\mathrm{dU}}{\mathrm{dr}} = \frac{-\frac{\mathrm{ar}}{2}\left[\left(\frac{\mathrm{ar}}{2}\right) + (\tau_{\mathrm{c}})\right]}{\left[(\ \tau_{\mathrm{c}}) \cdot \eta_0 + \eta_{\infty}\left(\frac{\mathrm{ar}}{2}\right)\right]} \tag{11}$$

The velocity profile, Fig. 2, is obtained after integrating the Equation 11, setting:

$$A = \frac{2\eta_0 \cdot |\tau_c|}{a\eta_\infty} \tag{12}$$

We obtain:

$$U(r) = \frac{\left(\frac{\Delta p}{L}\right)}{4\eta_\infty}\left(R^2 - r^2\right) + \left[\frac{\left(\frac{\Delta p}{L}\right)A}{2\eta_\infty} - \frac{|\tau_c|}{\eta_\infty}\right](r - R) + \left[\frac{|\tau_c|A}{\eta_\infty} - \frac{\left(\frac{\Delta p}{L}\right)A^2}{2\eta_\infty}\right] \tag{13}$$

With: $A = \frac{2\eta_0|\tau_c|}{\left(\frac{\Delta p}{L}\right)\eta_\infty}$ and $B = \ln\left|\frac{r+A}{A+R}\right|$

This velocity profile can be obtained for a given pressure drop.

## 4 Pressure Drop and Shear Stress

The shear stress at the wall can be estimated from the pressure drop value. In steady state flow conditions we can use a simple formula deduced from the force balance law, Fig. 3.

This formula, Eq. 14, traduces the relationship between wall stress and imposed pressure drop in the system. It can be easily observed that this equation is not dependent on the fluid rheology.

$$\tau_w = \frac{\partial p}{\partial z}\frac{r}{2} \tag{14}$$

In the laminar regime, pressure drop calculation is related to the determination of the oil apparent shear viscosity. When the viscosity is known (or non-Newtonian

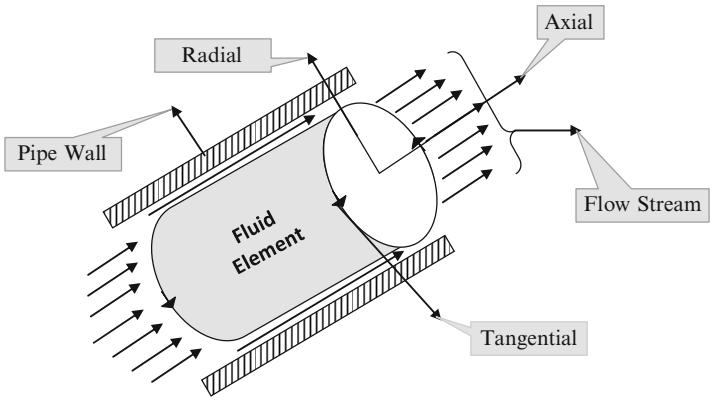


**Fig. 3** Force balance on a fluid portion

fluid rheology is known), the pressure drop calculation can be achieved using the Eq. 14. The problem is to get the fluid rheological knowledge [3–5]. The stresses at the wall are different when flow regime is laminar or turbulent [6, 7]. So, the first step consists on getting the apparent viscosity law [8–11]. The pressure drop (ΔP/L) in a pipe is given by:

$$\frac{\Delta p}{L} = f\frac{\rho U^2}{R} \tag{15}$$

$U$ is the average velocity of the flow, $R$ is the pipe radius, $\rho$ the flowing phase volume mass and $f$ the friction factor which is only dependent upon the Reynolds number of the flow. This friction factor in the laminar Poiseuille flow case is given by:

$$f = \frac{16}{R_e} \text{ and } R_e = \frac{\rho UD}{\mu} \tag{16}$$

From the velocity profile, Eq. 13, we can compute the gradient rate tensor of the global flow $L$, the macroscopic deformation rate tensor $D$ and the gradient rate tensor of the local flow $\varsigma$.

$$L_{ij} = \frac{\partial u_i}{\partial u_j}, D_{ij} = \frac{1}{2}\left(\frac{\partial u_i}{\partial u_j} + \frac{\partial u_j}{\partial u_i}\right), \varsigma = (L - \xi D) \tag{17}$$

These tensors are introduced in the constitutive equation of the Phan-Thien and Tanner model [1] (see appendix) to obtain a system of partial differential equations. This system can be solved numerically.

$$\begin{cases} \dfrac{\partial \tau_{rr}}{\partial t} = -\dfrac{\sigma_i}{\lambda_{i,0}}\ \tau_{rr} - AA\ \ \zeta.\ \tau_{rz} \\ \dfrac{\partial \tau_{rz}}{\partial t} = -\dfrac{\sigma_i}{\lambda_{i,0}}\ \tau_{rz} - AA\ [\ \xi.\ \tau_{zz} + (\ \xi - 2).\ \tau_{rr}] + 2\dfrac{\eta_m}{\lambda_{i,0}} AA \\ \dfrac{\partial \tau_{zz}}{\partial t} = -\dfrac{\sigma_i}{\lambda_{i,0}}.\ \tau_{zz} - AA(\ \xi - 2)\ \tau_{rz} \end{cases} \tag{18}$$

with:

$$AA = \frac{-\frac{ar}{2}\left[\left(\frac{ar}{2}\right) + (\tau_c)\right]}{\left[(\ \tau_c)\eta_0 + \eta_\infty\left(\frac{ar}{2}\right)\right]} \tag{19}$$

## 5 Results and Discussions

Figures 4 and 5 represent the variation of the stresses according time and pipe radius obtained from the resolution of the mathematical system (18). Maximum stresses levels are at the wall. The tangential stresses are practically fifteen times superior to the normal ones.

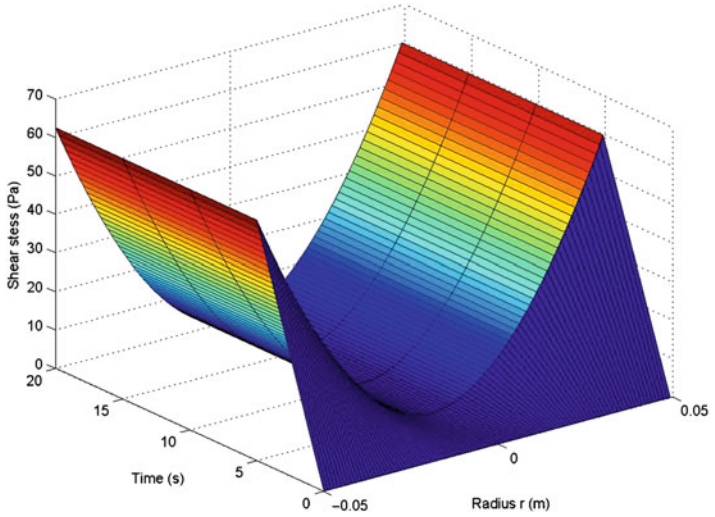


**Fig. 4** Shear stress according to time and pipe radius, Algerian crude oil

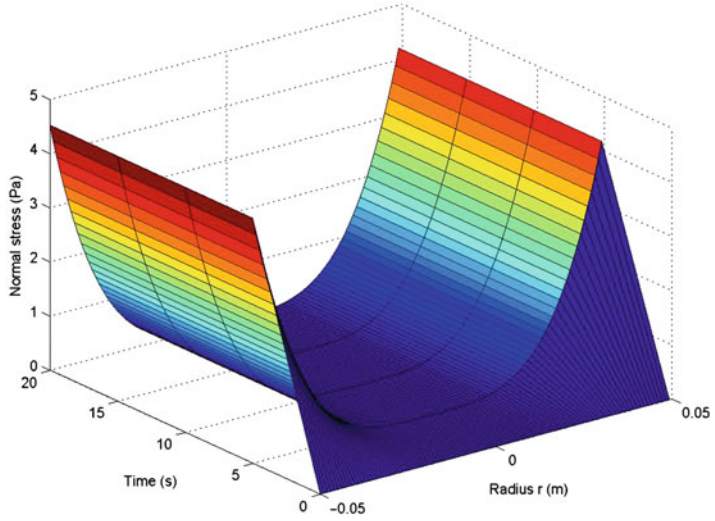


**Fig. 5** Normal stress according to time and pipe radius, Algerian crude oil

The Figs. 6–8 show the comparison between results obtained with the analytic model (Eqs. 14 and 15) and MPTT model concerning the pressure drop variation according to the mean velocity for the Algerian crude oil at three different temperatures.

On these figures, it can be noticed that the Krieger & Dougherty model is well adapted. One can conclude the good agreement between these results. The MPTT model predicts correctly the tendency of parietal constraints. The prediction is better beyond the flow velocity of 2 m/s.

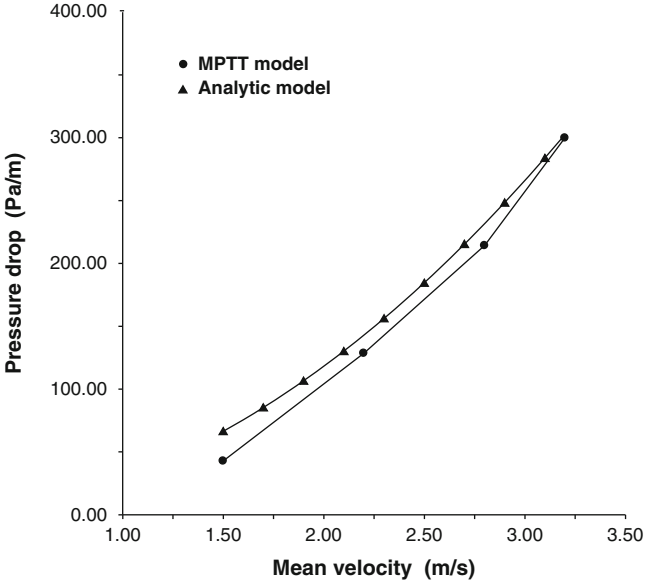


**Fig. 6** Comparison between MPTT model and analytic model for pressure drop according to mean velocity of Algerian crude oil, (63°F)

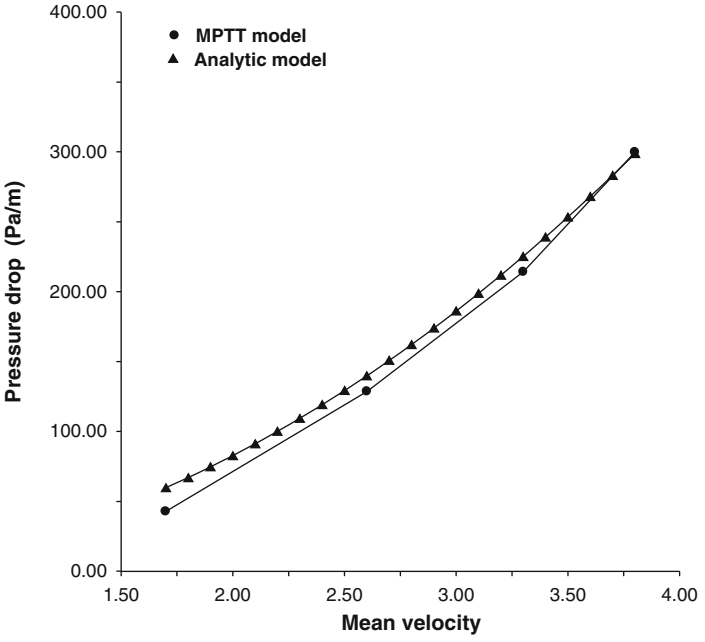


**Fig. 7** Comparison between MPTT model and analytic model for pressure drop according to mean velocity of Algerian crude oil, (68°F)

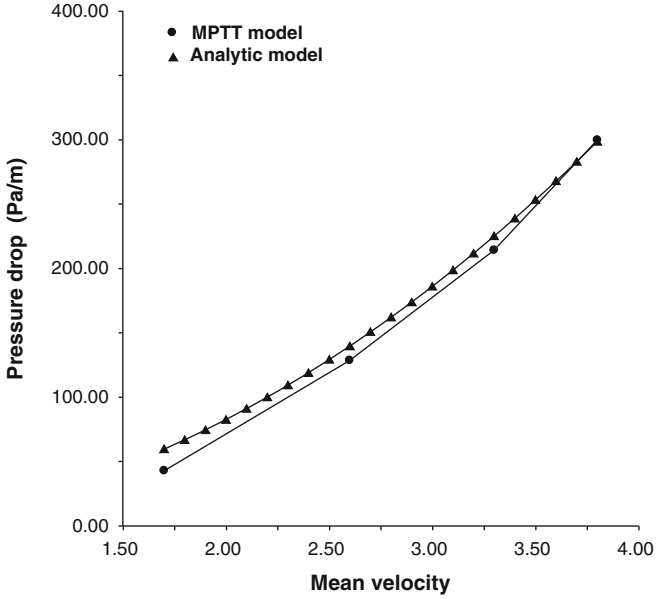


**Fig. 8** Comparison between MPTT model and analytic model for pressure drop according to mean velocity of Algerian crude oil, (74°F)

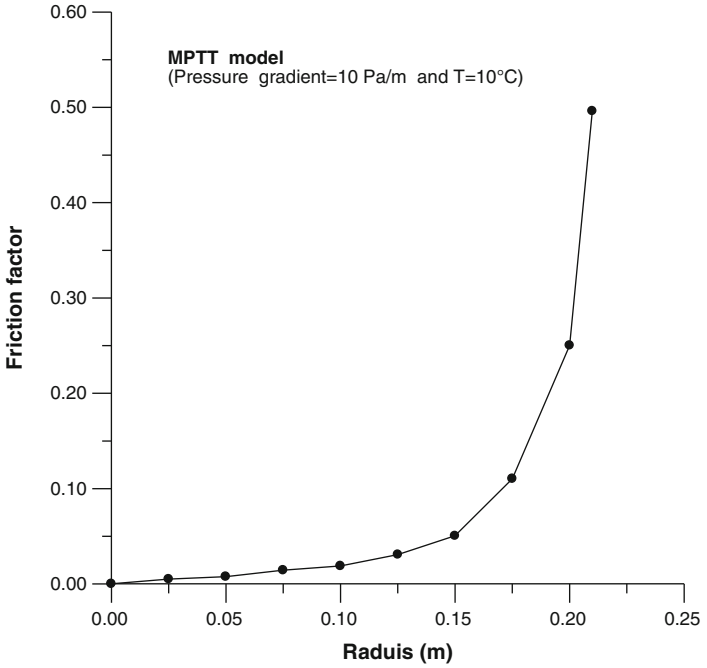


**Fig. 9** Friction factor according to pipe radius for $\Delta p/L = 10\ Pa/m$ and T=10°C

Finally, from shear stress profile obtained with the MPTT model, the friction factor evolution can be obtained as shown in Fig. 9 for the fluid temperature case T = 10°C. Near the internal pipe wall the friction factor increases considerably to reach the value of 0.5.

## 6 Conclusions

Crude oil is a non-Newtonian fluid presenting a complex behaviour. So, the modelling approach of its flow characteristics is not easy because the traditional methods are not satisfactory. This work has tested the Phan-Thien and Tanner model developed from polymers rheology. Application has concerned the Algerian crude oil flow. This model is adapted because it seems in our opinion more realistic, because based on a micro-structural description of the fluid. The obtained results seem to be acceptable and realistic. It should be noticed that the model of Phan-Thien and Tanner offers greatest flexibility on configurations choice and boundary conditions. Next step is to apply more complex boundary conditions in order to have a better modelling of the crude oil flow. Finally the rheological characteristics knowledge of crude oil is also an important step to study some important phenomenon such as pipelines corrosion. Thermal conditions must be complete the next work.

## References

1. N. Phan Thien, R.-I. Tanner, A new constitutive equation derived from network theory. J. Non-Newton. Fluid Mech. **2**, 353–365 (1977)
2. E.G. Barry, Pumping non-Newtonian waxy crude oils. J. Instate Petrol. **57**(554), 74–85 (1971)
3. M. Rudman, H.M. Blackburn, L.J.W. Graham, L. Pullum, Turbulent pipe flow of shear-thinning fluids. J. Non-Newton. Fluid Mech. **118**, 33–48 (2004)
4. A. Saniere, I. Hénaut, J.F. Argillier, Pipeline transportation of heavy oils, a strategic, economic and technological challenge. Oil Gas Sci. Technol. Rev. IFP **59**(5), 455–466 (2004)
5. A. Sinquin, T. Palermo, Y. Peysson, Rheological and flow properties of gas hydrate suspensions. Oil Gas Sci. Technol. **59**(1), 41–57 (2004)
6. Cheng Chang, Q. Dzuy Nguyen, Rønningsen Hans Petter, Isothermal start-up of pipeline transporting waxy crude oil. J. Non-Newton. Fluid Mech. **87**, 127–154 (1999)
7. I. Masalova, A. Ya, P.S. Malkin, K. Wilson, The rheological characterization and pipeline flow of high concentration water-in-oil emulsions. J. Non-Newton. Fluid. Mech. **112**, 101–114 (2003)
8. A. Farah Marco, C. Oliveira Roberto, Caldas Jorge Navaes, Rajagopal Krishnaswamy, Viscosity of water-in-oil emulsions: variation with temperature and water volume fraction. J. Petrol. Sci. Eng. **48**, 169–184 (2005)
9. M. Kane, M. Djabourov, Rheology and structure of waxy crude oils in quiescent and under 147 shearing conditions. J. Fuel **83**, 1591–1605 (2004)
10. G. Vinay, A. Wachs, I. Frigaard, Start-up transients and efficient computation of isothermal waxy crude oil flows. J. Non-Newton. Fluid Mech. **143**, 141–156 (2007)
11. D. Dan, G. Jing, Apparent viscosity prediction of non-Newtonian water-in-crude oil emulsions. J. Petrol. Sci. Eng. **53**, 113–122 (2006)

# Corrosion Risk Assessment of Pipelines Based on Cathodic Protection Survey

**Luciano Lazzari**

**Abstract** This paper deals with a methodological approach for external corrosion risk assessment of buried and submerged pipelines based on data achieved through a Cathodic Protection Survey. The main techniques used, for example, CIPP (Close Interval Potential Profile) and TGM (Transversal Gradient Method) are described. Interpretations and analyses of data are illustrated using practical case studies. As well the prioritization of intervention is discussed using a risk matrix approach.

## 1 Cathodic Protection Principles

### *1.1 Introduction*

Buried pipelines are protected against corrosion by a combination of cathodic protection (CP) and a coating. This combined protection system represents the optimum from both technical and cost-effective point of view.

CP is an electrochemical method of corrosion prevention which can be applied to metals exposed to conductive environments. As shown in Fig. 1, this technique utilises the circulation of a continuous current between an electrode (anode) placed in the environment and the metallic structure to be protected (cathode). This cathodic current lowers the potential of the metal and reduces, or even halts, its corrosion rate.

The circulating current is obtained either by *galvanic anodes* (also called *sacrificial anodes*) or by *impressed current*, thus defining the two types of CP systems. In the case of galvanic anodes, CP is achieved through galvanic coupling with a less noble metal (Fig. 1a). For example, aluminium and zinc are used for the protection of steel in sea water, magnesium is employed for the protection of steel in soil and fresh water; pure iron is usually utilised for the protection of stainless steel and copper alloys.

L. Lazzari (✉)
Department of CMIC "G.Natta", Politecnico di Milano, Via Mancinelli, 7 – 20131 Millan, Italy
e-mail: Luciano.lazzari@polimi.it

T. Boukharouba et al. (eds.), *Integrity of Pipelines Transporting Hydrocarbons*, NATO Science for Peace and Security Series C: Environmental Security,
DOI 10.1007/978-94-007-0588-3_18, 

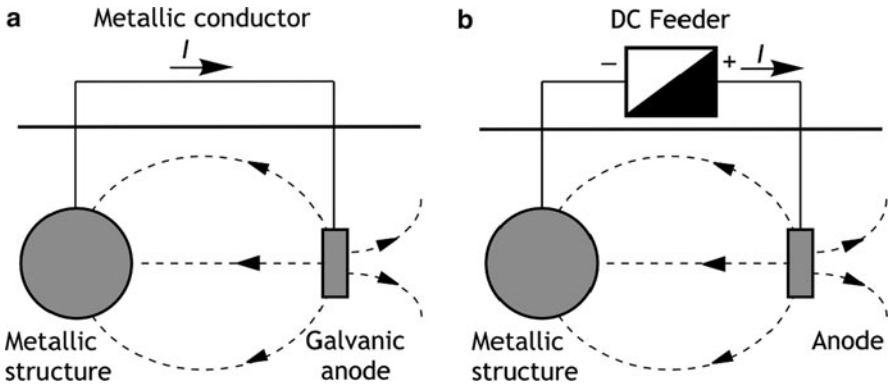


**Fig. 1** Types of cathodic protection: (**a**) by galvanic anodes; (**b**) by impressed current system [1]

Impressed current systems make use of a DC generator (Fig. 1b), with the positive pole connected to an anode, generally made of insoluble metal, (for example silicon cast iron, graphite, activated titanium) and the negative pole connected to the structure.

### *1.2 Protection Potential*

The cathodic current brings the metal potential below the equilibrium potential ($E < E_{eq}$) thus inhibiting the corrosion or oxidation process. These conditions are referred to as *thermodynamic immunity*. Equilibrium potential, $E_{eq}$, can be defined as the *protection-potential*, below which corrosion stops. The well known protection-potential value for steel is –0.85 V CSE (copper sulphate reference electrode). Table 1 reports protection-potentials of metals in soil and sea water [1].

### *1.3 Protection Current Density*

To obtain CP, that is to lower the potential below the protection-potential, it is necessary to supply an adequate current to the structure. This current is determined by the so-called *protection current density*. Table 2 reports protection current density for steel in various environments [1].

## 2 Cathodic Protection Monitoring

CP conditions are verified by means of potential measurements. Figure 1 reports the electrical scheme of the measurement which is carried out using a high-impedance voltmeter connected to the structure (positive) and a reference electrode (negative).

**Table 1** Protection potentials used in soil and sea water [1]

| | Soil | Sea water | |
|---|---|---|---|
| Metallic materials | V CSE | V SCE | V ZN |
| Carbon and low alloy steels: | | | |
| - Normal conditions | −0.85 | −0.80 | +0.25 |
| - Anaerobic conditions | −0.95 | −0.90 | +0.15 |
| - In concrete | −0.75 | −0.70 | +0.35 |
| Copper and its alloys | −0.45 to 0.60 | −0.50 | +0.55 |
| Lead | −0.50 to 0.65 | −0.45 to 0.60 | +0.60 |
| Zinc | −1.00 | −1.05 | 0 |
| Aluminium | −0.8 | −0.9 | +0.15 |
| Stainless Steels | −0.40 | −0.50 | +0.55 |

**Table 2** Typical values of the protection current density for steel in various environments [1]

| Environment | Protection current density $(mA/m)^2$ |
|---|---|
| Bare steel | |
| Soil | |
| Neutral aerated | 20–150 |
| Water saturated | 2–20 |
| Hot pipeline | 30–60 |
| Concrete | |
| Atmospherically exposed | 5–15 |
| Water saturated | 0.2–2 |
| Fresh water | |
| Room temperature | 30–160 |
| Warm to hot | 50–160 |
| Sea water | 50–550 |
| Acid solutions | 50–1.500 |
| Coated steel | |
| Soil | 0.01–1 |
| Sea water | 0.1–10 |

Copper/copper sulphate reference electrodes are most commonly used for these measurements.

Two potential values can be measured:

- the so-called on-potential when the CP system is operating, i.e., protection current flows in soil,
- the so-called off-potential which the instantaneous reading taken after a T/R switch off, that is when protection current in soil is interrupted. The off-potential, also called true potential, does not include the ohmic drop contribution

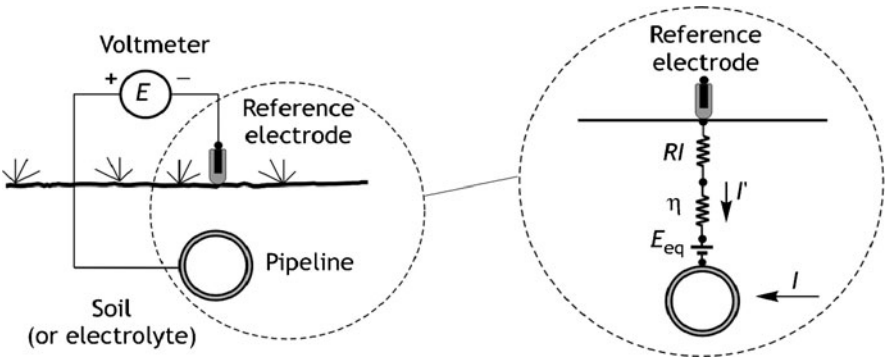


**Fig. 2** Electrical scheme for potential measurement in soil [1]

caused by the protection current flowing in soil. The on-potential measured through a reference electrode depends on electrode position with respect to the structure. The measured value, $E$, is the sum of three contributions, as schematically shown in Fig. 2.

$$\mathrm{E} = \mathrm{E_{eq}} + \eta + \mathrm{IR} \tag{1}$$

Where $E_{eq}$ is metal equilibrium-potential against the reference electrode used, η is overpotential measured with respect to the equilibrium-potential and *IR* is ohmic drop that depends on the reference electrode position, environment resistivity and the circulating current.

The sum ($E_{eq}$ + η) is the "true-potential", also indicated as $E_{off}$, which can also be expressed through the free corrosion-potential:

$$\mathrm{E_{off}} = \mathrm{E} - \mathrm{IR} = (\mathrm{E_{eq}} + \eta) = (\ \psi + \mathrm{E_{corr}}) \tag{2}$$

Where ψ is the overpotential with respect to the free corrosion-potential $E_{corr}$. The reference electrode should be placed at the ground level on the vertical of the structure to minimize IR drop contribution in soil. To eliminate such contribution the on – off technique can be used.

## 2.1 Criteria Established by Standards

EN 12954 [2] standard and NACE RP0169-2005 revision [3] specify different criteria to ascertain CP conditions to be used when particular conditions apply. It has to be emphasized that each criterion mentioned by the standards is to be considered equivalent, so that once a criterion fits the protection is deemed established.

### 2.1.1 True Potential or Off-Potential Criterion

This is the most used criterion and consists of assessing CP condition by checking that IR-drop-free-potential (i.e., true-potential) is equal or more negative than −0.85 V CSE. Different procedures can be used:

- on-off technique,
- corrosion coupons with an embedded reference electrode.

### 2.1.2 300 mV Potential Swing Criterion

This is used in on-condition, i.e., when protection current flows through the soil to the structure, and has the following meaning:

- on-potential is compared to free-corrosion-potential (measured before applying CP). A negative shift of 300 mV assures that CP is achieved,
- furthermore, although such a negative shift includes an IR drop contribution, it has the meaning that a "net cathodic current" enters the structures so that a strong reduction of corrosion rate applies of approximately one of magnitude for every 100 mV shift.

### 2.1.3 100 mV Potential Decay Criterion

This can be adopted when on-off technique can be used. CP is established when, after current interruption, a potential shift of 100 mV toward more positive value is measured in a time of 4–24 h.

## *2.2 On-Potential Interpretation*

Although the on-potential includes the ohmic drop contribution, its measurement is useful for a first hand interpretation of CP level. An on-potential, $E_{on}$, more negative than protection potential ($E_{on} < -0.85$ V CSE) implies the following:

- a 'cathodic current' reaches the structure and reduces the free corrosion rate (that is, when CP is not applied) of more than one or two order of magnitude,
- in high-resistivity environments, where the *IR* drop is high, reading errors may be high as well, but highly resistive media are not as aggressive, so corrosion risk is low,
- if CP is verified taking the on-potential measurement, the corrosion rate can be considered significantly reduced.

The on-potential, $E_{on}$, can be used to estimate the equivalent coating defect size, assuming that the total ohmic drop is given by $E_{prot} - E_{on}$, when $E_{on}$ is measured on

the vertical line of the defect. The ohmic drop, caused by a defect of equivalent diameter, $d_{eq}$, is given by [1]:

$$E_{prot} - E_{on} = i_o \pi d_{eq}^2 \frac{\rho}{8\pi d_{eq}} = \frac{i_o \rho d_{eq}}{8} \tag{3}$$

The meaning of the equivalent defect diameter, $d_{eq}$, is the result of all defect surface area for each square meter of coated surface. It follows that the coating efficiency is: $\xi = 1 - \pi {d_{eq}}^2/4$.

Then, taking $E_{prot} = -0.85$ V CSE and protection current density of bare steel in soil $i_o = 0.1$ A/m$^2$, the on-potential, $E_{on}$, is given by:

$$E_{on} \cong -0.85\left(1 + 0.015 \cdot \rho d_{eq}\right) \tag{4}$$

This provides the relationship between on-potential, environmental resistivity, ρ, and the maximum diameter, $d_{eq}$, of a coating defect still under full protection (that is, potential more negative than −0.85 V CSE). Figure 3 plots the relationship in double-logarithmic scale, where each straight line is an on-potential value. It is clear that if resistivity is very high, the critical defect size is small and vice versa. In a case study, this approach was applied assuming an average soil resistivity of 100 Ωm, by taking a mean value of the on-potential of −1.2 V CSE, an equivalent coating defect diameter, $d_{eq}$, of about 100 mm (equivalent surface area 0.02 m$^2$/m$^2$) was still under full protection. Similarly, an on-potential of −1.5 V CSE, states that an equivalent coating defect diameter, $d_{eq}$, of about 150 mm (equivalent

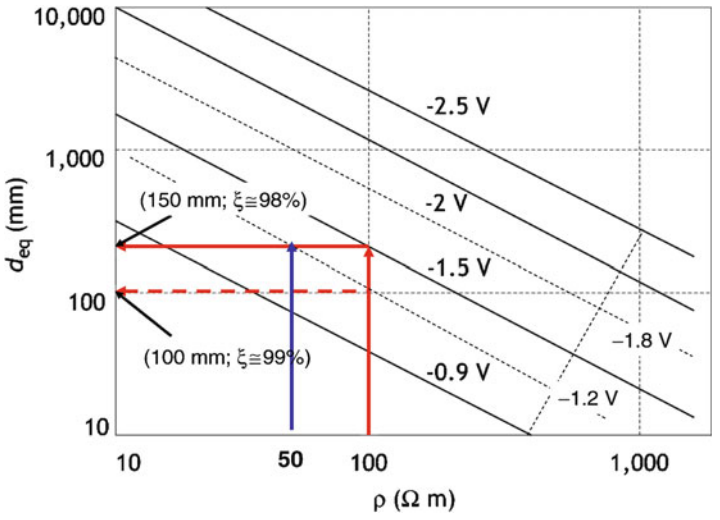


**Fig. 3** Relationship between soil resistivity, equivalent defect coating size and on-potential [1]

surface area 0.03 $m^2/m^2$) is protected. Such equivalent defect sizes correspond to a coating efficiency, ξ, of about 99% and 98% respectively. These values of the coating efficiency can be considered conservative and thus acceptable in practice. In other words, for coated pipelines and flowlines present in the field an on-potential between −1.2 V and −1.5 V CSE assures full CP with a high degree of confidence from a reliability viewpoint.

## 2.3 *"Instant off" Potential Measurements*

The on-off technique is based on the experimental evidence that when the protection current is interrupted, the *IR* drop disappears in a very short time, on the order of $10^{-6}$ s. Therefore, by taking the potential reading shortly after current interruption, the *IR* drop is no longer included.

Obviously, by interrupting the current, overpotential is also eliminated but over a much longer period than *IR* drop, ranging from milliseconds for activation overpotential to seconds or even days for concentration overpotential. The latter is the prevailing one in CP. Figure 4 reports a typical potential recording obtained by means of a high frequency acquisition voltmeter (at least 10 Hz sampling frequency) where the so-called *off-potential*, $E_{off}$, is the potential value recorded immediately after current interruption.

This technique is applied by locating the reference electrode close to the structure, typically in the case of a pipeline in the vertical position. The measurements are carried out with the cathodic protection switched alternatively off and on at intervals for instance of 3 s off and 12 s on (this to prevent any significant depolarisation of the structure).

This method can be used to detect stationary interference at insulating joints, provided on-off potential measurements carried out at both sides of the

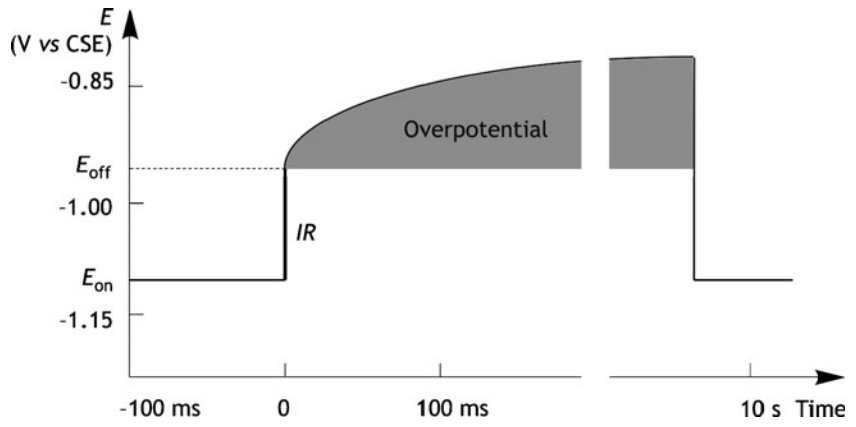


**Fig. 4** Theoretical profile of instant off potential measurement [1]

insulating joints. At unprotected side, when on- and off-potentials are equal, no interference occurs. On the contrary a shift in the negative direction of off-potential means an anodic interference.

## 2.4 Under Protection Conditions Analysis

When either on or off-potential falls in the range of underprotection condition, that is, $-0.65\ \text{V} > E > -0.85\ \text{V}$ CSE, a residual corrosion rate, $i_{\text{residual}}$, takes place:

$$\mathrm{i_{residual}} = \mathrm{i_{corr}} 10^{\frac{E-E_{corr}}{0.1}} \tag{5}$$

Where $i_{\text{corr}}$ (mm/year or $\text{A/m}^2$) is a free corrosion rate (that is, when CP is not effective) $E$ (V) is measured potential (in the protection interval), $E_{\text{corr}}$ (V) is free corrosion potential and constant 0.1 instead of 0.06 is conservatively taken as Tafel slope of iron (V/decade). Equation 5 is derived from Tafel's law, where free corrosion rate, $i_{\text{corr}}$, replaces the exchanged current density and the free corrosion potential, $E_{\text{corr}}$, replaces the equilibrium potential.

Assuming a free corrosion potential $E_{\text{corr}} = -0.55$ V CSE and a free corrosion rate $i_{\text{corr}} = 0.1$ mm/year, when measured potential is $-0.85$ V, the corrosion rate is reduced to a minimum of 1,000 times, when potential is $-0.75$ V, the corrosion rate is reduced to a minimum of 100 times for instance, when potential is $-0.65$ V, the corrosion rate is reduced to a minimum of ten times.

In conclusion, under protection conditions, where on-off potential practically coincide because ohmic drop in soil is low due to the low flowing current, the residual corrosion rate is fairly low and even negligible when approaching the protection-potential. When potential falls in the range $-0.75\ \text{V} > E > -0.84$ V the residual corrosion rate is below 10 μm/year.

### 2.4.1 Interpretation Criteria of Potential Measurement

On the basis of standards and norms, interpretation criteria of potential measurements are reported in Table 3.

# 3 Insulating Joints

Stray-current corrosion occurring internally at insulating joints is a typical corrosion attack taking place when electrical interference is present. The corrosion mechanism is the same as the usual external interference: the non protected structure, that is not electrically connected to the CP feeding system, is located

**Table 3** Interpretation criteria of potential measurements

| Eon potential | Eoff potential | Protection level by standard | Interpretation criteria |
|---|---|---|---|
| Eon > −0.30 V | Eoff > −0.50 V | | Severe corrosion |
| | −0.50 V > Eoff > −0.65 V | | Free corrosion conditions |
| | −0.65 V > Eoff > −0.75 V | No | Underprotection (residual corrosion rate higher than 10 μm/year) |
| | −0.75 V > Eoff > −0.80 V | No | Underprotection (corrosion rate below 10 μm/year). Acceptable |
| | −0.80 V > Eoff > −0.85 V | Y | Underprotection (corr. rate below 10 μm/year). Fully acceptable |
| −1.0 V > Eon > −1.5 V | −0.85 V > Eoff > −1.15 V | Y | Protection range |
| | −0.95 V > Eoff > −1.05 V | Y | Optimum protection range |
| | Eoff < −1.15 V | No | Overprotection conditions |
| | Eoff < −1.30 V | No | Severe overprotection conditions (hydrogen evolution) |

nearby the groundbed. The current can enter the structure and leave it toward the protected pipeline at the crossing point zone. Interference corrosion becomes stronger the closer the interfered structure is to the groundbed.

## *3.1 Interference Current*

An interference corrosion occurs at insulating joint when an electrolyte is present inside the pipeline. In this case, the interfering current by-passes the joint internally causing corrosion. A typical situation in the oil and gas industry is the following: a flowline from the producing well to the manifold of the oil centre is electrically separated at both ends from the well casing and from the grounding system by means of insulating joints and cathodically protected by an impressed current CP system, as shown in Fig. 5.

The CP current can enter the grounding system or the well casing, which are not electrically connected to the negative pole of the T/R, and accordingly return to the T/R, by-passing the joint, through the electrolyte inside the flowline [1].

Interference current, and accordingly the corrosion rate, is high when:

- ΔE across the insulating joint is high,
- the ohmic resistance within the electrolyte is low,
- at given geometry (pipeline diameter, internal coated pipe length and electrolyte content) the electrolyte resistivity is low (Fig. 5).

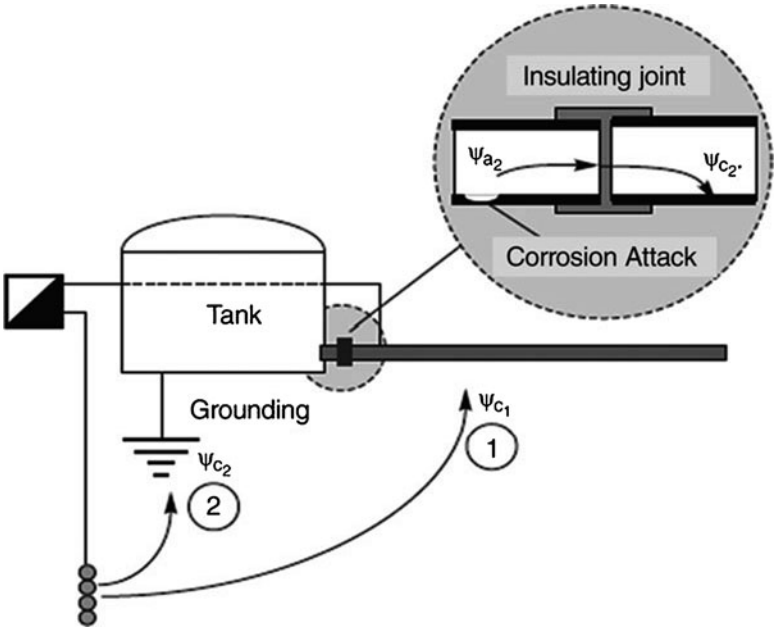


**Fig. 5** CP system of a flowline in an oil centre [1]

## *3.2 Potential Measurements*

To verify the correct CP conditions, potential measurements are carried out. To eliminate the IR drop contribution, the so called "on-off technique" is applied. The normal schematic potential trend occurring in the on-off measurement is reported in Fig. 3. The vertical line recorded at current interruption (also known as instant-off) represents the ohmic drop contribution. The correspondent potential value, $E_{off}$, is the true potential, not including the ohmic drop contribution. In the presence of an insulating joint, the potential trend is different, as schematically shown in Fig. 6 where the depolarisation is so rapid to be mixed with the ohmic drop contribution [4] For the correct potential interpretation, the use of high frequency acquisition datalogger voltmeter was required in order to detect the ohmic drop contribution, although partially masked by the rapid depolarisation. As a consequence, the true-potential cannot be measured by the on-off technique. For practical applications, we propose to adopt as true-potential value the reading detected after about 50 ms from the current interruption. This procedure was confirmed by comparison to the readings taken by means of a fixed reference electrode, located in a position very closed to the pipeline. In conclusion, when rapid depolarization occurs, as discussed in the previous paragraph, internal corrosion is very likely to occur. Table 4 shows a proposal for criteria to interpret insulating joint (IJ) interference conditions and efficiency.

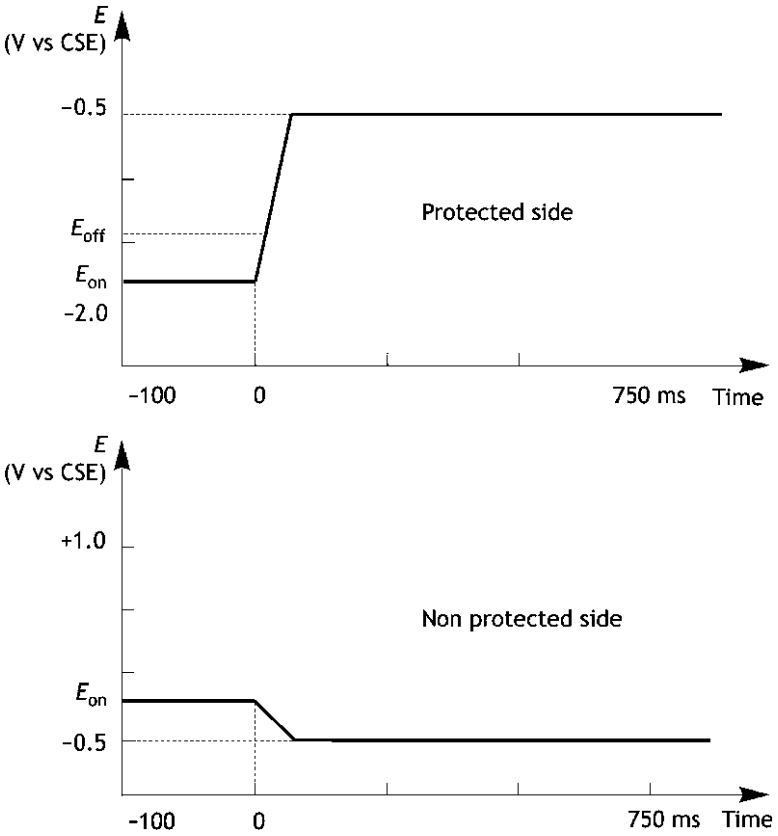


**Fig. 6** Example of typical potential recording in presence of internal insulating joint corrosion [1, 2]

## 4 Coating Defect Localisation

The localisation of coating defects in a pipeline is important for the so-called coating integrity check-up. To do this, two methods are used: electrochemical and electromagnetic, both often used in an integrated way [1]. Electromagnetic methods have the advantage of not requiring an electrical connection with the structure, but they do not indicate the CP level. On the contrary, electrochemical methods are more expensive, since they require longer periods of time and a larger number of operators, however, they do provide more accurate results.

### *4.1 Electromagnetic Methods*

Electromagnetic methods are based on a very simple principle. An alternating current (AC) signal is injected into the pipeline and then measured along the

**Table 4** Interpretation criteria of IJ efficiency

| Case | Protected side | NON protected side | ΔV (Eoff – Eon) non protected side | Interpretation |
|---|---|---|---|---|
| 1 | | | Eon = Eoff | IJ efficient |
| | | | ΔV > 0 | IJ efficient |
| 2 | | | 0 < \|Eoff − Eon\| < 50 mV | Interference negligible |
| | | | ΔV > 0 | IJ efficient |
| 3 | Eoff < −0.85 | Eoff > −0.85 | \|Eoff − Eon\| > 50 mV | Interference: light cathodic |
| | | | ΔV < 0 | IJ efficient |
| 4 | | | \|Eoff − Eon\| < 50 mV | Interference: light negligible anodic |
| | | | ΔV < 0 | IJ efficient |
| 5 | | | \|Eoff − Eon\| > 50 mV | Anodic Interference |
| | | | | IJ efficient |
| 6 | | | Eoff − Eon = 0 | Probable presence of galvanized steel |
| | | | ΔV > 0; ΔV < 0 | IJ efficient |
| 7 | Eoff < −0.85 | −0.7 > Eoff > −0.85 | \|Eoff − Eon\| < 50 | Probable presence of galvanized steel; negligible interference |
| | | | ΔV < 0 | IJ efficient |
| 8 | | | \|Eoff − Eon\| > 50 | Probable presence of galvanized steel; anodic interference |
| 9 | Eoff < −0.85 | Eoff < −0.85 | Eoff − Eon > 0 | IJ NOT EFFICIENT |
| 10 | Eoff > −0.85 | Eoff > −0.85 | Eoff − Eon = 0 | IJ Efficiency not valuable |

pipeline as it escapes from coating defects or poorly coated sections. This allows their localisation. Moreover, since the signal's intensity at one point depends on the presence of previous defects, it is convenient to proceed investigating by successive steps, first, by measuring a few points along the pipeline, and then by intensifying the measurements in between, to better identify the exact point of AC signal leakage.

Two methods are used: *Pearson's method*, based on the conductivity measurement and *inductive method*, based on the inductance measurement.

### 4.1.1 Pearson's Method

This method consists of sending an alternating current signal along the pipeline by a feeder connected to the pipeline (for example, at a test point) through a temporary GB (Fig. 7). The signal frequency is chosen as a function of pipeline coating; for example, low frequencies of about 200 Hz are used for bituminous coatings, while greater frequencies, over 1 kHz, are usually used for epoxy resins. If there

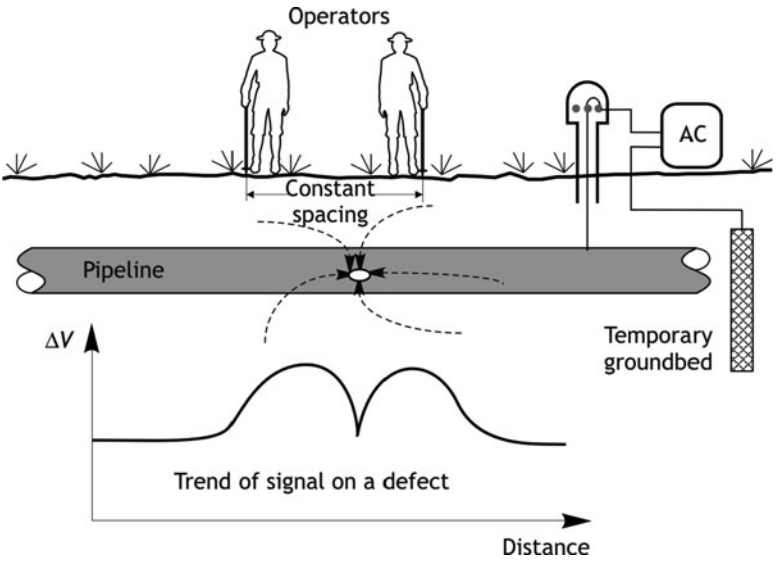


**Fig. 7** Pearson method to detect coating defects [1]

is a defect, the alternating current signal leaves the pipeline with an intensity proportional to the defect size. The signal along the pipeline is taken by two operators walking in tandem, using two portable electrodes. When the electric field intensity increases due to the presence of a fault, the signal intercepted by operators increases. Very often, an acoustic system is used to facilitate signal detection.

### 4.1.2 Inductive Method

This method is based on the principle that a high frequency alternating current (usually 10–20 kHz) injected into the pipeline creates a variable magnetic field around it, whose intensity is proportional to the circulating current in the pipeline. Before and after the presence of a fault, a sharp variation on the inducted magnetic field occurs, which can be detected by moving a magnetic field detector over the pipeline (Fig. 8). This method is better adapted than the previous one to determining coating degradation, rather than to detecting fault location. In general, the interpretation is as follows: a pronounced signal attenuation indicates poor quality coating; a slope change indicates a variation in the coating degradation rate; sharp variations indicate the presence of defects or metal contacts with other structures. Using this method, the reading is taken by one operator who measures the field intensity at predefined intervals.

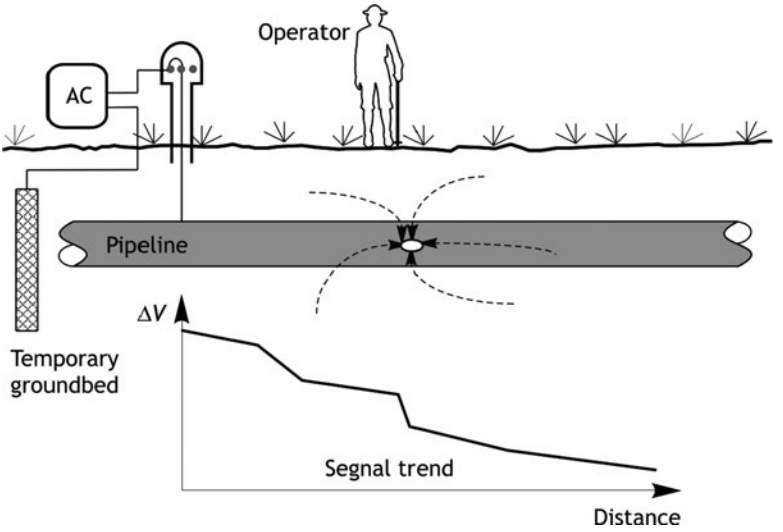


**Fig. 8** Water injection flowlines and trunklines network "General data"

## *4.2 Electrochemical Methods*

### 4.2.1 On-Off Potential Profile

The localisation of coating defects can be worked out by examining the potential profile along the pipeline, as schematically illustrated in Fig. 9. To obtain the profile, an electrical connection with the pipeline is required and the measurement must be synchronised with the operator's movement.

The $E_{on}$ potential, by itself, may provide useful information. However, because of the *IR* drop, small defects cannot be detected. In this case, the $E_{off}$ potential profile has to be used.

Two distinct effects are recorded in correspondence with defects: a peak towards more positive potential values of both $E_{on}$ and $E_{off}$ (polarisation is less and therefore the potential is more positive) and a decrease in ohmic drop as the difference $|E_{on} - E_{off}|$, because, although the current density increases locally, coating contribution to the ohmic drop prevails.

### 4.2.2 Transversal Gradient Method

At a coating defect, current density increases correspondingly and provokes an increase in the ohmic drop in the soil. This is the basis of the so-called *transversal gradient method*, where the *IR* drop between a central reference electrode, placed vertically over a pipeline, and a lateral one located in a "remote" position, usually 10–50 m away from the pipeline, is measured. In the absence of coating defects,

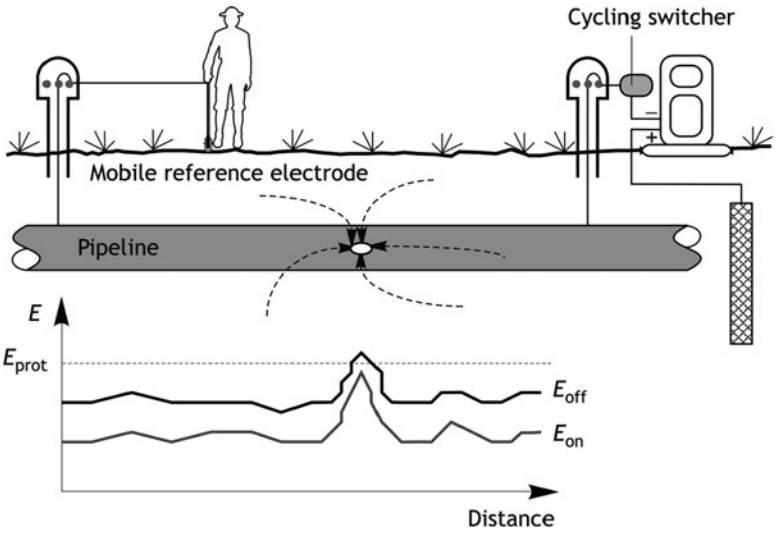


**Fig. 9** On-Off potential profile along a pipeline with coating defects [1]

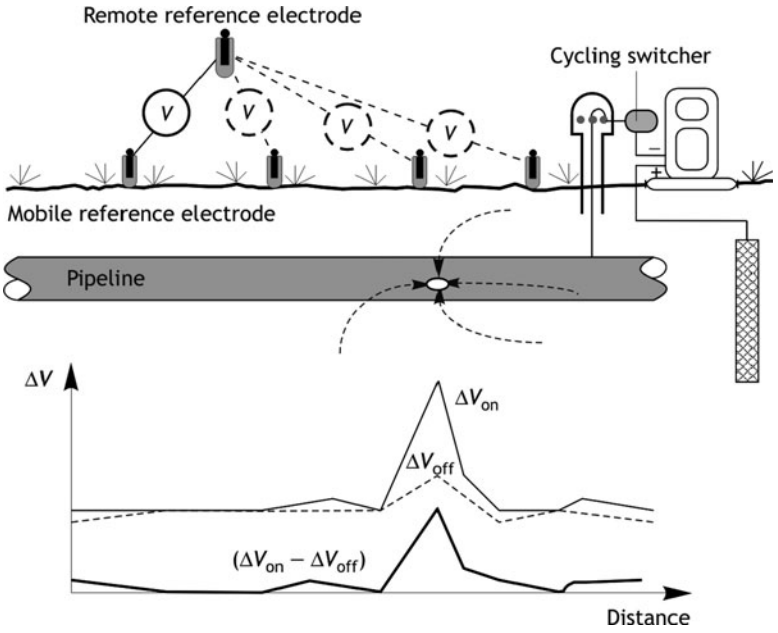


**Fig. 10** Illustration of the lateral on/off IR drop measurement [1]

the lateral ohmic drop is very low, usually less than 10 mV even in very resistive environments. On the other hand, when a defect is present the ohmic drop is about one order of magnitude higher, and thus easily detected. Figure 10 reports an

example of such a measurement. During surveys, the protection current is often increased to improve sensibility of the technique by increasing the ohmic drop.

Due to inevitable current circulation in the soil from various sources, such as stray currents, measurement of the ohmic drop is affected by some disturbances that do not allow correct data interpretation. To overcome this inconvenience, the on-off technique must be used, exploiting the superimposed effects principle, since during '*on*' periods all *IR* drop contributions are measured, while during the '*off*' period the *IR*-drop related CP is not, so that, the difference between the two measurements is the *IR* drop caused only by cathodic current:

$$\Delta V_{on} = R_L \left(I_{nat} + I_{cp}\right) \tag{6}$$

$$\Delta V_{off} = R_L \, I_{nat} \tag{7}$$

$$I_{cp} = \frac{\Delta V_{on} - \Delta V_{off}}{R_L} \tag{8}$$

Where $I_{nat}$ is current circulating in soil during the measurement, $I_{cp}$ is CP-related current and $R_L$ is lateral resistance. The on-off *IR* drop difference is generally plotted against pipeline length, as illustrated in Fig. 10, showing *IR* drop peaks which indicate location of defects. Where coating is integral, the *IR* drop is near zero or a few millivolts, as a function of the type of coating and soil resistivity. This method has a great advantage of not requiring an electrical connection to the pipeline.

### 4.2.3 Combination of On-Off Profiles and Gradients

This is the most sophisticated measurement for localising and quantifying coating defects, while simultaneously providing effective protection conditions. Measurement along the pipe is taken, according to the on-off procedure already illustrated, simultaneously for both methods: the on-off potential profile and the lateral *IR* drop.

The equivalent coating defect size can be calculated without knowing either soil resistivity or circulating current, by using the relationship that links lateral ohmic drop ($\Delta V_{on} - \Delta V_{off}$) to defect size from equation:

$$\Delta V_{on} - \Delta V_{off} = \frac{\rho I}{2\pi}\left(\frac{1}{H} - \frac{1}{\sqrt{H^2 + d^2}}\right) = C\frac{\rho\, I}{2\pi} \tag{9}$$

Where C is a constant which depends only on $H$, the burial depth, and on $d$, the electrode spacing. On the other hand, resistance $R$ located at the defect is given by the ohmic drop contribution measured by the on-off technique.

$$R = \frac{E_{off} - E_{on}}{I} \tag{10}$$

By eliminating the current $I$, and introducing the resistance of a coating defect with size $d_{eq}$:

$$R = \frac{\rho}{2\pi d_{eq}} \tag{11}$$

We obtain:

$$d_{eq} = C\frac{\Delta V_{on} - \Delta V_{off}}{E_{off} - E_{on}} \tag{12}$$

This allows a ranking of the equivalent defect size.

## 5 Risk Assessment Approach

A formal engineering risk evaluation of equipment is referred to as a **Failure Mode, Effect and Criticality Analysis** (FMECA), that ranks perceived risks in order of seriousness: Criticality (Risk) = Effect (Consequences) × Mode (Probable frequency):

1. **Failure criticality**: Potential failures are examined to predict the severity of each failure effect in terms of safety, decreased performance, total loss of function and environmental hazards.
2. **Failure effect**: Potential failures assessed to determine probable effects on process performance and the effects of components on each other.
3. **Failure mode**: Anticipated operational conditions used to identify most probable failure modes, the damage mechanisms and likely locations.

Failure Modes is the combination of damage on operational (and accidental) loads. Corrosion is not a cause of failure but is a contribution to the mode.

Failure mode:

- local leakage
- longitudinal/transverse rupture
- collapse or buckling

Corrosion damage (corrosion morphology):

- uniform corrosion and erosion
- isolated pitting
- flow induced localised corrosion and erosion (mesa-corrosion)
- longitudinal and transverse cracking
- longitudinal and transverse grooving (weld corrosion)

Loads:

- pressure (internal and external)
- forces (tensional/hoop stresses, compressive, bending/torsional)
- impacts (collisions, dropped objects)

**Table 5** Criticality index used for risk assessment

| | |
|---|---|
| Probability (P) | Low chance of occurrence. . . . . .almost certain to occur |
| Seriousness (S) | Not serious, minor nuisance. . . . . .total failure, safety hazard |
| Detection (D) | Easily detected. . . . . .unlikely to be detected |
| Ranking Value (C) | 1 2 3 4 5 6 7 8 9 10 |

**Table 6** Criticality matrix

| | Consequence of failure | | |
|---|---|---|---|
| Failure probability | High | Medium | Low |
| High | 1 | 2 | 3 |
| Medium | 2 | 3 | 4 |
| Low | 3 | 4 | 5 |

The analysis determines the probability of each failure mode occurring (P), the seriousness (consequences) of the failure (S) and may also include the difficulty of detecting the failure (D). As shown in Table 5, the criticality index (C) provides a numerical ranking ($C = P \times S \times D$) that enables management to focus on audit procedures (appropriate maintenance and corrosion control strategies, including inspection activities) on items of plant, or processes, that are deemed to have either high/unacceptable risks or low/acceptable risks.

This approach forms the basis of various commercial software based systems used by the industry to assess criticality and corrosion risks. Similar systems are available as part of maintenance strategies and risk based inspection [5, 6] (Table 5).

Criticality/risk analyses can be carried out at all project stages:

- **at design** where the aim is to identify hazards and minimise risk by targeting corrosion mitigation procedures,
- **during operation** where the aim is to focus inspection and monitoring on critical areas and to eliminate poor corrosion mitigation procedures.

A standard part of such evaluations is to use a matrix display to highlight or quantify the risks. Examples of such systems include a $3 \times 3$ matrix (as per Table 6) and a $5 \times 5$ matrix (as per Table 7 [6]).

## *5.1 Managing the Corrosion*

Corrosion processes found in many industries, including oil/gas production, are widely understood and mitigation procedures are well established. However, unacceptable problems such as leaks and emissions still occur. An often accepted general conclusion is that: the cause of corrosion related failures is human error/poor management control.

**Table 7** Criticality matrix [6]

| Likelihood/ consequence | A | B | C | D | E |
|---|---|---|---|---|---|
| 5 | Medium/high | Medium/high | Medium/high | High | High |
| 4 | Medium | Medium | Medium/high | Medium/high | High |
| 3 | Low | Low | Medium | Medium/high | High |
| 2 | Low | Low | Medium | Medium | Medium/high |
| 1 | Low | Low | Medium | Medium | Medium/high |

These causes include lack of inspection/monitoring, poor communication, mal-operation, insufficient design review and inattention to warnings/technical information. An overall system is therefore required to manage not only technical corrosion issues but also human response and actions.

Good corrosion control/mitigation to ensure adequate safety procedures requires good design. The continuing review of safety-critical elements as part of the safety case should provide a driver for improvement of feedback from the field into new designs. Most organisations conduct periodic reviews with formal audits at "hold points" during the design process. These include HAZOP studies and Engineering Reviews, hence introduction of corrosion related safety checks at these stages of the design process would be recommended. The means of conducting inspections and corrosion monitoring, including provision of adequate access for personnel, monitoring instrumentation and inspection equipment is often crucial, yet this aspect of design is frequently neglected until too late in the process. The use of Risk Control Systems during design would assist in the overall management process. Typical approaches are currently adopted by industry to manage safety and corrosion and are based on the legislative requirements and further recommendations are then made for further improvement of the audit and verification systems.

## 6 Case Study

This case study here reported deals with a corrosion risk assessment of a water injection trunklines and flowlines in an Oil and Gas plant. Aim of the study was the following:

- to assess the performance of the existing cathodic protection systems and to provide recommendations if needed,
- to assess the actual protection levels of all buried protected structures and the integrity status of the existing cathodic protection units and all their components,
- to recommend remedial actions to guarantee correct protection levels of all plant facilities, including those ones affected by electrical interference,
- to develop proposals for any required interventions to extend the operating life of the cathodic protection systems for the remaining life of the Field.

## 6.1 Cathodic Protection Philosophy

Water injection trunklines and flowlines are protected by a combination of CP and external coatings. All flowlines, trunklines and export pipeline located outside the plant area are electrically isolated from foreign structures by isolating joints or flanges. All buried metallic structures inside the plant area (piping; earth ground system; steel concrete reinforcement) are assumed to be properly electrically interconnected. A simplified layout of the water injection flowlines and trunklines is reported in Fig. 11. Table 8 reports the general data for the investigated flowlines.

**CP system** consisted of an impressed current as follows:

- N.1 Transformer Rectifier Unit,
- N.1 deep anode groundbed,
- Magnesium anodes (number and position unknown).

CP operating data for the water injection systems have been gathered in two steps, before and after the repair intervention of a number of damaged components, and hereinafter reported as *first survey* and *second survey*.

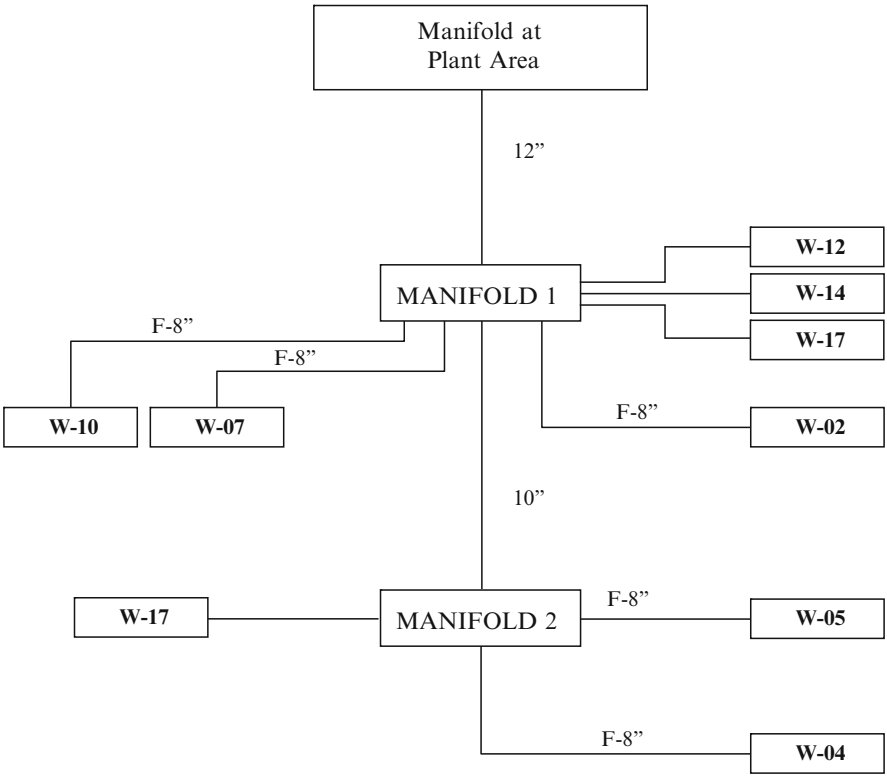


**Fig. 11** Water injection pipeline network

**Table 8** Water injection flowlines and trunklines network "General data"

| Item (−) | Start up (year) | Length (m) | Diameter (in.) |
|---|---|---|---|
| F-8″-W-02 | 2003 | 3.100 | 8 |
| F-8″-W-07 | 2000 | 6.000 | 8 |
| F-8″-W-10 | 2002 | 4.800 | 8 |
| F-8″-W-04 | 2002 | 3.400 | 8 |
| F-8″-W-05 | 2002 | 1.800 | 8 |
| F-W12 | | | |
| F-W14 | | | |
| F-W-13 | | | |
| F-W-17 | | | |
| T-M1-12″ | 2000 | 6.400 | 12 |
| T-M2-10″ | 2002 | 11.000 | 10 |

After the first survey, the following repair actions were performed:

- M1: installation of cables.
- M2: installation of a surge diverter into the junction box. Cables connected.
- W2: installation of new cables and connections.
- W4: surge diverter reconnected.
- W5: surge diverter reconnected.
- W13: new test points on insulating joint with a surge diverter installation.
- W10: new test points with a surge diverter installation and new connections.
- W7: box of IJ has been extended of 0.60 m.

All damaged boxes have been replaced. On-potential measurements taken during the second survey are reported in Table 9.

### 6.1.1 CP Criteria Used

Reference has been made to applicable international normative. For pipeline networks, outside the plant area, when instant-off-potential measurements were available, the criteria reported in Table 1 were used.

When on-potential measurements only were available, a potential more negative than −1.20 V vs. CSE was considered indicative of acceptable protection conditions on the basis of on-potential interpretation discussed in previous paragraphs. Different criteria have been used for buried structures within the plant area; this is the case of cathodic protection of so called *complex structures*, where the cathodes to be protected, buried piping, tank bottom, etc., are inevitably in contact with other metallic structures like reinforced concrete foundations and copper-earth-ground system.

**Table 9** Water injection pipe network "CP operating data"

| | | Second survey | Notes | | |
|---|---|---|---|---|---|
| Area | Position | Protected side [mV] | Unprotected side [mV] | Casing [mV] | |
| Plant area | Injection | −1.987 | | | |
| | TP1 | −1.878 | | | |
| | PC/Gas | −1.778 | −1.778 | | Gas crossing |
| | TP2 | −1.813 | | −1.348 | Mg anode: −1.353 mV |
| | TP3 | −1.782 | | −985 | Casing: −446 mV, Mg anode: −1.353 mV |
| | TP4 | −1.648 | | | |
| | TP5 | −1.592 | | −932 | |
| | TP6 | −1.408 | | −956 | |
| | TP7 | −1.389 | | −905 | |
| M1 | all | −1.157 | | | |
| M2 | M8 arrival | −1.125 | −929 | | |
| | W5 start | −933 | −905 | | |
| | W13 start | −927 | −902 | | |
| | W4 start | −1.101 | −1.070 | | |
| M1 – M2 | Start | −1.231 | −1.231 | | Insulating joint box |
| | TP1 | −1.231 | | −982 | P.C. by Mg anode |
| | TP2 | −1.180 | | | |
| | TP3 | −1.174 | | −333 | |
| | TP4 | −1.087 | | | |
| | TP5 | −1.080 | | | |
| | TP6 | −1.121 | | | |
| | TP7 | −1.148 | | | |
| | TP8 | −1.095 | | | |
| | TP9 | −1.179 | | | |
| | M9 arrival | −1.125 | −929 | | |
| M8 – W2 | 8″ W start | −1.053 | −1.030 | | Insulating joint box |
| | TP1 | −1.120 | | | |
| | TP2 | −1.075 | | −802 | Casing: −302 mV, Mg anode: −983 mV |
| | Wellhead arrival | −1.026 | −821 | | |
| M8 – W12/7 | W7&12 start | −1.095 | −1.053 | | Insulating joint box |
| | PT1 | −1.065 | | −1.083 | |
| | PT2 | −1.178 | | | Casing: −302 mV, Mg anode: −983 mV |
| | PT3 | −1.030 | | −1.242 | |
| | W12 arrival | −978 | | | |
| | W12 start | −978 | | | |
| | Wellhead arrival | −902 | | | |

(continued)

**Table 9** (continued)

| Area | Position | Second survey | | Notes |
|---|---|---|---|---|
| | | Protected side [mV] | Unprotected side [mV] | Casing [mV] | |
| M8 – W10 | W10 start | −1.101 | −1.094 | | Insulating joint box |
| | PT1 | −1.065 | | −223 | |
| | PT2 | −1.150 | | −375 | |
| | Wellhead arrival | −1.060 | −598 | | |
| M8 – W14 | W14 start | −1.102 | −236 | | Natural potential −395 mV |
| | PT1 | −980 | | | Sand |
| | Wellhead arrival | −1,162 | −340 | | |
| M9 – W4 | W4 start | −1.101 | −1.070 | | Insulating joint box |
| | PT1 | −1.160 | | −285 | |
| | PC/Gas | −1.160 | | −285 | M5 – M10 Crossing |
| | PT2 | −1.160 | | −285 | |
| | Wellhead arrival | −1.142 | −691 | | |
| M9 – W5 | W5 start | −933 | −905 | | Insulating joint box |
| | PT1 | −1.102 | | −420 | |
| | Wellhead arrival | −1.095 | −550 | | Surge diverter disconnected |
| M9 – W13 | M9 start | −927 | −902 | | Natural potential −368 mV |
| | PP2 | −1.024 | | | |
| | PP3 | −1.015 | | | |
| | Wellhead arrival | −1.035 | −650 | | |

### 6.1.2 On-Potential Assessment

On the basis of the theory discussed and the plot of Fig. 3, some important conclusions on CP protection conditions can be drawn from an analysis of the measured on-potential. This is of particular importance in this case study, since a thorough on-off procedure technique could not be followed because not all supplied current to pipelines could be interrupted at one time. When the on-potential is known, for instance around −1.5 V vs. CSE by the application of the plot of Fig. 3, it can be stated that at such on-potential (−1.5 V vs. CSE), assuming a soil resistivity close to 100 Ωm, all possible coating defects smaller than 0.15 m in equivalent diameter are in protection condition. In other words, it can be stated that, with an on-potential of −1.5 V vs. CSE, a pipeline is in full protection with a coating efficiency higher than about 98%. Therefore, it is our opinion that all three pipelines are in full protection condition because it is certain that the coating efficiency is higher than 98%. In fact, the average protection current density is less than 50 μA/m$^2$, which means a calculated coating efficiency of 99.9% or 99.5%

on the basis of a protection current density of bare steel of 50 mA/m$^2$ or 10 mA/m$^2$, respectively, as follows:

$$\xi = 1 - \frac{i}{i_{bare}} = 1 - \frac{0.05}{50} = 0.999 \text{ and } \xi = 1 - \frac{i}{i_{bare}} = 1 - \frac{0.05}{10} = 0.995 \quad (13)$$

In this zone, on-off-potentials were measured against both fixed (FRE) and portable (PRE) reference electrodes. Measured potentials were −1.1 to −1.3 V CSE as on-potential by FRE and −1.1 to −1.5 V CSE as on-potential by PRE. To this zone, 300 mV swing criterion and on-potential assessment apply, thus it can be concluded that protection condition is achieved, provided to assure the same coating efficiency in the future, by a periodic check by carrying out a coating integrity survey.

### 6.1.3 External Corrosion Risk Assessment

The risk of external corrosion on surveyed pipelines was evaluated on the basis of the on-potential assessment, taking into account the interpretation criteria reported in Tables 3 and 4. As discussed in the previous paragraph, from the on-potential readings it was estimated a value of the off-potential and then the criteria applied. What was reasonably assumed is that there is confidence to have full protection with an on-potential of −1.5 V vs. CSE, provided a coating efficiency higher than about 98%. This assumption was deemed reasonable and then acceptable because it was known that the coating condition was good, as proved by recent excavations in areas nearby.

The importance of this approach is based on the possibility of carrying out few measurements of the on-potential and not the off-potential, as required by standards. Nevertheless, a reliable evaluation of corrosion-related risk is possible, provided a critical analysis of the on-potential measurements. To rank the criticality of different zones of crossing pipelines, a matrix can be used where likelihood of consequences can be stated on the basis of the area crossed (isolated or in a plant area) and the size which is related to the amount of hydrocarbon releasing amount, and likelihood of occurrence (leakage by corrosion) should be related to the on-potential measured. In the case study, the on-potential could be ranked as *low* for readings more negative than −1.5 V vs. CSE, and as *high* for readings more positive than −0.85 V vs. CSE and *medium* in between. On the basis of the survey results, the risk of external corrosion was considered low for almost all investigated zones.

**Acknowledgments** The author wishes to thank the Organizing Committee of the NATO Workshop 2010 for this special opportunity to publish this work.

## References

1. L. Lazzari, P. Pedeferri, *Cathodic Protection* (Polipress, Milan, 2006)
2. EN 12954 *Cathodic Protection of Buried or Immersed Metallic Structure – General principles and Application for Pipelines*, European Committee of Standardization, 2001
3. NACE RP0169-2005, *Recommended Practice: Control of External Corrosion on Underground or Submerged Metallic Piping Systems*, NACE International, Houston, 2005
4. B. Bazzoni, P. Fassina, L. Lazzari, V. Sia, Potential measurement interpretation on insulating joints. Mater. Perform. 26–30 Sept. 2000
5. API RP 580, Recommended practice for risk-based inspection, American Petroleum Institute, Washington, DC
6. API RP 581, Risk-based inspection technology, American Petroleum Institute, Washington, DC

# Above Ground Coating Integrity Assessment: Experience with SUMED Pipelines

**Saher Shawki**

**Abstract** External corrosion protection of the buried pipelines is primarily achieved by coatings and supported by cathodic protection. The coating damage occurs during pipeline installation, or due to aggressive soil. Coating integrity assessment is aimed to improve the safety of pipeline operation regarding personnel and environment as well as economic security. Inspection practice is intended to identify coating defect location and estimate corrosion activity of the pipeline. The inspection program includes the following steps:

- pre-assessment: collect information on pipeline physical characteristics and operating history,
- indirect inspection: field measurements,
- direct examination: evaluation of pipeline coating performance,
- post-assessment: analysis of data collected, coating defect repair, mitigate corrosion protection faults including cathodic protection system.

The techniques and measuring equipment for above ground coating inspection are well established as for Close Interval Potential Survey (CIPS) and Direct Current Voltage Gradient (DCVG) methods. However, analysis of the gathered inspection data is rather uncertain. The accuracy determining coating defect location and assessment depends on the vast experience of the inspection team dealing with diverse pipelines conditions. The paper describes in details the inspection technique, the required equipment to perform the measurement, and the means of data analysis. A comprehensive example is given by the survey works carried out on SUMED transmission pipelines between Suez (Red Sea) and Alexandria (Mediterranean Sea).

S. Shawki (✉)
Central Metallurgical R&D Institute, El-Tebbin, Helwan, Egypt
e-mail: sahersan@yahoo.com

T. Boukharouba et al. (eds.), *Integrity of Pipelines Transporting Hydrocarbons*,
NATO Science for Peace and Security Series C: Environmental Security,
DOI 10.1007/978-94-007-0588-3_19, 

## 1 Pipeline Status

In the last decade hydrocarbon pipelines, existing and planned, showed a dramatic rise in number and mileage. The expansion is to meet the increasing demand in fuel oil and natural gas. Pipeline networks covers oil/gas producing and consuming countries as well as International or Transcontinental Lines. The Mediterranean area is best representation: Algeria, Libya, and Egypt as producing countries are linked by land-based and undersea lines with Italy, Spain, and turkey as consumer countries. Pipelines are routed through land for thousands of miles everywhere in arid (desert) and in urban areas. It is estimated that 25% of pipeline failures in the past were due to corrosion. For most buried pipeline, experience has shown that external corrosion is more dominant than internal corrosion. Pipelines which are more than 15–20 years old, and are coated with traditional barrier coatings (epoxy, P.E., P.U., etc.) show marked degradation of the coatings over time. This is mainly due to aggressive soils or to wrong – handling of the coated pipes during construction.

## 2 Why Coating Inspection

Construction and operation of pipelines is very expensive. The consequences of corrosion failure are devastating as for the safety of personnel and environment, even threatens the social security. For these reasons protection against soil corrosivity is given highest levels by barrier coatings supported by cathodic protection systems.

An important aspect of assuring and maintaining pipeline performance is implementation of integrity management programs by above ground coating inspection techniques. In USA, Federal and State laws and regulations necessitate that: transmission pipelines owners have to implement external corrosion direct assessment surveys at service durations of 3–7 years. The Standard Recommended Practice NACE RP0502-2007 [1] is approved by the American National Standards and well recognized in many countries. The expected results of integrity surveys are to reduce risks for people, property and environment, as well as, reduce economic losses. Insurance of pipelines against accidents is very common. At least a discount of 25% of insurance bill is granted if the results of integrity survey are presented to the Insuring Body.

## 3 The Survey Techniques

The best accepted method of evaluating the protection level of pipelines is through the use of potential measurements. Potential values on pipelines have traditionally been recorded only at test stations (posts) located at distances 1–3 km along the

pipeline routing. But potential monitoring only at test posts provides limited information. It is possible that serious corrosion can be occurring on the pipeline even when recorded potential values at test posts satisfy the criteria for protection i.e. $> -850$ mV against copper/copper sulfate reference electrode. The coating anomalies would not be detected unless a detailed inspection and potential survey is performed. The data provided by the coating inspection surveys plays a key role in decision making as to when and where coating defects should be repaired. Above ground coating inspection program includes the following steps:

- pre-Assessment: To collect information on pipeline physical characteristics, operating history, and the cathodic protection system in application,
- field Measurements: To identify the location and severity of coating faults, and areas at which corrosion activity might be occurring,
- direct Examination and Post Assessment: To analyze the collected data, evaluate coating performance, repair critical defects and upgrade cathodic protection system involved.

The details of each step are as follows.

## *3.1 Pre-Assessment*

A comprehensive list of the required information of this step is as follows:

| Pipeline installation and protection data | |
|---|---|
| 1. General: | |
| Line designation | |
| Fluid | Crude oil/gas/products |
| Location | Map |
| Installation date | |
| Pipe size | (inch) |
| Burial depth | (meters) |
| Total length | km |
| Material | X 50, 80 |
| Insulating flanges | Number and location |
| 2. Coating Data: | |
| Type | Polyethylene H.D./P.U./P.V.C. |
| Thickness | (mm) |
| Insulating properties | Resistivity (Ω cm) |
| 3. Tested section: | |
| Location | |
| Total length surveyed | (km) |
| Test points | |
| Number | |
| Locations | Map |
| Connection | Other pipeline links |
| Valves | km |

(continued)

| Pipeline installation and protection data (continued) | |
|---|---|
| Number | |
| Locations | |
| Soil | |
| Description | Sand/clay/rock |
| pH value | |
| Chloride content | |
| Resistivity (corrosivity range) | (Ω cm) |
| 4. Cathodic protection: | |
| Power supply units | |
| Number | |
| Type | T/R or solar |
| Location | |
| 5. Monitoring data (during survey period): | |
| Normal potential ($Cu/CuSO_4$) | (mV) |
| Protective current | (A) |
| T/R voltage output | (V) |
| Pipe/soil potential (range) | (mV) |
| Potential attenuation | (mV/km) |
| Interference and/or stray currents | |
| 6. Survey techniques: | |
| Close interval potential survey (CIPS) | |
| Intervals-time | 4 s. ON,1s.OFF |
| Intervals-distance | 2 m |
| Voltage gradient survey (VGS) | |
| Intervals-distance | 2 m above line, 1 m perpendicular |

## *3.2 Field Measurement*

Above ground coating inspection techniques depending on direct current (D.C.) are well established. These include the following methods:

### 3.2.1 Close Interval Potential Survey (CIPS)

Pipe–to-soil potential is measured at very close distance (every 2–5 m). Simple equipment are required to perform the measurement:

- $Cu/CuSO_4$ reference electrode,
- data logger,
- trailing wire,
- current interrupter.

The arrangement is shown in Fig. 1.

The trailing wire is connected to a test-post and the operator moves along the pipeline route placing the reference electrode in the soil every 2 m. The measured

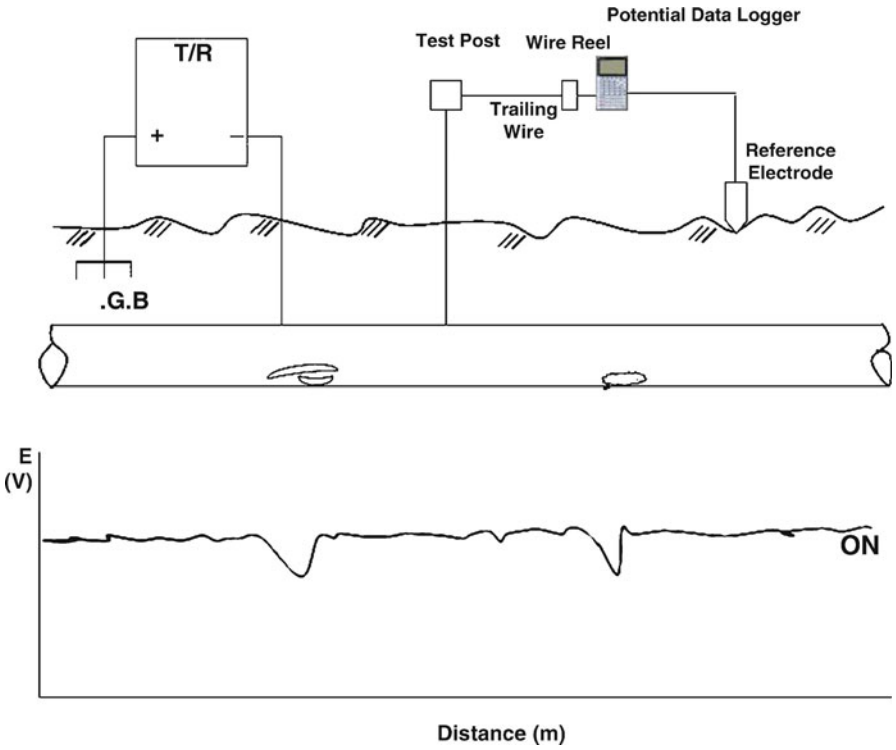


**Fig. 1** Close interval potential measurements

potential is recorded by the data logger. A computer program is used to transfer and process the recorded data. The potential data is expressed by a graph against distance. The recorded potential falls down, than normal value, in allocation of coating defect. The method is simple and one operator can cover a distance of 3 km per day. One major defect is that soil variance can show a decrease in potential that can be mixed-up with indication of a coating defect. To overcome the ambiguity an improved technique is used.

## Interrupted Close Interval Potential Survey

Synchronized timers (current interrupters) are used to switch all cathodic power sources attached to the line in order to get representative readings of the instant OFF potential. The ON potential and instant OFF potential are registered by the data logger at the same time for each reference cell location. This technique is now the most widely used method. From the gained results, regions of defective coating are postulated. Typical (schematic) results are shown in Fig. 2.

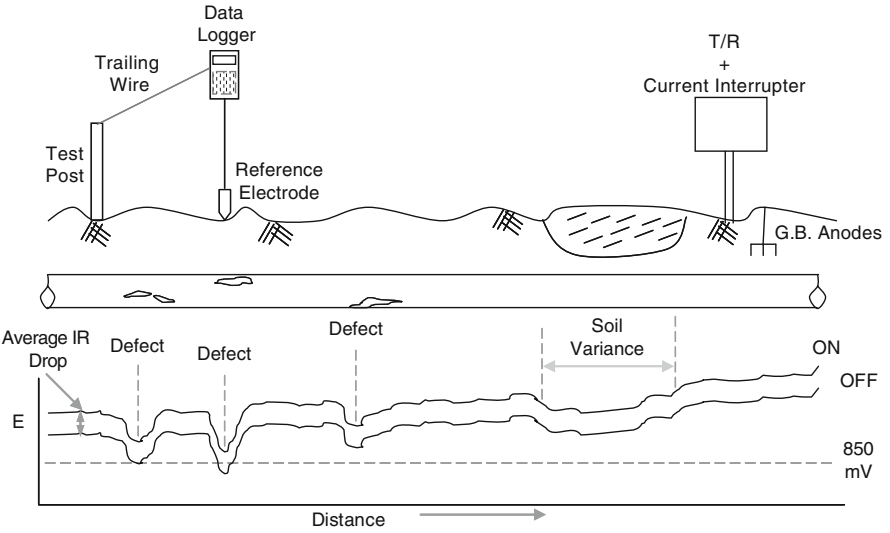


**Fig. 2** Interrupted close interval overline optional survey

## Direct Current Voltage Gradient Method

When c.p. current flows through resistive soil to the bare steel exposed at a coating defect, a voltage gradient is generated between the bare and coated points. Generally, the larger the coating defect, the greater the current flow and the greater the resulting voltage gradient.

In this method, the voltage gradient is traced by measuring the path difference between 2 reference electrodes using a sensitive millivoltmeter. There is no direct connection to the pipeline, so there are no trailing wires.

In surveying a pipeline, the operator walks the route placing the 2 reference electrodes (with 2 m apart) at a regular short interval. As a coating fault is approached, the voltmeter will signify voltage value higher than the signal in any intact coating location along the pipeline route. The voltage value progressively decreases as the reference electrodes get nearer to the coating defect. When the defect place is passed, the voltage signal will reverse in sign ($\pm$) and the value slowly decreases as the surveyor moves away from the coating defect.

The fault location is accurately determined when there is no or very small value of voltage signal, that is the fault is sited midway between the 2 reference electrodes (Fig. 3). The same procedure is repeated perpendicular to the pipe. The coating epicenter is accurately decided at the point where the 2 midway positions cross.

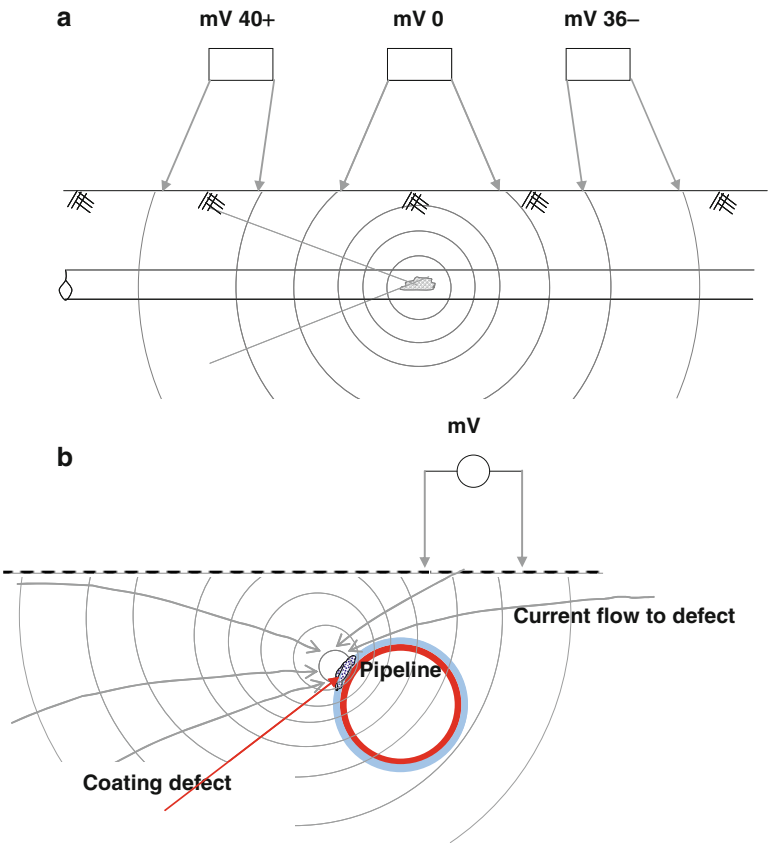


**Fig. 3** Direct current voltage gradient measurement: (**a**) over-the-line, (**b**) perpendicular to the pipe

## *3.3 Analysis of Survey Results*

### 3.3.1 Interrupted CIPS

- Instant "OFF" value of potential $E_{OFF}$ is the most important value which contributes to the level of protection of the pipe and points out to the areas of active corrosion.
- While "ON" potential $E_{ON}$ is the voltage lost to overcome the soil resistance and does not really contribute to the cathodic protection of the pipe.
- The difference between $E_{ON}$ and $E_{OFF}$ is the IR drop.
- The average value of IR drop is decided from CIPS graphs. The values depend mainly on the soil resistivity since the applied current is constant and the coating resistivity is the same.
- Suspected location of a coating defect can be seen from CIPS graphs if the IR drop at a decreased value of potential is smaller than the average IR drop.

### 3.3.2 Direct Current Voltage Gradient Method

The exact location of the coating defect is determined according to the scheme described above. However to determine the severity of the defect additional measurement should be performed as follows:

Sizing Coating Defects

At each defect, the voltage drop OL/RE (over-the-line-to-remote-earth) i.e. perpendicular to the pipe, is measured using two reference electrodes (say 2 m apart) and a millivoltmeter. The two electrodes are moved till two consecutive readings show no value i.e. remote earth (Fig. 4).

The total value of the readings (say 4 readings) is the defect OL/RE. The defect severity is calculated as follows:

$$\% \text{ IR} = \text{Defect OL/RE (mV)} \tag{1}$$

$$E_{ON} - E_{OFF}(\text{mV}) \tag{2}$$

The severity of the defect is then categorized as follows:

- <15% can be neglected,
- 15–35% defects should be repaired,
- >35% active corrosion at defect location and the coating should be repaired as soon as possible.

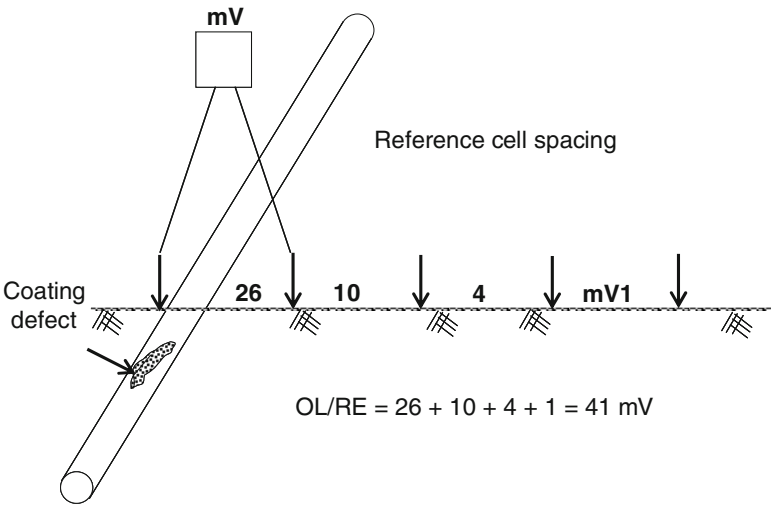


**Fig. 4** Over-the-line/remote-earth measurements

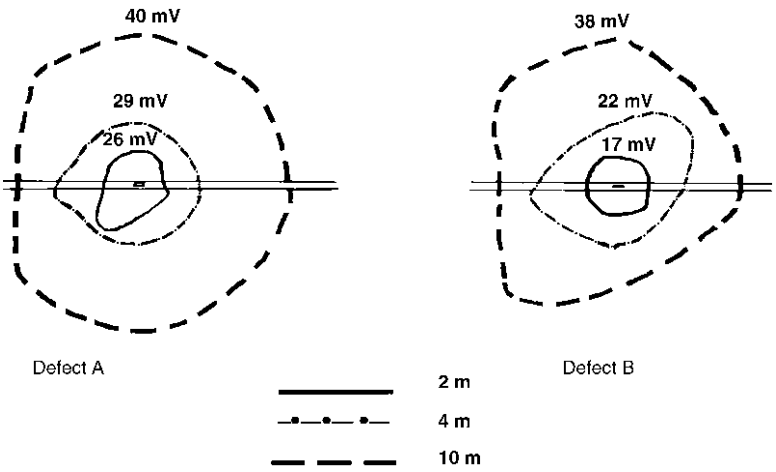


**Fig. 5** Field measurements: equi-potential lines in coating defect locations

Experience had shown that defect sizing or severity with the above scheme is very approximate. Attempts to modify methods of voltage gradient measurements and calculation are in progress [2].

(a) One trial to verify the defect intensity estimation was suggested as follows:
(b) place one measuring cell on the epicenter of the defect and move the other cell in perpendicular direction to the line until there is no change in the measured potential measurement. Accordingly, one voltage only is considered ($V_{RE}$) and the corresponding distance from the line is measured (say 10 m),
(c) the potential difference between two cells is then measured over the line ($V_{OL}$), for the same distance, in good coating area (not far from the defect to avoid the effect of the soil variation),
(d) the results of field experiments on two defect locations are shown in Fig. 5.

The defect intensity (D.I.) can be calculated as follows:

$$\text{D.I.} = \frac{V_{RE} - V_{OL}}{V_{OL}} 100 \tag{3}$$

## 4 Coating Inspection Project of SUMED Pipelines

SUMED transmission (crude oil) pipelines are two 40″ parallel lines (10 m apart) extending for 315 km between the Port of Suez at the Red Sea and Sedi-Kerir Port (west of Alexandria) at the Mediterranean Sea. The lines were constructed in 1974 and 1975. The lines are routed in a desert area for 112 km, crossing the River Nile at Cairo, then extends for 203 km till the Mediterranean in desert and agriculture lands.

The lines are coated with polyethylene (PE) and cathodically protected by impressed current. The protection current is supplied by 7 Transformer/Rectifier (T/R) stations and 2 Solar Energy stations distributed along the route.

A Coating Integrity Assessment Program was conducted in 2003. The following are examples of the survey results: Figures 5–8 are examples of the produced potential- distance graphs obtained in one section of the pipeline (35 km). The applied protective current in this section was constant at 8 A.

The following information can be deduced from the CIPS graphs:

- The IR drop ranges between 400 and 600 mV specifying high resistivity soil.
- OFF potential ($E_{OFF}$) values are over – 850 mV indicating adequate protection of the pipeline section.
- Defect locations are suspected when there is potential drop in OFF values corresponding to the ON potential drop.

Voltage gradient measurements were carried out only for areas of defect suspected points indicated by CIPS. The measurements were carried out for a length over the line of at least 20 m before and 20 m after the suspected points. The exact location of any ascertained coating defect is given with reference to a nearest construction mark. The following table is a model of the data obtained on one surveyed section of the pipeline.

Voltage gradient technique of OL/RE was also conducted for the confirmed coating defects. The values of% IR (defect severity) are also given in the Coating Defect Table. The location data given in the table is dispatched to the pipeline operation section to execute the Post Assessment stages of the program i.e. excavation

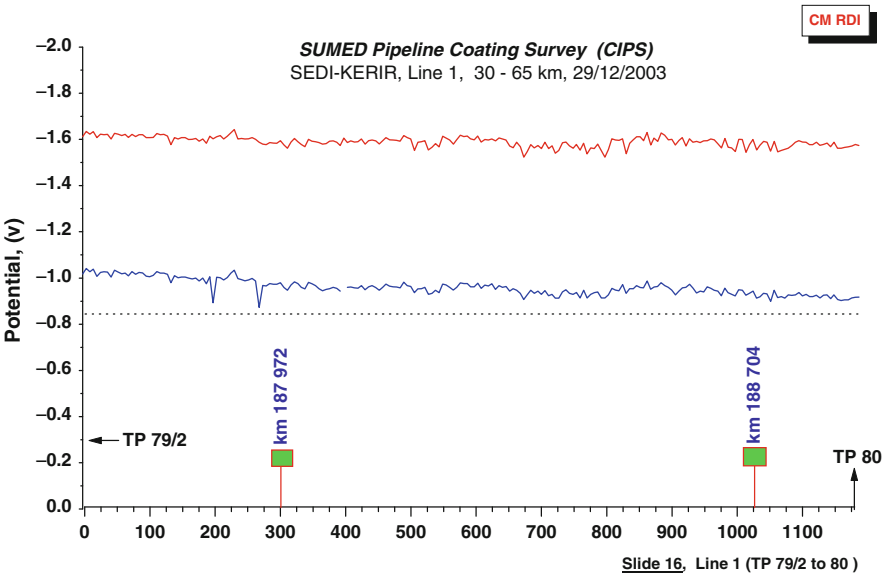


**Fig. 6** CIPS graph showing no defect in the measured distance

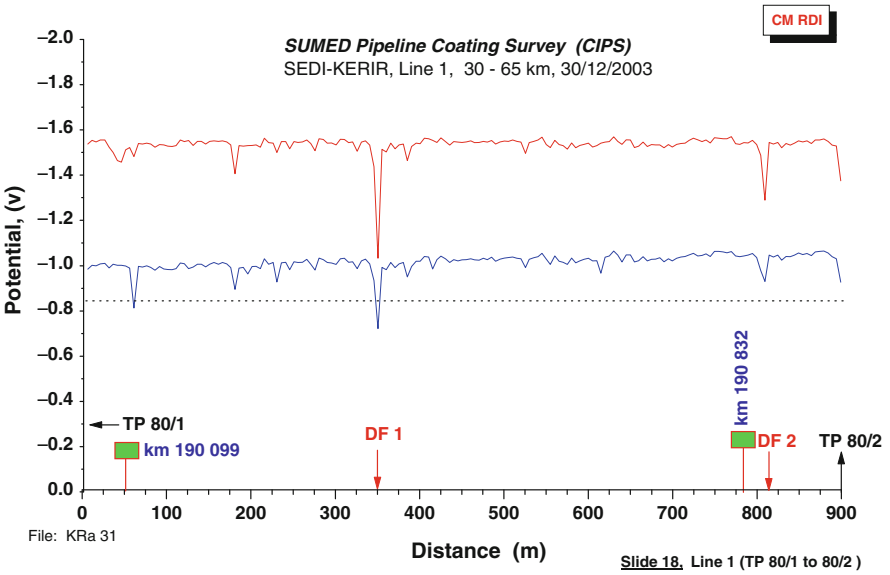


**Fig. 7** CIPS graph showing 2 coating defects

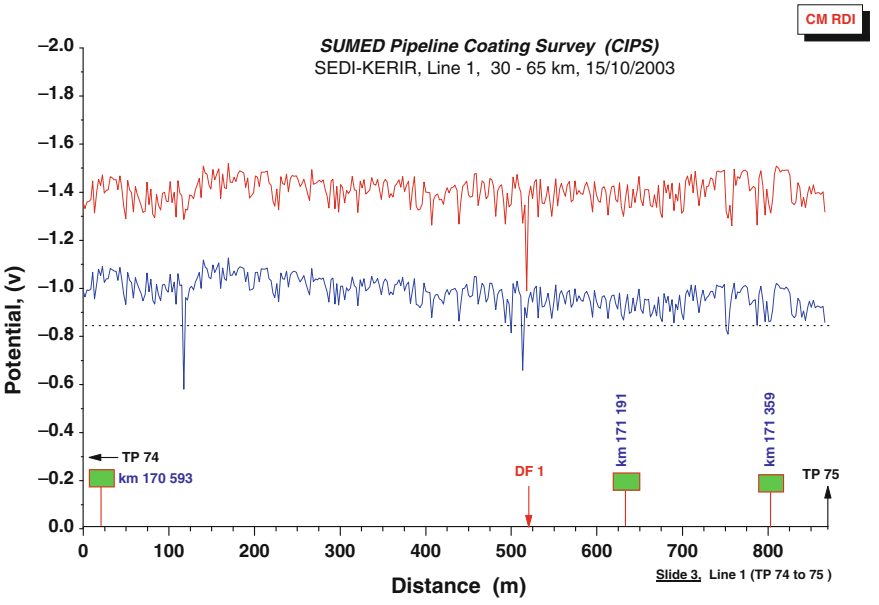


**Fig. 8** CIPS graph showing one coating defect irrespective of spike of deceptive potential spikes

and repair. The accuracy of the findings was estimated to be over 95% for location. The defect severity could be decided only in two categories: namely% IR less than or over 15%.

Coating Defect: SEDI-KERIR – Line 1 (30–65 km)

| Distance | | | Location | | % IR | | |
|---|---|---|---|---|---|---|---|
| Form | To | DF n°. | Reference | Meter form | <15% | >15% | DF length (m) |
| TP37 | TP73/1 | 1 | TP73 | +70 | | 40 | Dis. |
| TP73/1 | TP74 | No defect | | | | | |
| TP74 | TP75 | 1 | Km 171191 | −110 | | 30 | Dis. |
| TP75 | TP76 | 1 | Km 172956 | +40 | 11 | | Dis. |
| TP76 | TP76/1 | No defect | | | | | |
| TP76/1 | TP76/2 | 1 | Km 175616 | −60 | 8 | | Dis. |
| | | 2 | Km 175616 | +65 | 12 | | Dis. |
| TP76/2 | TP76/3 | No defect | | | | | |
| TP76/3 | TP76/4 | 1 | TP76/4 | −20 | | 54 | Dis. |
| TP76/4 | TP77 | 1 | TP76/4 | +90 | | 32 | Dis. |
| TP77 | TP77/1 | No defect | | | | | |
| TP77/1 | TP78 | 1 | Km 182396 | −10 | 15 | | Dis. |
| | | 2 | Km 183234 | +80 | 14 | | Dis. |
| TP78 | TP78/2 | No defect | | | | | |
| TP78/2 | TP79 | No defect | | | | | |
| TP79 | TP79/1 | 1 | Km 186128 | +60 | 9 | | Dis. |
| TP79/1 | TP79/2 | No defect | | | | | |
| TP79/2 | TP80 | No defect | | | | | |

## 5 Conclusions

Potential data loggers coupled with computer programs have made it economical to perform a detailed coating inspection along transmission hydrocarbon pipelines. The computerized potential logs resulting from two well established techniques CIPS and DCVG are used for coating integrity program.

The main advantage of the said technique is resolving the exact location of the coating defects and their intensity. In addition the measurements provide detailed information for analyzing the level of cathodic protection, IR drop values of the earth, interfering current, etc. In total, economic control of pipeline corrosion protection, against aggressive soil and coating degradation, can be achieved.

## References

1. NACE RP0502-2002, *Pipeline External Corrosion Direct Assessment Methodology* (NACE, Houston, 2002)
2. O.C. Moghissi, J.P. Mckinney, M.E. Orazem, *Corrosion/2009* Paper #146, 2009